

CHAPTER 3

Polar Stratospheric Ozone: Past and Future

Lead Authors:

P.A. Newman
J.A. Pyle

Coauthors:

J. Austin
G.O. Braathen
P.O. Canziani
K.S. Carslaw
P.M. de F. Forster
S. Godin-Beekmann
B.M. Knudsen
K. Kreher
H. Nakane
S. Pawson
V. Ramaswamy
M. Rex
R.J. Salawitch
D.T. Shindell
A. Tabazadeh
D.W. Toohey

Contributors:

D. Allen
L.M. Avallone
S.R. Beagley
G.E. Bodeker
C. Brühl
J. Christy
B. Connor
M. Dameris
A.R. Douglass
S. Eckermann
M. Gelman
F. Goutail
P. Hamill
Y. Koshelkov
K. Labitzke
U. Langematz
R. Lin
E. Manzini
T. Nagashima
E.R. Nash
J. Nash
S.J. Oltmans
D. Parker
K. Pfeilsticker
G. Pitari
W.J. Randel
E. Rozanov
M.L. Santee
C. Schnadt
M.D. Schwarzkopf
T.G. Shepherd
M. Shitamichi
P. von der Gathen
D.W. Waugh
P.O. Wennberg

CHAPTER 3

POLAR STRATOSPHERIC OZONE: PAST AND FUTURE

Contents

SCIENTIFIC SUMMARY	3.1
3.0 INTRODUCTION	3.5
3.1 TRENDS OF OZONE AND TEMPERATURE IN THE POLAR STRATOSPHERE	3.6
3.1.1 Polar Ozone Trends	3.6
3.1.2 Polar Temperature Trends	3.10
3.2 BASIC POLAR STRATOSPHERIC PROCESSES	3.13
3.2.1 Transport and Dynamics	3.13
3.2.1.1 The Polar Vortex: Mean Structure	3.13
3.2.1.2 Polar Vortex: Causes of Interannual Variability and Its Implications	3.13
3.2.1.3 Polar Transport and Mixing	3.19
3.2.2 Polar Stratospheric Clouds	3.21
3.2.2.1 Observations of PSC Physical Properties and Their Interpretation	3.21
3.2.2.2 Particle Composition	3.24
3.2.2.3 Denitrification	3.25
3.2.2.4 Dehydration	3.28
3.2.3 Polar Ozone Chemistry	3.28
3.2.3.1 Chlorine	3.29
3.2.3.2 Bromine	3.33
3.2.4 The Polar Summer Lower Stratosphere	3.37
3.2.4.1 Summertime NO _x Chemistry	3.38
3.2.4.2 Summertime HO _x Chemistry	3.39
3.2.4.3 Summertime Cl _y Chemistry	3.40
3.3 QUANTIFICATION OF POLAR OZONE LOSS: OBSERVATIONS AND MODELS	3.41
3.3.1 Approaches to Quantify Chemically Induced Ozone Loss in the Arctic	3.42
3.3.1.1 Approaches That Use Explicit Transport Calculations	3.42
3.3.1.2 Approaches That Use the Relation of Ozone to an Inert Tracer	3.43
3.3.2 Arctic Ozone Loss During the Last Decade	3.45
3.3.2.1 Ozone Loss Rates Near the Maximum of the Ozone Concentration	3.45
3.3.2.2 Vertical Profiles of Ozone Loss	3.45
3.3.2.3 Effect of Ozone Loss on the Total Ozone Column	3.48
3.3.2.4 Chemical Ozone Loss in the Arctic Winter 1999/2000	3.50
3.3.3 Consistency Between the Different Observational Techniques	3.50
3.3.4 The Effect of Denitrification on Ozone Loss	3.51
3.3.5 Model Studies of Arctic Ozone Loss	3.54
3.3.5.1 Chemical Transport Models	3.54
3.3.5.2 Specific Model Studies	3.55
3.3.6 Quantifying Antarctic Ozone Loss	3.57
3.3.7 Model Studies of Antarctic Ozone Loss	3.57
3.3.8 Conclusion	3.58
3.4 CAUSES OF POLAR STRATOSPHERIC TEMPERATURE TRENDS	3.58
3.4.1 Introduction	3.58
3.4.2 Modeling Techniques	3.58

3.4.2.1	Fixed Dynamical Heating (FHD) Models	3.59
3.4.2.2	General Circulation Models (GCMs)	3.59
3.4.3	Causes of Polar Stratospheric Temperature Trends	3.59
3.4.3.1	Polar Ozone	3.59
3.4.3.2	Well-Mixed Greenhouse Gases (WMGHGs)	3.63
3.4.3.3	Combined Changes in WMGHGs and Stratospheric Ozone	3.63
3.4.3.4	Stratospheric Water Vapor	3.64
3.4.3.5	Solar Changes	3.64
3.4.3.6	Volcanoes	3.64
3.4.4	Timing of the Springtime Cooling Trend	3.65
3.4.5	Summary and Conclusions	3.65
3.5	CHEMICAL-CLIMATE MODELING OF THE PAST AND FUTURE POLAR STRATOSPHERE	3.66
3.5.1	Introduction	3.66
3.5.2	The Uncertainties in Chemistry-Climate Models	3.68
3.5.2.1	Temperature Biases	3.68
3.5.2.2	The Simulation of Polar Stratospheric Clouds	3.69
3.5.2.3	The Position of the Upper Boundary of the GCM	3.72
3.5.2.4	Predictions of Planetary Waves	3.73
3.5.2.5	Stratospheric Water Vapor Changes	3.75
3.5.3	Model Assessments	3.75
3.5.3.1	The 1960-2000 Time Frame: Ozone Depletion	3.77
3.5.3.2	The 2000-2020 Time Frame: Start of Ozone Recovery	3.77
3.5.3.3	The 2020-2060 Time Frame: Complete Ozone Recovery	3.79
3.5.3.4	Attribution of Model Ozone Changes	3.80
3.5.4	Summary	3.80
	REFERENCES	3.81
	APPENDIX 3A: SATELLITE MEASUREMENTS IN THE ANTARCTIC AND ARCTIC	3.104

SCIENTIFIC SUMMARY*

- **Springtime Antarctic ozone depletion remains very large.** Severe depletion, leading to minimum values around 100 (Dobson units (DU)), has been seen every year since the early 1990s. The main processes are well understood.
- **Some estimates of the severity of the Antarctic ozone hole, e.g., the area enclosed by the 220-DU contour, show an increase at some times in recent years, and therefore it is not yet possible to say that the ozone hole has reached its maximum.** Much of the change appears to be associated with processes at the edge of the polar vortex and is consistent with meteorological variability and the almost constant halogen loading. The observations do not show evidence of ozone recovery; this is expected due to the slow decrease of stratospheric chlorine and bromine to pre-ozone-hole levels (see Chapter 1).
- **Meteorological observations show that the Antarctic polar vortex is persisting later than was observed during the 1970s.** Over the last decade, the vortex has broken up in the early-December period in contrast to a breakup in late-November during the 1970 to 1980 period.
- **There was very large local ozone depletion in the Arctic vortex in 1999/2000, reaching 70% by early April in a narrow region around 20 km.** Integrated column losses were greater than 80 DU. The winter of 1999/2000 was characterized by persistent low temperatures and a strong vortex. In contrast, in the warmer more disturbed polar vortex of 1998/1999, the estimated loss was very small. These observations are consistent with our expectation that Arctic ozone losses are largest in cold stratospheric winters.
- **The Arctic winter/spring ozone column continues to be variable, reflecting the variable meteorology of the Northern Hemisphere (NH) stratosphere.** Lower column ozone was present during the cold winter of 1999/2000 than in the warmer, more disturbed winters of 1998/1999 and 2000/2001, reflecting the variability in the dynamical and chemical processes that control the ozone layer in the NH stratosphere. It is not possible to isolate the importance of these factors just from observations; model studies are needed to do this. The Arctic Oscillation can be used as an index to describe variability, but not causality.
- **The magnitude of chemical loss of ozone for all Arctic winters during the last decade has now been studied with a variety of observationally based approaches.** There is generally good agreement between different analyses for quantifying losses: for the 1999/2000 winter, agreement was better than 20% in the Arctic stratosphere around 20 km.
- **Satellite and radiosonde observations show that the springtime Arctic and Antarctic lower stratospheres have cooled.** However, because of large variability in the Arctic spring, the magnitude of the trend is uncertain there. During the 1979 to 2000 period the linear temperature trend exceeds -1.5 K/decade at 70°N and 70°S .
- **Modeling studies now demonstrate that the stratospheric ozone depletion has exerted an important influence on the springtime cooling of the Arctic lower stratosphere over the 1980 to 2000 period, but the degree of attribution is hindered by the large dynamical variability in this region.** In Antarctica modeling studies reaffirm that ozone loss is the major cause of the springtime cooling and the increased persistence of the Antarctic polar vortex. Well-mixed greenhouse gases and stratospheric water vapor increases also contribute to the annually averaged cooling.
- **A laboratory study of the rate of formation of ClOOCl (the chlorine monoxide dimer), the initial step for the most important polar ozone loss cycle, suggests it is up to 25% faster (depending on temperature) than previous estimates based on data extrapolations to low polar temperatures.** This leads to faster calculated rates of chemical ozone loss.

* Editor's note added in press: The preparation and review of this Assessment report were completed by August 2002. The observations of the unusual Antarctic ozone hole of 2002 occurred thereafter and hence are not included here. Such subsequent observations will, of course, be included in future reports and assessments.

POLAR OZONE

- **In situ observations of the rate of decay of chlorine monoxide (ClO) at sunset are consistent with the new laboratory rate for $\text{ClO} + \text{ClO} + \text{M}$ and recommended cross sections for ClOOCl .** This suggests that errors in model representation of the partitioning of ClO and its dimer cannot account for discrepancies between modeled and measured Arctic ozone losses observed in January.
- **Modeling studies of the latitudinal, seasonal, and diurnal variations in bromine monoxide (BrO) column abundances agree well with observations from a number of ground sites, indicating that the processes that govern bromine partitioning in the polar regions are reasonably well understood.**
- **Observations of BrO in the winter Arctic vortex by in situ and remote detection techniques are in broad agreement and consistent with a total bromine budget of $\sim 20 \pm 4$ parts per trillion.** This result now allows for more accurate assessment of the contribution of bromine to polar ozone loss. At present, the fractional contribution of bromine to total ozone loss ranges between 30% and 60%, depending on temperature and abundances of ClO. Considering the observed leveling off of abundances of sources of chlorine (reported in Chapter 1), the role of bromine in polar ozone loss will continue to increase relative to that of chlorine until the current upward trends of the bromine source gases reverse.
- **New laboratory and field studies have led to refinements in the recommendations for the rate constants of several key reactions that couple the photochemistry of odd hydrogen (HO_x) and nitrogen oxides (NO_x) (species that are largely controlled by natural processes) and to the discovery of a new process (near-infrared photolysis of peroxyxynitric acid (HNO_4)).** Together with new observations of HO_x , NO_x , and ozone in late spring and summer, these studies have demonstrated that our understanding of the photochemistry of HO_x and NO_x in the lower summertime stratosphere is fundamentally sound.
- **Removal of nitrogen compounds (denitrification) has been observed to occur in the Arctic lower stratosphere in several cold winters.** Denitrification of up to 70% of the total reactive nitrogen was observed at some levels of the lower stratosphere in winter 1999/2000. Observations and modeling results show that denitrification in the 1999/2000 Arctic lower stratosphere increased ozone loss by as much as 30% at 20 km in spring.
- **Our understanding of what causes denitrification has improved considerably by the discovery of large nitric-acid-containing particles in the Arctic polar lower stratosphere during the winter of 1999/2000.** Sedimentation of these particles can account for observed Arctic denitrification, although the mechanism of formation of these sedimenting particles remains uncertain. Sedimentation of ice containing dissolved nitric acid, which has been the preferred mechanism in stratospheric models, was not the dominant mechanism in the Arctic in 1999/2000. These observations show that denitrification can occur at higher temperatures than previously thought.
- **Synoptic and mesoscale motions (baroclinic and gravity waves) can lead directly to, and enhance, polar stratospheric cloud (PSC) formation in both hemispheres.** For the first time, operational meteorological analyses have been demonstrated to contain credible information about the gravity-wave field in high latitudes.
- **Model calculations suggest that the magnitude and vertical extent of denitrification could increase considerably in a future colder Arctic stratosphere, leading to increased ozone loss over a broader altitude range in the lower stratosphere.** The denitrification mechanism is not well represented in current global models, which is one of the limiting factors in the ability of the models to reproduce the large ozone losses observed in cold Arctic winters and to reliably predict future ozone losses in the Arctic.
- **The chemical composition of liquid and solid PSC particles has been measured directly for the first time.** Measured compositions are in agreement with model calculations for liquid particles and nitric acid trihydrate, which have been used in stratospheric models for many years. These measurements give confidence in the micro-physical models that are central to simulations of polar ozone loss.

- **Significant chemical loss of ozone (~0.5 parts per million by volume) in the lower stratosphere during January has been observed in several cold Arctic winters.** The observations indicate that the loss occurred exclusively during periods when the air masses are exposed to sunlight. These January ozone losses cannot be fully explained with our current understanding of the photochemistry. For some cold Arctic winters the ozone loss during January contributes about 25% to the overall loss of ozone over the winter.
- **Coupled chemistry-climate simulations broadly reproduce past trends in total ozone over the Antarctic.** The coupled chemistry-climate models have studied the future evolution of minimum Antarctic ozone. These models suggest that the minimum column ozone may have already occurred or should occur within the next decade, and that recovery to 1980 levels may be expected in the 2045 to 2055 period. The model response is driven mainly by the changes in stratospheric halogen loading, with a small delay in ozone recovery due to cooling of the lower stratosphere.
- **The area of the Antarctic ozone hole depends on processes near the edge of the polar vortex.** Area estimates amongst the coupled chemistry-climate models are uncertain because vortex-edge temperatures are near the threshold for PSC formation and these temperatures are difficult to predict.
- **Coupled chemistry-climate models now capture the typical interannual variability of Arctic ozone levels.** However, temperatures are often near the threshold for PSC formation and, hence, the initiation of perturbed chemistry. This places severe constraints on model predictions of past and future ozone behavior. A number of coupled chemistry-climate models run for this Assessment suggest that minimum Arctic ozone would occur within the next two decades, depending on the meteorology. Very low Arctic ozone columns, similar to those seen in the Antarctic, are not predicted by these models (in contrast to earlier simpler calculations considered in the previous Assessment). Such low levels in the Arctic would require weak dynamical forcing that is unprecedented in NH observations.

3.0 INTRODUCTION*

This chapter provides an update on our understanding of recent changes in polar ozone and of the polar vortex, and considers possible future developments. It builds on earlier Assessments, concentrating mainly, but not exclusively, on work reported since the previous United Nations Environment Programme/World Meteorological Organization (UNEP/WMO) assessment report (WMO, 1999).

The previous Assessment reported that the Antarctic ozone hole continued unabated, with essentially near-complete destruction of ozone in late winter/spring in the lower stratosphere, and that the factors controlling the depletion (meteorological preconditioning, halogen activation, ozone depletion in sunlight) were well understood. In the Arctic, substantial ozone losses were reported in several winters during the 1990s, depending on the meteorological conditions. The Assessment highlighted the vulnerability of the Arctic to large ozone losses in a cold winter while chlorine abundances remain high during the next decade or so. Less chemical loss was to be expected in the Arctic in winters with a warm, disturbed vortex. Difficulties with the precise quantification of Arctic ozone loss were indicated. The previous Assessment highlighted specific uncertainty issues surrounding the understanding of the different types of polar stratospheric clouds (PSCs), and the process of denitrification, which can limit our ability to model present and future polar ozone loss.

The coupling between atmospheric chemistry and climate has been recognized increasingly in recent assessments. In WMO (1999) a late-winter/springtime cooling in the Arctic polar lower stratospheric temperatures of ~3 to 4 K/decade was noted (although with the large dynamical variability in that region the statistical significance of the trend was not high), and the role of ozone, water vapor, and the well-mixed greenhouse gases was explored. Three-dimensional (3-D) coupled chemistry-climate models were used for the first time to look at the possible recovery of the ozone layer; these models all indicated a delay in recovery beyond the time of the peak in stratospheric halogen abundance.

Since the previous Assessment there has been considerable progress in basic research that we report below. Satellite datasets on ozone and temperature have been further extended. In addition, scientific impetus has been provided by several major field campaigns to study the

Arctic stratosphere. Results are reported here from the National Aeronautics and Space Administration (NASA) Photochemistry of Ozone Loss in the Arctic Region in Summer (POLARIS) campaign, aimed at understanding the summer polar stratosphere; the European Union (EU) Third European Stratospheric Experiment on Ozone (THESEO), a polar and middle-latitude campaign; and the joint NASA/EU Stratospheric Aerosol and Gas Experiment (SAGE) III Ozone Loss and Validation Experiment (SOLVE)-THESEO 2000. These campaigns produced new data to address some of the uncertainties remaining after the previous Assessment.

Section 3.1 updates polar ozone measurements in both Antarctica and the Arctic, concentrating on the winter and spring seasons when the largest ozone depletion is observed. The total ozone columns are considered, and updated information on various possible indicators of ozone recovery, suggested in the previous Assessment, is presented briefly. The updated polar temperature trends are also presented here.

Section 3.2 reviews our understanding of the relevant physical and chemical processes controlling the polar vortex and its composition. The Arctic field campaigns have provided new data on a disturbed winter with considerable exchange between polar and middle latitudes (1998/1999) and on the cold polar winter of 1999/2000, which led to large local ozone depletion. Many new complementary constituent measurements provide an important constraint on chemical loss processes. Important new measurements of particles were also made in the winter polar stratosphere, leading to advances in our understanding of particle composition and denitrification. Improved understanding of the dynamics in and around the polar vortex has also been developed.

Section 3.3 looks in detail at our quantitative understanding of polar ozone loss. In earlier assessments it was recorded that models often fail to quantify correctly the observed ozone loss. A variety of methods to derive ozone loss from measurements are reviewed in this section. Estimated losses in recent Arctic and Antarctic winters are considered and compared with each other and with model estimates.

In the previous Assessment (WMO, 1999), it was recognized that the future development of the ozone layer does not depend just on changes in stratospheric halogen loading but also, very importantly, on a number of other factors connecting chemistry and climate. These factors are discussed in Section 3.4. Temperature changes are

* Editor's note added in press: The preparation and review of this Assessment report were completed by August 2002. The observations of the unusual Antarctic ozone hole of 2002 occurred thereafter and hence are not included here. Such subsequent observations will, of course, be included in future reports and Assessments.

POLAR OZONE

particularly important, since polar heterogeneous chemistry is strongly temperature dependent, and furthermore, temperature changes are related to the strength of the polar vortex, descent within the vortex, and mixing with lower latitudes. The attribution of the trends in polar stratospheric temperatures (presented in Section 3.1.2) is discussed, and the roles of changes in well-mixed greenhouse gases, ozone, water vapor, and aerosol particles are reviewed. Future stratospheric temperature changes are discussed.

Finally, in Section 3.5, possible future states of the polar stratosphere are explored in sensitivity calculations using coupled chemistry-climate models. Results from these models were reported for the first time in an assessment in WMO 1999, and the models are still being developed. An extensive review of the present uncertainties in chemistry-climate models is presented here, followed by some examples of sensitivity calculations to consider the polar stratosphere during the next 50 years.

3.1 TRENDS OF OZONE AND TEMPERATURE IN THE POLAR STRATOSPHERE

3.1.1 Polar Ozone Trends

Ozone is primarily produced in the midlatitudes and tropics by photodissociation of oxygen by hard ultraviolet (UV) radiation (below 242 nm) and is transported toward the poles by the Brewer-Dobson circulation. The result is an annual cycle in ozone, shown by the climatological values in Figure 3-1. Because of the stronger Brewer-Dobson circulation in the Northern Hemisphere (NH), the Arctic is both warmer and has larger column ozone amounts than the Antarctic. In the NH, there is usually a maximum in the column in late winter/early spring. At the South Pole, there is less annual variation (larger annual variations are expected at the vortex edge). In recent years, the annual cycle has been modified by polar ozone depletion, most obviously in the Southern Hemisphere (SH).

Figure 3-1 also shows recent year-round ozone measurements from the Arctic Ny Ålesund station (78.9°N, 11.9°E) and the South Pole station, updating polar observations since the previous Assessment. The Antarctic observations in the last few years continue to show the extremely low spring ozone values that have characterized the ozone hole during the 1990s. The low Antarctic values begin with the chemical ozone losses during August and September and end upon the breakup of the vortex in November or December. During the Arctic summer, ozone is destroyed photochemically, especially at these high latitudes during continuous sunlight condi-

tions (Brühl et al., 1998), and the climatological seasonal minimum is reached in autumn.

In the Arctic, the March-to-April ozone maximum is occasionally reduced below the climatology in some years (e.g., in 1997, the cyan triangles in Figure 3-1) because of severe chemical ozone loss and reductions in ozone transport (Andersen and Knudsen, 2002). In these low-ozone years, the column ozone rapidly increases with the breakup of the vortex (e.g., early April 1997). Of the most recent winters, 1999/2000 also has somewhat lower ozone columns than the climatology, as discussed later. Extremely low Ny Ålesund column ozone values at the beginning of 1996 (Figure 3-1, dark red triangles) can partially be explained by the early onset of the ozone depletion that year (see Section 3.3.2). The lowest 1996 values occur in an “ozone mini-hole” event (Weber et al., 2002) (see Section 3.2.1.2). A complicating factor in the upper panel in Figure 3-1 is that occasionally Ny Ålesund is outside the vortex, as is evident from the large variations on a broad range of spatial and temporal scales.

Extremely high Ny Ålesund column ozone values in December 1998 (Figure 3-1, gray diamonds) and February 2001 (red circles) were caused by sudden warmings and the associated ozone transport. The warmings in those years also resulted in high temperatures, thereby preventing the formation of polar stratospheric clouds.

The largest ozone depletion occurs in the polar vortices during springtime. Figure 3-2 shows the springtime ozone values in the Arctic and Antarctic (63° to 90°) since 1970 (updated from Newman et al., 1997). The Arctic column ozone averages were extremely low during the mid-1990s, but have been relatively high in four of the last five winters. As noted in the previous paragraph and as is apparent in Figure 3-1, these higher ozone values are associated with stratospheric sudden warmings. The downward secular ozone trend apparent through 1997 and its reversal over the last few years can be associated with a long-term variation of stratospheric warmings.

Figure 3-2 also shows that the Antarctic ozone hole continued to display the low values over the last 4 years that were apparent during the early and mid-1990s. The notably higher value in October 2000 resulted from greater dynamical activity, as is also apparent in Figure 3-1.

The polar column ozone averages of Figure 3-2 in the 63° to 90° region generally coincide with the polar vortices. However, in the NH the vortex is usually smaller and the 63° to 90° region may contain air outside the vortex. The absolute minimum in the NH occurred in 1997, when the vortex was cold, very large, and pole-centered. However, the column chemical ozone loss in the vortex was probably larger in 1995, 1996, and 2000 (see Section 3.3.2.3). However, Andersen and Knudsen

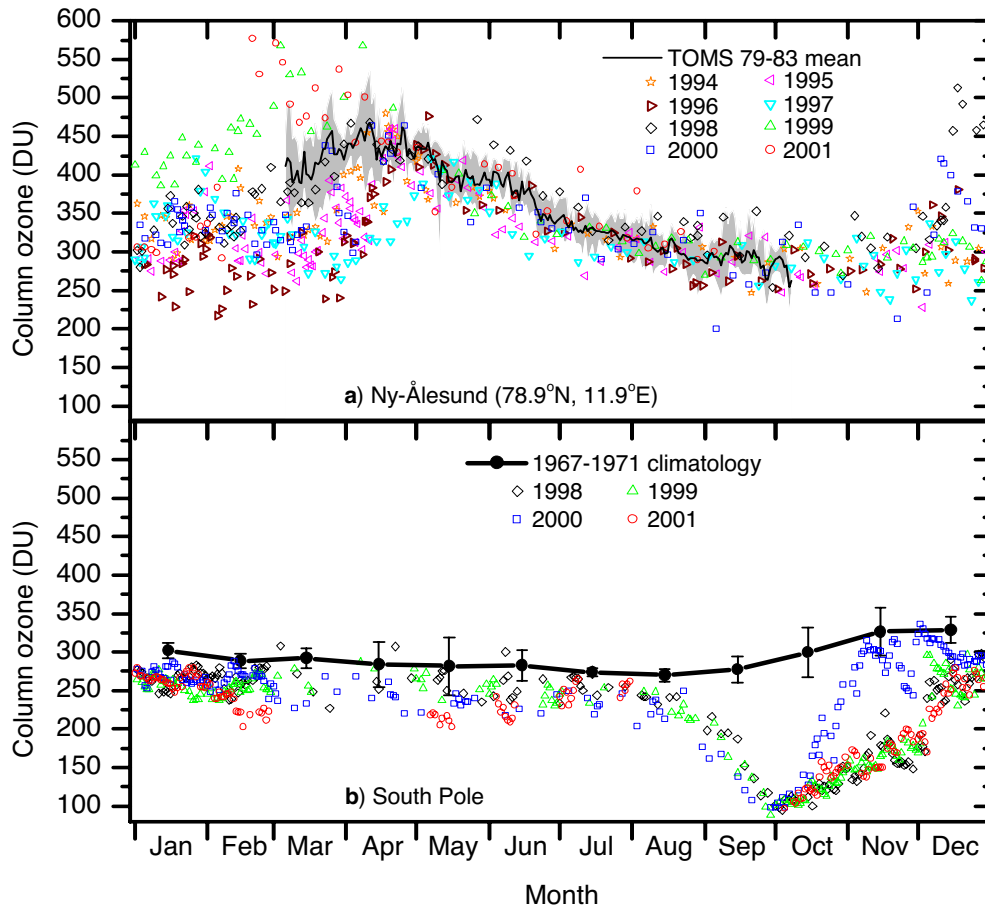


Figure 3-1. The column ozone determined from (a) ozonesondes launched from Ny Ålesund and (b) ozonesonde and Dobson measurements at South Pole, as a function of day of year. Symbols give individual measurements. The solid line in panel (a) is the daily TOMS mean column ozone for the Ny Ålesund station from 1979 to 1983, with the shading indicating the range. The solid line in (b) is a climatology for the South Pole from 1967 to 1971 (with 1σ error bars indicated). Courtesy Peter von der Gathen (Alfred Wegener Institute) and Samuel Oltmans (NOAA-CMDL).

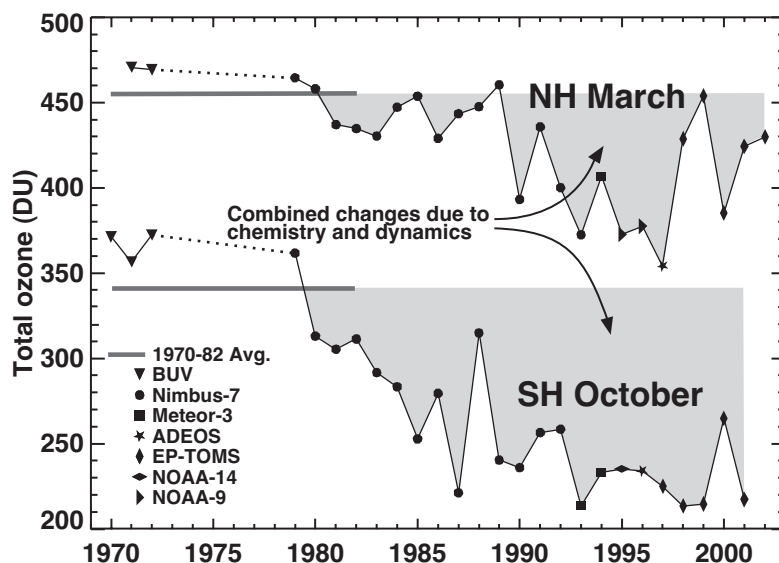


Figure 3-2. Average total ozone poleward of 63° latitude in March in the Northern Hemisphere (NH) and October in the Southern Hemisphere (SH). Symbols indicate the satellite data that have been used in the different years. The horizontal gray lines represent the average total ozone for the years prior to 1983 for the NH and SH. The lighter gray shading shows the combined differences resulting from chemical losses and dynamical processes. Updated from Newman et al. (1997).

POLAR OZONE

(2002) have argued that about 75% of the 63° to 90°N depletion from 1992 to 2000 relative to the 1979-to-1982 average is due to ozone depletion inside the vortex, so the plot does give a good indication of the Arctic vortex depletion.

Large total column ozone trends have been seen in both the Arctic and Antarctic polar vortices during the spring (Figure 3-3). To obtain these trends with better correlation with the polar vortices, a potential vorticity coordinate (equivalent latitude) remapping technique was applied to a trend analysis of homogenized satellite data from the Total Ozone Mapping Spectrometer (TOMS) and the Global Ozone Monitoring Experiment (GOME) (Bodeker et al., 2001; see also Appendix 3A for satellite data descriptions). In this coordinate the centers of the vortices are at 90° and the edges at about 60° to 75° (as shown by the x points in Figure 3-3). After a regression model including trends and variability (seasonal cycle, quasi-biennial oscillation (QBO), solar cycle, volcanic effects, and El Niño-Southern Oscillation (ENSO)) was applied to the data from 1978 to 1998, statistically significant linear trends were obtained.

The largest Arctic negative trend ($1.04 \pm 0.39\% \text{ yr}^{-1}$) is observed in March, whereas the largest Antarctic negative trend ($2.51 \pm 0.62\% \text{ yr}^{-1}$) is observed in October (updated from Bodeker et al. (2001) to include the additional years 1999 and 2000). In the Arctic vortex the 1978 to 1998 trend was largely due to severe vortex depletions in the 1990s (Section 3.3.2). The addition of the warmer winter of 1998/1999, when no significant ozone depletion in the vortex occurred, reduced the downward trends. In the Antarctic vortex trends have weakened due to saturation of the ozone losses. Hence, the trends, with 1999 and 2000 data included, have slightly smaller negative trends than previous estimates in the Antarctic spring column ozone. In the Arctic, Figure 3-3 shows steep gradients in the trends across the edge of the vortex. It also reveals statistically significant negative ozone trends in May, June, and July just inside the Antarctic vortex, which were not found in previous trend analyses, but confirms earlier findings (Roscoe et al., 1997; Lee et al., 2001) (see Section 3.3.7).

Because the ozone loss mainly occurs in the 12- to 20-km layer, the partial column ozone from 12 to 20 km

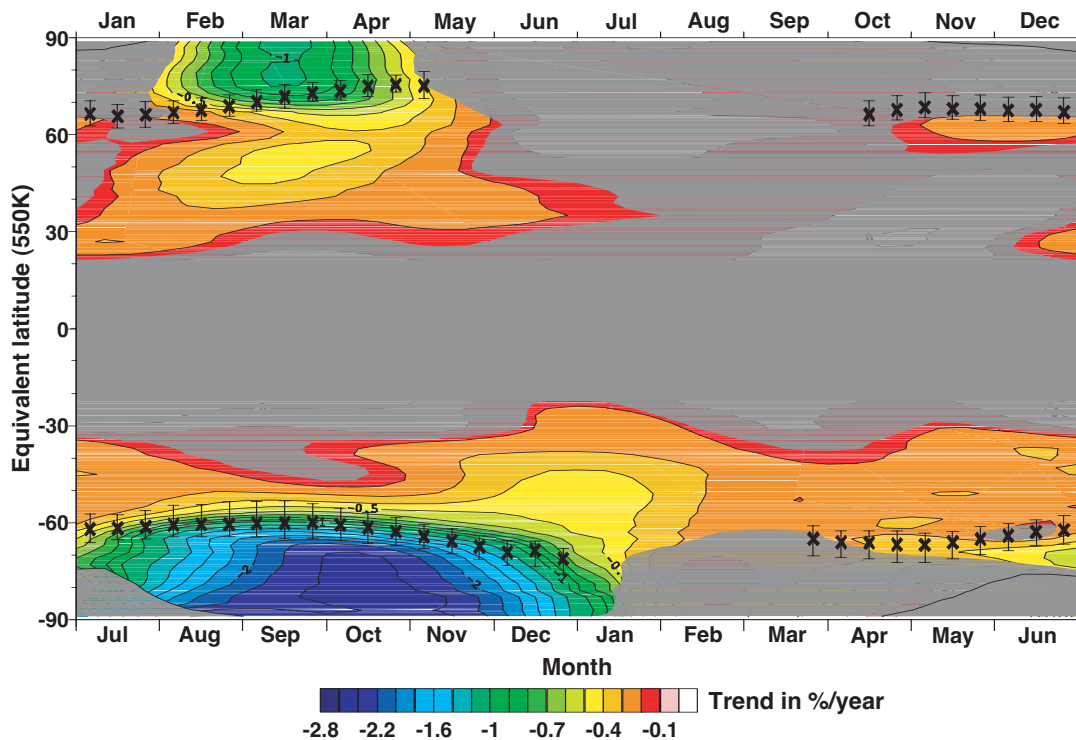


Figure 3-3. Total column ozone trends as a function of equivalent latitude and season using corrected TOMS and GOME data from November 1978 to December 2000. Gray shaded regions indicate where trends are statistically insignificant (at 95% confidence). The crosses show the mean position of the vortex (remnant) edge(s) over the time period when the position could be determined, and the “error bars” on each cross show the mean width of the vortex boundary (Nash et al., 1996). The equivalent latitude is calculated on the 550-K isentropic surface (Bodeker et al., 2001).

provides a good representation of the long-term decrease of the stratospheric ozone in Antarctica and could be used as an indicator of ozone recovery (see WMO, 1999). Figure 3-4 gives monthly averaged partial column ozone in September, October, and November (SON) based on ozonesonde observations at Syowa (1968 to 2001). The partial column ozone has decreased considerably from the early 1970s (~80% in September, ~85% in October, ~80% in November). The October partial column has not shown appreciable change since 1992. On the other hand, the September and November partial columns continued to show small reductions during the 1990s. The averaged partial column ozone over the 3 months (September to November) has also shown decreases during the 1990s, with relatively smaller interannual variability. Because Syowa is located near the vortex edge region, these September and November ozone reductions during the 1990s may be related to cooling near the vortex collar.

Spatially averaged characteristics of the Antarctic ozone hole from 1979 to 2001 based on the total column ozone observed by satellites (TOMS series for 1979-2001, and Television Infrared Observation Satellite (TIROS) Operational Vertical Sounder (TOVS) for 1995) are shown in Figure 3-5. These parameters include the maximum area, the minimum total column ozone, the ozone mass deficiency, and the date of the ozone hole's disappearance. The maximum area of the ozone hole increased rapidly during the 1980s and gradually during the 1990s, with year-to-year variations, and reached a maximum in 2000. The minimum total ozone, which usually appears in late September or in early October, has been approximately 100 Dobson units (DU) since 1993 (Figure 3-5) after the considerable decrease during the 1980s and the early 1990s. The ozone mass deficiency in the ozone hole (O_3 MD) is defined as the ozone mass deficiency from 300 DU in the sunlit area poleward of 60°S averaged for 105 days (1 September to 15 December). O_3 MD varied in concert with the Antarctic ozone hole area and was at the highest level ever in 2000. The date of the disappearance of the Antarctic ozone hole (disappearance of the total ozone values below 220 DU) has generally been occurring later in the season. As a whole, observations show that the Antarctic ozone hole has been slightly larger in the last few years in comparison with the mid-1990s. These observational results could be explained by ozone decreases near the vortex edge (e.g., Bodeker et al., 2001, 2002; Lee et al., 2001). Although the size of the Antarctic polar vortex has not increased, it has been stronger, as shown in Figure 3-6. There has been a tendency toward a cooling of the vortex due to ozone depletion, and the polar vortex has been more persistent, with some interannual variability (the temperature trends and persistence of the Antarctic polar vortex are discussed in

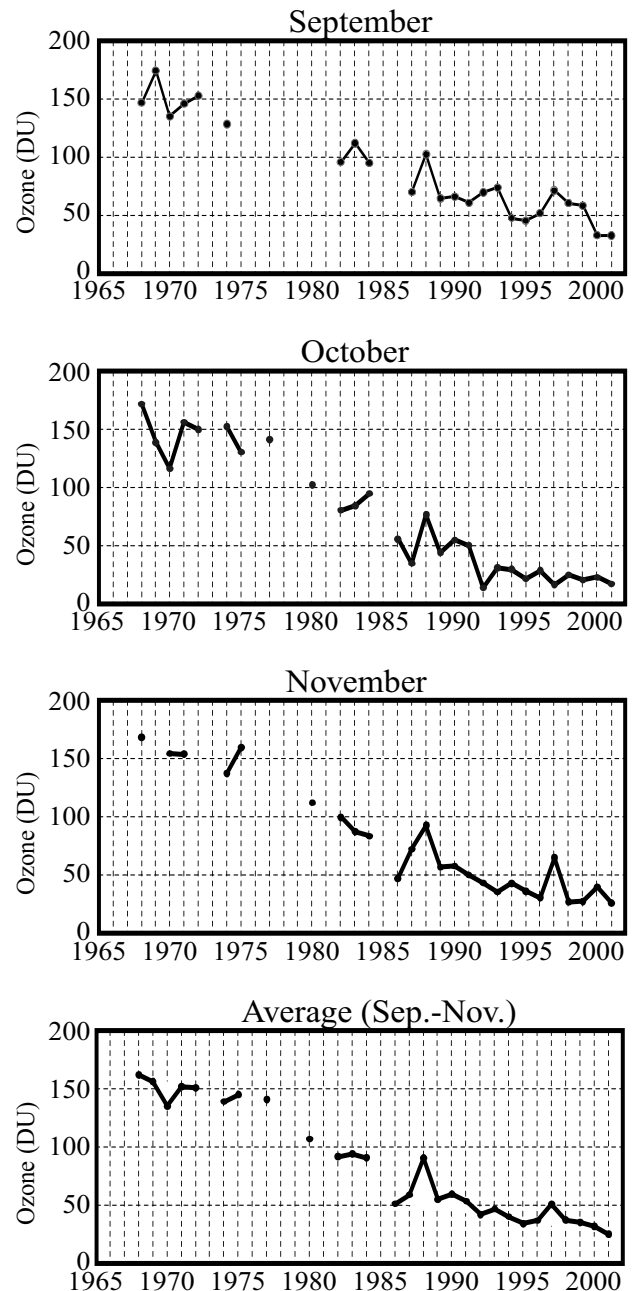


Figure 3-4. Partial column ozone in the 12- to 20-km layer in September, October, and November, and the average for September-November, over Syowa in Antarctica from 1968 to 2001. Update of Figure 4-27 of WMO (1999) by Japan Meteorological Agency.

the next section, Section 3.1.2). These conditions could result in more extensive polar stratospheric clouds (PSCs) in the sunlit vortex edge, and larger chemical depletion of ozone. This expands the area of the hole, and delays its disappearance into the late-spring period.

POLAR OZONE

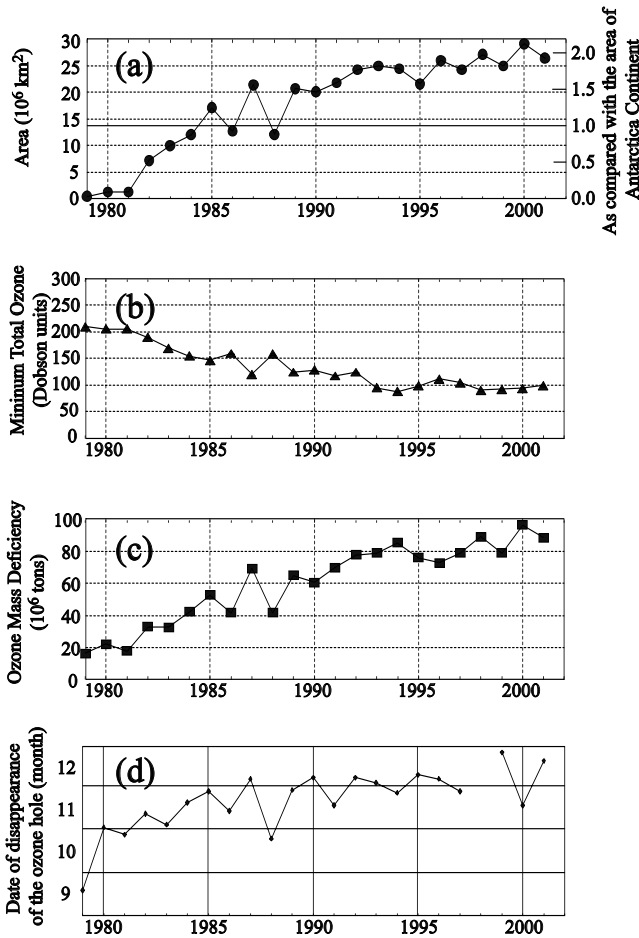


Figure 3-5. Evolution of the Antarctic ozone hole (defined by total ozone values below 220 DU) based on satellite data for the period 1 September to 1 December of each year. Panel (a) shows the maximum area covered by ozone hole values (left axis in millions km²; right axis gives size relative to Antarctic area), (b) the minimum total column ozone measured each year, (c) the maximum ozone mass deficiency from 300 DU during the period 1 September to 15 December (in Mt), and (d) the date of disappearance of the ozone hole values (Uchino et al., 1999; data updated to 2001).

The ozone hole has expanded in area somewhat since the early 1990s. The top panel of Figure 3-5 displays the maximum area of the ozone hole observed in the 1979 to 2001 period. There appears to be a steady increase of ozone hole size since the early 1990s. However, maximum values are sensitive to the timing of individual dynamical events in the early-September period (e.g., the 30 million km² single-day value in 2000). Figure 3-7 dis-

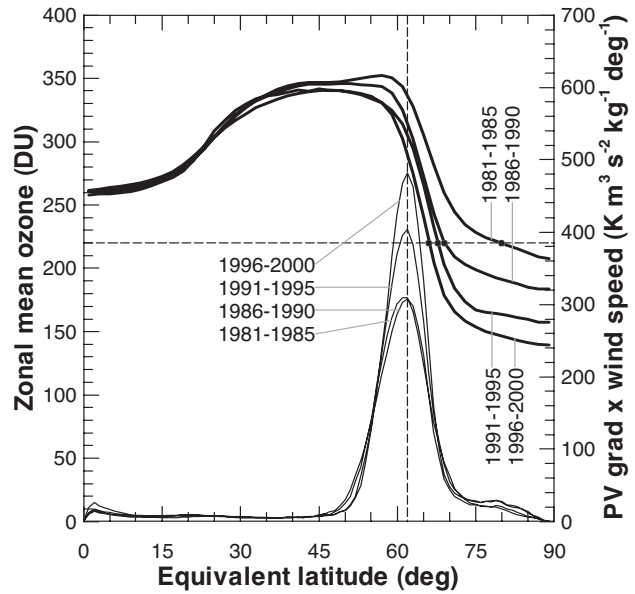


Figure 3-6. October SH average zonal mean total column ozone (top four thick solid lines plotted against the left ordinate) and October average vortex strength (gradient of potential vorticity (PV) multiplied by zonal wind speed; thin solid lines plotted against the right ordinate) for each of the four analysis periods (Bodeker et al., 2002).

plays the average size of the ozone hole (determined by the area enclosed by the 220-DU total ozone contour) over this same period, as determined from TOMS observations (see Appendix 3A for TOMS data description). Again, larger sizes are observed in the 1998 to 2001 period as compared with the 1992 to 1997 period. These size estimates are generally consistent with predictions that the ozone hole would have slight growth over the 1992 to 1995 period and maximum sizes occurring in the period after 1996 (Schoeberl et al., 1996).

3.1.2 Polar Temperature Trends

Substantial observational temperature data on the polar stratosphere are available from ~1979, including radiosonde and satellite measurements, and analyses of various types (Ramaswamy et al., 2001). Figure 3-8 illustrates the time series of temperatures at 70°N (March) and 70°S (November) from National Centers for Environmental Protection (NCEP) reanalyses and Climate Prediction Center (CPC) analyses (for descriptions, see WMO, 1999, Chapter 5). There are large interannual variations manifest in both hemispheres that generally complicate the determination of statistically significant trends.

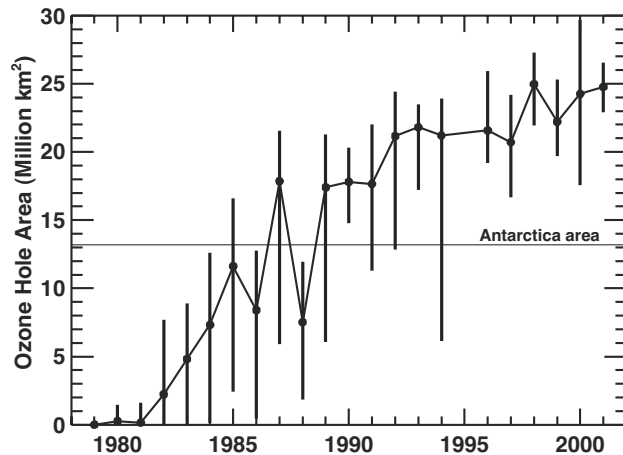


Figure 3-7. Area of the Antarctic ozone hole (defined by total ozone values below 220 DU) based on TOMS satellite data. The points show the average of the daily areas (in millions km²) between 7 September and 13 October. The vertical lines show the range of values over this same period.

The Microwave Sounding Unit channel-4 (MSU-4) data and the Stratospheric Sounding Unit (SSU) derived temperature trends (1979 to 1998) for 70°N and 70°S are shown in Figure 3-9 (see also Figures 3-39 and 3-40). These are an update to the 1979 to 1994 trends presented in Ramaswamy et al. (2001). The 70° latitude is chosen for comparison, because this is the highest latitude for which SSU trend data are available. Both MSU-4 (black line) and SSU-15X (gray line) signals originate from a range in altitude in the stratosphere and do not correspond to one particular height. The SSU peak signal corresponds to a pressure of roughly 50 hPa and shows a statistically significant (at the 2 σ level) cooling of nearly 3 K/decade at 70°N in March, April, and May (MAM) and 70°S in September, October, and November (SON), and approximately 1.2 K/decade for the annual average temperature change at both poles. The instrument also shows cooling significant at the 1 σ level for most other seasons. The MSU-4 data (peak signal from approximately 100 hPa) also shows a significant cooling during the spring in both hemispheres (−1.8 K/decade at 70°N and −1.1 K/decade at 70°S) and at both poles. These MSU-4 trends are roughly half the magnitude of the SSU trend. The observed satellite trends for this period indicate cooling in all seasons at both 70°N and 70°S.

It should be noted that the magnitude and statistical significance of the trends in both regions are dependent on the end-year considered. This is more crucial for the Arctic, especially during winter/spring when

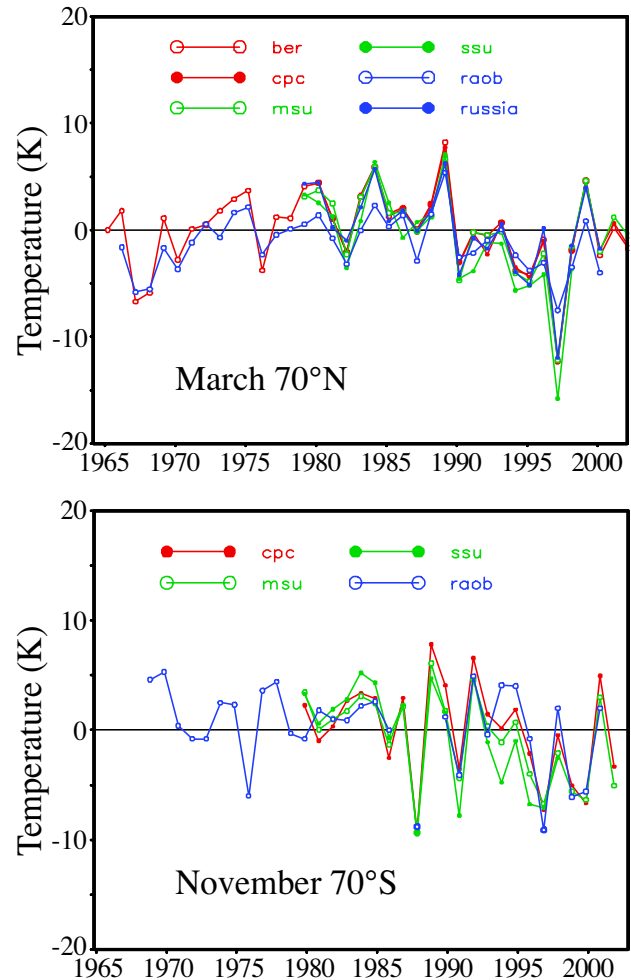


Figure 3-8. Zonal mean temperature deviation from the long-term mean in the lower stratosphere during March at 70°N (top) and November at 70°S (bottom). The red filled circles are 50-hPa NCEP/CPC objective analysis data; the open red circles are from the 50-hPa Freie Universität Berlin analyses; the open green circles are the MSU channel-4 satellite data (approximately a layer mean between 12 and 22 km); the filled green circles are the SSU channel-15X data (approximately a layer mean between 12 and 28 km); the open blue circles are the UK Meteorological Office adjusted and gridded radiosonde (RAOB) data at 50 hPa, and the filled blue circles are 50-hPa Russian radiosonde data from high northern latitudes. For each dataset, the deviation was determined with respect to the monthly mean of the time series (see Ramaswamy et al. (2001) for further details on the datasets). Figure assembled in cooperation with the Stratospheric Processes and Their Role in Climate (SPARC) Stratospheric Temperature Trends Assessment project.

POLAR OZONE

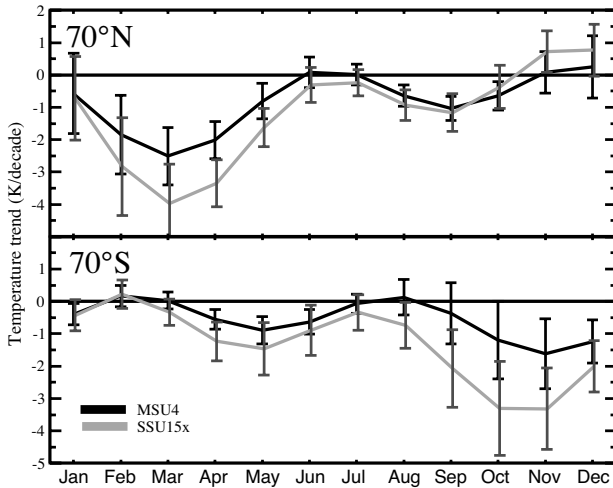


Figure 3-9. Stratospheric temperature trends for the period 1979 to 1998 at 70°N (top panel) and 70°S (bottom) for MSU-4 (black line) and SSU-15X (gray line) for each month of the year. The error bars represent the 95% confidence limits of the trend estimates. Figure provided by W.J. Randel (NCAR).

the time series reveals large interannual variations in temperatures (see Figure 3-8; also Labitzke and Van Loon, 1995). The trend sensitivity can be appreciated by comparing the latest (1979 to 1998) MSU trend at 70°N (March, as shown in Figure 3-9) with the corresponding MSU trends shown in WMO (1995, Figure 8.11 for the period 1979 to 1991).

Comparison of the satellite 1979 to 2000 annual-mean trends with those obtained for the 1979 to 1994 period (WMO, 1999) shows that there is now a statistically significant cooling at the 95% confidence level in the mid-to-high southern latitudes (Ramaswamy et al., 2002a). The northern midlatitudes continue to exhibit a statistically significant cooling trend (see WMO, 1999) while the higher latitudes (Arctic region) now have a cooling trend significant at the 90% confidence level. As in the satellite data, the 1979 to 2000 sonde trends yield an annually averaged cooling trend in the northern polar region. The sonde trend is somewhat smaller than the satellite trend (see Figure 3-39), although this may be partially due to the time period for the trend analysis being longer in the sonde data (note that 3 of the last 4 years have been relatively warmer; see Figure 3-8). The CPC analysis at 50 hPa also shows a cooling at both poles, consistent with the satellite data and sonde data.

Because ozone is radiatively active in both the infrared and the ultraviolet, large chemically driven polar ozone losses can potentially alter the dynamics of the strat-

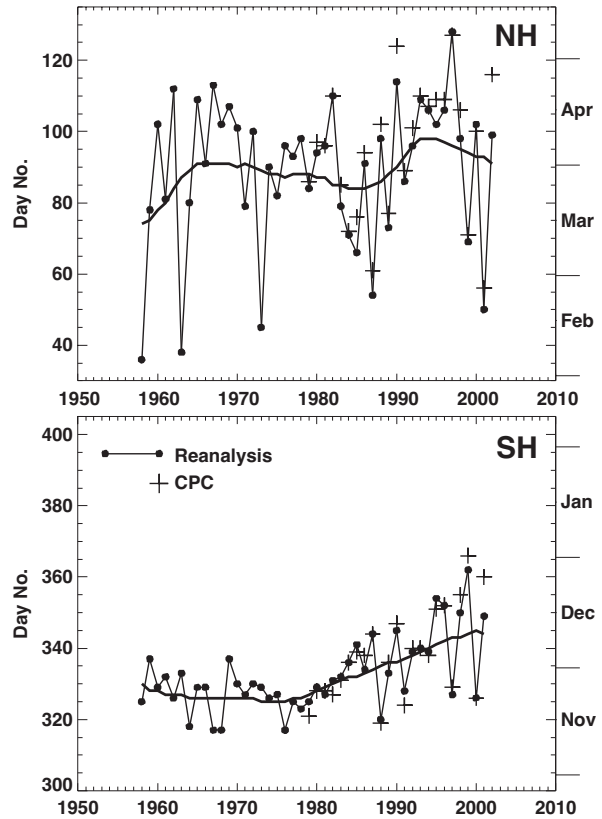


Figure 3-10. The vortex breakup date from 1958 to 2002 on the 500-K surface in the Northern (top) and Southern (bottom) Hemispheres using the method described in Nash et al. (1996; see also Waugh et al., 1999). The thin lines with filled dots are the dates calculated from the National Centers for Environmental Prediction/National Center for Atmospheric Research (NCEP/NCAR) reanalysis data. The thick lines are these same data time-filtered to remove the year-to-year fluctuations. The crosses are the breakup dates calculated from the NCEP/Climate Prediction Center analyses for the period 1979 to 2002.

osphere by cooling the polar stratosphere (Kiehl et al., 1988; see also WMO, 1990). Randel and Wu (1999a) have shown such an Antarctic cooling using radiosonde and conventional meteorological analyses, and Compagnucci et al. (2001) using MSU retrievals. This cooling strengthens the meridional temperature gradient, thereby strengthening the Antarctic polar vortex. Waugh et al. (1999) and Zhou et al. (2000) have additionally shown that the Antarctic vortex has strengthened over the last two decades, with breakup dates occurring later in the spring, consistent with the polar cooling forced by the ozone loss. Figure 3-10 displays these stratospheric polar

vortex breakup dates in the NH (top) and SH (bottom), as determined using a wind average along the edge of the polar vortex (see Nash et al., 1996). The SH breakup date shows variations of 1 to 2 weeks, with a trend from late November in the 1980s to mid-December over the last few years. The NH breakup dates also show considerable variation, but without a linear trend. As discussed in Waugh et al. (1999), the variations in dynamics (i.e., eddy wave driving) do not explain the longer term trends of the breakup in the SH. Hence, the observed late breakups in the SH (and possibly the NH) are presumably related to radiative changes from ozone losses.

3.2 BASIC POLAR STRATOSPHERIC PROCESSES

3.2.1 Transport and Dynamics

This section discusses the structure and dynamics of the polar stratosphere, including trace gas transport. Section 3.2.1.1 gives a brief overview of the mean vortex structure, providing a context for the later assessment. Section 3.2.1.2 assesses recent studies of the dynamics and structure, including variability and trends. An important point is the apparent delay in polar vortex breakdown in springtime of the Southern (and possibly Northern) Hemispheres; extending the cold winter season is a critical factor in increasing the likelihood of chemical ozone loss, but even in the absence of chemical processes, the continued isolation of the polar region into the springtime leads to a “dynamical” ozone deficit. Section 3.2.1.3 examines transport processes, including the mean meridional circulation and issues of transport inside, outside, and across the boundary of the polar vortex; these play a crucial role in fixing the distributions of ozone and other trace gases, which impacts both the physical processes (such as radiative heating) and chemical ozone loss.

3.2.1.1 THE POLAR VORTEX: MEAN STRUCTURE

The winter stratospheric circulation is dominated by the polar night jet, which is at the edge of the polar vortex. Understanding the polar vortex dynamics is central to our ability to understand recent ozone change and to predict future ozone.

The polar vortex structure is well understood: absence of solar heating in winter leads to low temperatures, which are offset by the adiabatic warming caused by the descending branch of the Brewer-Dobson circulation. This circulation is caused by the damping of planetary and gravity waves in the middle atmosphere (e.g., Fels, 1985). An illustration of the polar vortex (Figure 3-

11) shows the polar night jet (peaking near 60°N at about 45 km) and the strong descent (shown by the meridional stream function). Descent in the polar region leads to (diabatic) downward transport, carrying ozone and other trace gases from the mesosphere to the lower stratosphere during winter (e.g., Rosenfield and Schoeberl, 2001).

The asymmetry of the polar vortices in the two hemispheres is a consequence of the different topographic features: the weaker wave activity propagating from the SH troposphere provides less forcing and therefore a weaker Brewer-Dobson circulation than in the NH (e.g., Randel and Newman, 1998). The Antarctic vortex is more symmetric, stronger, and colder than the Arctic, as illustrated by the 50-hPa geopotential height distributions in middle winter (Figure 3-12). Even in the absence of chemical ozone destruction, these dynamical differences lead to substantially more ozone in the Arctic than in the Antarctic vortex, especially in springtime.

The main impacts of these dynamical differences on Arctic (compared with Antarctic) ozone arise from the stronger diabatic descent, which transports trace species downward more rapidly, the weaker isolation of the Arctic, and the decreased likelihood of PSC formation. Since PSCs form at temperatures near 195 K at 50 hPa (see Section 3.2.2), they can form every winter in the Antarctic vortex core, but only on colder-than-average days in the Arctic (e.g., Pawson et al., 1995; Pawson and Naujokat, 1999).

While these basic mechanisms that determine the vortex structure and tracer transport in polar regions are now well understood, there are important aspects for which the complexity is only partially described. Recent results pertaining to these uncertainties are assessed in the next section (3.2.1.2).

3.2.1.2 POLAR VORTEX: CAUSES OF INTERANNUAL VARIABILITY AND ITS IMPLICATIONS

Differences between the hemispheres, caused by the stronger wave driving in the NH, are also evident in the year-to-year variations. Figure 3-9 shows what appear to be robust temperature trends in the springtime, but interpretation of such trends is complex, because of the large interannual variability of high-latitude temperature (Figure 3-8), which varies with time of year and is different in the two hemispheres (Figure 3-13; e.g., Scaife et al., 2000b). Southern Hemispheric variability peaks in late winter and spring (e.g., Kuroda and Kodera, 1998), whereas variability in the NH is large throughout the season (e.g., Labitzke, 1982). The variability of the stratosphere (defined in terms of departures from the long-term mean) is characterized by a “see-saw” of temperature and mass

POLAR OZONE

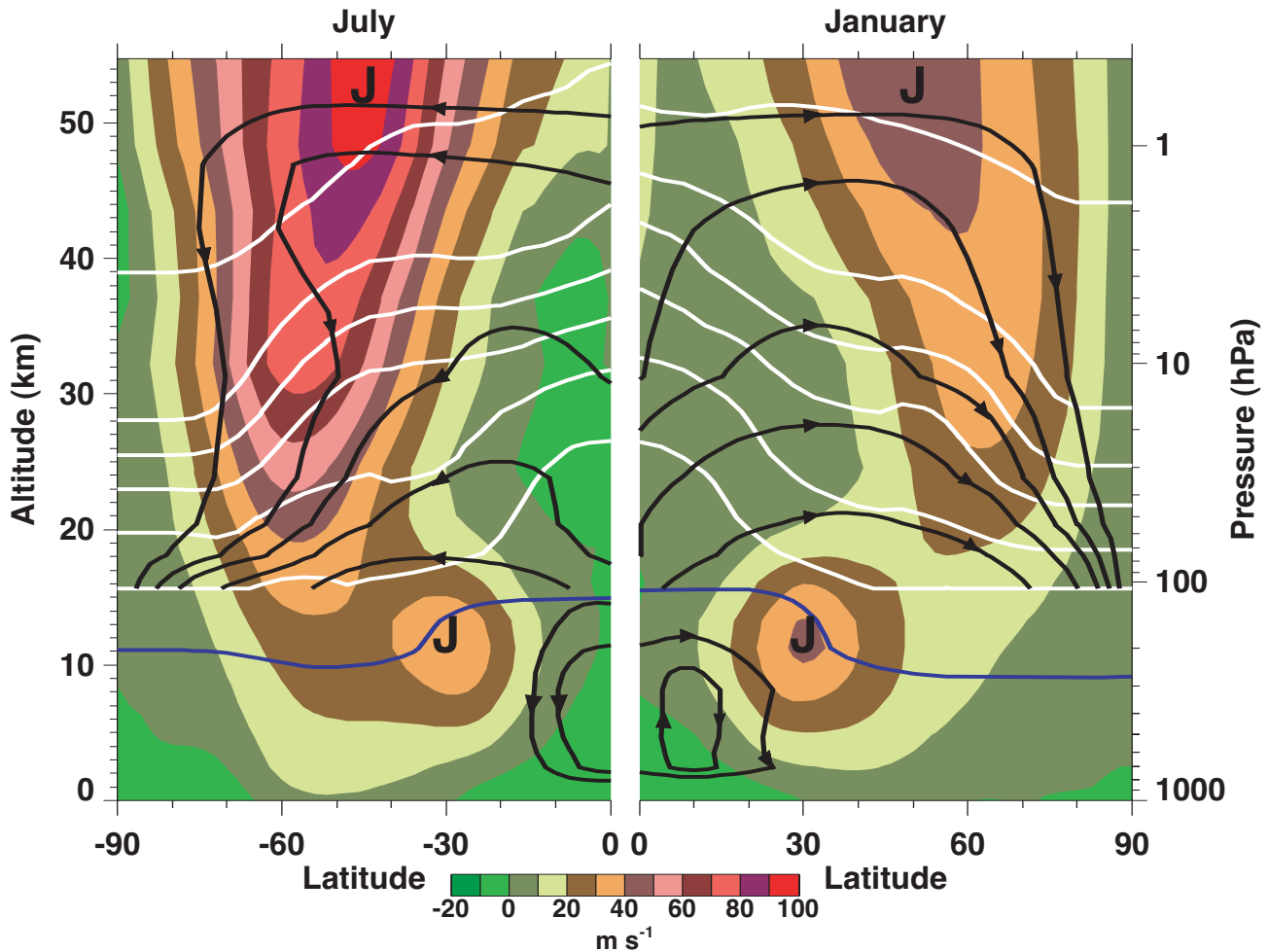
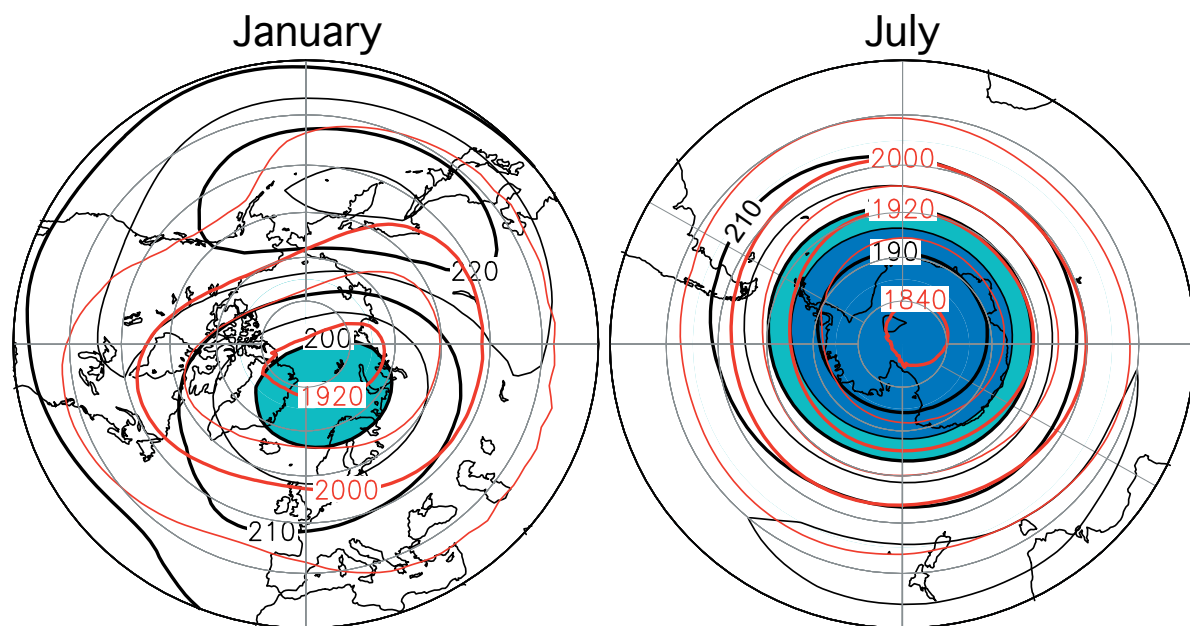


Figure 3-11. Zonal-mean sections of zonal velocity (shaded), the mean meridional streamfunction (black lines), and an atmospheric trace gas (white contours) for midwinter (July in the Southern Hemisphere and January in the Northern Hemisphere). The data were obtained from multiannual climatologies. The figure illustrates the stronger polar night jet in the Southern Hemisphere, the stronger subtropical jet in the northern winter, along with consistent differences in the strength and structure of the mean meridional circulation and trace gas distributions.

between the polar region and midlatitudes (e.g., Labitzke, 1982; Kodera et al., 1996): anomalously weak wave forcing leads to a strong polar vortex and a weak Brewer-Dobson circulation, with a cold polar region and warmer midlatitudes (the converse is true for strong wave forcing). Newman et al. (2001) demonstrated the quantitative linkage between the upward-propagating wave activity through the tropopause region and the strength of the polar vortex.

The occurrence of a strong, cold polar vortex leads to anomalously low ozone in the polar region, because the transport of ozone-rich air is weak and because the potential for PSC processing, a precursor to chemical ozone loss, is enhanced. This means that in years with weak tro-

pospheric wave forcing, a stronger polar vortex will result in less ozone in the polar region. Chipperfield (1999) reported results from a 6-year simulation using the SLIMCAT chemical transport model (CTM), driven by the United Kingdom Meteorological Office (UKMO) analyses of the meteorology. The horizontal winds and temperatures are taken from the UKMO analyses, and the vertical motion is diagnosed using a radiation scheme. The model simulates the interannual variations in chlorine activation during northern winters and reproduces the repeatable pattern of activation observed during southern winters. Chipperfield and Jones (1999) utilized the same model to evaluate the relative contributions of photochemical and dynamical processes to interannual



Geopotential Height (gpdm) and Temperature (K) at 50 hPa

Figure 3-12. Polar stereographic projections for January in the Northern Hemisphere and July in the Southern Hemisphere. The geopotential height (red contours; geopotential decameters (gpdm)) and temperature (black contours; K) for 50 hPa are shown. Light-blue shading indicates regions colder than 200 K, while dark-blue shading shows regions colder than 195 K. Data are 19-year means from the United Kingdom Meteorological Office-processed TOVS data (Scaife et al., 2000b).

variability in northern high-latitude ozone, and showed that dynamical variations dominate interannual variability. Hadjinicolaou et al. (2002) find similar results using a long run of the same transport model, driven by European Centre for Medium-Range Weather Forecasts (ECMWF) analyses but using a simplified chemical scheme.

In the NH, the anomalies in polar vortex strength are a part of what is now known as the Arctic Oscillation (AO) (Thompson and Wallace, 1998). The AO and its Southern Hemispheric counterpart are also referred to as the annular modes. The annular structure of the AO in the stratosphere can be traced to the surface, with a strong link to the North Atlantic Oscillation (NAO) in the NH (Thompson and Wallace, 1998). Whereas there is some debate about the role of the stratosphere in forcing anomalies in the tropospheric component of the AO (e.g., Perlwitz and Graf, 2001; Ambaum et al., 2001), that is beyond the scope of this Assessment of stratospheric ozone. This discussion focuses on the stratospheric component of the AO.

A high (low) AO index corresponds to a strong (weak) vortex and low (high) polar ozone column values (Thompson and Wallace, 2000; Hartmann et al., 2000). Thompson et al. (2000) estimated that approximately 40% of recent apparent polar ozone loss in March could be

explained by the tendency of the AO to remain positive in the springtime, which describes a strong, cold, and isolated polar vortex. However, on the basis of the observations alone, it cannot be determined whether the signal in ozone is caused by the AO anomaly, or whether the AO anomaly is a consequence of ozone depletion, or whether both are coherently forced by some other factor.

There is strong evidence that the AO signal originates near the subtropical stratopause and propagates poleward and downward through the mechanism of wave forcing (e.g., Baldwin and Dunkerton, 1999, 2001; Kuroda and Kodera, 1999; Kodera et al., 2000; Christiansen, 2001). Kodera and Kuroda (2000) show how the interannual variability of wave forcing can cause such anomalies to take different phases in different years.

Isolating causes of variability and the factors that drive trends is not straightforward. Apart from the link between the AO strength and the upward propagation of planetary waves, other mechanisms have been related to the polar vortex. Model simulations reveal that a substantial year-to-year variability in the stratospheric vortex (and, hence, the AO) can exist in the absence of variations in boundary conditions or other forcing mechanisms (e.g., Yoden et al., 1999; Hamilton et al., 1999). This variability, forced by internal dynamics of the atmosphere, means that

POLAR OZONE

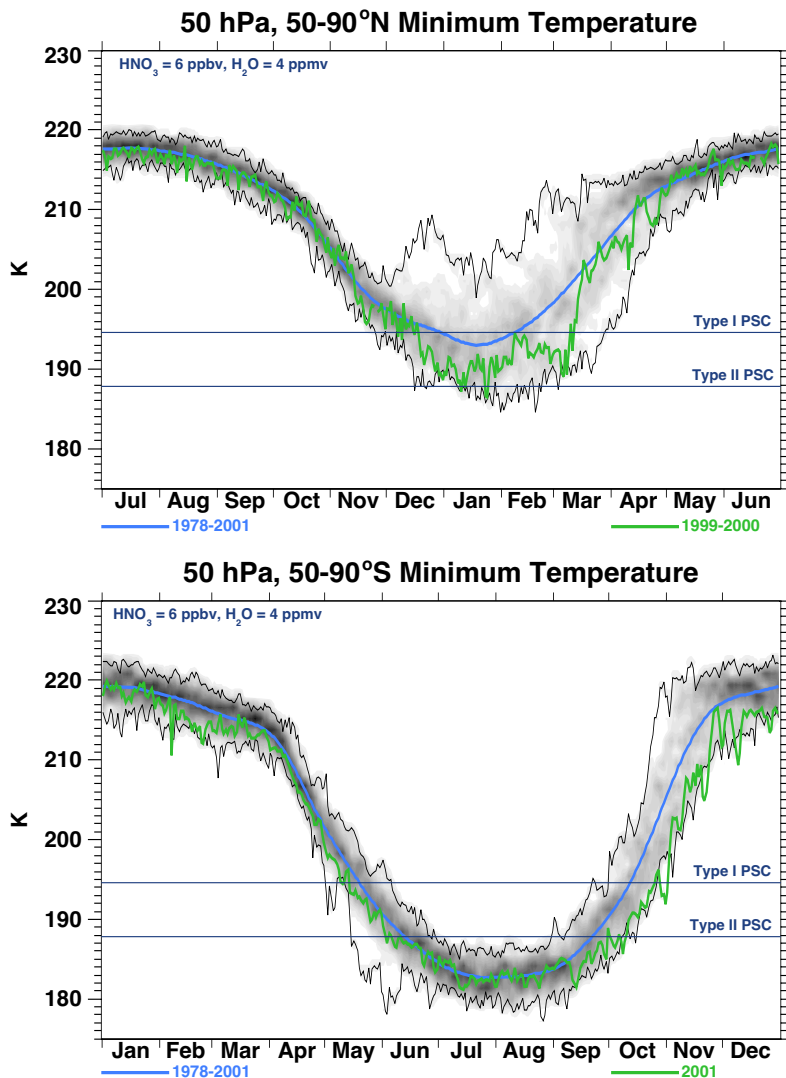


Figure 3-13. Time series showing binned distributions of 50-hPa minimum polar temperatures for 50°-90°N (top) and 50°-90°S (bottom). The blue line shows the 1978-2001 mean, and the thin black lines show the maximum-minimum values. Shading shows the density of observations, with heavy shading indicating a high probability and light shading indicating a low probability. Data are binned into intervals of 5 days by 2 K, and therefore the maximum number of observations in any bin is 95 (for 19 years of data). The green line shows the values for 1999-2000 (top panel) and 2001 (bottom panel). The seasonal cycles are offset by 6 months so that the seasonal progression in each hemisphere is contrasted. Thresholds for PSC formation are indicated by the horizontal lines. Data were processed as in Scaife et al. (2000b).

many factors often invoked as causes of interannual variability in the real atmosphere may or may not be significant. Despite this, there is some evidence of coupling between the polar vortex and other atmospheric variations; the main relationships that have been studied are the QBO of tropical winds, the 11-year variability of solar radiation, the phase of the ENSO, and major volcanic eruptions. Although polar vortex composites grouped according to these mechanisms show apparent signals, several factors complicate their interpretation and robustness. The most severe complications are that the observational record covers only about four decades and that some of the forcing factors vary in unison. For instance, following Labitzke and van Loon (1997) and grouping northern midwinter polar vortex structure according to the solar cycle (high or low) and the phase of the QBO (East or West) leads to 12 winters in the low/West category, with a strong polar vortex; however, 5 of these 12

winters coincide with ENSO cold events or volcanic eruptions, which have the same anomalies (see Figure 3-14). Determining robust relationships from observations on the basis of these overlapping factors and the internal variability is thus impossible.

Models have been used to address these questions. The SKYHI general circulation model (GCM) with an artificially forced QBO reproduces observed QBO-related interannual variability in the Arctic vortex (stronger when the tropical winds are westerly, weaker when easterly) and variations in wintertime stationary wave patterns (Hamilton, 1998). Shindell et al. (1999b) found that the QBO significantly modulated the strength and propagation of planetary-wave energy in the troposphere in the Goddard Institute for Space Studies (GISS) model, leading to higher (3- to 5-K) zonal-mean temperatures at high southern latitudes for late winter and early spring during the QBO easterly phase. Niwano and Takahashi

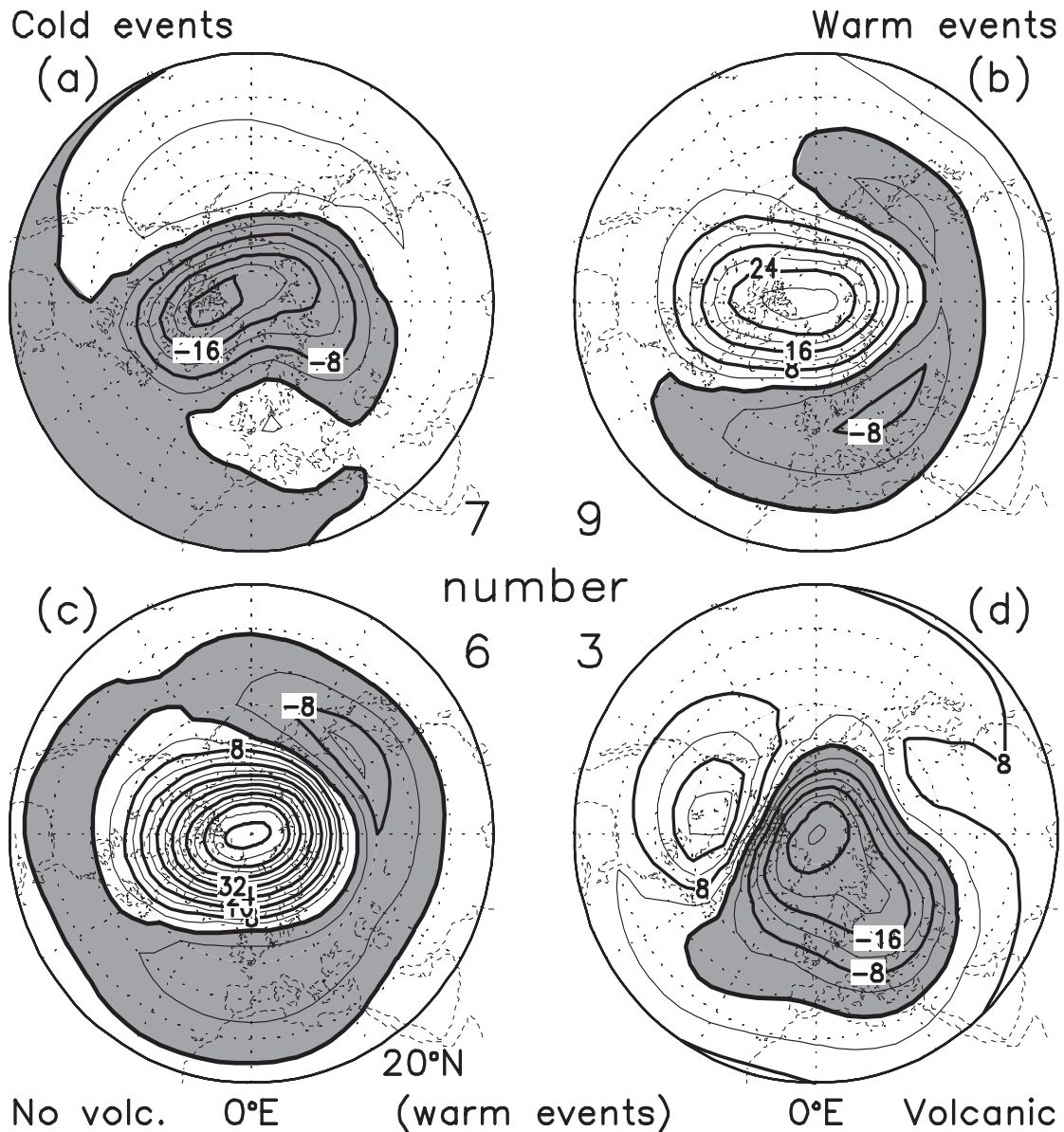


Figure 3-14. The anomalies in January/February 30-hPa geopotential height revealed by composite anomaly plots for ENSO and volcanic events, 1958-1997, as determined from Freie Universität Berlin analyses. The two top panels are (a) the composite anomaly of the seven winters with ENSO cold events, and (b) that for the nine warm events. The anomalies are in gpm and are relative to the mean of the years with no ENSO events. The lower two panels show the warm-event anomalies of panel (b), but further split into (c) the 6 years with no volcanic events and (d) the 3 years with them. These results were updated from van Loon and Labitzke (1987) and Labitzke and van Loon (1989).

(1998) studied the influence of the QBO on the NH winter circulation; their model reproduced the relationship between the polar vortex strength and the QBO phase and a related NAO pattern in the troposphere. These and earlier studies have worked on the premise that the lower stratospheric winds impact planetary wave propagation, whereas more recent work (Gray et al., 2001) has shown

that the polar vortex anomalies are more strongly related to winds near the tropical stratopause (which are indirectly affected by the QBO).

There are two important factors in isolating the impacts of solar forcing on the circulation and climate. First, stratospheric ozone changes modulate the response of the temperature to the changes in solar irradiance

POLAR OZONE

(Haigh, 1994). However, studies of solar impacts on ozone, mostly using two-dimensional (2-D) models, have been plagued by an inability to reproduce the solar-ozone relationship detected in observations (e.g., Brasseur, 1993; Hood and Zhou, 1999). Second, inclusion of the correct spectral dependence of solar irradiance variations in the atmospheric heating rate calculations is essential to capture the correct vertical structure of heating rates (Haigh, 1999; Shindell et al., 1999a; Larkin et al., 2000). However, even incorporating these feedbacks, climate model studies generally remain inconclusive about the role of solar-induced perturbations in the variability of the Arctic polar vortex.

Volcanic aerosol loading can possibly impact polar ozone by perturbing stratospheric chemistry and transport. Chemical perturbations from heterogeneous reactions on aerosols are discussed in Section 3.2.2. Increased volcanic aerosol loading of the tropical lower stratosphere leads to a warmer tropical lower stratosphere some months after a volcanic eruption (e.g., Robock, 2000), which is discussed in more detail in Chapter 4. The polar response to this tropical warming has a northern polar vortex remaining anomalously cool in the winter following the eruption (e.g., Kodera, 1994), as shown in Figure 3-14. Figure 3-14 shows that the three volcanic eruptions affected winters with ENSO warm events and that they “reverse” the ENSO anomalies, leading to anomalously strong, cold polar vortices (van Loon and Labitzke, 1987; Labitzke and van Loon, 1989), thereby increasing the likelihood of negative polar ozone anomalies. Based on only three events (and because of the factors discussed above), these results must be interpreted with caution. This relationship has also been isolated in models (Kirchner et al., 1999; Ramachandran et al., 2000).

Although temperatures low enough for PSC formation occur on the large scales (e.g., Pawson and Naujokat, 1997, 1999), the likelihood of their occurrence is enhanced by the temperature perturbations induced by medium-scale waves (e.g., Grewe and Dameris, 1997; Sato et al., 2000; Teitelbaum et al., 2001), as well as by inertial gravity waves (e.g., Dörnbrack et al., 2001, 2002). The temperature perturbations induced by these waves can cause sufficient additional cooling for PSCs to form in locations where the large-scale flow would not support them. This is particularly important on the vortex edge, where the processed air can be irreversibly transported into the middle latitudes (in the presence of breaking waves) and where the air masses are more likely to be illuminated, enhancing the potential for ozone depletion.

Ozone mini-holes occur because of synoptic-scale, reversible advection (e.g., McKenna et al., 1989; Newman et al., 1988) related to upper tropospheric anticyclonic

structures. The high tropopause, coupled with ascending motion, leads to extremely low total ozone values with lifetimes of up to several days. Steinbrecht et al. (1998) show that correlations in tropopause height correlate with ozone concentration changes in the region up to 23 km, illustrating the depth of the disturbances. However, the low ozone values themselves are short-lived features that are unrelated to chemical loss. The dynamical forcing that causes ozone mini-holes also causes adiabatic cooling, which can lead to synoptic-scale temperature perturbations of sufficient magnitude to allow PSC formation (e.g., McKenna et al., 1989; Grewe and Dameris, 1997). The importance of baroclinic disturbances in producing PSC formation near the polar vortex edge has been discussed by Hood et al. (2001) and Teitelbaum et al. (2001). Orsolini and Limpasuvan (2001) showed how these disturbances are linked to the storm tracks, which vary in unison with the AO. There is thus a flow-dependent nature to the likelihood of synoptic-scale PSC formation and to the likelihood that PSCs contribute to ozone loss on the vortex edge region.

Just as baroclinic waves help PSC formation on the synoptic scales, mesoscale disturbances from gravity waves are also important. Volkert and Intes (1992) demonstrated PSC formation in wave crests over Scandinavia in their model of topographically forced gravity waves. The importance of gravity-wave PSCs was also demonstrated by Deshler et al. (1994) and Meilinger et al. (1995). High-resolution radiosonde data have recently provided much-needed information on stratospheric gravity-wave morphologies in and around the Antarctic (Pfenniger et al., 1999; Zink and Vincent, 2001) and Arctic (Whiteway and Duck, 1999; Yoshiki and Sato, 2000). Although the microphysical effects of a background spectrum of gravity waves are smaller than first thought (Bacmeister et al., 1999), it is now accepted that mesoscale temperature decreases due to large-amplitude gravity waves, particularly mountain waves, can lead to temperatures low enough for PSC formation (Carslaw et al., 1998b, 1999; Schulz et al., 2001), and lead to structure inside larger scale PSCs (Toon et al., 2000). PSCs are discussed in Section 3.2.2 of this chapter.

Important advances have been made in our ability to model lower stratospheric gravity waves and, especially, to resolve such waves in global meteorological analyses. Dörnbrack et al. (2001) demonstrated that the high-resolution ECMWF operational meteorological analyses capture gravity-wave structures over Scandinavia. This represents an important advance for applying the analyses to our understanding of the gravity-wave morphology and its importance for PSC formation. An additional advance of some importance was made by

Dörnbrack et al. (2002), who detected inertia-gravity waves over Scandinavia in the ECMWF analyses and in situ data, noting their role for PSC formation. The isolation of gravity waves in such operational analyses points to their potential utility in mountain wave forecasting and analysis, meaning that the off-line models that have been used for such studies could eventually become unnecessary.

Another important role played by gravity waves (from all sources) is that they transport momentum into the middle atmosphere; as these waves break, they deposit momentum to the mean flow, constituting an important driving mechanism for the Brewer-Dobson circulation. The importance of these waves for driving the flow and reducing biases in global models is discussed in more detail in Section 3.5.2.1.

3.2.1.3 POLAR TRANSPORT AND MIXING

This section discusses in detail the physical processes that lead to the redistribution of trace gases in the polar regions. Trace gas distributions are determined by the balance between the slow, mean-meridional circulation and the more rapid, quasi-isentropic mixing (e.g., Holton, 1986); the following discussion examines these components of transport in and around the polar vortex and the exchange across the vortex edge.

Manney et al. (2002) examine impacts of using different meteorological analyses, which affect the amount of exchange between middle latitudes and the vortex. Despite the uncertainties, the consensus is that the vortex remains quite isolated in wintertime. Vertical transport leads to descent of tracers in and around the vortices, while mixing redistributes ozone and trace gases on isentropic levels; there is some exchange across the vortex edge, associated with large-scale mixing events.

Descent in the Polar Vortex

Descent inside the polar vortex builds up (or maintains) lower stratospheric ozone over the winter, making it an important process to understand. The descending branch of the Brewer-Dobson circulation is driven by wave forcing of the flow (see Section 3.2.1.1). Descent rates can be determined in several manners: (1) “directly” from the vertical velocities produced in routine meteorological analysis systems, such as the UKMO (Swinbank and O’Neill, 1994) and the Data Assimilation Office (DAO) (Rood et al., 1997), (2) based on the cross-isentropic transport determined by diabatic heating rates, and (3) using measurements of long-lived trace gases with well-understood vertical gradients. The various estimates are in reasonably good agreement, showing stronger

descent in the upper stratosphere than in the lower stratosphere and unmixed descent from the upper to the lower stratosphere. The strongest unmixed descent occurs in the Antarctic vortex. Descent in the Arctic vortex is more variable; it occurs on the vortex edge when the temperature is higher there (e.g., Manney et al., 1999).

Schoeberl et al. (1995) used Halogen Occultation Experiment (HALOE) methane (CH_4) data to estimate the descent rate as 1.8 km/month inside the Antarctic vortex in February to October 1992 (see Appendix 3A for HALOE data description). Descent rates over Antarctica were deduced from the Improved Stratospheric and Mesospheric Sounder (ISAMS) carbon monoxide (CO) data for April to July 1992 by Allen et al. (2000) and from the Polar Ozone and Aerosol Measurement (POAM) III H_2O data by Nedoluha et al. (2000). Abrams et al. (1996) demonstrated strong descent in the upper stratosphere (3.2 km/month at 40 km) with weak descent in the lower stratosphere (0.8 km/month at 20 km) based upon the Atmospheric Trace Molecule Spectroscopy (ATMOS) data from November 1994. Kawamoto and Shiotani (2000) also used HALOE data and UKMO meteorological analyses to investigate the interannual variability of the descent rate, using the February-October (winter) averages in 1992 to 1997 HALOE CH_4 data (see Appendix 3A for POAM and HALOE data descriptions). They found that the descent varies between 1.2 and 1.8 km/month using the 0.6 parts per million by volume (ppmv) CH_4 contour inside the polar vortex and is consistent with the wave driving determined from the UKMO analyses. To summarize, the various estimates of polar descent rates give reasonably consistent results, given that they are presented for different levels, seasons, and years.

The Vortex Core

The degree of mixing within the vortex core has come under scrutiny because of assumptions about representing the bulk behavior of the vortex with irregular temporal and spatial sampling. If the core is well mixed, then measurements anywhere within the vortex will suffice to characterize its behavior. If the core is not well mixed, then more frequent sampling at separated locations is necessary to do this. Schoeberl et al. (1990) assumed that the vortex was relatively well mixed in assessing ozone loss using Earth Resources-2 (ER-2) data from the Airborne Arctic Stratospheric Expedition (AASE)-I mission during the Arctic winter of 1988/1989. Richard et al. (2001) used ER-2 data from the SOLVE-THESEO 2000 campaign to show that tracer-tracer relationships inside the vortex during the Arctic winter of 1999/2000 are distinct and compact, suggesting a rapid mixing in the Arctic vortex. Whereas current evidence suggests that the Arctic vortex

POLAR OZONE

is relatively well mixed in the absence of intrusions of air from the vortex edge, Lee et al. (2001) present evidence that the Antarctic vortex is separated into two regions: a strongly mixed vortex core and a weakly mixed ring of air extending to the vortex boundary.

Transport Across the Vortex Edge and Mixing

The balance of mass and trace gases in and around the polar vortex is determined by the downward transport and exchange across the vortex edge. Any vertical gradient in the vortex-averaged mass flux will be compensated for by flow across the vortex edge. The discussion below will separate the transport across the vortex edge in winter from transport occurring as the polar vortex breaks down.

Planetary-wave breaking can be responsible for vortex shrinking as well as sharpening of the vortex edge (e.g., Thuburn and Lagneau, 1999). A number of studies have shown considerable variability in the width of the Antarctic vortex edge when it is perturbed (Teitelbaum et al., 1999; Perez et al., 2000), which results in nonlinear irreversible transport and mixing of vortex air into mid-latitudes (Teitelbaum et al., 1999). Lidar observations at Dumont d'Urville (66.4°S, 140°W) allow sampling at and around the moving vortex edge (Godin et al., 2001); observations of Mt. Pinatubo aerosols, made during October and November 1992, show the sharpness of the vortex edge and low mixing between the inner vortex and the outside air above 400 K.

The first obstacle to determining the cross-vortex flow is to unambiguously define the vortex edge. Chen (1994) defined it as the potential vorticity (PV) contour that has the smallest lengthening rate; he found a vertical dependence to the transport across the edge, with more transport out of the vortex at potential temperatures lower than 400 K than at higher levels. Tuck et al. (1995) reached similar conclusions using ER-2 data, showing also that the vortex edge region can be quite wide. This viewpoint of the polar vortex as a reasonably well isolated entity is now generally accepted, but the amount of "leakage" from the vortex (as a function of altitude) is not yet well understood. Different proposed definitions of the vortex edge include the wind maximum and the strongest gradients in PV (e.g., Bowman, 1996; Nash et al., 1996). The uncertainty in defining the vortex edge remains, so there is no unambiguous estimate of the vertical structure of cross-vortex transport. Mechanisms for the transport are at least qualitatively understood and are discussed here.

Recent results continue to sustain our understanding of the vortex edge impermeability (Chen, 1994) and of the polar vortex as a quasi-isolated containment

vessel. Norton and Chipperfield (1995) and Jones and MacKenzie (1995) had argued that ozone-depleted air from the polar vortices makes only a small contribution to middle-latitude ozone loss. High-resolution, single-level models with weak dissipation (e.g., Jukes and McIntyre, 1987; Mo et al., 1998; Thuburn and Lagneau, 1999; Sobel and Plumb, 1999) have further confirmed that the export of air from the polar vortex is constrained. Vincent and Tranchant (1999) also found little mixing across the vortex edge at 520 K in the Antarctic. Li et al. (2002) used a CTM driven by analyzed winds to show that less air is indeed exported from the Antarctic polar vortex to middle latitudes than descends into the troposphere.

Laminae and filaments could be an important mechanism in the mixing of air across the quasi-impermeable vortex edge. Such structures are common in winter and spring. As pointed out in the previous Assessment (WMO, 1999) the filaments/laminae, i.e., material sheets that tilt outward with increasing height (Schoeberl and Newman, 1995; Newman and Schoeberl, 1995) with initial horizontal scales of a few thousand kilometers, can lead to irreversible mixing on the time scale of 20 to 25 days over which they decay. Laminae have been detected in a variety of data types, including in situ aircraft observations (Newman et al., 1996); sondes and lidar (Bird et al., 1997; Orsolini et al., 1997; Teitelbaum et al., 2000); and satellites (Manney et al., 1998, 2000). They have been successfully modeled (e.g., Orsolini et al., 1997). Waugh and Dritschel (1999) analyzed the relationship between Rossby wave breaking and vortex structure. These studies show that filamentation can lead to vortex air being peeled off and eventually mixed irreversibly into the surf zone, although some air may rejoin the polar vortex. Furthermore Manney et al. (1998, 2001) have also shown that lamination processes within the polar vortex did not result from exchange across the vortex edge but rather from transport variations within the vortex.

Hence, there is a need to assess the behavior of laminae and the magnitude of their contribution to the total exchange between the vortex and midlatitudes. Appenzeller and Holton (1997) attempted to diagnose the production of tracer laminae using satellite data and meteorological analyses, as a first step in determining their contribution to transport. Nevertheless, there arose some limitations regarding the use of such a diagnostic (Kettleborough and Holton, 1999), because (1) it does not include small vertical scales that are relevant in defining tracer lamination, and (2) there can be reversible contributions. In other words, the proposed diagnostic could overestimate the transport and mixing.

A principal challenge to modeling polar ozone in the NH and the effects of polar processes on middle lati-

tudes is to ensure that the models produce the appropriate balance among the many processes that contribute directly or indirectly to the polar lower stratospheric ozone tendency. Both transport and photochemical processes contribute. The year-to-year variability in meteorological fields is significant, and the northern vortex may be cold and strong, as in the 1996/1997 and 1999/2000 winters, or warmer and more disturbed, as in the 1997/1998 winter (Sinnhuber et al., 2000; Guirlet et al., 2000). Simulations have focused on replicating observations for ozone and other trace gases, and quantifying model sensitivity to various processes (Chipperfield and Pyle, 1998). Such studies point out the importance of developing a better understanding of the physical processes (e.g., those leading to denitrification), so that model parameterizations respond appropriately to changes in temperature, water vapor, or nitric acid (HNO_3) that may result from climate change.

Millard et al. (2002) utilized diagnostics developed by Lee et al. (2001) to quantify the importance of polar processes to ozone change at middle latitudes. Both the chemical processes that contribute to polar ozone loss and the transport processes that impact mixing between high latitudes and middle latitudes vary depending on the meteorology of a particular year. CTMs have been utilized to address questions concerning specific winters. For example, Lefèvre et al. (1998) utilized a CTM forced by winds from ECMWF to show that both transport and photochemical processes contributed to the record-low ozone observed by TOMS during northern spring 1997 (Figure 3-2). Like the studies of Guirlet et al. (2000), their results are broadly consistent with observations. However, as shown by Douglass et al. (2001), the model results separating photochemical and transport contributions are sensitive to the vertical velocity and to the ozone vertical gradient.

The breakdown of the polar vortex, whether by a major midwinter warming or in the final warming, allows vortex air to be mixed relatively easily with air from middle latitudes. Atkinson and Plumb (1997) showed that as the Antarctic vortex breaks down, a substantial amount of ozone-depleted air is transported to middle latitudes. Once there, it can effectively mix with the ambient air masses. Effective diffusivity has been used as a diagnostic for mixing by Allen and Nakamura (2001), who show increases in mixing lengths as the polar vortices break up.

3.2.2 Polar Stratospheric Clouds

PSCs play two important roles in polar ozone chemistry. First, the particles support chemical reactions leading to active chlorine formation, which can catalyti-

cally destroy ozone. Second, nitric acid (HNO_3) removal from the gas phase can increase ozone loss by perturbing the reactive chlorine and nitrogen chemical cycles in late winter and early spring.

PSCs are divided into two main categories. Type I PSC particles contain nitric acid, either in the form of liquid ternary solutions with water and sulfuric acid or as solid hydrates of nitric acid. Type II PSCs are made of ice particles. Knowledge of PSC particle sizes, number concentrations, composition, phase, and evolution is central to efforts to develop prognostic models of how PSCs affect the chemistry of the polar stratosphere. In situ observations of PSCs from balloons or aircraft are often used to obtain detailed information on cloud particle size distribution and composition. Remote sensing platforms, such as lidar and satellites, provide complementary information on phase and large-scale time evolution of PSCs, respectively. We now briefly review recent advances in our understanding of PSC properties and their effect on denitrification and dehydration.

3.2.2.1 OBSERVATIONS OF PSC PHYSICAL PROPERTIES AND THEIR INTERPRETATION

In Situ

The previous Assessment (WMO, 1999) described considerable improvements in our understanding of liquid PSCs but highlighted the outstanding uncertainties in the properties of solid particles. Solid nitric-acid-containing PSC particles are important because, in contrast to the submicron liquid aerosol, they may be present with sufficiently low number concentrations ($<10^{-2} \text{ cm}^{-3}$) to allow a few particles to grow to large sizes, leading to sedimentation and denitrification. Our understanding of the range of solid-particle number concentrations and sizes that can form in the polar stratosphere has improved since the previous Assessment as a result of new in situ observations.

Observations in the Arctic stratosphere at altitudes from 16 to 20 km in January to March 2000 detected a population of large nitric acid particles with very low number concentrations (Fahey et al., 2001; Northway et al., 2002a); see Figure 3-15. Large particles, with sizes and number concentrations similar to those observed by Fahey et al. (2001), were detected by the Multiangle Aerosol Spectrometer Probe (MASP) (Carslaw et al., 2002). These measurements (Fahey et al., 2001; Northway et al., 2002a) are very important because they provide conclusive evidence that such large particles are composed principally of nitric acid (probably present as nitric acid hydrates).

POLAR OZONE

Observations of large nitric acid particles raise several questions. The most obvious question is how these particles compare with previous observations in the Arctic and Antarctic. Balloonborne instruments such as the optical particle counter (OPC) (e.g., Deshler et al., 1991, 1994; Deshler and Oltmans, 1998; see also WMO, 1999, and references therein), which has flown in many previous Arctic winters, are capable of detecting particles up to 20 μm in diameter with number concentrations greater than about $6 \times 10^{-3} \text{ cm}^{-3}$. However, this is higher than the average particle concentrations ($\sim 10^{-4} \text{ cm}^{-3}$) measured by Fahey et al. (2001). It is interesting to note that in earlier Antarctic measurements, the OPC instrument, which operated at a different inlet flow rate, detected large PSC particles with number concentrations as low as 10^{-4} cm^{-3} (Table 3-1). The forward scattering spectrometer probe (FSSP) instrument, which measured PSC size distributions during the 1989/1990 Arctic winter (Dye et al., 1992), detected PSCs with total number concentrations of about 10^{-3} cm^{-3} . Some particles were observed up to 13-

μm diameter with concentrations of $\sim \text{few} \times 10^{-4} \text{ cm}^{-3} \mu\text{m}^{-1}$, similar to those observed by Fahey et al. (2001). These large particles were attributed to ice (Wofsy et al., 1990), although some of them could certainly have been nitric acid trihydrate (NAT). Thus populations of very few ($\sim 10^{-4} \text{ cm}^{-3}$) large PSC particles have been observed previously, but it is only through recent measurements (Fahey et al., 2001) that we have learned that such large particles are indeed enriched in nitric acid.

The second question is whether these large particles present at very low number concentrations can denitrify the stratosphere. Simple calculations presented by Fahey et al. (2001) demonstrate that large nitric acid particles can grow to their optimal observed sizes in about 5 to 8 days, implying that they must have nucleated several kilometers above the aircraft flight altitude. Instantaneous downward flux calculations of nitric acid contained in such large particles indicate that the large particles were capable of causing significant denitrification (Fahey et al., 2001; Northway et al., 2002b). Three-dimensional model simulations of particle growth further show that the observed PSC sizes are consistent with growing NAT and/or nitric acid dihydrate (NAD) particles (Carslaw et al., 2002). However, it is important to note that PSCs with size distributions differing from those measured in winter 1999/2000 have been observed in previous winters in both hemispheres (see Table 3-1). Model simulations by Jensen et al. (2002) show that previously observed PSC particle size distributions (Dye et al., 1992; Hofmann and Deshler,

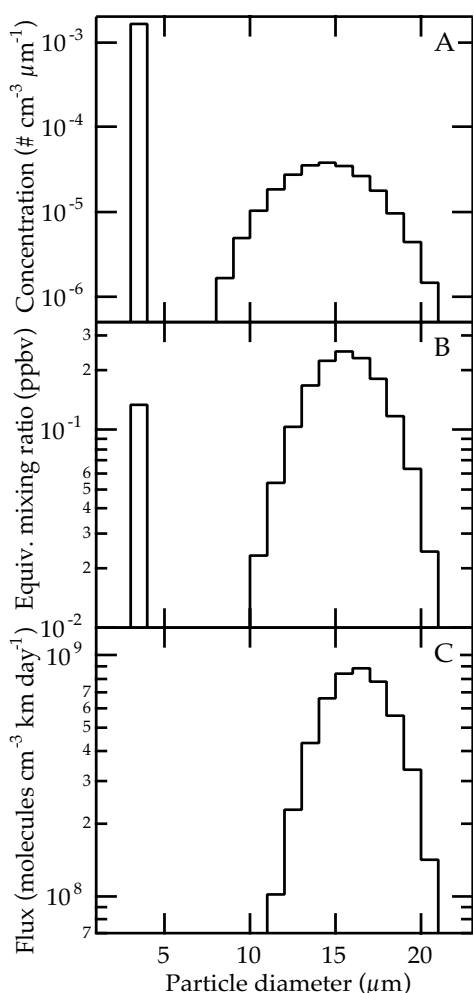


Figure 3-15. Results from the statistical simulation of total reactive nitrogen (NO_y) values observed by the ER-2 NO_y instrument on 20 January 2000 (Fahey et al., 2001). Panels show (A) the adjusted best-fit size distribution and number concentration, (B) the equivalent gas-phase mixing ratio of HNO_3 derived from the distribution, and (C) the derived flux of HNO_3 at 60 hPa ($\sim 19.5 \text{ km}$). The size distribution is given by the Gaussian functions in the caption of Figure 3 of Fahey et al. (2001) adjusted to account for size-dependent sampling efficiency. The adjustments, which are in addition to a basic particle enhancement factor of 12.8, range from +30% to -10% over the size range and are calculated with a fluid dynamical model of the particle separator. The concentration integral of the large (small) mode is $2.3 \times 10^{-4} \text{ cm}^{-3}$ ($2 \times 10^{-3} \text{ cm}^{-3}$) with an estimated uncertainty of $\pm 30\%$. The lower limit of the vertical axis in (A) corresponds to the detection of a single particle over the 800-s observation period. The total gas-phase HNO_3 of the large (small) mode is 1.5 ppbv (0.2 ppbv). The HNO_3 flux of the combined distribution is $5 \times 10^9 \text{ molecules cm}^{-3} \text{ km day}^{-1}$ or $2.2 \text{ ppbv km day}^{-1}$ at 60 hPa. Adapted from Fahey et al. (2001).

Table 3-1. Observations of solid PSC number density and particle size.

Number Density (cm ⁻³)	Average Diameter (µm)	Atmospheric References	Location
10 ⁻¹ -1	1-2	Voigt et al. (2000a, b)	Arctic
10 ⁻³ -10 ⁻²	1-4	Dye et al. (1992) ^a	Arctic
10 ⁻⁴ -10 ⁻²	4-10	Hofmann and Deshler (1991) ^a	Antarctic
10 ⁻⁵ -10 ⁻³	10-20	Fahey et al. (2001) ^b ; Northway et al. (2002a) ^b	Arctic

^a Note that these measurements are mode diameters of a lognormal distribution. Some particles, most likely containing nitric acid, were observed up to 13 µm in diameter (Wofsy et al., 1990).

^b These observations on the average show PSC number densities of about 2×10^{-4} cm⁻³ with a mode diameter centered near 14 µm, assuming a nitric acid trihydrate (NAT) composition.

1991), with number concentrations in the range of 10⁻² to 10⁻³ cm⁻³, are also capable of efficiently denitrifying the polar stratosphere.

A third question is how these large nitric acid particles form in the polar stratosphere. Both homogeneous (Tabazadeh et al., 2001) and heterogeneous (Tolbert and Toon, 2001; Drdla et al., 2002) freezing mechanisms have been suggested to account for the formation of large nitric acid particles. For such nucleation mechanisms to operate, the cooling caused by synoptic-scale uplift of air masses (Teitelbaum et al., 2001; Spang et al., 2001; Hendricks et al., 2001; Saitoh et al., 2002) can provide favorable conditions for solid PSCs to form. Laboratory observations show that concentrated aqueous nitric acid aerosols can homogeneously crystallize into hydrates of nitric acid (Disselkamp et al., 1996; Bertram and Sloan, 1998a, b; Prenni et al., 1998; Salcedo et al., 2001). The stratospheric particle system has also been studied using thin films, where gas-phase nitric acid and H₂O are absorbed by cold aqueous sulfuric acid solutions (Iraci et al., 1994, 1995, 1998). The results of these thin-film experiments show that HNO₃ uptake in sulfuric acid can cause freezing of nitric acid hydrates in solution. Tabazadeh et al. (2001) have recently extrapolated the laboratory homogeneous freezing rates of Salcedo et al. (2001) and obtained nucleation rates sufficient to produce large nitric acid particles in a microphysical model. Note that the nucleation rates extrapolated from Salcedo et al. (2001) are much higher than upper limits derived from earlier bulk freezing experiments with 1-milliliter samples, which used stratospheric temperatures and liquid-phase compositions (Koop et al., 1995, 1997). Modeling studies (Drdla et al., 2002) further show that heteroge-

neous freezing can also produce large particles if only a very small fraction (<0.1%) of stratospheric aerosol particles contained an effective freezing nucleus, although it is not clear what the freezing nucleus should be (Biermann et al., 1996). In addition to direct homogeneous and heterogeneous freezing mechanisms, the large particles may also form by a gradual sedimentation from the base of “mother clouds” containing much higher number concentrations of small solid particles (Füglister et al., 2002; Dhaniyala et al., 2002), such as those generated by lee wave clouds (Carslaw et al., 1998a).

The freezing mechanisms described above are all capable of producing low number concentrations of sedimenting nitric acid particles. However, model simulations do strongly suggest that the large nitric acid particles, observed during the winter of 1999/2000, were unlikely to have nucleated in synoptic-scale ice clouds, which were not sufficiently prevalent in the days preceding the observations (Carslaw et al., 2002; Drdla et al., 2002). Further analysis of satellite data in the Antarctic also seems to suggest that large nitric acid particles formed in the winter of 1992 independent of synoptic-scale ice clouds (Tabazadeh et al., 2000). Formation of denitrifying particles when polar temperatures are above the ice frost point will allow denitrification to occur at higher temperatures than previously assumed in 3-D chemical models (see Section 3.2.2.3).

A final question is whether these large particles observed in situ can also be detected by lidar. Aircraft lidar observations in January to March 2000 detected regions of enhanced aerosol backscatter in regions where large nitric acid particles were detected (Flentje et al., 2000). However, Flentje et al. (2000) inferred an approx-

POLAR OZONE

imate size for the particles based on the sedimentation speed of the particle layer, rather than directly from the lidar signal. Their derived particle sizes are in reasonable agreement with in situ observations (Fahey et al., 2001).

Overall, the assessment of both the Arctic and Antarctic studies, on observed and inferred PSC particle sizes, indicates that large nitric acid particles cannot initially nucleate on synoptic-scale ice clouds. However, the formation mechanism of large nitric acid particles still remains uncertain. Thus, more laboratory and field studies are needed to better test which of the above mechanisms is most likely to dominate the rate of large nitric acid particle production in the polar stratosphere.

Remote

Lidar observations are useful for constraining PSC particle sizes. Depolarization measurements by lidar can also provide strong evidence for the presence of solid PSC particles. As indicated above, only large solid PSC particles can cause denitrification, and lidar observations provide valuable information on the horizontal and vertical extents of solid PSC particle distributions in the stratosphere.

Lidar studies provide new estimates of the occurrence of solid PSC particles, which is an important parameter for constraining microphysical models. Toon et al. (2000) have reanalyzed lidar observations from all DC-8 flights during the 1989/1990 Arctic winter and find that large solid PSC particles are more common in the Arctic stratosphere than the smaller liquid PSC particles (Type Ib). Three years of lidar observations from Ny Ålesund (79°N) (Biele et al., 2001) have shown that at least 50% of PSCs contained solid particles, with some of these clouds being of Type Ib, normally attributed to pure liquid clouds. Several studies have also derived new estimates of solid particle number concentrations. Gobbi et al. (1998) have analyzed many Antarctic lidar vertical profiles and estimate that solid PSC particles constituted less than 1% of the available condensation nuclei (therefore, typically less than 0.1 particles cm^{-3}). Toon et al. (2000) derived similar values for the 1989/1990 winter Arctic stratosphere. Biele et al. (2001) and Tsias et al. (1999) estimate that many depolarizing clouds must typically contain fewer than about 0.005-0.01 cm^{-3} solid particles and that such particles can rarely grow to their equilibrium sizes. In summary, all the lidar studies discussed here suggest that large solid particles that can cause denitrification are widely distributed in both hemispheres.

Some clouds observed by lidar are consistent with high number densities of small solid nitric acid particles (typically $>1 \text{ cm}^{-3}$ and $<2 \mu\text{m}$ in diameter) (Tsias et al., 1999; Toon et al., 2000; Hu et al., 2002). These clouds are frequently associated with the outflow from mountain

waves (e.g., Hu et al., 2002). Efficient NAT nucleation on numerous small ice particles formed in wave clouds could be an important mechanism for generating such a dense population of small solid PSC particles (Carslaw et al., 1998a, 1999; Wirth et al., 1999; Larsen et al., 2002). Some studies suggest that small solid PSC particles generated by wave clouds may also play a central role in producing large nitric acid particles that lead to denitrification (see the previous section on in situ observations).

Satellite instruments are also capable of observing PSC particles. Stratospheric Aerosol Measurement (SAM) II (McCormick et al., 1981), Cryogenic Limb Array Etalon Spectrometer (CLAES) (Mergenthaler et al., 1997), Polar Ozone and Aerosol Measurement (POAM) (Steele et al., 1999; Fromm et al., 1997, 1999; Bevilacqua et al., 2002), and Improved Limb Atmospheric Sounder (ILAS) (Kondo et al., 2000; Irie et al., 2001) instruments have taken many aerosol extinction vertical profiles of PSCs in the Arctic and Antarctic stratosphere over the last two decades (see Appendix 3A for satellite data descriptions). Several recent studies have paired up aerosol extinction measurements with water and nitric acid gas-phase measurements onboard the same (Tabazadeh et al., 2000; Stone et al., 2001; Nedoluha et al., 2000; Dessler et al., 1999) or different satellites (Santee et al., 2002) to determine the scale and magnitude of denitrification and dehydration in both polar regions (see Sections 3.2.2.3 and 3.2.2.4).

3.2.2.2 PARTICLE COMPOSITION

Inferred Particle Compositions

PSCs that exist at temperatures greater than the ice frost point have long been accepted to be composed of nitric acid and water, either in the form of a nitric acid hydrate or as supercooled solution droplets of nitric acid, sulfuric acid, and water (supercooled ternary solution, STS). Numerous attempts have been made to infer the composition of nitric-acid-containing PSCs by comparing particle volumes (either measured directly or derived from satellite extinction) and/or gas-phase nitric acid concentrations with equilibrium model calculations assuming various particle compositions (WMO, 1999; Hopfner et al., 1998; Steele et al., 1999; Santee et al., 2002; Saitoh et al., 2002; Strawa et al., 2002). These studies have provided strong support for the existence of STS droplets, but confirmation of the presence of different nitric acid hydrates has been more difficult to establish (WMO, 1999). This difficulty may be due to the fact that nitric acid hydrate particles, which can be considerably larger than STS droplets, are often not in thermodynamic equilibrium (e.g., Tsias et al., 1999; Biele et al., 2001).

Direct Determinations of Particle Composition

New in situ observations using an aerosol mass spectrometer have measured PSC particle composition (Schreiner et al., 1999, 2002; Voigt et al., 2000a, b; Larsen et al., 2000, 2002). The mole ratio of nitric acid to water observed using an aerosol mass spectrometer in a mountain-induced gravity wave cloud over Scandinavia (Voigt et al., 2000b) shows close agreement with an STS droplet composition predicted by a model. The same aerosol mass spectrometer flown in January 2000 detected NAT particles, identified by a H_2O to HNO_3 mole ratio of 3:1 and confirmed to be solid particles from co-located backscatter measurements (Voigt et al., 2000a; Larsen et al., 2000); see Figure 3-16. These direct observations of particle composition in PSCs are important because they confirm that the thermodynamic models used to predict liquid aerosol compositions (e.g., Carslaw et al., 1997a) are reliable, and that NAT, long predicted to exist in the stratosphere (Hanson and Mauersberger, 1988), actually does exist there.

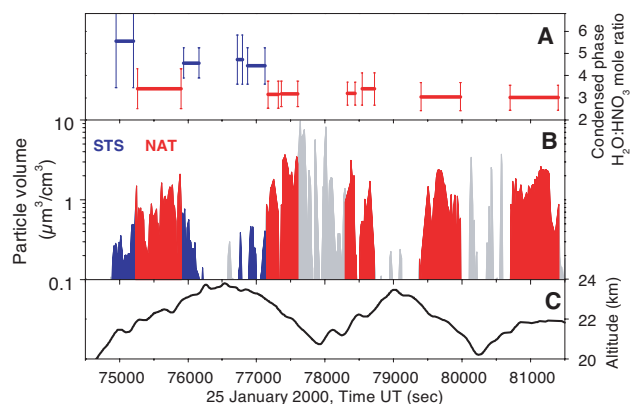


Figure 3-16. In situ observations of PSCs using an aerosol mass spectrometer, showing particles with a $\text{HNO}_3/\text{H}_2\text{O}$ ratio consistent with supercooled $\text{HNO}_3/\text{H}_2\text{SO}_4/\text{H}_2\text{O}$ droplets. Panel A displays the measured molar ratios, panel B shows particle volume, and panel C shows the balloon altitude. The red color indicates the presence of nitric acid trihydrates (NAT), blue indicates supercooled ternary solution (STS) particles, and gray represents particles with insufficient information to derive molar ratios. Adapted from Voigt et al. (2000a).

3.2.2.3 DENITRIFICATION

Observations of Denitrification

In situ Arctic observations from the ER-2 aircraft in January to March 2000 detected the most severe and extensive denitrification observed in the Arctic stratosphere (Popp et al., 2001); see Figure 3-17. Average removal of as much as 60% of total reactive nitrogen (NO_y) was observed throughout the core of the vortex near 20 km (Figure 3-17). Waibel et al. (1999) have also analyzed balloonborne observations of denitrification in 1995. These observations reveal an approximate 50% reduction in NO_y at 20 km. Using tracer measurements to eliminate deficits due to mixing (see Section 3.3.1.2), Waibel et al. (1999) concluded that at least 82% of the observed NO_y loss at 20 km was due to denitrification. Sugita et al. (1998) and Hintsa et al. (1998) have also observed similar levels of Arctic denitrification near 20 km, in 1995 and 1996 winters, respectively. Together, these observations show that some Arctic air parcels were

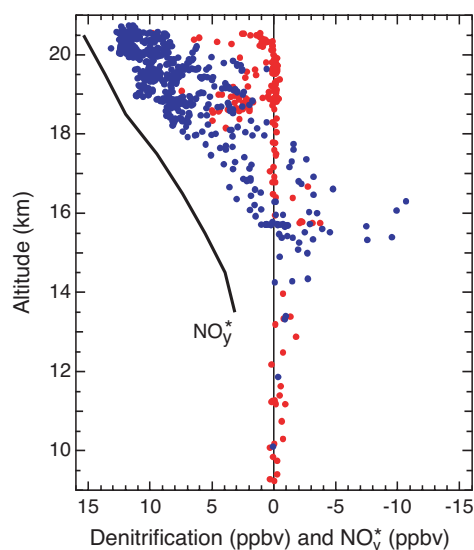


Figure 3-17. Vertical profiles of redistributed NO_y in the 1999-2000 Arctic vortex. Positive values of denitrification represent NO_y removal. Blue and red symbols represent measurements made at greater than 70°N and less than 70°N equivalent latitude, respectively. The solid black line representing NO_y^* (the maximum available NO_y at a given altitude) was determined from altitude-bin-averaged N_2O values for measurements made throughout the winter at equivalent latitudes greater than 70°N . Maximum ER-2 flight altitudes of 20 to 12 km represent a potential temperature of approximately 460 to 475 K. Adapted from Popp et al. (2001).

POLAR OZONE

severely denitrified (>50%) near 20 km in several cold winters.

Figure 3-18 shows the time evolution of HNO_3 in both hemispheres for a number of winters on three potential temperature surfaces, based on Microwave Limb Sounder (MLS) observations (see Appendix 3A for MLS data description). Large irreversible depletions (>80%) in HNO_3 vapor amounts occur only in the SH (Santee et al., 1999), but much smaller irreversible depletions (~20%) have also been observed in cold Arctic air parcels (Dessler et al., 1999; Santee et al., 2000, 2002). However, large permanent depletions in HNO_3 concentrations (>40%) have been observed in cold Arctic winters by satellite instruments with finer vertical resolution than MLS (~6-km vertical resolution), such as the ILAS instrument, which has a 1- to 2-km vertical resolution (Kondo et al., 2000; Irie et al., 2002; see also Appendix 3A for satellite data descriptions). Thus, extensive denitrification does occur in both hemispheres based on both in situ and remote sensing observations. However, severe denitrification in the Arctic must be narrow in depth because if the denitrified layers were deeper than 6 km, then MLS would have been able to detect this irreversible loss in gas-phase nitric acid (Tabazadeh et al., 2001). Individual nitric acid vertical profiles from the ILAS instrument (Kondo et al., 2000; Irie et al., 2002) during the winter of 1996/1997 further show that the vertical range of denitrification in the Arctic is typically ~2 to 3 km deep (from about 18 to 21 km), with immediate nitrification occurring below this altitude range.

Tabazadeh et al. (2000) have shown that denitrification over a broad altitude range (>10 km in depth) occurs rapidly in the Antarctic when the duration of an average PSC event is about 2 weeks (defined to be the time spent by an isentropic air parcel below 195 K at 450-K potential temperature). Tabazadeh et al. (2000) suggest that deep extensive denitrification currently occurs only in the Antarctic because average Arctic PSC events last nearly half as long as those in the Antarctic. Antarctic denitrification rapidly occurs during the mid- to late-June time period (see Figure 3-18). The short persistence of PSC events in the NH limits the extent of severe denitrification to only a few kilometers, as observed in many past cold Arctic winters (Popp et al., 2001; Sugita et al., 1998; Hintsä et al., 1998; Kondo et al., 2000; Irie et al., 2001, 2002). In Section 3.3.4, the effect of denitrification depth on ozone loss is assessed for both hemispheres.

Model Simulations of Denitrification

Improvements in our understanding of PSC particle sizes and number concentrations (Section 3.2.2.1)

now allow for more sophisticated treatments of denitrification in models. Current 3-D chemical transport models include highly simplified representations of denitrification that are now recognized to be incorrect. These models assume that nitric acid is carried downward on sedimenting ice particles wherever temperatures are lower than the ice frost point (Chipperfield et al., 1993; Considine et al., 2000). Removal of nitric acid on sedimenting ice particles is clearly not operating in the Arctic because models, using this assumption, have been unable to produce any denitrification by this mechanism (Chipperfield and Pyle; 1998; Davies et al., 2002).

Drdla et al. (2002) have used a coupled microphysical-chemistry trajectory model to show that synoptic-scale ice clouds could not have caused the massive denitrification observed during the 1999/2000 winter. They concluded that the large nitric acid particles that caused denitrification were not nucleated on ice particles.

Jensen et al. (2002) have used a one-dimensional version of the Community Aerosol and Radiation Model for Atmospheres (CARMA) microphysics cloud model to show that solid nitric acid number densities in the range of 10^{-2} to 10^{-3} cm^{-3} are the most efficient in causing rapid denitrification. The CARMA cloud model has also been used to show (see Figure 4 in Tabazadeh et al., 2001) that the vertical range over which denitrification occurs is normally quite deep in the Antarctic (>10 km) but limited in the Arctic, in general agreement with many observations of denitrification in both hemispheres (i.e., Santee et al., 1999; Popp et al., 2001; Sugita et al., 1998; Hintsä et al., 1998; Kondo et al., 2000; Irie et al., 2001, 2002). The Arctic denitrified layers are shallow in depth mainly because the stratosphere, even in cold winters, is too warm below about 17 km for nitric acid hydrate particles to exist.

Waibel et al. (1999) simulated denitrification by assuming that ice acted as the nucleus for NAT formation. Most of the denitrification calculated in the model was caused primarily by sedimentation of NAT particles, with a fixed number concentration of 5×10^{-3} cm^{-3} , released upon ice evaporation. In these 3-D model simulations, in which a simplified treatment of horizontal transport was used, NAT particles were assumed to be in equilibrium with gas-phase nitric acid.

Davies et al. (2002) have included a parameterization in a 3-D CTM of NAT particle sedimentation assuming sizes and number concentrations representative of those observed by Fahey et al. (2001). NAT particles were assumed to be in equilibrium with gas-phase nitric acid in these simulations. The calculated denitrification magnitude was similar to that observed in winter 1999/2000. In contrast, the modeled denitrification was significantly less than observed when NAT was allowed

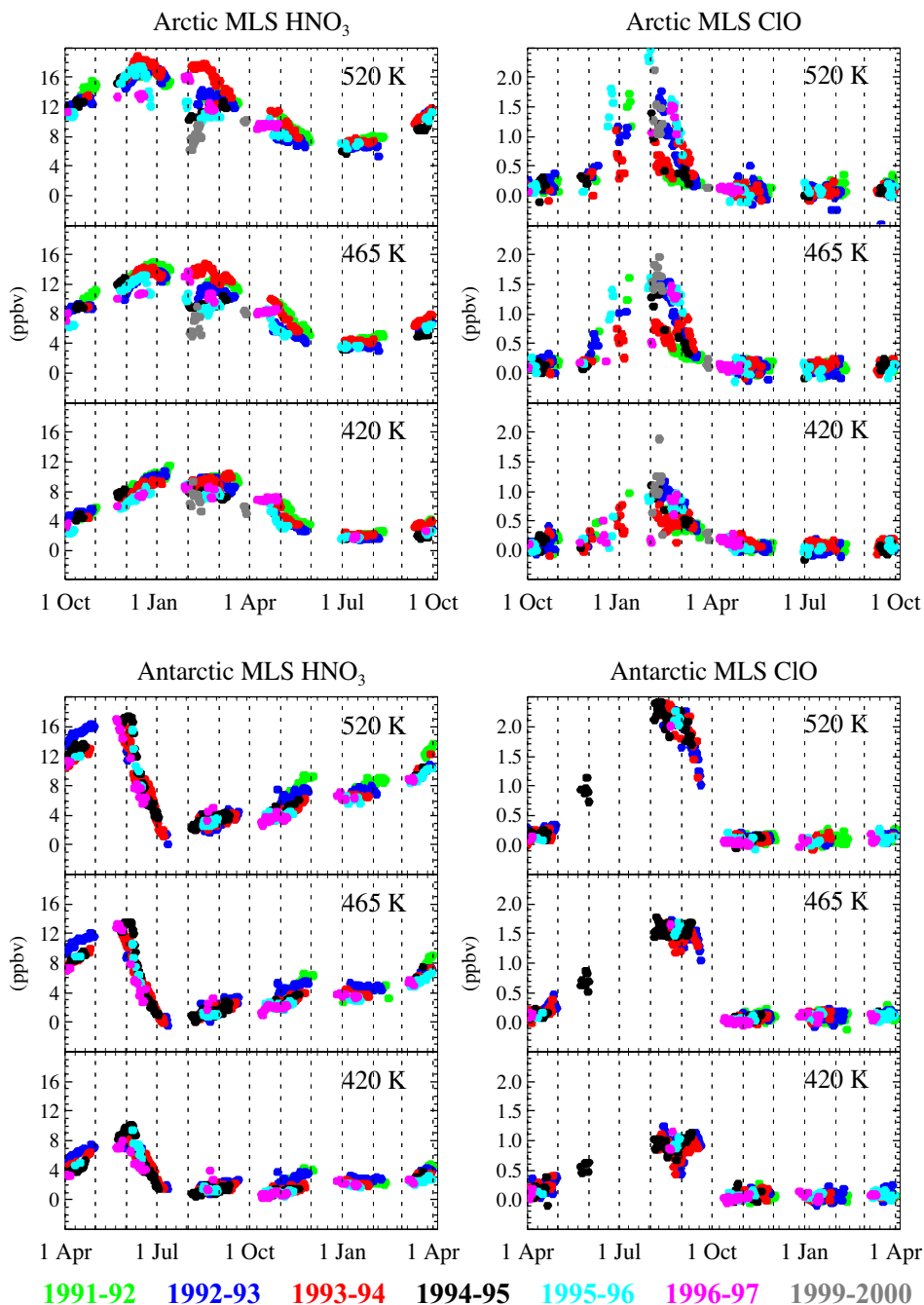


Figure 3-18. Time series of Upper Atmosphere Research Satellite (UARS) MLS HNO_3 (left, ppbv) and ClO (right, ppbv) at 520 K (~ 21 km), 465 K (~ 19 km), and 420 K (~ 17 km) for both the Northern (top) and Southern (bottom) Hemispheres. Values shown are averages of data points with solar zenith angle $< 88^\circ$ (daylight) in the 70° - 80° equivalent latitude bin. These values represent the best estimates of the abundances at these particular potential temperature surfaces based on the MLS measurements; it should be borne in mind, however, that correlations between these levels may have been introduced either during the retrieval process (since the retrieval pressure grid is finer than the width of the averaging kernels) or through interpolation of the retrieved data onto potential temperature surfaces, and thus the true number of completely independent pieces of information is likely to be less than the number of surfaces shown here. For the daily averages in this equivalent latitude bin the precision is roughly 0.15 ppbv for HNO_3 and 0.05 ppbv for ClO . Different years are represented by different colors as indicated in the legend. The x-axis tick mark increment is 10 days; dotted vertical lines demark calendar months. The 1991 to 1997 and 2000 data are adapted from Santee et al. (1999) and (2000), respectively.

POLAR OZONE

to nucleate only on ice particles. This result is consistent with previous simulations (Carslaw et al., 2002; Drdla et al., 2002) showing that the observed large nitric acid particles could not have nucleated on synoptic-scale ice clouds during the winter of 1999/2000.

Mann et al. (2002) have developed a 3-D model of denitrification that takes into account the time dependence of both growth and sedimentation of large NAT particles. In these simulations, NAT particle growth times are on the order of several days, and therefore the magnitude of denitrification strongly depends on individual particle growth cycles. In fact, the extent of modeled denitrification is strongly amplified when areas of low temperature are stable and concentric with the vortex, allowing for individual particles to persist for a longer time and to grow to larger sizes. Thus the area of low temperatures by itself is perhaps not the best indicator for predicting the severity of denitrification in the Arctic.

In summary, new model calculations show that the long-accepted mechanism of nitric acid removal on sedimenting ice particles cannot account for observed levels of denitrification. Denitrification is most likely caused by sedimentation of large nitric acid particles. Various models are able to reproduce, in broad terms, the observed levels of denitrification by assuming sedimentation of large nitric acid particles. In addition, recent model calculations show that Arctic denitrified layers are normally shallow in depth because the stratosphere is too warm below about 17 km to allow for large particles to carry much nitric acid beyond this altitude. Establishing the formation mechanism of the large nitric acid particles will be important for the development of realistic models of denitrification. The sensitivity of ozone loss to denitrification is discussed in Section 3.3.4.

3.2.2.4 DEHYDRATION

Figure 3-19 shows the time evolution of water vapor in the SH during 1998 (Nedoluha et al., 2000). Severe dehydration is observed over a 10-km altitude range. Similar results are also obtained from analysis of MLS water vapor data during the Antarctic winter of 1992 (Stone et al., 2001; see also Appendix 3A for MLS data description). In the Arctic, removal of ~1 ppm of water vapor over a 1- to 2-km altitude range has been observed by the ILAS instrument (Pan et al., 2002). The lack of extensive and deep dehydration in the Arctic is also supported by in situ observations (Vömel et al., 1997; Hintsä et al., 1998; Herman et al., 2002). Overall, the Arctic climate, even in cold years, is too warm to allow for formation of widespread persistent ice clouds that lead to dehydration. The sensitivity of ozone loss to dehydration is discussed in Section 3.3.4.

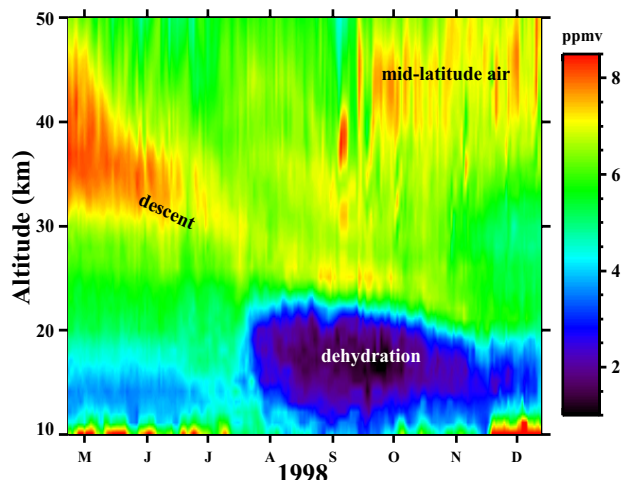
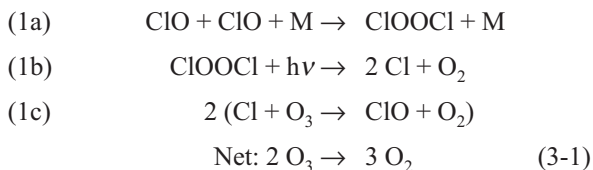


Figure 3-19. The water vapor mixing ratio as measured by POAM in the Southern Hemisphere from 27 April 1998 to 12 December 1998. Profiles are obtained from daily averages of the measurements from POAM, which generally provides 14 measurements per day. Measurements from both inside and outside of the vortex are included. The POAM measurement latitude biannually cycles from 88°S at the equinoxes (March 21 and September 21) to 62°S at the solstices (June 21 and December 21). Adapted from Nedoluha et al. (2000).

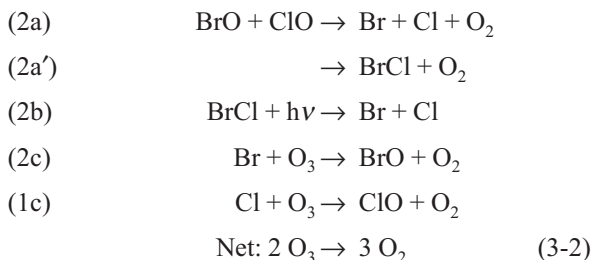
3.2.3 Polar Ozone Chemistry

The chemical loss of polar ozone during winter and spring occurs primarily by two gas-phase catalytic cycles that involve halogen oxide radicals:

Cycle 1



Cycle 2



Abundances of chlorine monoxide (ClO) in the polar vortex are greatly elevated by reactions of inactive chlorine reservoir species on various types of polar stratospheric clouds (PSCs) that form when temperatures drop below about 195 K (see Section 3.2.2). Abundances of bromine monoxide (BrO) determine the removal rate by Cycle 2, which contributes about 50% to the total chemical loss rate of polar ozone (Chipperfield and Pyle, 1998). In contrast to ClO, the abundance of BrO is not strongly affected by reactions involving PSCs because less than half of the available inorganic bromine budget is sequestered in reservoirs such as bromine nitrate (BrNO₃) and hydrogen bromide (HBr) prior to processing.

Since the previous Assessment, new studies have addressed the rates of ozone destruction by Cycles 1 and 2 in an effort to reconcile apparent discrepancies between measured and modeled chemical loss rates of Arctic ozone (see Section 3.3). The chlorine and bromine cycles are discussed separately below in Sections 3.2.3.1 and 3.2.3.2. Model calculations reveal that, at present and for the foreseeable future, winter polar ozone loss will be dominated by reactions involving ClO and BrO (e.g., Chipperfield and Pyle, 1998; Shindell et al., 1998b).

3.2.3.1 CHLORINE

A number of modeling studies have had difficulty accounting for observed chemical loss rates of Arctic ozone, particularly during midwinter when insolation is weakest (see Section 3.3). As a consequence, attention has focused on reducing uncertainties in key rate parameters, in particular those for formation and photolysis of the chlorine oxide dimer (ClOOC1), i.e., parameters k_{1a} (first-order reaction-rate constant) and J_{1b} (photolysis rate). These reactions determine the rate of ozone loss by Cycle 1, such that uncertainties in these kinetic parameters couple directly into the uncertainties in modeled ozone loss rates. Results of these studies are summarized in the section below on chlorine photochemistry.

The loss of polar ozone via Cycles 1 and 2 is determined by the temporal evolution of ClO. Numerous studies have examined the seasonal variations of inorganic chlorine partitioning, including production of high abundances of reactive chlorine (ClO_x, defined as [ClO] + 2 [ClOOC1]) by PSCs (“activation”); maintenance of high abundances of ClO_x throughout the winter; and deactivation of ClO_x back to hydrogen chloride (HCl) and chlorine nitrate (ClNO₃) (“recovery”). These results are summarized in the section below on chlorine seasonal evolution.

Simultaneous measurements of most of the major inorganic and organic chlorine species provide the ability to examine the overall chlorine budget for the Arctic and

Antarctic stratospheres during periods of rapid ozone loss. These investigations can assess the possible role of species not considered in standard models, such as higher oxides of chlorine. The results of these studies are summarized below (the section on the chlorine budget).

Chlorine Photochemistry

Our understanding of the key kinetic parameters governing ozone loss by Cycle 1 (k_{1a} and J_{1b}) has improved through new laboratory studies and atmospheric observations. Bloss et al. (2001) found k_{1a} to be up to 25% larger than the value recommended in the Jet Propulsion Laboratory (JPL) *Publication 00-3* compendium (Sander et al., 2000; hereafter referred to as *JPL 00-3* in this chapter) at temperatures below 210 K. The impact of this increase on calculated ozone loss rates depends on the manner in which the models treat ClO. In the case of models constrained by observed abundances of ClO, the rate of ozone loss due to Cycle 1 is roughly proportional to the increase in k_{1a} . For models that allow ClO and ClOOC1 to repartition within the constraint of constant active chlorine, the total loss rate is largely independent of this change in k_{1a} , because ClO abundances respond in the opposite sense to the change in the rate constant (Figure 3-20). Thus, the maximum effect of an increase in k_{1a} based on the results of Bloss et al. (2001) is to increase total ozone loss rates by no more than 25% under cold polar conditions. Such an increase is insufficient to resolve fully the factor-of-2 discrepancies between modeled and measured Arctic ozone loss rates during January found in several recent studies (e.g., Woyke et al., 1999; Becker et al., 2000).

The recommended absorption cross section for ClOOC1 has not changed since the previous Assessment. However, there have been several important laboratory and theoretical studies (Moore et al., 1999; Kaledin and Morokuma, 2000; Toniolo et al., 2000) of the product yields from photolysis of ClOOC1 at wavelengths longer than 300 nm, the spectral region that contributes most to the overall photolysis rate of ClOOC1. These new results reduce a significant uncertainty in our knowledge of ozone loss rates. Only the production of chlorine atoms and chloroperoxy radical (ClOO), leading to 2Cl + O₂ upon the rapid thermal decomposition of ClOO at polar temperatures, results in catalytic loss of ozone; production of ClO + ClO from ClOOC1 photolysis leads to a null cycle that has no effect on ozone. Moore et al. (1999) recently reported that two chlorine atoms and molecular oxygen (O₂) are the primary products of photolysis of ClOOC1 at 248 nm and at 308 nm. The ClOO product rapidly decomposes to atomic chlorine (Cl) and O₂ due to excess vibrational energy. This conclusion is further supported by

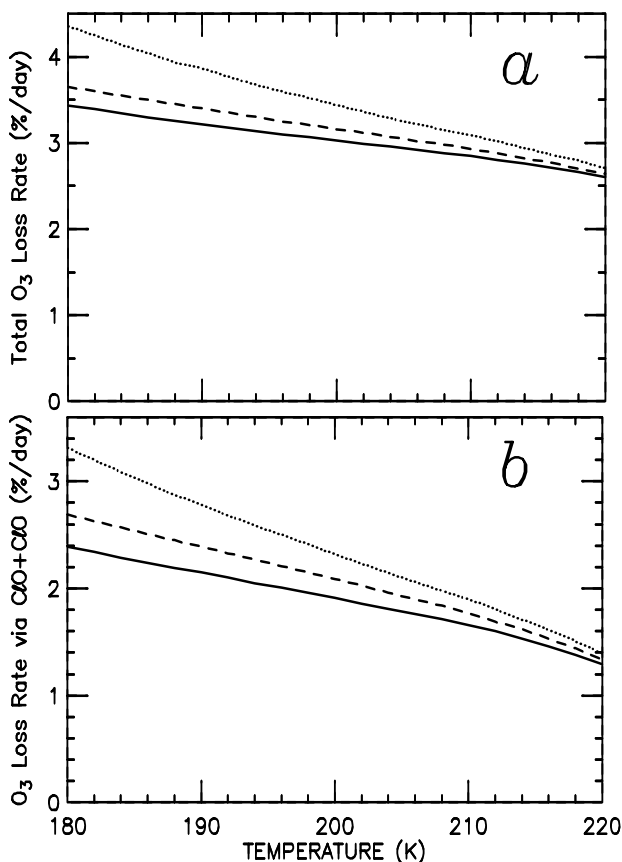


Figure 3-20. (a) Calculations of 24-hour average total chemical ozone loss rate for an air mass at 70°S, 50 hPa, as a function of temperature for mid-September conditions (e.g., ClO + 2·ClOOCl = 2 ppb; BrO + BrCl = 10 ppt; O₃ = 2 ppm; declination = 5°S) assuming the following: case 1, JPL 00-3 (Sander et al., 2000) kinetics (solid line); case 2, the Bloss et al. (2001) value for k_{1a} and the noontime concentration of ClO fixed at the same value used in case 1 (dotted line); and case 3, the Bloss et al. value for k_{1a} and the noontime concentration of ClO+2·ClOOCl fixed at the same value used in case 1 (dashed line). (b) Same as (a), except chemical loss rates due to just the ClO + ClO cycle are shown. Case 2 approximates the effect of the Bloss et al. value for k_{1a} on a model calculation constrained by measured ClO. Case 3 approximates the effect of Bloss et al. k_{1a} within a free-running CTM or GCM, where ClO and ClOOCl are allowed to equilibrate. Adapted from Bloss et al. (2001).

electronic structure calculations (Kaledin and Morokuma, 2000; Toniolo et al., 2000). These studies reduce the uncertainties of the product yield of ClOOCl photolysis

at key wavelengths for chemical loss of polar ozone relative to earlier laboratory investigations.

Several new sets of atmospheric observations provide quantitative tests of our understanding of k_{1a} and J_{1b} . Recent balloonborne in situ observations of the rate of decay of ClO immediately after sunset in the Arctic vortex (Vömel et al., 2001) are explained better by the larger value for k_{1a} at temperatures near 190 K than by the value recommended by *JPL 00-3* (Figure 3-21). An analysis of data obtained during five winters (1996 to 2000) (Solomon et al., 2002) found good agreement between measurements of column ClO and model calculations employing the value of J_{1b} / k_{1a} from *JPL 00-3*, in contrast to an earlier report, using only data for 1996, that indicated the ratio J_{1b} / k_{1a} might be 50% too low (Solomon et al., 2000). A similar conclusion had been reached in a study of earlier ground-based ClO observations over Antarctica (Shindell and de Zafra, 1995).

The chemical loss rate of ozone, particularly during early winter, is also sensitive to the dependence of J_{1b} on solar zenith angle (SZA). Avallone and Toohy (2001) concluded, based on an examination of in situ observations of ClO obtained at SZAs between 79° and 90°, that the photolysis rate of ClOOCl varied with SZA in a manner generally consistent with recommended absorption cross sections for ClOOCl. An analysis of the data they presented using the larger Bloss et al. (2001) value for k_{1a} yields values for J_{1b} that agree well with photolysis rates using *JPL 00-3* cross sections. The significantly smaller value for J_{1b} based on absorption cross sections of Huder and DeMore (1995) appears to be inconsistent with these results and those of Shindell and de Zafra (1995), Raffalski et al. (1998), Stachnik et al. (1999), and Solomon et al. (2002). Furthermore, there is no evidence from any of these studies that supports the notion that ClOOCl may photolyze at an appreciable rate in optically thin spectral regions (i.e., >420 nm). Such a process could enhance ozone loss rates at high SZAs and account for some of the discrepancy between measured and modeled ozone loss rates in midwinter (Rex et al., 2002b; see also Section 3.3).

Chlorine Seasonal Evolution

Another element critical in accounting for ozone loss is the temporal evolution of the ozone-destroying halogen radicals. Mixing ratios of ClO remain elevated (~1 to 2 parts per billion by volume (ppbv)) from May/June until September (Figure 3-18) for all years over Antarctica for which observations are available (WMO, 1995; WMO, 1999; Santee et al., 2000; Wagner et al., 2001, 2002; Solomon et al., 2002), in the region where temperatures between 14 and 24 km remain very low

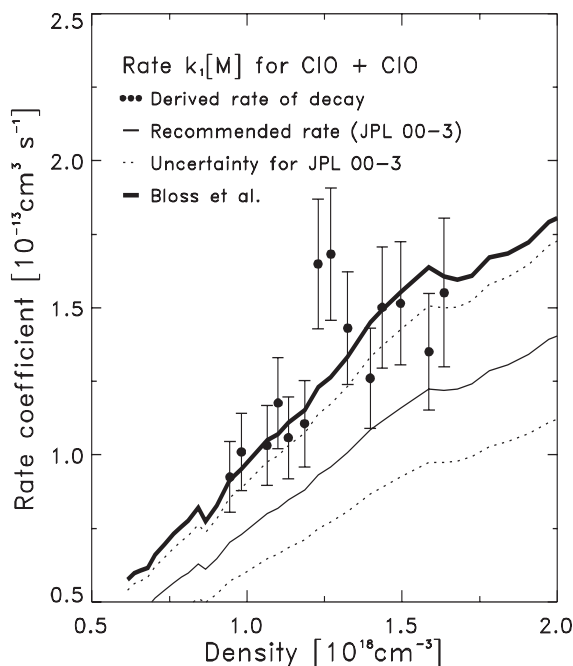


Figure 3-21. Derived rate of decay of ClO (points with 1σ error bars) from atmospheric observations of ClO obtained in the Arctic vortex during SOLVE-THESEO 2000 compared with the product of $M\cdot k_{1a}$ from the JPL 00-3 (Sander et al., 2000) recommendation (thin solid line) and from the laboratory study of Bloss et al. (2001) (thick solid line). Uncertainties for the JPL 00-3 rate are given by the dashed lines. Uncertainties for the laboratory measurement of Bloss et al. (2001) are not shown for clarity, but they are approximately the same size as the error bars for the results based on the ClO observations. Adapted from Vömel et al. (2001).

(below PSC thresholds) for several months (Figure 3-13, bottom). In addition, the southern polar vortex remains intact well into the spring season. Under these conditions, the total amount of ozone destroyed over Antarctica is nearly complete for an 8- to 10-km-thick altitude layer, a condition that is relatively insensitive to the chemical loss rate at contemporary abundances of inorganic chlorine (WMO, 1999).

Three-dimensional CTMs are able to simulate the seasonal evolution of ClO in the Antarctic polar vortex remarkably well (Ricaud et al., 1998; Solomon et al., 2000, 2002). Figure 3-22 compares ground-based column measurements of ClO above Scott Base, Antarctica (77.8°S), with calculations from the SLIMCAT model. Comparisons for the ClO mixing ratio at 480 K are also shown. During mid- to late winter, the rise of ClO is determined primarily by increasing solar illumination at

midday. The good agreement between theory and observations of column ClO during this time period suggests that the altitude range over which chlorine is activated is well reproduced by the model. During early spring, the short-term fluctuations in ClO are related to movement of the vortex over Scott Base, and the longer-term decline in ClO is the result of recovery into the reservoirs HCl (the primary sink for ClO_x in the denitrified Antarctic vortex)

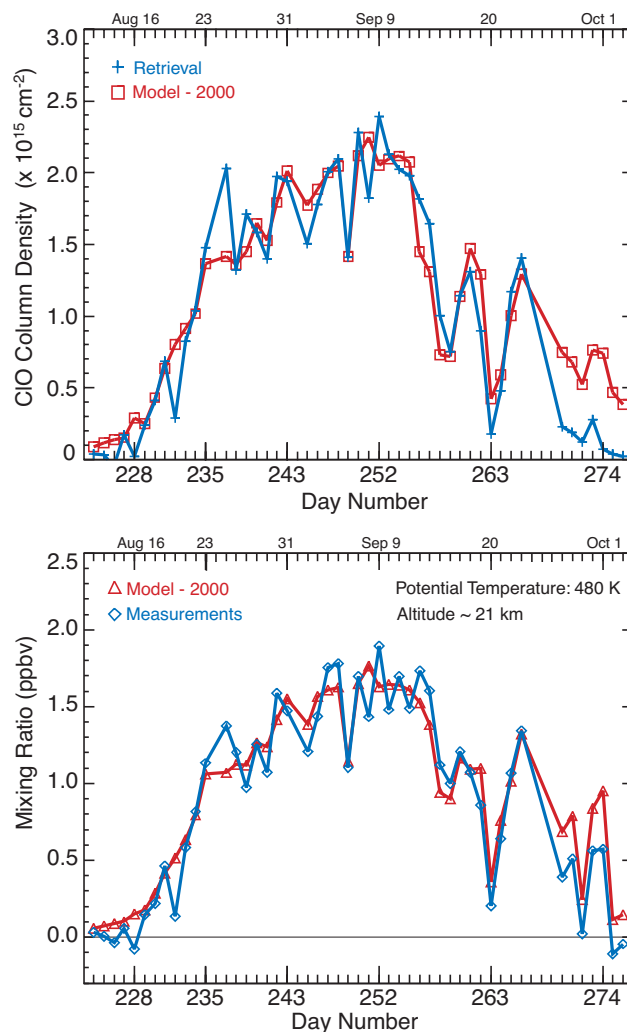


Figure 3-22. Top panel: Retrieved ClO column density (day-night difference) for 11 August through 4 October 2000 over Scott Base, Antarctica (78°S) (blue line), and the same quantity calculated using the SLIMCAT model assuming JPL 97-4 (DeMore et al., 1997) kinetics (red line). Bottom panel: Same as top panel, except for ClO mixing ratio (day-night difference) at 480 K. Adapted from Solomon et al. (2002).

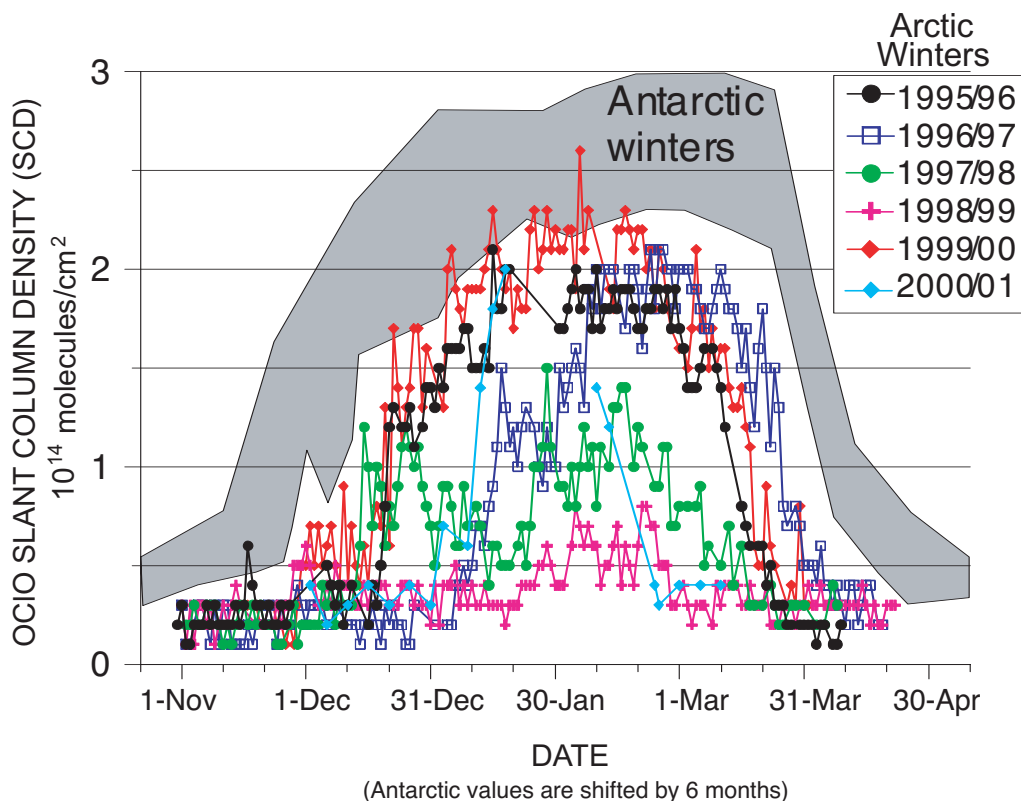


Figure 3-23. Daily maximum slant column density (SCD) of OCIO, at SZA of 90°, measured by GOME for a number of Arctic and Antarctic winters. Data for individual Arctic winters are shown, as indicated, whereas the range of data for Antarctic winters is shown by the shaded region. The time associated with the Antarctic measurements has been shifted by 6 months to facilitate comparison with Arctic observations at comparable seasons. The air mass factor (ratio of SCD to vertical column density) depends on the height profile of OCIO, which is not known a priori. Consequently, the SCD is the preferred choice for comparison of Arctic and Antarctic data. Adapted from Wagner et al. (2001, 2002).

and ClNO_3 (Solomon et al., 2002). As a result of widespread suppression of gas-phase HNO_3 in SLIMCAT, high abundances of ClO are sustained throughout the early spring season (September) until ozone is nearly completely removed. In October, HCl is observed to reappear much faster than ClNO_3 in the core of the vortex due to the shift in partitioning of Cl/ClO and nitric oxide/nitrogen dioxide (NO/NO_2) to favor Cl and NO driven by exceedingly low ozone, while ClO recovers mainly to ClNO_3 in the edge region of the Antarctic vortex (e.g., Douglass et al., 1995; Ricaud et al., 1998). Because most models simulate these features reasonably well, they are able to account for Antarctic ozone loss in a quantitative manner.

The situation for the Arctic winter is quite different, because chemical ozone loss depends more critically upon the details of chlorine activation and deactivation, and the timing of the breakup of the northern polar vortex. During cold Arctic winters, high levels of ClO are observed throughout the polar vortex (Raffalski et al., 1998;

Stachnik et al., 1999; Klein et al., 2000; Santee et al., 2000). Considerably more year-to-year variability is seen in Arctic measurements of ClO compared with Antarctic data, and peak values of Arctic ClO for cold winters are somewhat lower than observed in the Antarctic (Figure 3-18). Recent GOME measurements of chlorine dioxide (OCIO) (Figure 3-23), which indicate much greater year-to-year variability in active chlorine for the Arctic as well as considerably higher levels of active chlorine for the Antarctic (Wagner et al., 2001, 2002), provide a picture consistent with the MLS observations of ClO. The GOME observations of Antarctic OCIO are also consistent with earlier ground-based observations of OCIO (Miller et al., 1999; see also Appendix 3A for satellite data descriptions).

The MLS and GOME measurements show that elevated levels of ClO_x in the Arctic, even for cold years, decline rapidly in early spring, in contrast to the Antarctic, where high ClO_x persists well into spring (Figures 3-18 and 3-23). Consequently, the total quantity of ozone destroyed

in the Arctic vortex depends strongly on the rate of chlorine deactivation, which in turn is related to the extent of denitrification (e.g., Rex et al., 1997; Waibel et al., 1999; Tabazadeh et al., 2000) and the efficiency of chlorine reactivation (e.g., Solomon, 1999; Hanisco et al., 2002; Drdla and Schoeberl, 2002). Abundances of ClO_x over the Arctic decrease rapidly when temperatures increase above ~ 200 K, because of photochemical release of NO_x from nitric acid that remains in excess of reactive chlorine throughout the winter. During this recovery period, observations have shown that ClNO_3 is the primary inorganic chlorine species, representing $>80\%$ of the available chlorine (Chapter 3 of WMO, 1995). It has long been assumed that chlorine can be readily reactivated on PSCs during this recovery period (provided temperature drops below ~ 195 to 200 K), leading to significant additional ozone loss. However, a recent study based on analyses of in situ observations of hydroxyl radical (OH) and hydroperoxyl radical (HO_2) (Hanisco et al., 2002) concludes that key heterogeneous reactions that reactivate chlorine proceed more slowly than currently recommended rates. The consequences of this finding have yet to be explored in photochemical model studies of Arctic ozone loss.

Most important, however, 3-D chemistry and transport models (Ricaud et al., 1998; Massie et al., 2000; van den Broek et al., 2000) as well as trajectory simulations (Woyke et al., 1999; Danilin et al., 2000) are able to simulate well the high levels of ClO observed in the Arctic, indicating that chlorine activation schemes used in photochemical models are relatively accurate in describing large-scale features of chlorine activation. Recent model simulations also suggest that the rate and extent of halogen activation in the polar vortex are not as sensitive to PSC composition as previously thought (Carslaw et al., 1997b; Becker et al., 1998; Woyke et al., 1999; Danilin et al., 2000). This lack of sensitivity arises because most heterogeneous halogen activation rates are much faster at low temperatures than deactivation rates of ClO_x for air parcels outside of PSCs (e.g., Solomon, 1999).

Although models simulate the seasonal evolution of ClO in the Arctic reasonably well for cold winters, they have some difficulty for warm winters, where minimum temperatures are close to the threshold for formation of PSCs (e.g., Klein et al., 2000). For the winter of 1998/1999, ground-based observations of ClO from Ny Ålesund, Spitzbergen (78.9°N), revealed little or no enhancements above background levels, whereas the SLIMCAT model predicted ClO mixing ratios as high as 1.0 ppbv. This discrepancy has been attributed to a small cold bias (~ 1 K) in the UKMO temperatures input to the SLIMCAT model (Klein et al., 2000; Knudsen et al., 2002), although it is also possible that the PSC nucleation scheme in SLIMCAT is

unrealistic at temperatures near NAT thresholds. In either case, such a problem highlights the extraordinary sensitivity of Arctic ClO to temperatures and microphysics schemes for winters where the minimum temperatures are very close to the threshold for formation of PSCs.

Chlorine Budget

Ideally, an assessment of the chlorine budget should be based on simultaneous measurements of the primary inorganic (e.g., HCl, ClNO_3 , ClO, ClOOCl) and organic (e.g., chlorofluorocarbons and other chlorine-containing halocarbons) chlorine species. A significant number of studies, all of which lack observations of ClOOCl , have indicated good agreement between the inorganic and organic chlorine budget for the lower polar stratosphere (e.g., von Clarmann et al., 1995; Engel et al., 1997; Mickley et al., 1997; Ricaud et al., 1998; Michelsen et al., 1999; Pierson et al., 1999). For example, balloon-borne microwave and whole-air sampler measurements of $[\text{HCl}] + [\text{ClO}] + 2[\text{ClOOCl}^*]$ versus N_2O for air in the core of the Arctic vortex on 27 January 1995 (Stachnik et al., 1999), made under conditions of highly elevated ClO, agree well with estimates of inorganic chlorine based on the measured decomposition of organic halocarbons. The above-mentioned studies relied on calculated concentrations of ClOOCl , termed ClOOCl^* , assuming a steady-state relation with measured ClO. Their validity is supported by the good agreement between laboratory rates for k_{1a} and J_{1b} (needed to calculate ClOOCl^*) and values inferred for these kinetic parameters from the time rate of change of ClO in the atmosphere (Avallone and Toohey, 2001; Vömel et al., 2001).

Also, these findings are consistent with reasonably good agreement (differences of about $\pm 15\%$) between the disappearance of organic chlorine (CCl_y) species and the appearance of inorganic chlorine (Cl_y) species observed for the summer polar stratosphere (Section 3.2.4.3), a region of the atmosphere for which the contribution to Cl_y is dominated by HCl and ClNO_3 .

3.2.3.2 BROMINE

Cycle 2 ($\text{BrO} + \text{ClO}$; see beginning of Section 3.2.3) makes important contributions to polar ozone loss. As shown below in the section on bromine monoxide abundances, there is now reasonably good agreement between measurements of BrO obtained by various techniques. This is a significant advance in our understanding because important differences had been noted in the previous Assessment (WMO, 1999). This convergence of measurements allows for fairly accurate assessment of the contribution of bromine to chemical loss of polar ozone.

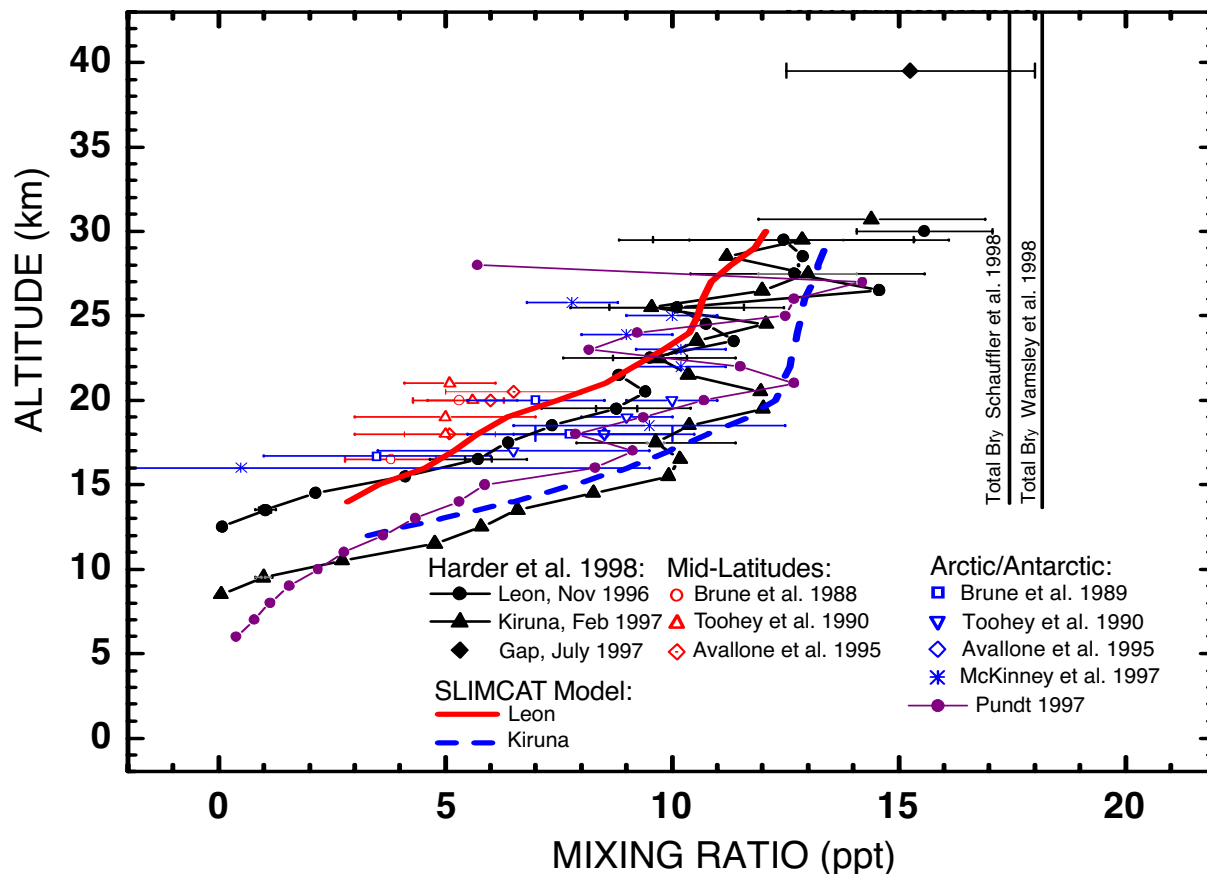


Figure 3-24. Measurements of profiles of BrO obtained at midlatitudes, in the Arctic and the Antarctic, by the in situ resonance fluorescence technique (red and blue open symbols and blue * symbol) and by the remote Differential Optical Absorption Spectroscopy (DOAS) technique (closed symbols). Also shown are two estimates of total inorganic bromine (total Br_y) loading at the top of the atmosphere based on measured abundances of brominated source gases (thin vertical lines). Calculations of profiles for BrO from the SLIMCAT model, appropriate for conditions of the DOAS observations of BrO from León, Spain (42.6°N), and Kiruna, Sweden (67.9°N), are shown by the red solid and blue dashed lines. See Harder et al. (1998) for the full citation of the references given on the figure. Adapted from Harder et al. (1998).

Profiles of inorganic bromine (Br_y) based on measurements of BrO have recently been compared with estimates based on the observed falloff (with increasing height) of the organic source species. These comparisons, discussed in the section on bromine trends and budget, show a slight offset that may result from either direct influx of ~3 parts per trillion by volume (pptv) of inorganic bromine across the tropical tropopause or some organic species not accounted for. Finally, profile measurements of BrO discussed also in the bromine budget section have been used to determine trends in total bromine loading that can be compared with trends based on the organic bromine (CBr_y) content of the lower atmosphere.

Bromine Monoxide (BrO) Abundances

Harder et al. (1998) compared in situ BrO measurements from the ER-2 aircraft and a balloon flight with profiles of BrO obtained by the Differential Optical Absorption Spectroscopy (DOAS) technique (Figure 3-24). There is a systematic difference in these two sets of observations, where DOAS measurements are somewhat larger than in situ, although this is within the combined uncertainties of the measurements. Consequently, the estimates of the inorganic bromine budget based on these sets of measurements have ranged from ~16 pptv (in situ) to ~20 pptv (DOAS) (Avallone et al., 1995; Pfeilsticker et

al., 2000). It is important to note that, because these sets of observations were obtained 5 years apart, more than half of this difference can be explained by trends in the bromine source gases, as discussed in the next section.

Sinnhuber et al. (2002) compared ground-based zenith sky measurements obtained at 11 sites with simulations from the SLIMCAT model in an effort to examine the detailed processes that govern the partitioning of BrO. Comparisons for three sites are shown in Figure 3-25. The simulated abundances of BrO generally agree to within ~10% of the observations over a wide range of seasons, latitudes, and solar zenith angles. The results are consistent with a total stratospheric bromine loading (sum of organic and inorganic) of 20 ± 4 pptv, in agreement with the values deduced from previous remote measurements of BrO.

The SLIMCAT model tends to overestimate BrO column abundances at high latitudes, typically when ClO abundances are elevated (Figure 3-25). Conversely, Friess et al. (1999) find a discrepancy in the opposite sense between BrO slant column measurements made at Kiruna, Sweden (67.9°N), in winter and SLIMCAT model calculations that use *JPL 97-4* kinetics (DeMore et al., 1997; hereafter referred to as *JPL 97-4* in this chapter) and a bromine loading of 20 pptv (the model underestimates midday measured BrO columns by 20 to 40%). Sinnhuber et al. (2002) note that the discrepancy highlighted in their study can be reduced by increasing the rate constant for reaction 3-2a' to the upper limit of the uncertainty of the *JPL 00-3* recommendation. Friess et al. (1999), however, report that the discrepancy they found is evidence for several pptv of BrO in the free troposphere. The Friess et al. (1999) interpretation is consistent with interpretations based on other remote observations of BrO (e.g., Harder et al., 1998; Fitzenberger et al., 2000).

The discrepancies outlined above have a relatively minor impact on ozone loss rates calculated directly from Cycle 2 or on observed abundances of ClO and BrO in the polar vortices. However, they do raise questions about the completeness of our understanding of coupled bromine/chlorine chemistry. Similar questions have been raised based on aircraft observations of BrO at 20 km (in situ) and 12 km (remote) within the perturbed polar vortex. Specifically, Avallone and Toohey (2001) report that mixing ratios of BrO did not drop to near-zero as expected with increasing SZA after sunset, when reservoir species like bromine nitrate (BrNO₃), bromine chloride (BrCl), and hypobromous acid (HOBr) are expected to sequester nearly all available reactive bromine. Similarly, Wahner and Schiller (1992) previously reported non-zero BrO column abundances above 12 km in darkness that were difficult to explain. Avallone and Toohey (2001) suggest

that thermal decomposition of a weakly bound molecule, such as BrOOCl (bromochloroperoxide), may be able to maintain a few pptv of BrO following sunset, but note that such a process would have little impact on ozone loss rates because of the rapid decline of ClO at sunset. The existence of adducts of bromine and chlorine oxides has been postulated in theoretical studies (Gleghorn, 1997; Bridgeman and Rothery, 1999; Gomez and Pacios, 1999; Papayannis et al., 2001) and has been observed in an argon matrix (Johnsson et al., 1995).

The previous Assessment noted the spectroscopic detection of bromine dioxide (OBrO) in the midlatitude stratosphere, with implied mixing ratios as high as 20 pptv (Renard et al., 1997). As such, OBrO would be the dominant nighttime reservoir for inorganic bromine in the midlatitude stratosphere. The same group has since reported the presence of smaller amounts of OBrO in the nighttime, polar stratosphere (Renard et al., 1998). However, abundances of even a few hundredths of a part per trillion (ppt) of OBrO in the nighttime stratosphere are contrary to our present understanding of bromine photochemistry (Chipperfield et al., 1998). Erle et al. (2000) recently reported measurements of upper limits for OBrO that are appreciably smaller than values observed by Renard et al. (1997, 1998), indicating that one of the sets of observations is in error or that abundances of OBrO are highly variable. The explanations for non-zero BrO mixing ratios in darkness and possible detection of OBrO remain a mystery.

Bromine Trends and Budget

During the Arctic winter of 1998/1999, vertical profiles of all known major organic bromine species were measured between 9 and 28 km (Pfeilsticker et al., 2000) (Figure 3-26). The expected profile for inorganic bromine that was inferred from the source gases agrees well (i.e., differences are within the measurement uncertainties) with a second profile that was estimated from spectroscopic observations of BrO and a photochemical model estimate of the BrO/Br_y ratio (see Figure 3-26) (Pfeilsticker et al., 2000). This result indicates that the budget of bromine and its photochemistry in the lower stratosphere are reasonably well understood. For early 1999, the mixing ratio of total bromine estimated at 25 km in air of 5.6-year mean age was 18.4 (+1.8, -1.5) pptv based on organic precursor measurements, and 21.5 ± 3.0 pptv from BrO measurements. This slight offset allows for the possibility of a bromine influx of 3.1 (-2.9, +3.5) pptv from the troposphere to the stratosphere (Pfeilsticker et al., 2000).

Attempts to quantify temporal trends in inorganic bromine in the stratosphere traditionally have been ham-

POLAR OZONE

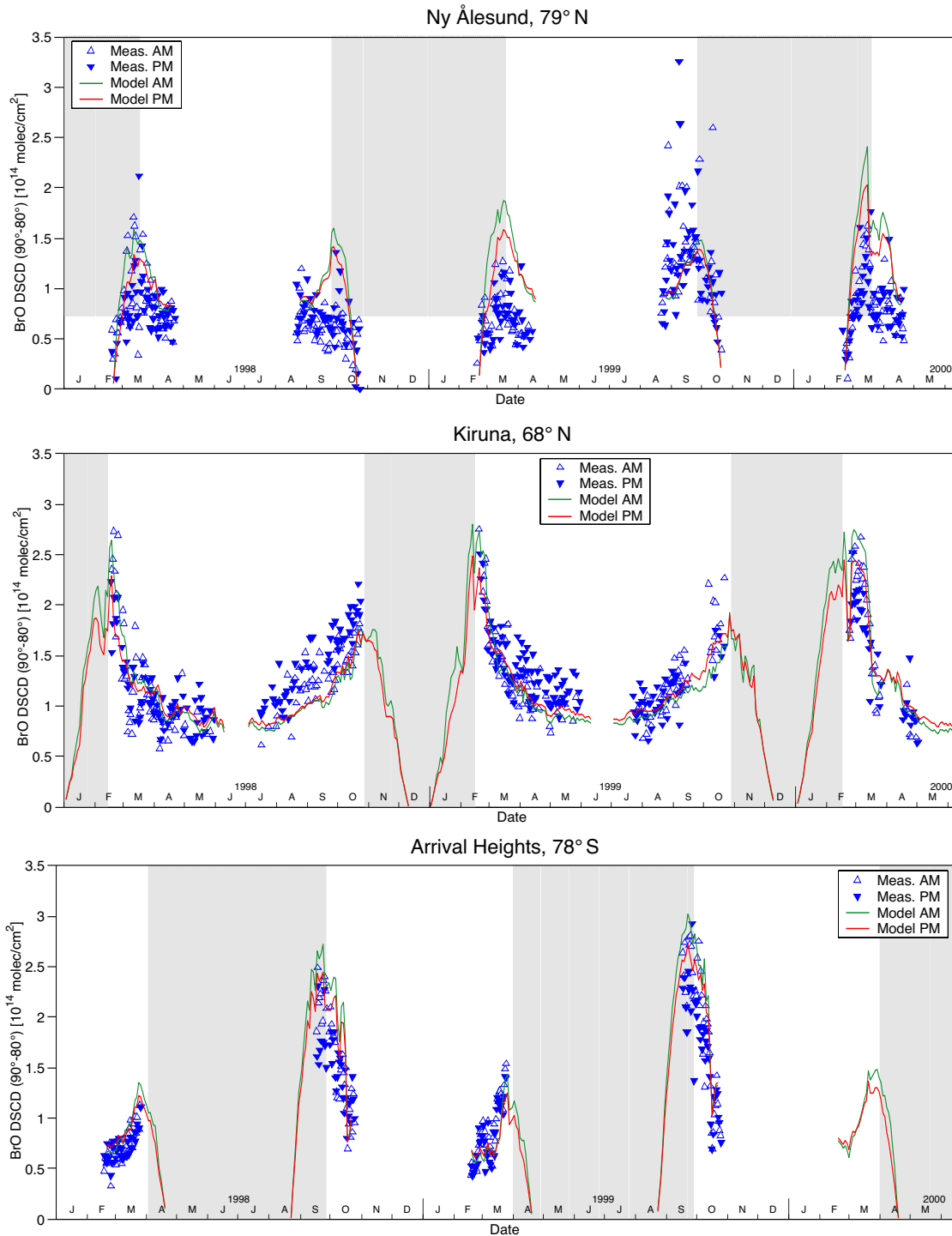


Figure 3-25. Comparison of measured and modeled differential slant column densities (DSCD) of BrO over Ny Ålesund, Spitzbergen (78.9°N), Kiruna, Sweden (67.9°N), and Arrival Heights, Antarctica (78°S). The differential slant columns were calculated from observations and model results obtained between solar zenith angles of 90° and 80° for the morning (AM) and evening (PM). However, when a solar zenith angle of 80° was not reached at high latitude (shaded regions), local noon values were used as a reference instead. Calculated values of BrO are from the SLIMCAT model. Adapted from Sinnhuber et al. (2002).

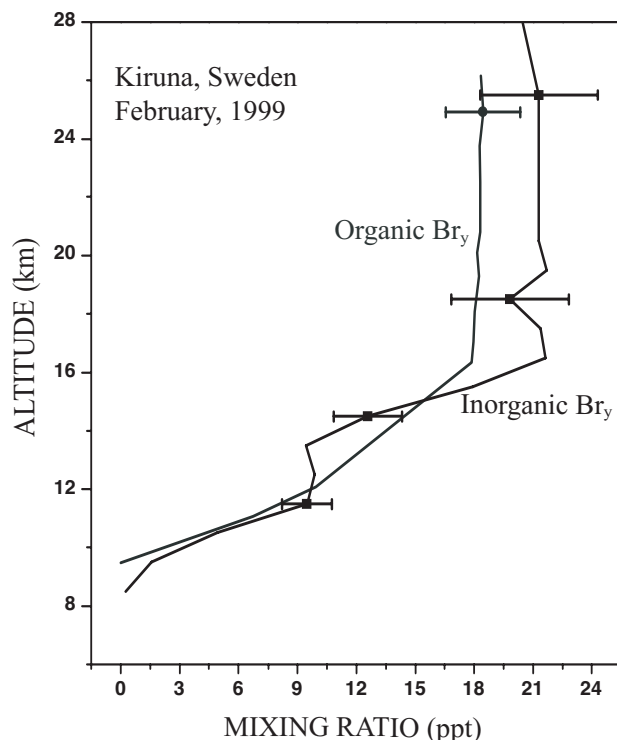


Figure 3-26. Vertical profile of total inorganic bromine (labeled Inorganic Br_y) based on the observed falloff of brominated source gases (labeled Organic Br_y) and based on measured BrO and a model calculation of the BrO/Br_y ratio. Measurements were obtained in the Arctic vortex, above Kiruna, Sweden (67.9°N), during the winter of 1998/1999. Adapted from Pfeilsticker et al. (2000).

pered by the lack of long-term observations and the relatively small quantities (~10 pptv or less) of the bromine species. However, a recent analysis of stratospheric measurements of BrO may shed some light on this issue, which is important in the context of polar ozone loss because the source of bromine to the stratosphere is expected to have increased by nearly 30% over the past decade (Wamsley et al., 1998).

Pfeilsticker et al. (2000) have taken the approach of estimating the abundance of total inorganic bromine (Br_y) based on measurements of BrO and model calculations of the BrO/Br_y ratio (Figure 1-8 in Chapter 1 of this Assessment; see also Figure 2.12 of EC (2001)). They rely on separate measurements of carbon dioxide (CO₂) or sulfur hexafluoride (SF₆) and model simulations to determine the age of air versus altitude. Their analysis of stratospheric data obtained between 1996 and 2000, reported in EC (2001), is consistent with a rate of increase of total bromine of about 0.7 pptv/year, broadly consis-

tent with the increase in tropospheric organic bromine over this time period (Figure 1-8).

This result suggests that the contribution of bromine to ozone loss in the polar regions has increased faster than that of chlorine because of abundances of bromine that continue to increase at a time when those of chlorine are leveling off (see Chapter 1). Model studies indicate that catalytic cycles involving BrO account for as much as 60% (depending on abundances of ClO and temperatures) of the total chemical loss of ozone in the Arctic for cold winters (Chipperfield and Pyle, 1998). The contribution of BrO reactions to the total loss of Antarctic ozone is somewhat less than for the Arctic because of lower temperatures and widespread denitrification in the SH vortex. Considering the observed leveling off of chlorine source gases, the relative role of bromine in polar ozone loss will continue to increase until the upward trend of bromine source gases reverses. However, since ozone loss by the BrO cycle also depends on ClO, future major declines in Cl_y are expected to lead to reductions in chemical loss of polar ozone essentially independent of changes to Br_y (Chipperfield and Pyle, 1998).

3.2.4 The Polar Summer Lower Stratosphere

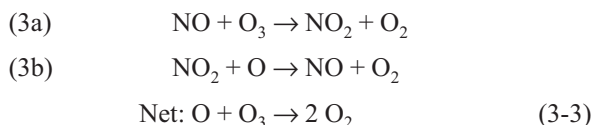
In both hemispheres, the annual cycle of total ozone has a strong decrease from the spring maximum to a minimum by mid-fall (e.g., Dobson, 1966; Dütsch, 1974; Bowman and Krueger, 1985; see also Figure 3-1). Column abundance of ozone declines by ~35% at high northern latitudes during summer (Toon et al., 1999; Lloyd et al., 1999). The rate of chemical ozone destruction in late spring/early summer is as large as in the winter polar stratosphere. This large decline, and the fact that the summer circulation is weak and quite zonally symmetric, makes the summer period a good test of understanding. Models typically have been unable to capture the full magnitude of the decline. To address this issue, the POLARIS experiment was flown from Fairbanks, Alaska, with three deployments during the early spring, summer, and early fall of 1997. This mission examined the seasonal ozone decrease using a complete payload of instruments aboard the NASA ER-2 high-altitude aircraft (Newman et al., 1999).

The summer lower stratosphere is mixed by waves that penetrate in the presence of the weak summer west-erlies (Wagner and Bowman, 2000). Orsolini (2001), however, has shown that remnants of polar vortex air can retain their identity until well into the summer in the lower stratosphere. Rosenlof (1999) has studied the annual cycle of ozone transport in high northern latitudes. She found

POLAR OZONE

that the seasonal cycle in transport was an important contributor to the seasonal march of ozone at high latitudes during middle to late summer, with the eddy contribution to ozone reduction more than offsetting the ozone increase by advection at this time. In early summer, transport is weak and in situ photochemical destruction dominates the ozone tendency. In contrast, Pierce et al. (1999) using a Lagrangian model with HALOE data found that the transport term was important (see Appendix 3A for HALOE data descriptions).

In situ measurements of nitrogen oxides (NO_x), odd hydrogen (HO_x), and ClO_x radical species (Fahey et al., 2000) and long-lived tracers of stratospheric transport (Toon et al., 1999) confirm the summertime loss of ozone is due primarily to the gas-phase catalytic cycle:



Fahey et al. (2000) calculated the ozone chemical tendency based on measurements of radicals from the major families and found that chemical processes dominate overall tendency in the midsummer. Although this ozone loss process is generally understood (Brühl et al., 1998), ozone abundances calculated using two- or three-dimensional models tend to exceed observations for high-latitude summer (e.g., Chipperfield, 1999). This discrepancy has been attributed to inadequacies in model transport (e.g., Fahey and Ravishankara, 1999).

New measurements of NO_x , HO_x , and ClO_x species in the summer polar stratosphere have provided quantitative tests of our understanding of processes that regulate the abundance of radicals in each family. Measurements in the summer polar stratosphere are particularly useful because heterogeneous reactions, normally the dominant loss process for NO_x , proceed at slower rates than gas-phase loss reactions because of uninterrupted periods of solar illumination that restrict the buildup of dinitrogen pentoxide (N_2O_5) (e.g., Gao et al., 1999; Osterman et al., 1999). In the sections that follow, we briefly assess recent advances in our understanding of stratospheric photochemistry based on these observations.

3.2.4.1 SUMMERTIME NO_x CHEMISTRY

Observations of NO , NO_2 , HNO_3 , and NO_y obtained in the summer polar stratosphere revealed higher levels of NO_x (relative to total NO_y) and NO_2 (relative to HNO_3) than could be accounted for by constrained photochemical box models using the *JPL 97-4* (DeMore et al.,

1997) set of recommended kinetic parameters (Gao et al., 1999; Jucks et al., 1999; Osterman et al., 1999; Cohen et al., 2000; Perkins et al., 2001) (Figure 3-27). During polar summer, production and loss of NO_x are regulated primarily by the $\text{OH} + \text{NO}_2$ and $\text{OH} + \text{HNO}_3$ reactions for a broad range of altitudes (e.g., Osterman et al., 1999). New laboratory data for $\text{OH} + \text{NO}_2$ (Dransfield et al., 1999; Brown et al., 1999a) and $\text{OH} + \text{HNO}_3$ (Brown et al., 1999b) led to a re-evaluation of the rate constant for both of these reactions in the *JPL 00-3* compendium (Sander et al., 2000). Use of the *JPL 00-3* kinetic parameters significantly improves the agreement between measured and modeled ratios of NO_x/NO_y and NO_2/HNO_3 (Gao et al., 1999; Jucks et al., 1999; Osterman et al., 1999; Cohen et al., 2000; Perkins et al., 2001; Salawitch et al., 2002b) (Figure 3-27).

It has also been proposed that the reaction of $\text{OH} + \text{NO}_2$ produces HOONO (pernitrous acid) in addition to HNO_3 (nitric acid) (McGrath and Rowland, 1994; Mathieu and Green, 2000; Golden and Smith, 2000, and references therein). Recent spectroscopic observations indicate a yield for HOONO of about 5% at 253 K and 26 hPa (Nizkorodov and Wennberg, 2002). The formation of the HOONO isomer is also supported by several recent kinetic studies (Donahue et al., 2001; Hippler et al., 2002). Implications of HOONO production have yet to be fully explored, but box model calculations of Golden and Smith (2000) indicate this process leads to small increases in calculated NO_x , and small decreases in calculated ozone, for the high-latitude summer stratosphere.

Simultaneous measurements of ozone, NO , NO_2 , ClO , and HO_2 during polar summer provide a stringent test of our understanding of the rapid photochemistry linking NO to NO_2 (Del Negro et al., 1999). Photolysis rates for NO_2 (J_{NO_2}) inferred from the chemical measurements are in excellent agreement with values calculated with radiative models and those measured with a spectroradiometer (Del Negro et al., 1999). Recently, this comparison has been extended to larger SZAs of 80° to 93° (Gao et al., 2001a). Values of J_{NO_2} derived from the in situ chemical measurements agree well (differences $<11\%$) with results from a multiple-scattering actinic flux model. The linearity of the correlation between these two computations of J_{NO_2} over the SZA range 80° to 93° demonstrates that the model scattering calculation is accurate for twilight conditions (Gao et al., 2001a).

Loss of ozone by NO_x chemistry in the summer polar regions may become more important in the future because of rising levels of NO_2 (Liley et al., 2000; McLinden et al., 2001). Nitrous oxide (N_2O), the source gas for NO_x and NO_y , is rising at about 3% per decade (e.g., McLinden et al., 2001). Interestingly, concentra-

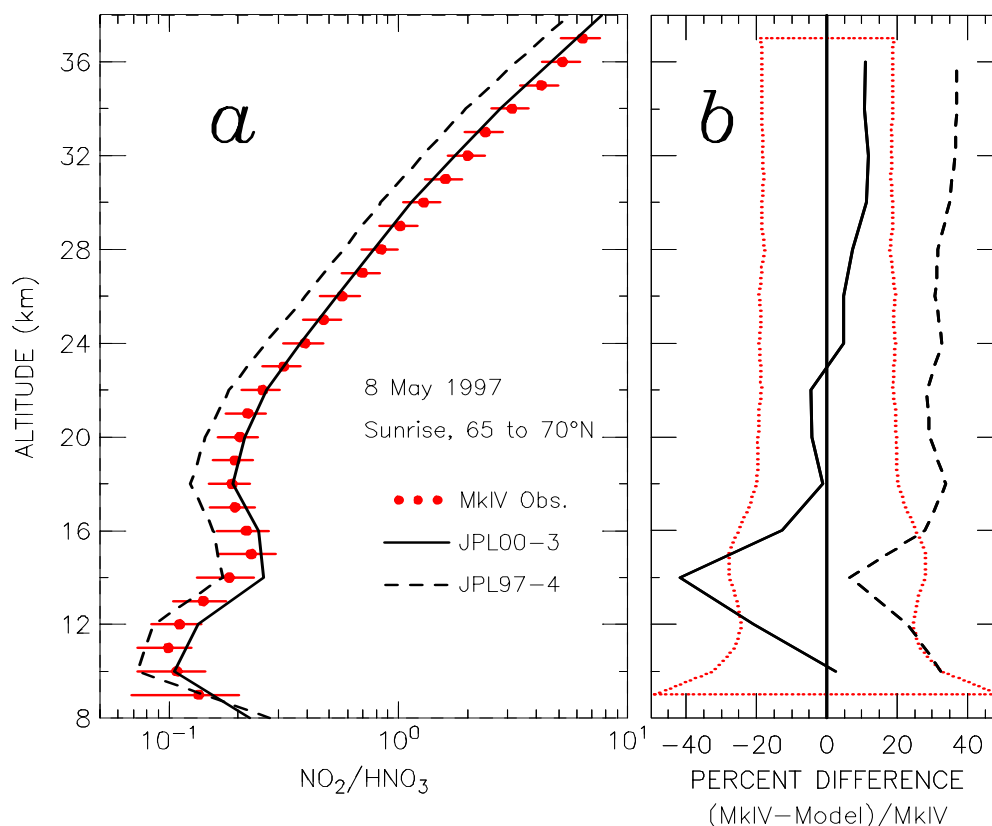


Figure 3-27. (a) MkIV observations (red points with error bars) of the NO_2/HNO_3 ratio at sunrise obtained during a balloon flight in the Arctic stratosphere on 8 May 1997. Constrained photochemical steady-state model calculations of the ratio, for the solar zenith angle of the observations, are shown for kinetic parameters from the JPL 00-3 (Sander et al., 2000) evaluation (solid line) and from the JPL 97-4 (DeMore et al., 1997) evaluation (dashed line). Error bars on the observations represent 1σ precision, based on considerations such as residuals in the spectral fitting, combined in quadrature with spectroscopic uncertainties. (b) Percentage difference between measured NO_2/HNO_3 and values from the two model calculations. The red dotted lines denote the 1σ measurement uncertainty. After Osterman et al. (1999) and Salawitch et al. (2002b).

tions of NO_2 at SH midlatitudes have been observed to be increasing at a faster rate of 5% per decade (Liley et al., 2000). This increase has been interpreted as being due to rising N_2O as well as declining levels of ozone, which alter the NO/NO_2 partitioning and the diurnal variation of NO_x (McLinden et al., 2001); see also Chapter 4.

3.2.4.2 SUMMERTIME HO_x CHEMISTRY

Measurements of OH and hydroperoxyl radical (HO_2) in the high-latitude stratosphere during late spring provide an important test of our understanding of HO_x sources throughout the day because abundances of these species are nearly in photochemical steady state under the slowly varying SZA conditions up to 93° (Wennberg et al., 1999). Observed abundances of OH and HO_2 in the lower stratosphere significantly exceed those from stan-

dard model calculations for $\text{SZA} > 80^\circ$ (Wennberg et al., 1999; Salawitch et al., 2002b) (Figure 3-28).

An important change in the *JPL 00-3* kinetics evaluation, relative to the *JPL 97-4* evaluation, is that the recommended reaction probability for BrNO_3 hydrolysis dropped from 0.8 to about 0.2 for conditions of the high-latitude, springtime lower stratosphere. Consequently, a model using *JPL 00-3* kinetics (Figure 3-28) does not predict the observed “morning rise” of HO_2 ; the calculated nighttime buildup of HOBr , which releases HO_x at sunrise, is limited because of this rate change (Salawitch et al., 2002b). The OH and HO_2 measurements suggest the presence of a photolytic source of HO_x that operates more efficiently than known HO_x sources during twilight and that operates at an essentially constant rate for $80^\circ < \text{SZA} < 93^\circ$ (e.g., this photolytic process must occur

POLAR OZONE

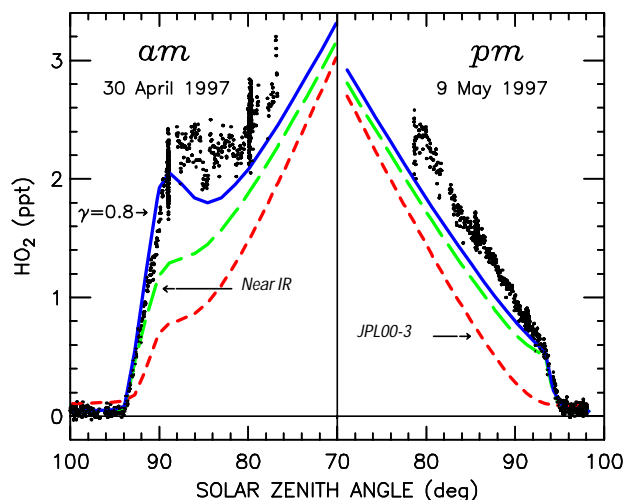


Figure 3-28. Observations of HO_2 obtained on the morning of 30 April 1997 and the afternoon of 9 May 1997 near 64°N in the lower stratosphere (Wennberg et al., 1999) compared with constrained photochemical model simulations using three sets of kinetic parameters: (1) JPL 00-3 (Sander et al., 2000) (red dashed lines); (2) allowing for near-IR photolysis of HO_2NO_2 based on cross sections and quantum yields from Roehl et al. (2001) (green dashed lines); and (3) allowing for near-IR photolysis of HO_2NO_2 and for a reaction probability of 0.8 for BrNO_3 hydrolysis (blue solid lines). After Salawitch et al. (2002b).

longward of 650 nm, which remains optically thin even for SZAs near 93°) (Wennberg et al., 1999).

Including a photolytic pathway for photolysis of HO_2NO_2 (peroxynitric acid) via excitation of purely vibration modes longward of 760 nm (the near IR) based on recent laboratory measurements of cross sections and quantum yields (Roehl et al., 2001), a process first suggested by Donaldson et al. (1997), leads to significant improvements in measured and modeled HO_x near twilight due to the rapid photolysis of HO_2NO_2 (Wennberg et al., 1999; Salawitch et al., 2002b) (Figure 3-28). The near-IR photolysis of HO_2NO_2 reduces calculated levels of this species, resolving a large discrepancy between standard model calculations and observations of HO_2NO_2 at high latitudes (Salawitch et al., 2002b). The lower calculated abundance of HO_2NO_2 also reduces the efficiency of the $\text{OH} + \text{HO}_2\text{NO}_2$ sink of HO_x , resulting in rather large (e.g., 20 to 60%) increases in 24 hour averaged HO_x for the high-latitude spring lower stratosphere and upper troposphere compared with models that neglect this process (Salawitch et al., 2002b). Nonetheless, the observed “morning rise” of HO_2 is still underestimated by a model

including near-IR photolysis of HO_2NO_2 . This discrepancy might be due to the actual rate of BrNO_3 hydrolysis proceeding at a faster rate than the JPL 00-3 recommendation, the presence of other twilight photolytic sources of HO_2 besides HOBr and HO_2NO_2 , less than 100% efficiency for production of H_2O from the $\text{OH} + \text{HO}_2\text{NO}_2$ reaction, or a systematic error in the measurements of OH and HO_2 (Wennberg et al., 1999; Salawitch et al., 2002b).

Balloonborne observations of OH , HO_2 , H_2O , and ozone obtained over Fairbanks, Alaska, also suggest important gaps in our understanding of several HO_x reactions (Jucks et al., 1998). Discrepancies between measured and modeled abundances of OH and HO_2 are reduced with a $\sim 25\%$ downward adjustment of the ratio of the rate constants for atomic oxygen ($\text{O} + \text{HO}_2$) and $\text{O} + \text{OH}$ and either a 25% reduction to the rate constant for $\text{OH} + \text{HO}_2$ (the primary HO_x sink) or a 25% increase in the HO_x production rate (Jucks et al., 1998). These modifications are within the uncertainties of the laboratory measurements and are consistent with the results of HO_x model/measurement studies discussed in the previous Assessment. The new insight provided by the simultaneous observations of OH and HO_2 is that the required modifications to the rate constants appear not to appreciably affect odd oxygen production rates in the upper stratosphere (Jucks et al., 1998).

3.2.4.3 SUMMERTIME Cl_y CHEMISTRY

The first in situ observations of ClONO_2 were obtained in the high-latitude stratosphere during the summer of 1997 (Stimpfle et al., 1999). These observations are in good agreement with values of ClONO_2 determined using a photochemical steady-state relation constrained by simultaneous observations of $[\text{ClO}]$ and $[\text{NO}_2]$ (the ratio of measured to modeled ClONO_2 is 1.15 ± 0.36). These results, together with a study that used balloonborne remote measurements (Sen et al., 1999), confirm the photochemical mechanism by which abundances of NO_x regulate the abundance of ClO in regions of the stratosphere that are NO_x -limited (i.e., mixing ratio of $\text{NO}_x >$ mixing ratio of ClO_x).

Simultaneous observations of ClONO_2 and HCl from a balloon (Sen et al., 1999) and the ER-2 aircraft (Voss et al., 2001) test our understanding of the kinetic processes that regulate the partitioning within the inorganic chlorine (Cl_y) family. Model calculations using JPL 00-3 recommendations agree extremely well with the balloonborne remote observations of both ClONO_2 and HCl (Figure 3-29), whereas the aircraft in situ measurements of the ratio $[\text{ClONO}_2]/[\text{HCl}]$ are ~ 55 to 60% lower than values based on a steady-state calculation (Voss et al., 2001). This dis-

crepancy has not been resolved and is the subject of ongoing investigations.

Simultaneous observations of the major inorganic and organic chlorine species in the summer polar stratosphere provide a test of the chlorine budget. The observed increase in the inorganic chlorine content (e.g., $\text{HCl} + \text{ClNO}_3 + \text{HOCl} + \text{ClO}$) of stratospheric air with decreasing N_2O , from both the ER-2 and MkIV, agrees well (differences less than $\sim 10\%$) with estimates of inorganic chlorine based on the observed disappearance of organic source molecules (Sen et al., 1999; Bonne et al., 2000) (Figure 3-29). However, the ER-2-based estimate of inorganic chlorine is $\sim 15\%$ less than the MkIV estimate for mixing ratios of N_2O below about 175 ppbv. This offset is probably due to differences in the measurements of ClNO_3 noted in the previous paragraph. These results extend the conclusions of the previous Assessment regarding the good quantitative link between abundances of inorganic chlorine species and their halogen sources to a new region of the atmosphere (i.e., polar summer) and to a new class of observations (i.e., in situ). These findings are particularly relevant for the discussion of the chlorine budget for the winter polar stratosphere (Section 3.2.3.1).

3.3 QUANTIFICATION OF POLAR OZONE LOSS: OBSERVATIONS AND MODELS

Quantification of the degree of chemical ozone loss in the polar stratosphere is hampered by the pronounced dynamically induced variability of the ozone layer in these regions in winter/spring. Precise quantification of the chemically induced contribution to observed changes in the ozone abundance are particularly difficult in the Arctic stratosphere, where the degree of ozone loss is smaller and the dynamic activity is more pronounced than in the Antarctic. Over the last decade a number of approaches have been developed to overcome these difficulties. Major challenges have been to (1) assess how reliable the results of these approaches are and, hence, how precise current estimates of the degree of Arctic ozone losses are, and (2) determine whether the degrees of ozone losses calculated by up-to-date chemical models agree with the observational results within the combined uncertainties of the models and the observations. The latter question is crucial to assess our current ability to make projections of future polar ozone losses in a potentially colder stratosphere.

Severe Arctic ozone loss has been reported for some recent cold Arctic winters. No significant loss was found during warmer winters. The large Arctic ozone losses result from increased levels of radical halogen

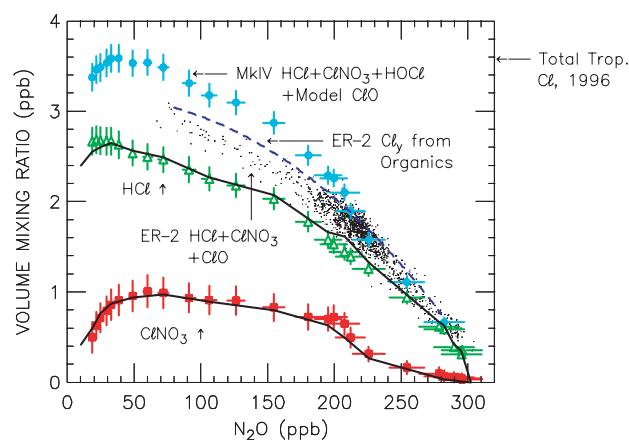


Figure 3-29. Measurements of chlorine species from balloon and in situ instruments during POLARIS. MkIV balloonborne measurements of the volume mixing ratio of HCl (green open triangles) and ClNO_3 (red solid squares) versus N_2O observed over Fairbanks, Alaska (64.8°N), on 8 May 1997 are shown, along with calculated values of HCl and ClNO_3 (solid black lines) found using a constrained photochemical model (Sen et al., 1999, updated for JPL 00-3 (Sander et al., 2000) kinetics). The dashed blue line shows an estimate of Cl_y based on ER-2 measurements of the organic source molecules during POLARIS (Sen et al., 1999). The sum $\text{HCl} + \text{ClNO}_3 + \text{HOCl}$ measured by MkIV plus calculated ClO (aqua solid dots) is also shown; calculated ClO makes a negligible contribution to this sum except for the highest altitudes (e.g., $\text{N}_2\text{O} < 50$ ppb) because the MkIV observations are obtained at twilight. Error bars for the MkIV measurements represent 1σ precision. ER-2 measurements of the sum $\text{HCl} + \text{ClNO}_3 + \text{ClO}$ are shown by the black dots (Bonne et al., 2000). Because the ER-2 observations are obtained at altitudes below ~ 20 km, species such as HOCl , Cl , etc., are estimated to make a negligible (e.g., < 20 ppt) contribution to the sum and are therefore neglected. Finally, the arrow in the right margin denotes the total chlorine content, 3.59 ppb, of the entire suite of tropospheric organic compounds for 1996 (WMO, 1999, Table 1-2).

species that result from heterogeneous chemical processing on the surface of polar stratospheric clouds (WMO, 1999; cf. also Sections 3.2 and 3.3.2 of this Assessment). Currently about 80 to 85% of the stratospheric chlorine is provided by the decomposition of anthropogenic organic chlorinated species (Zander et al.,

POLAR OZONE

1992, 1996; Gunson et al., 1994; Russell et al., 1996; Sen et al., 1999). Because the relevant ozone destruction cycles are linear to quadratic in the concentration of active chlorine, by far the largest fraction of the ozone losses discussed in this section is of anthropogenic origin. However, no quantitative study exists to precisely quantify the small degree of ozone loss that would be expected in a cold Arctic winter for natural levels of halogens in the stratosphere.

3.3.1 Approaches to Quantify Chemically Induced Ozone Loss in the Arctic

Two principal techniques are currently used to quantify chemically induced ozone losses in the Arctic:

- (1) Studies that take into account the effect of transport explicitly by using transport calculations based on meteorological analyses.
- (2) Studies that allow for transport effects implicitly by using the relation between ozone and a long-lived chemical tracer.

In the following, approaches that have been used in a consistent way for several winters are briefly assessed.

3.3.1.1 APPROACHES THAT USE EXPLICIT TRANSPORT CALCULATIONS

Bulk Advection

In this section, approaches are assessed that use explicit transport calculations to advect bulk quantities like vortex averages or gridded ozone fields and compare these with later measurements of ozone, a concept first published by Manney et al. (1994).

The “vortex average” technique involves analysis of the temporal evolution of the mean profile of ozone within the polar vortex on surfaces of potential temperature. Ozone measurements by ozonesondes (e.g., Knudsen et al., 1998; Rex et al., 1998; Lucic et al., 1999; Tzvetkova et al., 2002) or a remote sensing instrument, e.g., the POAM II satellite instrument (Bevilacqua et al., 1997) have been analyzed with this approach. The boundary of the polar vortex is usually defined by isolines of potential vorticity. Potential temperature and potential vorticity are conserved quantities in the polar stratosphere over time scales of a couple of weeks, so this coordinate system largely eliminates variability due to rapid and reversible dynamics. The slow irreversible descent of air across surfaces of potential temperature is usually accounted for by a diabatic correction calculated from descent rates using a radiative transfer model that is based on temperatures from a meteorological assimilation

system. In the absence of mixing across the vortex edge, changes in ozone can be attributed to chemical loss. The largest uncertainties connected with this approach are (1) possible mixing across the vortex edge, which may impact the average ozone abundance inside the polar vortex, (2) any time-varying bias in the sampling of the vortex, which may lead to changes in the derived vortex average, since ozone is not uniform within the vortex, and (3) uncertainties in the calculated diabatic corrections. Knudsen et al. (1998) used an approach based on domain-filling trajectory calculations to estimate the effect of mixing across the vortex edge for the Arctic winter of 1996/1997. For that winter, at the altitude of the maximum loss, they found an insignificant impact of mixing on the ozone loss derived from the vortex average technique.

In the “transport model” approach, a 3-D CTM is initialized with ozone observations during the early winter period. The model advects ozone passively, i.e., without chemical conversion, throughout the winter, using analyzed winds and, depending on the vertical transport scheme in the model, also temperatures. Ozone measurements throughout the winter are compared with the passively advected ozone. Evolving deficits between observed ozone and the model passive ozone indicate chemical loss. This approach has been used with the Reactive Processes Ruling the Ozone Budget in the Stratosphere (REPROBUS) model using data from the POAM satellite instruments and from the ground-based network of Système d’Analyse par Observation Zénithale (SAOZ) instruments (e.g., Lefèvre et al., 1998; Goutail et al., 1999; Deniel et al., 2000). Hansen et al. (1997), Guirlet et al. (2000), and Sinnhuber et al. (2000) have used this approach with the SLIMCAT model, using ozone lidar data, SAOZ data, and ozonesonde data, respectively. This approach relies on the assumption that the model transport scheme realistically represents the transport of air over a time period of several months. But when the derived ozone loss is averaged over the polar vortex, as is the case in many studies, the approach only depends on a correct representation of average transport properties like, e.g., vortex-averaged vertical subsidence and average rates of exchange of air across the vortex edge. Possible systematic errors in these average properties are the largest source of uncertainty in the transport model approach. Another source of concern is the initialization of the model ozone with data from a different type of instrument (usually measurements of the HALOE or MLS satellite instruments; see Appendix 3A for satellite data descriptions) than is used for the ozone observations later on. Systematic discrepancies between the different instruments make altitude-dependent correction factors necessary; these are often on the order of 5%, which is a substantial

fraction of the ozone changes observed over the course of warmer Arctic winters. The method is sensitive to the vertical variation of the correction, because early-winter measurements from one instrument at higher altitude are compared with late-winter measurements from another instrument at lower altitude.

Manney et al. (e.g., 1995a, b, 1996a, b, 1997) used a similar approach based on “trajectory ensemble” calculations to analyze ozone data of the MLS on the UARS satellite (see Appendix 3A for MLS data description). Trajectory calculations are started at all points on the gridded MLS data and are run forward in time for a few weeks. Succeeding MLS measurements are interpolated to the locations of the trajectories. The differences in ozone are attributed to chemistry. The results are stated as vortex-averaged ozone loss or are analyzed versus equivalent latitude, PV, etc. During the UARS north-looking yaw cycle, continuous time series of ozone loss can be derived, whereas only accumulated losses are stated across the south-looking yaw cycles, when measurements in the Arctic are not available. Schoeberl et al. (2002) advected ozone, using trajectory ensemble calculations initialized from early-winter ozone observations, over the course of the winter and then compared this early winter ozone with late-winter ozone observations. Again the advected and the observed ozone fields are averaged over the polar vortex before they are compared, thus reducing the sensitivity of the approach to transport features of individual air masses. The trajectory ensemble approach uses 3-D trajectory calculations that are several months long for the advection. Using trajectories instead of a grid-point advection scheme eliminates any potential bias due to numerical diffusion of the advection scheme. The largest uncertainty of the trajectory ensemble method comes from possible systematic biases in the long-term trajectory calculations, e.g., due to possible uncertainties in the vertical transport, which is based on calculated diabatic descent rates.

Lagrangian Ozone Measurements (Match)

“Match” is a Lagrangian technique to determine the rate of chemical ozone loss. In active Match campaigns, ozonesonde launches from a large network of about 35 ground stations are coordinated in real time to probe individual air masses twice over an interval of a few days (so-called “match events,” e.g., von der Gathen et al., 1995; Rex et al., 1997, 1998, 1999b, 2002a). The coordination is based on calculations of air parcel trajectories that allow for diabatic descent. Several hundreds to more than a thousand ozonesondes are launched in a Match campaign. The initial launch subsequently results in several

match events with later sondes at different altitudes. The coordination results in hundreds to thousands of match events per winter. Chemical ozone loss rates are derived from a statistical analysis of subsets of match events from a certain time period (typically 14 days long) and altitude region (typically 20 K broad) by calculating linear regressions of the difference in ozone between both measurements and the sunlit time that the air mass encountered. The overall ozone loss during the winter is calculated by accumulating the measured loss rates. Sasano et al. (2000) and Terao et al. (2002) have used a similar approach to analyze the ozone measurements from the ILAS satellite instrument (see Appendix 3A for ILAS data descriptions).

The largest uncertainties in this method are possible systematic errors in the trajectory calculations, including the calculated diabatic subsidence rates. Individual Match events depend on a correct representation of the motion of individual air masses by the trajectories. Therefore, the length of the trajectory calculations used in Match is limited to 10 days, and the majority of the Match events rely on ~5-7 days trajectories. But ozone loss rates are calculated in a statistical process from subsets of several tens of Match events, so that the derived average ozone loss rates are only sensitive to systematic trajectory errors, e.g., possible systematic biases in the calculated diabatic descent rates. A statistical analysis of the data shows that observed ozone losses occur exclusively during sunlit periods along the trajectories. This suggests that any systematic biases in the trajectory calculations, if present, are so small that they do not significantly affect the derived ozone loss rates (e.g., Rex et al., 1998, 1999b, 2002b).

3.3.1.2 APPROACHES THAT USE THE RELATION OF OZONE TO AN INERT TRACER

In midwinter, ozone abundances inside the polar vortex show a relatively compact relation to abundances of many long-lived tracer species such as nitrous oxide (N_2O) or methane (CH_4). In the absence of mixing, any reduction of ozone versus an inert tracer indicates chemical loss of ozone. This approach was first used by Proffitt et al. (1990). More recently, early-winter and late-winter measurements of ozone, N_2O , CH_4 , and HF by the HALOE satellite instrument have been used to identify chemical loss of ozone during various winters (e.g., Müller et al., 1996, 1997; see also Appendix 3A for satellite data descriptions). The evolution of the ozone-versus- N_2O relation through the winter of 1999/2000 was studied using data from in situ instruments onboard two balloon-borne platforms and the NASA ER-2 high-altitude aircraft (Salawitch et al., 2002a; Richard et al., 2001).

POLAR OZONE

Two fundamental issues affect the validity of the tracer relation approach. First, the existence of a compact universal relation between ozone and inert tracers has been questioned, and, second, the impact of mixing on results from studies of the ozone-versus-tracer relation has been discussed. Here we assess the current status of the discussion on these two points.

During polar summer the chemical lifetime of ozone in the middle and upper stratosphere is comparable with or shorter than transport time scales, so the ozone-tracer relationship in the Arctic stratosphere in fall is not expected to be compact and universal (Plumb and Ko, 1992). But in fall, the lifetime of ozone in the middle and lower stratosphere gets sufficiently long, and it can be expected that mixing within the early polar vortex leads to compacting of the ozone-tracer relations inside the vortex. These slowly evolving, more-compact relations inside the vortex are quite different from the extra-vortex relations, with less ozone inside at a given tracer level than outside. The degree of compactness and the definition of this inner vortex “early-winter relation” is critical for the validity of the tracer relation approach. Richard et al. (2001) and Salawitch et al. (2002a) used initial ozone-versus- N_2O reference relations measured well inside the polar vortex in midwinter (December/early-January). They showed that these relations were sufficiently compact and representative of initial conditions inside the polar vortex, an essential condition for the validity of the approach. But observations of the ozone-versus-methane relation measured well inside the Arctic vortex in midwinter for 1999/2000 were significantly lower (ozone differences of ~ 1.5 ppmv for values of $CH_4 = 0.5$ ppmv) than the suite of initial HALOE-based reference relations (Müller et al., 1999, and references therein) measured in the vortex edge region in October for earlier Arctic winters (Salawitch et al., 2002a). The validity of these early-winter HALOE reference relations is currently the subject of numerous ongoing investigations (see Appendix 3A for satellite data descriptions). Generally results from the tracer relation approach are more reliable when the initial reference relation is measured late (i.e., December/early-January) and deep inside the vortex.

The second issue brought up regarding the validity of tracer relation studies is related to mixing. These considerations apply also for studies that assess the degree of denitrification based on changes in the otherwise very compact relation between NO_y and N_2O . If the relation between two tracers is curved, as is the case for these species, the results of the tracer relation approach can be compromised by mixing between air masses that are widely separated in tracer space (e.g., Waugh et al., 1997; Michelsen et al., 1998; Rex et al., 1999a; Plumb et al.,

2000; Ray et al., 2002). Isentropic mixing across the edge of the polar vortex or mixing of air masses inside the vortex that underwent different descent during the winter are examples for such long-range mixing in tracer space. Furthermore, the ozone/tracer relations inside the vortex are different from the relations outside the polar vortex. After substantial ozone loss, these differences can be very pronounced (several ppmv). Hence, any mixing across the vortex edge directly impacts the ozone/tracer relation inside the vortex and could represent a potential source of uncertainty for the tracer relation approach.

One can attempt to distinguish mixing and chemical ozone loss (or denitrification) by using simultaneous measurements of two long-lived tracers (e.g., CH_4 and N_2O) to estimate the impact of mixing (Rex et al., 1999a). However, this method is dependent on the assumption that there had been a single mixing event after the bulk of the descent and is not applicable if there is intermittent mixing at descent (Plumb et al., 2000). A more general approach is the use of a linear combination of several long-lived tracers to form an artificial tracer that has a compact and linear relationship with ozone (or NO_y) (Esler and Waugh, 2002). Because of its linearity, this artificial relation is unaffected by mixing within the vortex, so deviations from this relationship can be more directly attributed to chemical ozone loss (denitrification). But mixing across the edge of the vortex edge is still a source of uncertainty, because the outside vortex relations are often different from the inside relations (for ozone versus N_2O this is always the case; for NO_y versus N_2O this is the case after denitrification inside of the vortex). These attempts to correct for the impact of mixing in tracer relation studies were mainly focused on studies that used the relation of NO_y versus N_2O to assess denitrification.

Salawitch et al. (2002a) noted that considerations that are valid for the NO_y -versus- N_2O relation (e.g., the relation χ_2 versus χ_1 in Plumb et al. (2000) resembles NO_y versus N_2O) should not be applied to the interpretation of the ozone-versus- N_2O relation in the vortex, because ozone mixing ratios, unlike NO_y , do not approach zero at the top of the vortex because of the influence of photochemistry at 40 km. Hence, the curvature of the ozone-versus- N_2O relation for low N_2O (i.e., N_2O between 10 and 40 ppbv) is much less pronounced than that of NO_y versus N_2O , and mixing cannot lead to the observed changes in the ozone tracer relations that have been observed e.g., by HALOE. More quantitatively, simultaneous measurements of multiple long-lived tracers have been used to argue that the impact of mixing on estimates of chemical ozone loss by the tracer relation approach for the Arctic winter of 1999/2000 was negligible. Based on

the temporal evolution of CO₂, CFC-11 (CCl₃F), N₂O, and ozone within the vortex, studies of Richard et al. (2001) and Salawitch et al. (2002a) demonstrated that the vast majority of the observed changes in the O₃/N₂O relations were due to chemistry and could not have been caused by dynamics. The isolation of the Arctic vortex for that winter was also noted by a multivariate analysis of the time evolution of nearly a dozen tracers with varying lifetimes (Ray et al., 2002). Rex et al. (2002a) showed that during January to March 2000, any mixing across the vortex edge would have led to an underestimation of the ozone loss by tracer relation studies, and therefore the results of tracer relation studies that rely on initial relations from early January can be regarded as conservative estimates of the loss. These results from the Arctic winter of 1999/2000 support the validity of the tracer relation approach, provided the reference relation is defined in midwinter, but it is currently not clear whether these results can be applied to other, more dynamically active winters (e.g., Salawitch et al., 2002a).

3.3.2 Arctic Ozone Loss During the Last Decade

Since the previous Assessment (WMO, 1999), a number of approaches to quantify the degree of chemical ozone loss in the Arctic have been used in a consistent way for several winters during the 1990s. Because of these long-term efforts, the extent and the variability of Arctic ozone losses are now well characterized for the last 10 years. Several techniques have revealed a large interannual variability of chemical ozone losses in the Arctic.

3.3.2.1 OZONE LOSS RATES NEAR THE MAXIMUM OF THE OZONE CONCENTRATION

The Match approach was used consistently over the last decade to study the evolution of chemical ozone loss at about 475 K potential temperature (~19 km altitude). At polar latitudes this level is close to the maximum concentration of ozone in the ozone layer. Figure 3-30 shows the measured ozone loss rates for the winters 1991/1992 to 2000/2001 (compilation of Match results based on Rex et al. (1997, 1998, 1999b, 2002a) and Schulz et al. (2000, 2001)). Little or no significant ozone loss was observed in 1997/1998 and 1998/1999. The accumulated ozone loss during the winter was particularly large in 1995/1996 and 1999/2000, when relatively large loss rates were sustained for extended periods of time. The chemical ozone loss rate in the Arctic stratosphere is clearly controlled by temperature. Blue shaded areas in Figure 3-30 indicate the geographical areas (A_{PSC}) where

temperatures have been below T_{PSC} (the NAT equilibrium temperature based on 5-ppmv water vapor and an average HNO₃ profile based on measurements; T_{PSC} is a convenient threshold that roughly indicates the onset of rapid heterogeneous chemistry in the stratosphere, independent of the actual composition of the PSCs). All periods of rapid chemical ozone loss in Figure 3-30 are associated with preceding large values of A_{PSC} . No significant chemical loss of ozone was observed in warm winters, when T_{PSC} was not reached or only barely reached.

3.3.2.2 VERTICAL PROFILES OF OZONE LOSS

The determination of vertical profiles of ozone loss requires quantification of ozone losses over a broad altitude range. Ozone loss observations are typically most reliable at levels around 475 K. Below 400 K or above 550 K the uncertainty of observational studies is typically significantly larger. The problems at lower levels are that (1) a strong vertical gradient in the average ozone mixing ratio profile largely amplifies the uncertainty introduced by diabatic descent, and (2) larger dynamical activity via synoptic-scale waves makes explicit transport calculations less reliable and leads to larger degrees of mixing, which is problematic for all approaches. Above 550 K, average poleward motion and influx into the polar vortex, followed by mixing, is the main problem. The strong diabatic descent at higher altitudes causes additional uncertainty only in winters when the vertical gradient in the average ozone mixing ratio profile is significant at these levels, which is not always the case (e.g., compare 1998/1999 with 1997/1998 in Figure 3-31).

Figure 3-31 shows ozone losses derived from the vortex average approach in the vertical region between $\Theta = 360$ and 570 K (update from Rex et al. (2002a) for various winters). Results at the lowest and highest levels shown are less reliable. It is based on several hundred ozonesonde measurements per winter inside the vortex from a network of about 35 sounding stations. The vortex-averaged ozone profiles have been plotted against the “spring-equivalent potential temperature” ($e\Theta$), which is the potential temperature that a given air mass reached at the end of March due to diabatic subsidence. Through use of $e\Theta$, which is a conserved quantity, diabatic effects are accounted for. In the absence of mixing across the vortex edge, any change in the vortex-averaged ozone versus $e\Theta$ profile indicates chemical loss of ozone. In Figure 3-31, the large interannual variability of the ozone loss stands out. During the winter of 1998/1999, no significant loss of ozone was found at any part of the profile. In contrast, the loss of ozone in 1999/2000 exceeded 70% in a ~1-km-thick region centered around 460 K. This local

POLAR OZONE

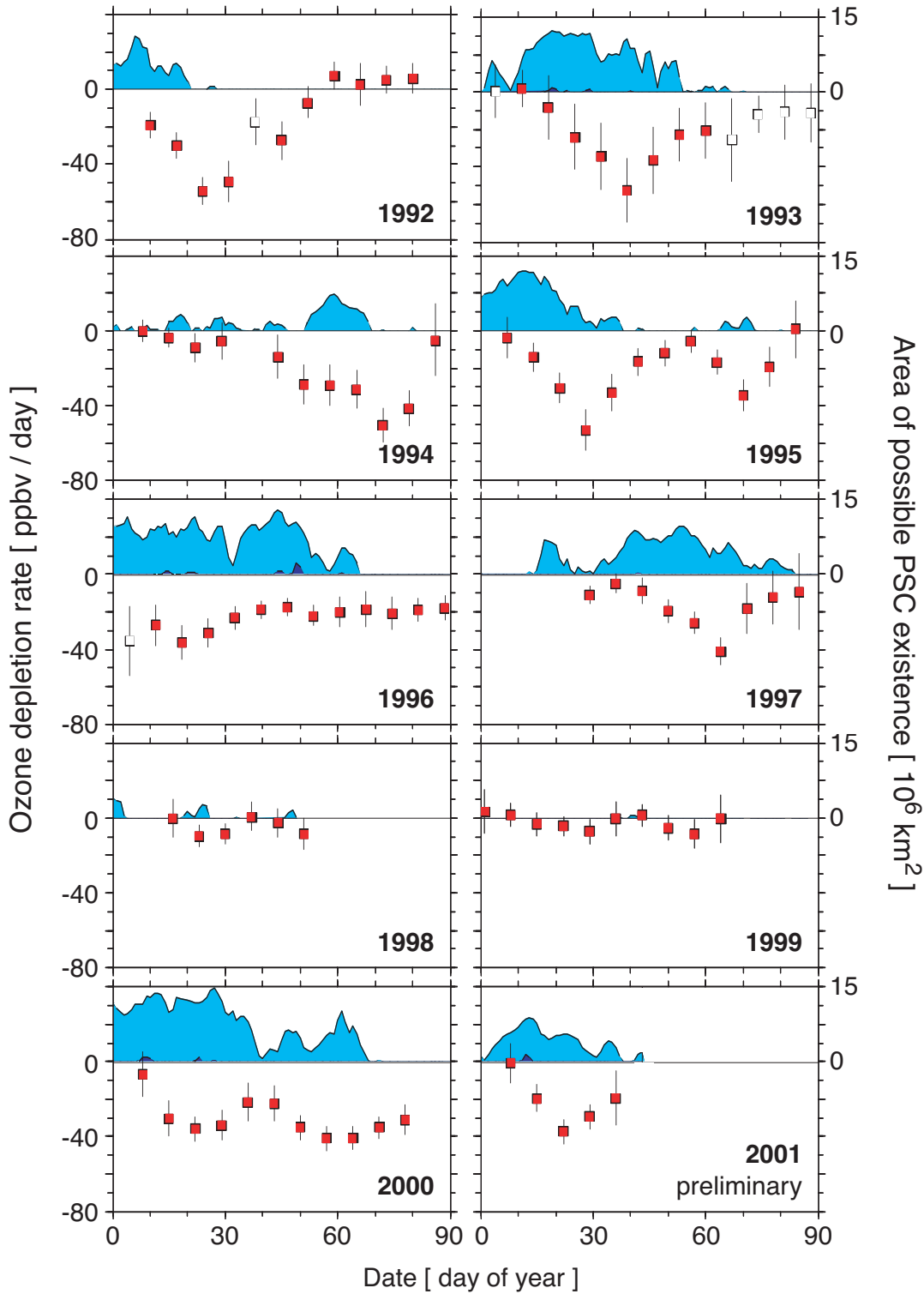


Figure 3-30. Ozone loss rates from Match at 475 K for various winters (squares) and A_{PSC} at 475 K (blue shaded areas). Red squares indicate 10 matches or more; white squares indicate fewer than 10 matches. Error bars are the 1σ errors of the fit of ozone differences (matches) as a function of sunlit time in the time period considered.

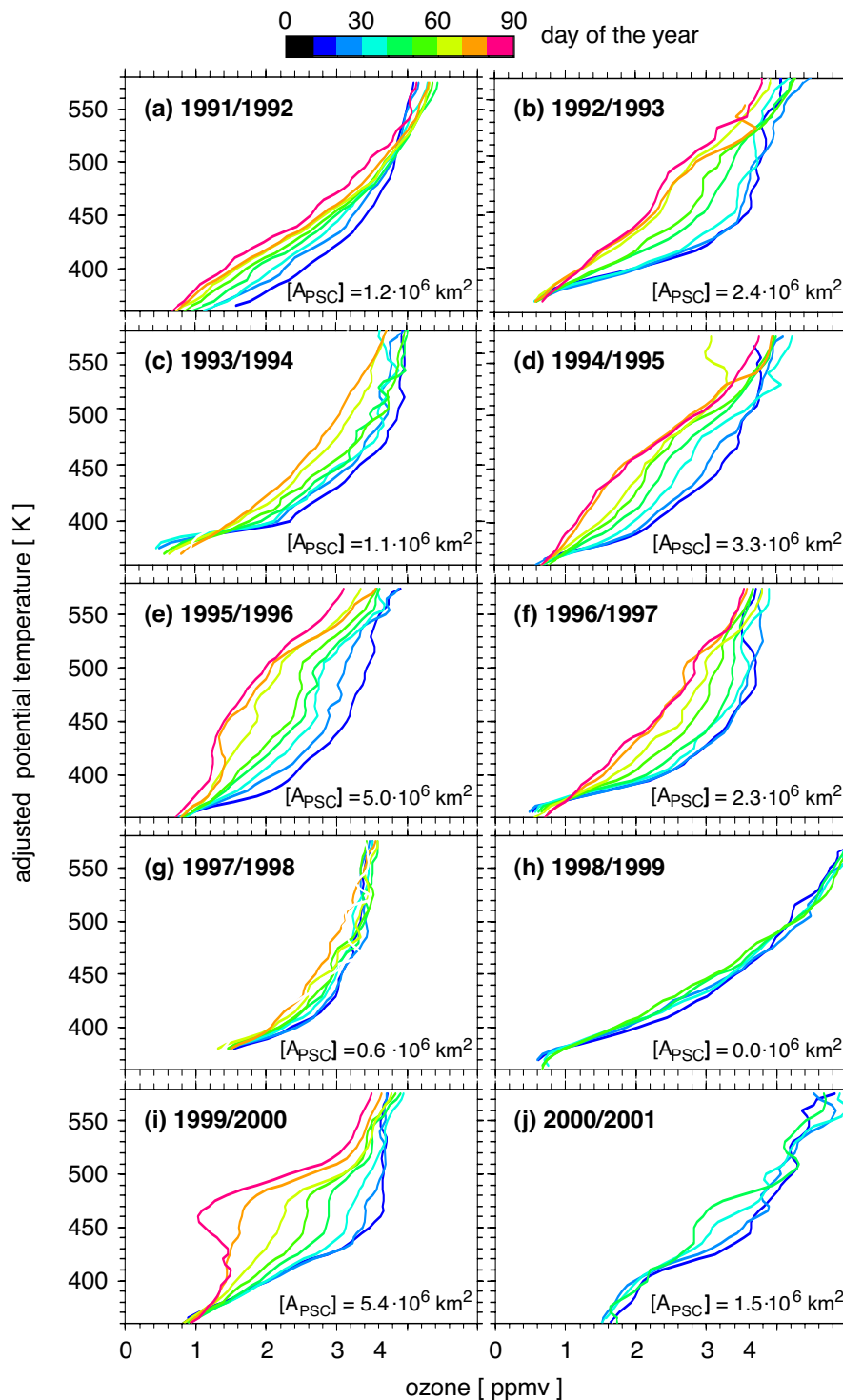


Figure 3-31. The evolution of the average ozone profile inside the Arctic polar vortex in spring-equivalent potential temperature ($e\Theta$) coordinates for various years; see text for a definition of $e\Theta$. The data from all ozonesonde measurements inside the vortex have been averaged into 10-day bins, centered around the day indicated by the color scale. The profiles typically rely on 20 to 50 individual measurements that, in most cases, sample the PV-space homogeneously. The average values for A_{PSC} ($[A_{PSC}]$) from 16 December to 31 March of each winter, between 400 and 550 K, are also given in each panel.

POLAR OZONE

loss is slightly more than in any previous Arctic winter, with 64% local loss in winter of 1995/1996 as the previous record. However, in 1995/1996, ozone loss occurred over a broader vertical region (e.g., ozone loss of more than 1 ppmv occurred between ~ 390 to 530 K in 1995/1996, compared with ~ 420 to 510 K in 1999/2000), and therefore the vertically integrated losses in both years are comparable.

The average value of A_{PSC} (denoted as $[A_{\text{PSC}}]$), averaged from mid-December to end of March between 400 and 550 K potential temperature, is given in Figure 3-31. Figure 3-32 shows the relation between $[A_{\text{PSC}}]$ and the average accumulated ozone loss between 400 and 550 K $e\Theta$. A surprisingly close quantitative relation between both quantities suggests that the chemical loss of ozone in the Arctic stratosphere in a given winter correlates strongly with the parameter $[A_{\text{PSC}}]$. The compactness of the relation shown in Figure 3-32 is currently not fully understood. Many mechanisms that influence Arctic ozone loss, e.g., the degree of denitrification, should correlate well with the parameter $[A_{\text{PSC}}]$. But other meteorological parameters, like the timing of low-temperature periods, which also impact the overall degree of ozone loss, are not expected to correlate with $[A_{\text{PSC}}]$. Figure 3-32 suggests that the effect of variability in these parameters has been relatively limited during the past decade. To reproduce the empirical relation shown in Figure 3-32 is a major challenge for global chemistry transport models.

The ability of models to reproduce the slope of the relation shown in Figure 3-32 is crucial, if models are to be used to predict the impact of climate changes on future ozone losses.

3.3.2.3 EFFECT OF OZONE LOSS ON THE TOTAL OZONE COLUMN

Estimating the total column loss of ozone also requires a good quantification of ozone loss in a broad vertical region. The region above 550 K is of less concern for ozone column loss estimates because it contributes little to the total column amount of ozone, due to the small ozone concentrations at these altitudes. But uncertainties in the ozone loss estimates at altitudes below 400 K make ozone column loss estimates generally less reliable than estimates of local ozone losses near 19-20 km. The ozone column loss has been estimated for all winters since 1993/1994 with the transport model approach. Figure 3-33 shows the difference between ozone columns as measured by the SAOZ UV-visible network in the Arctic (Ny Ålesund, Thule, Scoresbysund, Sodankylä, Salekhard, Zhigansk, and Harestua) and the column of passive ozone in REPROBUS (again, initialized with POAM measurements in early winter) above these stations. In many winters, large deficits of observed ozone compared with passively advected ozone have been observed. These deficits are attributed to chemical loss

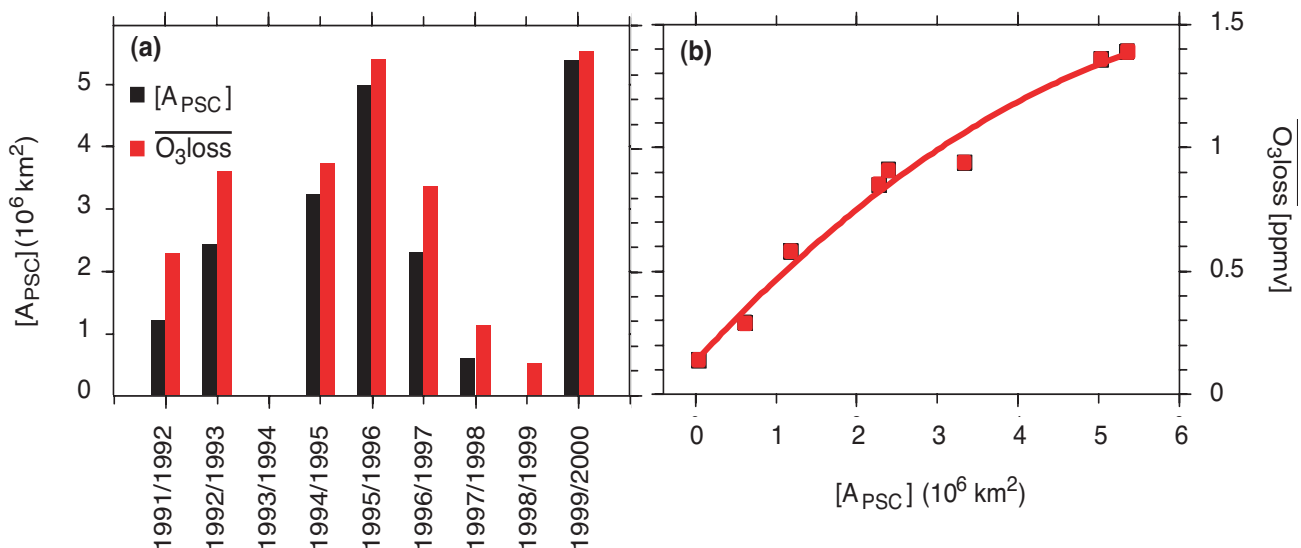


Figure 3-32. (a) Histogram of average values of A_{PSC} ($[A_{\text{PSC}}]$; black bars) and the average value for chemical loss of ozone from mid-January to the end of March, between 400 and 550 K (red bars). When the period of rapid ozone loss overlaps with the vortex break up, the vortex average approach cannot be used to estimate the overall loss of ozone. Those years (1994, 2001) have been omitted. (b) Scatter diagram of average ozone loss versus $[A_{\text{PSC}}]$.

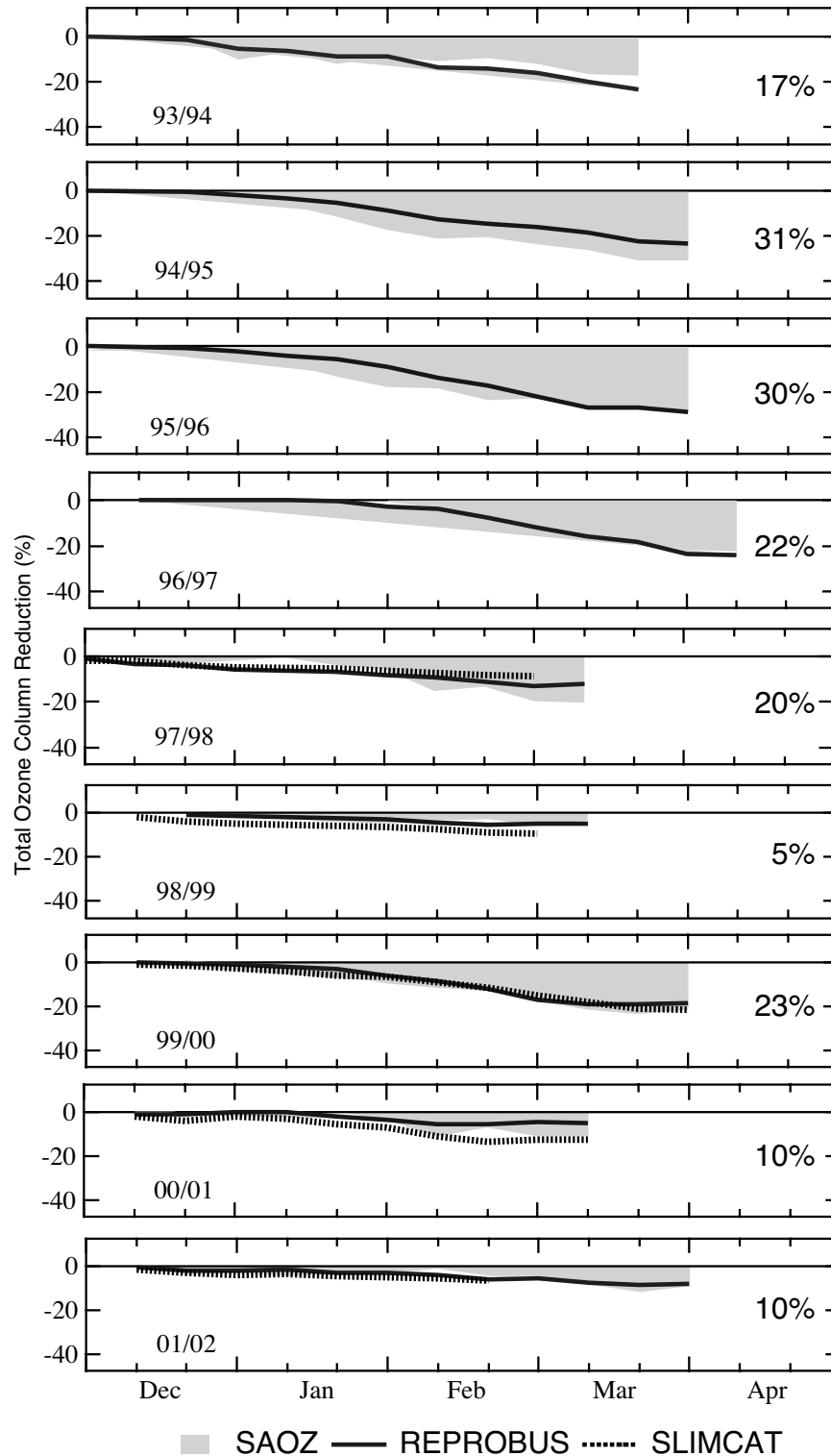


Figure 3-33. Total ozone reduction in the Arctic derived by comparing measurements of the SAOZ network (Ny Ålesund, Thule, Scoresbysund, Sodankylä, Salekhard, Zhigansk, and Harestua) with passive ozone in REPROBUS (gray shaded area) and modeled ozone losses (solid line, REPROBUS; dotted line, SLIMCAT). Written percentages on the right side of each panel are the cumulative SAOZ losses. Reproduced from EC (2001).

POLAR OZONE

of ozone. Associated with persistently low temperatures in the winters of 1994/1995, 1995/1996, 1996/1997, and 1999/2000, large chemically induced ozone reductions of 22 to 31% were observed inside the vortex. The ozone loss during the warmer winter of 1998/1999 was smaller and is hardly significant. In the relatively warm winter of 1997/1998, ozone column losses derived from the transport model approach were still significant (20%). In that winter, temperatures dropped below the PSC threshold only in very limited geographical regions inside the vortex and only during short periods (see Figure 3-30). From the vortex average approach (Figure 3-31) some limited ozone loss in 1997/1998 is also visible, but only below 450 K. During that year Match results at 475 K indicate no significant loss, but results for 450 K and below are not available from Match for that year.

3.3.2.4 CHEMICAL OZONE LOSS IN THE ARCTIC WINTER 1999/2000

The winter of 1999/2000 had the largest potential for PSC formation for at least the last 20 years. Because of the extensive SOLVE-THESEO 2000 campaign during the winter 1999/2000, all basic approaches outlined in Section 3.3.1 were used to study the ozone loss throughout the winter, resulting in a better characterization of the ozone losses in 1999/2000 than in any previous winter and providing a unique opportunity to compare results from the different techniques.

All approaches identified extensive chemical loss of ozone. Figure 3-34a shows the evolution of the vortex averaged ozone loss in a vertical section as determined with the Match approach. Ozone loss started at altitudes above 500 K in mid-January. The largest loss rates of 61 ± 4 ppbv per day (vortex average) were observed at 450 K in early March. Rex et al. (2002a) showed that the vertical structure and the time evolution of the observed ozone loss agree well with the vertical structure and the time evolution of observations of high levels of active chlorine. During the winter of 1999/2000 only approaches that are based on ozonesonde measurements, like Match and the vortex average approach, were able to capture the full extent of the ozone loss, i.e., cover the full altitude range of the loss and the time period from early January to late March in vertical resolution. Comparisons of the results with other approaches are possible for a slightly shorter period and focus on the region close to 450 K. Here the results of all approaches agree very well (see Section 3.3.3).

Figure 3-35 shows the impact of the cumulative ozone loss through the winter on the vortex-averaged vertical ozone profile at the end of March. In a layer of air

around 18 km altitude the degree of chemical ozone destruction reached 70%.

Table 3-2 gives an overview of various estimates for the deficit in the total column amount of ozone due to chemical loss of ozone. The numbers given are the difference between the actually observed column amount of ozone and the column amount of ozone that would have been present at a given day in the absence of chemical ozone loss, dynamics being equal. For comparable time periods the agreement between results from all approaches is within the error bars. The results from the SAOZ/transport model study are generally somewhat higher than the other approaches and have larger uncertainties. The results of the other approaches agree to better than 20%. Figure 3-34c shows the evolution of the total column loss from January through March, as determined by Match. By the end of March, the chemically induced ozone deficit amounted to between 90 and 100 DU. This is roughly the amount of total ozone that has been supplied to the polar vortex by dynamic effects during the same time, and therefore the total ozone column remained relatively constant during January to March (Rex et al., 2002a), which is in contrast to the natural, climatological increase of the Arctic ozone column during this season.

3.3.3 Consistency Between the Different Observational Techniques

Comparisons of the different approaches used to infer Arctic ozone loss are often hampered by the fact that the altitude range, horizontal extent (vortex definition), and time periods used in the various published works are different. These differences are partly unavoidable because of the constraints of the datasets used. But often the datasets can be reanalyzed for certain time periods and regions where they overlap, so that the results can be directly compared.

For winter 1999/2000 basically all approaches can be used to calculate the amount of ozone loss that occurred inside the polar vortex between 20 January and 12 March in the layer of air that subsided from about 475 to 450 K during that time. This subsiding layer of air is indicated in Figure 3-34a by the solid black lines. Figure 3-36 summarizes the accumulated ozone losses as determined for this layer of air with the various techniques. The average of the various estimates is 1.65 ppmv of ozone loss for this specific time period and vertical region. The results from all techniques are within $\pm 20\%$ of this value; all but two are within $\pm 10\%$ of the average.

The winter of 1999/2000 was characterized by relatively weak dynamic activity and perhaps less than average exchange of air across the vortex edge (see

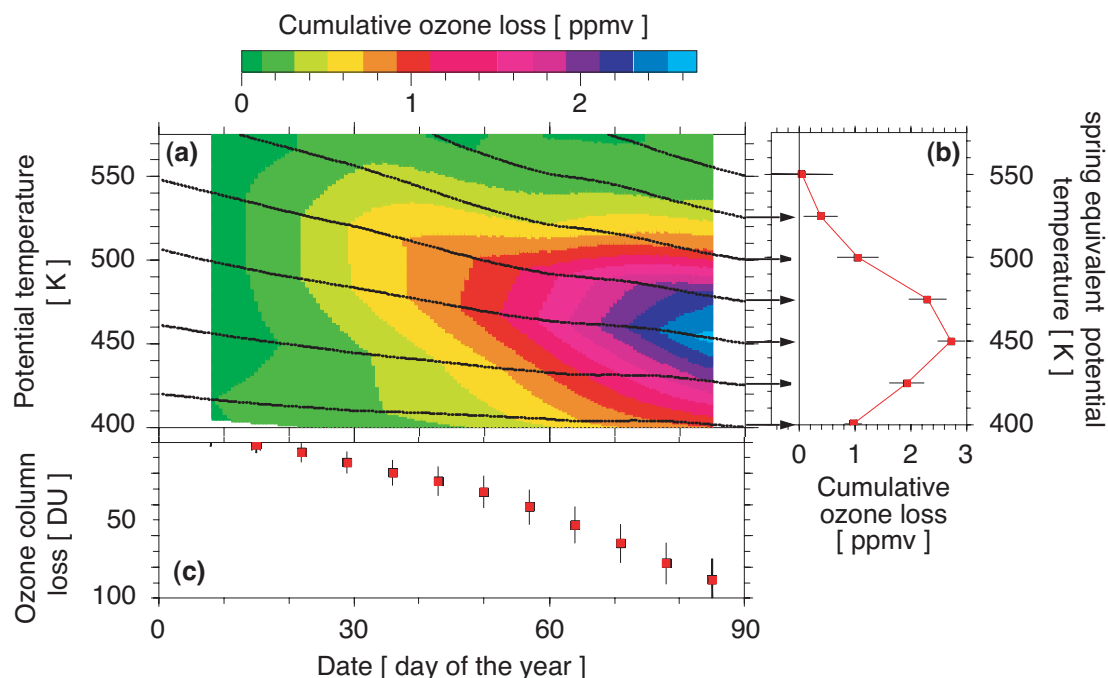


Figure 3-34. (a) Evolution of the cumulative ozone loss in subsiding air masses from Match for 1999/2000. The subsidence of air is indicated by the black lines (see text). (b) Profile of the cumulative ozone loss on 26 March 2000 from Match. (c) Accumulated chemical ozone loss in the partial column between $\theta = 400$ and 575 K from Match. Error bars are 1σ . Reproduced from Rex et al. (2002a).

Section 3.2.1). It is reasonable to assume that for the winter of 1999/2000 the agreement between different techniques to estimate the degree of chemical ozone loss from ozone observations may be better than for dynamically more active winters. However, to investigate this, Harris et al. (2002) reanalyzed data from past winters during the 1990s, using different techniques and datasets, focusing on time periods where the datasets overlap. On the basis of results from many winters, they found an agreement of generally better than 20% between techniques that use explicit transport calculations. Results from tracer relation studies showed slightly larger discrepancies compared with these results, when the initial tracer relation was measured early in fall. This agreement is 25% or better, when the initial tracer relation was measured in midwinter, e.g., in December.

On the basis of these studies, the results from current estimates of the degree of chemically induced Arctic ozone losses appear to have an accuracy of about 20%.

3.3.4 The Effect of Denitrification on Ozone Loss

The effect of denitrification on ozone loss has been quantified (to some extent) in both hemispheres. In the Antarctic (complete) denitrification is shown to cause a

10% increase in the column ozone loss (Brasseur et al., 1997; Portmann et al., 1996).

Evidence for a much more significant impact of denitrification (see Section 3.2.2.3) on Arctic ozone losses in recent cold winters has increased. Observational results indicate that the degree of ozone loss in the Arctic was significantly amplified by denitrification during the winters of 1994/1995, 1995/1996, and 1999/2000. Using model studies, Rex et al. (1997) concluded that in winter 1995/1996, observed ongoing chemical ozone loss in certain air masses more than 1 month after the last exposure to PSCs can only be explained by approximately 80% denitrification in about half of the air masses inside the polar vortex. In that winter the heavily denitrified layer of air was limited to a very narrow vertical region of less than 1 km thickness at about 20 km altitude.

Waibel et al. (1999) presented measurements of denitrification in the Arctic winter of 1994/1995, based on the NO_y -versus- N_2O relation, and used a chemical model to conclude that in the denitrified air masses the degree of ozone loss was enhanced by at least 30% compared with what would have occurred without denitrification. They show that the model results can come close to the observed ozone loss only when the observed denitrification is taken into account.

POLAR OZONE

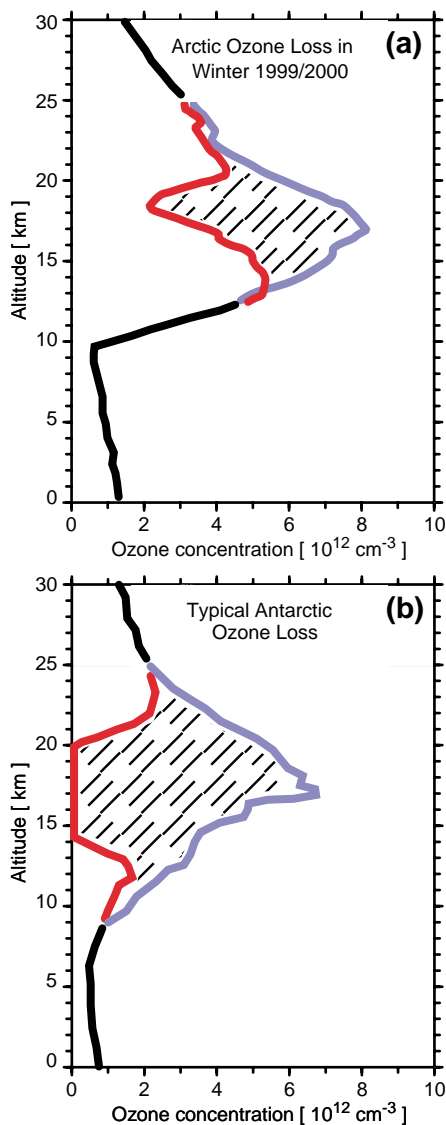


Figure 3-35. Comparison of ozone loss in the Arctic winter of 1999/2000 and typical Antarctic ozone loss. (a) Concentration profile of O_3 during late winter for observations from ozonesondes between 20 and 30 March 2000 in the Arctic (red). The profile of O_3^* (blue), the abundance of O_3 expected in the absence of any chemical loss, was estimated by allowing the early-winter vortex average O_3 profile from ozonesondes to descend by amounts based on cooling rates from the SLIMCAT model. For this calculation, the mixing ratio of O_3 was assumed to be conserved during descent and was converted to concentration in the last step. The profiles are shown for the altitude and pressure the air would have been at on 25 March. The difference between the profile of O_3^* and O_3 is hatched. This is an estimate, based on the vortex average approach, for the accumulated chemical loss of ozone during the winter. The black lines represent a typical late-March ozone profile above and below the vertical region where significant ozone loss occurred. Adapted from Rex et al. (2002a). (b) Illustration of the typical degree of ozone loss in the Antarctic. Typical midwinter (15 July 1997, blue) and late winter (13 October 1997, red) ozone profiles measured inside the Antarctic polar vortex at the Neumayer station at 71°S are shown. This panel is for illustration only, and no attempt has been made to correct for transport effects, which are weaker in the Antarctic compared with the Arctic. Poleward and downward transport between July and October supplies ozone to the Antarctic vortex, and therefore the hatched area in panel (b) is a conservative estimate of the chemical loss.

Table 3-2. Comparisons of chemical loss of column ozone, column [$O_3^* - O_3$] (see Rex et al., 2002a), inside the Arctic vortex for the winter of 1999/2000 as of the indicated date. N/A indicates that data for that date are not available.

Data Source	Method	Reference	Chemical Loss of Column Ozone (DU)		
			5 March 2000	15 March 2000	28 March 2000
OMS balloon	Tracer-tracer (O_3 vs. N_2O)	Salawitch et al. (2002a)	61 ± 14	N/A	N/A
HALOE	Tracer-tracer	Müller et al. (2002)	N/A	84 ± 13	N/A
POAM III satellite	Vortex-averaged descent	Hoppel et al. (2002)	51 ± 11	67 ± 11	N/A
SAOZ network	Transport model	EC (2001)	85 ± 24	98 ± 25	101 ± 30
Ozonesondes	Match	Rex et al. (2002a)	53 ± 11	71 ± 12	88 ± 13

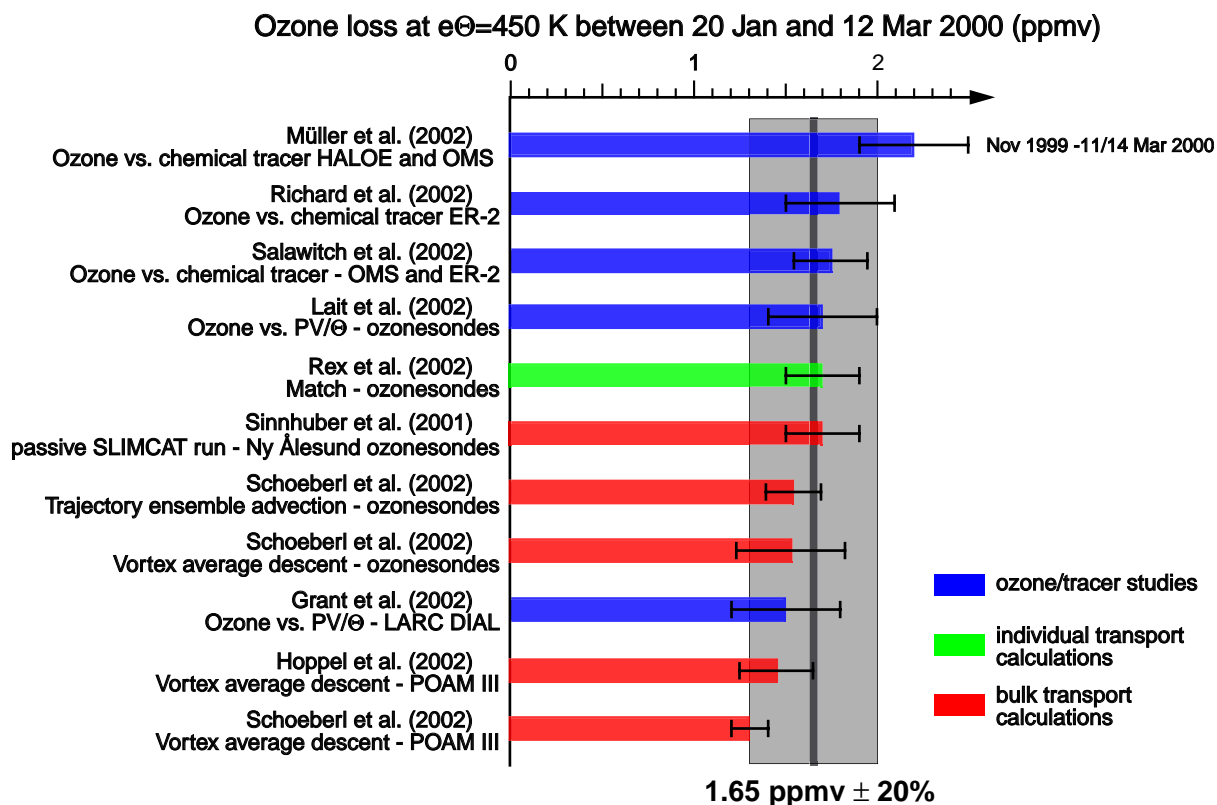


Figure 3-36. Overview of the results of various approaches to estimate the amount of Arctic ozone loss (ppmv) between 20 January and 12 March 2000. The results are stated for the layer of air that subsided from about 475 K at the beginning of the period to 450 K at the end. Results from studies that use the relation between ozone and an inert tracer are plotted in blue; studies that rely on bulk transport calculations are plotted in red; and results from the approach that relies on individual transport calculations are plotted in green. The error bars represent the 2-standard-deviation uncertainty of the loss estimate as estimated by the individual investigators. The average of the various estimates is 1.65 ppmv \pm 20%. (OMS = Observations of the Middle Stratosphere; LARC DIAL = NASA Langley Research Center Differential Absorption Lidar; other acronyms defined in text.) Based on Newman et al. (2002).

Gao et al. (2001b) present measurements of varying degrees of denitrification (also based on the NO_y -versus- N_2O relation) in different areas of the polar vortex, as characterized by fixed ranges of N_2O and potential temperature. Succeeding observations of the rate of ozone loss indicate largest loss rates at the N_2O levels that were most severely denitrified (about 30% larger losses than in less denitrified air). Gao et al. (2001b) show that these differences in the ozone loss rate cannot be explained by differences in solar exposure or initial chlorine activation and, hence, are most likely a result of the denitrification.

These observational studies have shown that denitrification in cold Arctic winters can cause up to a 30% increase in ozone loss at a given altitude, a result that is confirmed by model studies (Chipperfield and Pyle, 1998; Tabazadeh et al., 2000; Drdla and Schoeberl, 2002). The

more pronounced effect of denitrification on ozone loss in the Arctic, compared with the Antarctic, is the result of higher temperatures in the Arctic. In the Antarctic, reactivation of chlorine out of the reforming ClNO_3 reservoir via reactions on cold liquid aerosol particles (e.g., $\text{ClNO}_3 + \text{H}_2\text{O}$) can sustain a high level of active chlorine in spring (Portmann et al., 1996). This is much less effective in the Arctic, since the heterogeneous reaction of $\text{ClNO}_3 + \text{H}_2\text{O}$ is much slower at the higher temperatures typical for the Arctic spring. Therefore, the lifetime of active chlorine is strongly dependent on the rate of formation of ClNO_3 and, hence, the abundance of HNO_3 . The overall effect of denitrification on Arctic column ozone loss depends on the vertical range of severe denitrification. Currently, the effect of denitrification on Arctic ozone is limited to the altitude range of ~ 18 to 21 km, where most parcels are

POLAR OZONE

shown to be severely denitrified in cold winters (Hintsä et al., 1998; Kondo et al., 2000; Fahey et al., 2001). Microphysical studies have shown that the vertical range of severe denitrification in the Arctic lower stratosphere is very sensitive to the temperature (Waibel et al., 1999; Tabazadeh et al., 2001).

It is important to note that current denitrification schemes (e.g., in 3-D CTMs) have difficulties correctly representing the degree of denitrification in cold Arctic winters (e.g., Davies et al., 2002; see also Section 3.2.2.3). In light of the recent results showing that extensive denitrification (up to 80%) occurred in cold Arctic winters and that it had significant impact on the degree of ozone loss in those years, the correct representation of denitrification remains one of the major challenges for 3-D CTMs, when they are used to study the variability of chemical ozone loss in the Arctic (e.g., Chipperfield and Jones, 1999) or to predict future ozone losses in a potentially changing climate.

Dehydration, unlike denitrification, can moderate ozone loss for two reasons (Portmann et al., 1996; Chipperfield and Pyle, 1998). First, in a drier atmosphere it is harder for PSCs to form. Second, heterogeneous reaction rates that lead to active chlorine production drop exponentially with decrease in relative humidity. Sensitivity studies show that dehydration (to the level of ice saturation) in the Antarctic can decrease column ozone loss by about 20% (Portmann et al., 1996; Brasseur et al., 1997). No large-scale model calculations have yet been performed to evaluate the role that dehydration may play in Arctic ozone loss and recovery in the future. However, it is unlikely that climate change in the near future could cause extensive dehydration in the Arctic region. Some air mass trajectory statistical analyses indicate that even a substantial cooling of lower stratospheric temperatures (by 3 to 4 K) is still insufficient to trigger the occurrence of severe dehydration in the Arctic vortex (Tabazadeh et al., 2000).

3.3.5 Model Studies of Arctic Ozone Loss

Model investigation of polar ozone loss was the subject of intense research in recent years. Most studies concentrated on the Arctic region because of the high interannual variability of the Arctic ozone loss in relation to the year-to-year meteorological conditions. Three-dimensional CTMs, which proved to be particularly well fitted to the non-zonal character of the Arctic polar vortex, were used to estimate the overall degree of polar ozone loss for several winters. For more specific studies or highly constrained comparisons between models and ozone loss observations, photochemical box models were used.

3.3.5.1 CHEMICAL TRANSPORT MODELS

Studies using the transport model approach to estimate ozone loss from ozone measurements typically include a comparison with the ozone loss calculated by the chemistry module of the model. Chemical ozone loss inferred from the POAM II and III measurements was compared with that obtained from the REPROBUS model (Deniel et al., 1998, 2000). In the same way, total ozone measurements by the SAOZ network were compared with REPROBUS and SLIMCAT simulations for various Arctic winters from 1993/1994 (Figure 3-33; Goutail et al., 1999; EC, 2001). The agreement between the observed ozone loss and the model result varies from winter to winter. Two points can be seen in Figure 3-33. First, the overall interannual variability of the Arctic ozone loss is reasonably well represented by the models. The models reproduce a large fraction (about 60 to 100%) of the overall Arctic ozone loss. Second, in winters when substantial ozone loss was observed during January (1994/1995, 1995/1996, and 1999/2000), the models fall short of reproducing this January loss. Typically, by the end of January, only about 50% of the observed loss is accounted for by the models. The loss in January is partly why the overall loss at the end of the winter is sometimes underestimated (e.g., 1994/1995). In other winters the January loss contributes only a minor fraction to the overall loss (e.g., 1999/2000) or the model overestimates the loss rate later during the winter, and therefore the overall loss at the end of the winter is better reproduced than the time evolution of the loss (e.g., 1995/1996). Also, in 1995/1996 the simulated vertical distribution of the ozone loss at the end of March differs from that estimated from POAM II measurements, with the model resulting in larger losses at lower altitudes and smaller losses at higher altitudes compared with the observations (Deniel et al., 2000). It appears that a good agreement between observations and modeled total ozone loss at the end of the winter alone may be fortuitous and does not necessarily prove that the ozone loss mechanisms in the model are well reproduced.

Extensive modeling studies were performed as part of SOLVE/THESEO 2000 to estimate the ozone loss in the winter of 1999/2000. Sinnhuber et al. (2000) compared the chemical ozone loss estimated with SLIMCAT with that derived from the model ozone passive tracer and ozonesonde observations at Ny Ålesund (Figure 3-37). They found good agreement between the modeled ozone and observations, both indicating more than 2.5 ppmv ozone destruction by late March, corresponding to 70% ozone loss at the 450 K isentropic level, the largest ozone loss ever produced by SLIMCAT. The reason for the large loss of ozone in the model was extensive formation of

large denitrifying ice particles by the model's microphysical scheme. But the large-scale formation of ice clouds in the model was the result of a cold bias in the UKMO temperature fields used in SLIMCAT and is not consistent with observations during SOLVE/THESEO 2000. A later study performed by Davies et al. (2002) focused on the effect of denitrification on Arctic ozone depletion during the same winter using SLIMCAT and a denitrification scheme based on the formation of large NAT particles (see Section 3.2.2.3). When the model was forced by UKMO analyses, the ozone losses derived inside the vortex were very close to those derived by Sinnhuber et al. When ECMWF temperatures were used that were closer to observations in winter 1999/2000, the modeled active chlorine was in better agreement with ER-2 measurements, but the derived ozone loss was smaller than in observations and in Sinnhuber et al. (2002).

The KASIMA (Karlsruhe Simulation model of the Middle Atmosphere) CTM driven by ECMWF analyses was compared with ozone measurements by a Fourier transform infrared (FTIR) spectrometer and a millimeter wave radiometer in Kiruna for winter 1999/2000. The modeled total ozone loss underestimates the observations by 30% and 20%, respectively (Kopp et al., 2002).

The Langley Research Center (LaRC) Lagrangian chemical transport model (LCTM) was used in conjunction with HALOE and POAM III satellite observations to simulate the large-scale photochemical evolution of the Arctic vortex in 1999/2000 from a vortex ensemble of air mass trajectories using UKMO analyses (Pierce et al., 2002; see also Appendix 3A for satellite data descriptions). The model shows significant denitrification within the vortex in late December and early January. A significant overprediction of the level of chlorine activation is found in early March, but the predicted peak ozone loss rate is in good agreement with that inferred from the Match campaign during the same period. Conversely, it can be concluded that for a realistic level of active chlorine, the model would have significantly underestimated the observed ozone loss rate during that period.

Grooß et al. (2002) report simulations with the Chemical Lagrangian Model of the Stratosphere (CLaMS). This model simulates the dynamics and chemistry of multiple air parcels along their trajectories that are determined from ECMWF winds. The model includes mixing between neighboring air parcels. In this model study, the degree of denitrification was described from observations by using observed relations between NO_y and N_2O and the temperature history based on ER-2 measurements. The simulation was initialized on 10 February, and the ozone loss during the mid-February to mid-March

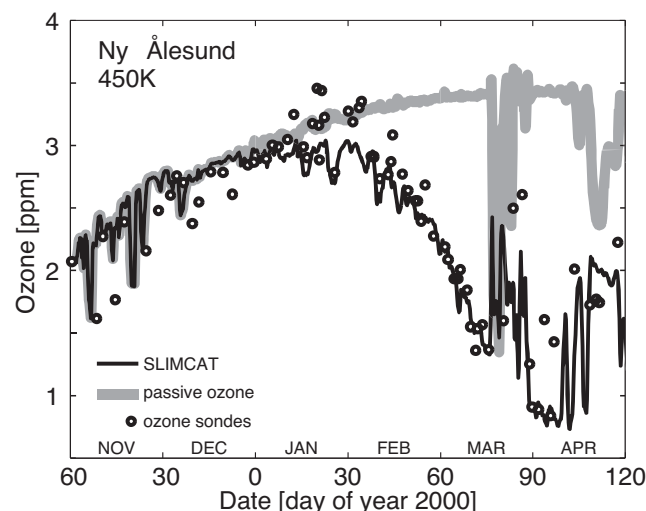


Figure 3-37. Ozonesonde measurements at Ny Ålesund (79°N) compared with the SLIMCAT three-dimensional transport model output for Ny Ålesund at the 450-K isentropic level. Ozone loss is indicated by the difference between the SLIMCAT's passive tracer (gray line) and SLIMCAT's ozone output (black line). Adapted from Sinnhuber et al. (2000).

period (up to 60% at 425 to 450 K) agrees roughly with estimates from observations.

The various 3-D model studies focusing on winter 1999/2000 reveal a consistent picture. The ozone loss after mid-February is well reproduced if the degree of denitrification in the model is correct, whether by coincidence as in Sinnhuber et al. (2000) or because it was specified from observations as in Grooß et al. (2002). Currently, 3-D CTMs are not able to reliably reproduce observed denitrification. This deficit limits the current ability to reliably reproduce the degree of ozone loss in cold Arctic winters.

3.3.5.2 SPECIFIC MODEL STUDIES

Several modeling studies using box models were conducted to compare specific ozone loss observations with model results and test our understanding of the chemical processes involved in the loss. These calculations are performed specifically for the air masses in which the ozone losses have been observed. Hence, the temperature and solar zenith angle history in these studies are much more constrained than in comparisons of vortex-averaged ozone losses. Becker et al. (1998, 2000) performed box model simulations along the trajectories of the Match dataset for 1991/1992 and 1994/1995. This analysis is illustrated in Figure 3-38, which compares the

POLAR OZONE

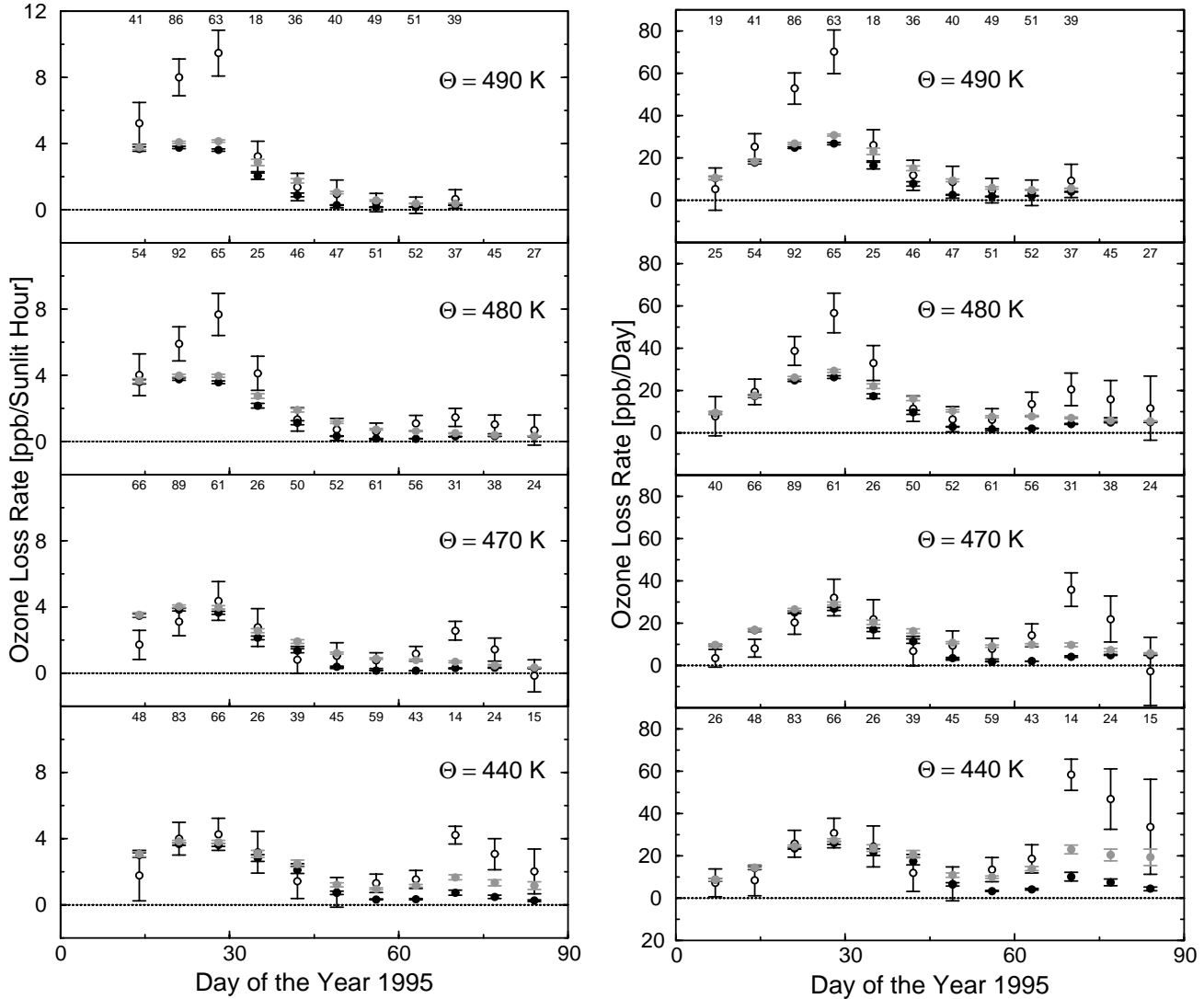


Figure 3-38. Time dependence of the ozone loss rates per sunlit hour (left panels) and the ozone loss rates per day (right panels) at various potential temperature levels in the 1994/1995 Arctic winter. Results of the Match analysis (open black circles) are compared with model results obtained with denitrification (solid gray circles) or without denitrification (solid black circles). Each point was deduced from Match trajectories with less than a ± 7 -day time interval and a ± 10 -K potential temperature interval. The number of matches contributing to each point is specified at the upper edge of each panel. The error bars correspond to the 1σ uncertainty of the linear regression.

ozone loss rates derived from simulations along the Match trajectories with the corresponding Match results at four potential temperature levels between 440 and 490 K for the winter of 1994/1995. It shows that the model underestimates the ozone losses observed by Match in late January by up to a factor of 2 above 475 K. During the other months, the observed losses are also underestimated by the model but within the large uncertainties of the model, mainly linked to the extent of denitrification. Match ozone loss rates were also compared with

SLIMCAT simulations for the winters of 1994/1995 and 1995/1996 (Kilbane-Dawe et al., 2001). The study suggests that Match may have overestimated the ozone loss rates above 525 K in January 1995 because of deficiencies in the ECMWF wind fields close to the top level of the ECMWF assimilation model (the top level has shifted to higher levels since then). In January 1995 at levels below 525 K and in January 1995/1996, SLIMCAT generally underestimated Match ozone loss rates by about 30 to 50%. It was found that the SLIMCAT photochemistry

was least able to reproduce observed ozone losses when low temperatures coincide with high solar zenith angles.

Woyke et al. (1999) used the tracer relation approach to quantify ozone loss in air masses that had been probed by a balloon payload providing observations of ClO, BrO, ozone, and long-lived tracers, on 3 February 1995. They used box model runs constrained by ClO and BrO concentrations observed by the balloon, to calculate the ozone loss throughout January along the back trajectories of the air masses. Using this highly constrained approach, they could explain only half of the observed ozone loss.

These results confirm that ozone losses observed during cold Arctic Januarys are currently not understood.

3.3.6 Quantifying Antarctic Ozone Loss

As emphasized in Section 3.1, Antarctic ozone depletion has been monitored by ground-based and satellite measurements since the mid-1980s. However, relatively few recent studies have concentrated on a detailed quantification of Antarctic ozone loss rates with state-of-the-art approaches to separate chemical loss from dynamical impacts. Hence, our quantitative knowledge of Antarctic ozone loss rates has not been as extensively tested as in the Arctic. The quantification of the accumulated overall ozone loss in the Antarctic is not challenging, because by the end of the winter, ozone is basically completely lost in a broad vertical region.

Hofmann et al. (1997) quantified Antarctic ozone loss from the analysis of 10 years of ozonesonde measurements at the South Pole and made recommendations for the detection of the recovery of the Antarctic ozone. Indicators for recovery include an end to springtime ozone depletion at 22 to 24 km and a 12- to 20-km ozone partial column value of more than 70 DU on 15 September. Bevilacqua et al. (1997) used POAM II ozone observations above Antarctica to derive vortex average ozone loss rates in August and September from 1994 to 1996 in the 450- to 800-K potential temperature range. Significant loss of ozone was found over the whole three-year period, except in 1994, when ozone loss was not observed in August, due to the sampling of the POAM instrument. The largest loss rates were found in September 1996 where they reached 0.1 ppmv/d below 500 K. From the analysis of the temporal evolution of total ozone at the Faraday station together with model calculations, Roscoe et al. (1997) showed that the ozone chemical depletion starts in June at the sunlit vortex edge, and Waters et al. (1999) showed that enhanced abundances of ClO are observed on the sunlit edge of the Antarctic vortex by late May or early June. Ozone loss rates were evaluated above the Antarctic station of Dumont d'Urville (66.4°S, 140°E)

from ozonesonde and lidar measurements on an interannual basis (Godin et al., 2001). Interpretation of the data required careful analysis of PV-equivalent latitude to determine whether each observation was inside, in the edge or outside the vortex at different isentropic levels. Measurements inside the vortex showed complete ozone destruction from 400 to 500 K, with ozone loss rates reaching 0.06 ppmv/d in the late-August to September period.

3.3.7 Model Studies of Antarctic Ozone Loss

The few recent model studies of the Antarctic ozone loss generally point to an agreement between models and observations. The SLIMCAT model was used to study the austral stratosphere in winter and spring 1996 together with ozonesonde measurements from various Antarctic stations (Lee et al., 2000). The model shows very good agreement with measured ozone values, and both the model and observations show that chemical ozone depletion follows the edge of polar night with little mixing poleward until the terminator reaches 80°S. In a follow-up study, Lee et al. (2001) analyzed the isentropic transport processes within the Antarctic polar vortex. Their calculations indicate two distinct regions within the vortex: a strongly mixed vortex core and a broad ring of weakly mixed air that remains isolated from the core between late winter and midspring and where the ozone loss is not complete. This result has an implication for the recovery of Antarctic ozone, since a cooling of the stratosphere could enhance the ozone loss in the edge region and delay the ozone recovery. In another study of Antarctic ozone loss, Wu and Dessler (2001) tested the current understanding of polar ozone chemistry with MLS version 4 measurements of ozone and ClO. By comparing the observed ozone loss estimated from the MLS ozone evolution at 465 K with a modeled ozone loss inferred from the simultaneous ClO measurements and a fixed BrO mixing ratio, they find a good agreement between both methods. However, MLS version 5 data, which has a better vertical definition of the ClO profile, resulted in a significant reduction of the ClO concentrations at 465 K compared with the version 4 data that had been used in Wu and Dessler (2001). This reduction would lead to a reduction in the modeled ozone loss rate in Wu and Dessler (2001). A slight change in the ozone profile in MLS version 5 data compared with version 4 data would also reduce the ozone loss rate deduced from observations. A quantitative study would be required to assess how the conclusions of Wu and Dessler (2001) would change if MLS version 5 data had been used (see Appendix 3A for MLS data description).

POLAR OZONE

3.3.8 Conclusion

Arctic chemical ozone losses during the last decade have been determined by a variety of approaches, and ozone loss rates are now better quantified in the Arctic than in the Antarctic. The uncertainty of state-of-the-art approaches to quantify Arctic ozone losses from ozone observations is below 20% for local losses between 400 and 550 K potential temperature and perhaps somewhat larger for total column loss estimates. Large interannual variability of the Arctic ozone loss, ranging from 0 to 70% loss at about 20 km for individual winters during the past decade, is driven by the variable extent of temperatures low enough for PSC formation in a given winter. Global CTMs reproduce a large fraction (60 to 100%, depending on the winter) of the observed ozone loss in the Arctic and its variability. The largest uncertainties are due to the current unrealistic representation of denitrification processes in 3-D CTMs and unexplained ozone losses during cold Arctic Januarys. These uncertainties currently prevent reliable predictions of future Arctic ozone losses in a potentially changing climate.

3.4 CAUSES OF POLAR STRATOSPHERIC TEMPERATURE TRENDS

3.4.1 Introduction

In the previous Assessment (WMO, 1999), it was recognized that the future development of the ozone layer does not depend just on changes in stratospheric halogen loading but also, very importantly, on a number of other factors connecting chemistry and climate. The observations of temperatures are discussed in Section 3.1.2, and the causes of trends in polar stratospheric temperatures are discussed here: the role of changes in well-mixed greenhouse gases (WMGHGs), ozone, water vapor, and aerosol particles are reviewed. Solar effects are also noted. The onset of low temperatures during the polar winter/spring, their duration, interannual variations, and the statistical significance of trends, over the past two decades, are issues that impact upon our knowledge of the chemistry-climate interactions and the detection and attribution of climate change in the polar stratosphere due to ozone and other greenhouse gases.

Observations, from radiosondes and satellites, have shown a general cooling of the polar lower stratosphere over the last few decades (WMO, 1999; Ramaswamy et al., 2001). For a number of reasons detection and attribution of temperature change in the lower stratosphere may be easier than at the surface (IPCC, 1996).

First, the observed temperature change in the stratosphere is large and the response time of the stratosphere is shorter, compared with the surface. There are relatively good satellite observations of both temperature and the important atmospheric constituents over the last few decades, corresponding to the timing of polar ozone depletion. There are also potentially fewer relatively uncertain mechanisms involved in stratospheric temperature change; many of the large and uncertain surface radiative forcings, such as the anthropogenic sulfate aerosol forcing, are expected to have a minimal effect on stratospheric temperatures. Further, the magnitude of the response in the stratosphere to a given mechanism has been shown to be reasonably well approximated by purely radiative processes, and therefore may be better quantifiable than the surface temperature response (Ramaswamy et al., 2001). However, the WMO (1999) ozone assessment acknowledged that the large variability of temperatures, particularly in the Arctic winter and spring, and a possible stratosphere-wide trend in stratospheric water vapor complicate the attribution issue. It is now recognized that ozone and WMGHG changes cannot be considered in isolation, and there is an increasing acknowledgement that it is important to attempt to quantify the feedbacks between temperature change, chemistry, and stratospheric dynamics, to understand better the stratospheric temperature response.

Since the previous Assessment there has been improved quantification of atmospheric constituent changes and development of more sophisticated stratospheric models, especially coupled chemistry-climate general circulation models. These have provided important insights into our understanding of polar temperature changes in the lower stratosphere.

This section uses the updated lower stratospheric high-latitude temperature trends (discussed in Section 3.1.2) and discusses the recent modeling efforts that have attempted to understand them. It concentrates on the analysis and understanding of past decadal-time-scale trends in the polar lower stratosphere; the upper stratospheric response is often more independent of latitude and is discussed in the global ozone chapter (Chapter 4).

3.4.2 Modeling Techniques

Several different types of model have been adopted for the study of stratospheric temperature change. Two types of commonly used models are briefly assessed here. Figure 3-39 compares the range of model results to observations, and Figure 3-40 shows individual model temperature trends.

3.4.2.1 FIXED DYNAMICAL HEATING (FDH) MODELS

Fixed dynamical heating (FDH) models and seasonally evolving fixed dynamical heating (SEFDH) models (WMO, 1999; IPCC, 2001) employ a method of calculating temperature changes using only a radiative transfer model. They have been shown to agree well with calculations using GCMs (Rosier and Shine, 2000; Ramaswamy et al., 2001), and, compared with these, they are generally faster and allow the use of more sophisticated radiative transfer schemes. In contrast to the FDH technique, SEFDH techniques include a calculation for the time evolution of temperature and have been shown to improve the temperature response in the high-latitude polar stratosphere, compared with GCM integrations (Forster et al., 1997; Rosier and Shine, 2000). This was a region where the equilibrium temperature response calculated with FDH models overestimated the cooling resulting from short-term polar ozone depletion. Both FDH and SEFDH techniques are unable to model the response of atmospheric dynamics.

3.4.2.2 GENERAL CIRCULATION MODELS (GCMs)

The GCM-Reality Intercomparison Project for SPARC (GRIPS) is currently performing an assessment of the performance of current middle-atmosphere GCMs (Pawson et al., 2000). Preliminary analysis of their results suggests that all models have a cold bias, at most levels in the troposphere and stratosphere, which may be indicative of errors in the radiative transfer, or input data (Pawson et al., 2000). This is particularly pronounced at the poles; one of the largest uncertainties remains the parameterization of small-scale gravity waves (see Sections 3.2.1.2 and 3.5.2.1). The upper boundary and vertical resolution may also be important for an accurate simulation (see Section 3.5.2.3). Because of large interannual variability, particularly in the Arctic temperatures (see Sections 3.1.2 and 3.5.2), either many transient integrations or many years of equilibrium experiments need to be performed for statistically significant trend calculations. It must be noted, however, that the real atmosphere has evolved through only one specific realization and that the global observational record spans only ~20 years. Experiments have been performed with both prescribed changes in atmospheric constituents and coupled chemistry-climate GCMs (discussed in more detail in Section 3.5). Although coupled chemistry-climate GCMs allow interaction between radiation, chemistry, and dynamics, they have two main drawbacks when attempting to attribute stratospheric temperature change to a particular cause. First, their complexity makes them

computationally expensive; it is therefore difficult to run them for long enough periods to produce statistically significant trends. Second, their simulation of the ozone change is imperfect; this is to be contrasted with GCMs that employ the ozone trends inferred from observations to determine the temperature response.

3.4.3 Causes of Polar Stratospheric Temperature Trends

This section assesses the role of different mechanisms on polar lower stratospheric temperature trends. A variety of recent model results are compared with the observed temperature trends (discussed in Section 3.1.2; see also Figure 3-9). Figures 3-39 and 3-40 summarize the findings for the lower stratospheric temperature response at 70°N and 70°S to (1) stratospheric ozone changes, (2) WMGHG changes, (3) combined changes in WMGHGs and stratospheric ozone changes, and (4) stratospheric water vapor changes. Annual and seasonal temperature trends are shown at pressures of 50 hPa and 100 hPa. Results are taken from studies by Ramaswamy and Schwarzkopf (2002), Rosier and Shine (2000; updated by M. Bourqui), Langematz et al. (2002), Smith (2001), Butchart et al. (2000), Shindell (2001), Austin (2002), Schnadt et al. (2002), and Forster and Shine (2002). Several factors affect the interpretation of the comparisons of the observations and model simulations presented in this section:

- (1) The satellite measurements comprise radiances from a range of altitudes. This introduces some uncertainty when model results at 50 and 100 hPa are compared with the satellite observations.
- (2) This section examines a single latitude belt in the polar regions where there is a large dynamical variability (see Figure 3-8).
- (3) The polar trends, especially for the winter/spring season, are influenced by the end-year considered for the analysis.

3.4.3.1 OZONE

The stratospheric cooling over Antarctica has been shown previously to be very well correlated with ozone losses (WMO, 1999; Randel and Wu, 1999a). Shine (1986) was the first to show that such a stratospheric cooling could be due to the direct radiative response of the ozone loss. GCM and radiative model studies since then have largely confirmed this early work (Mahlman et al., 1994; Ramaswamy et al., 1996; WMO, 1999). In the NH, studies have also found a correlation between

POLAR OZONE

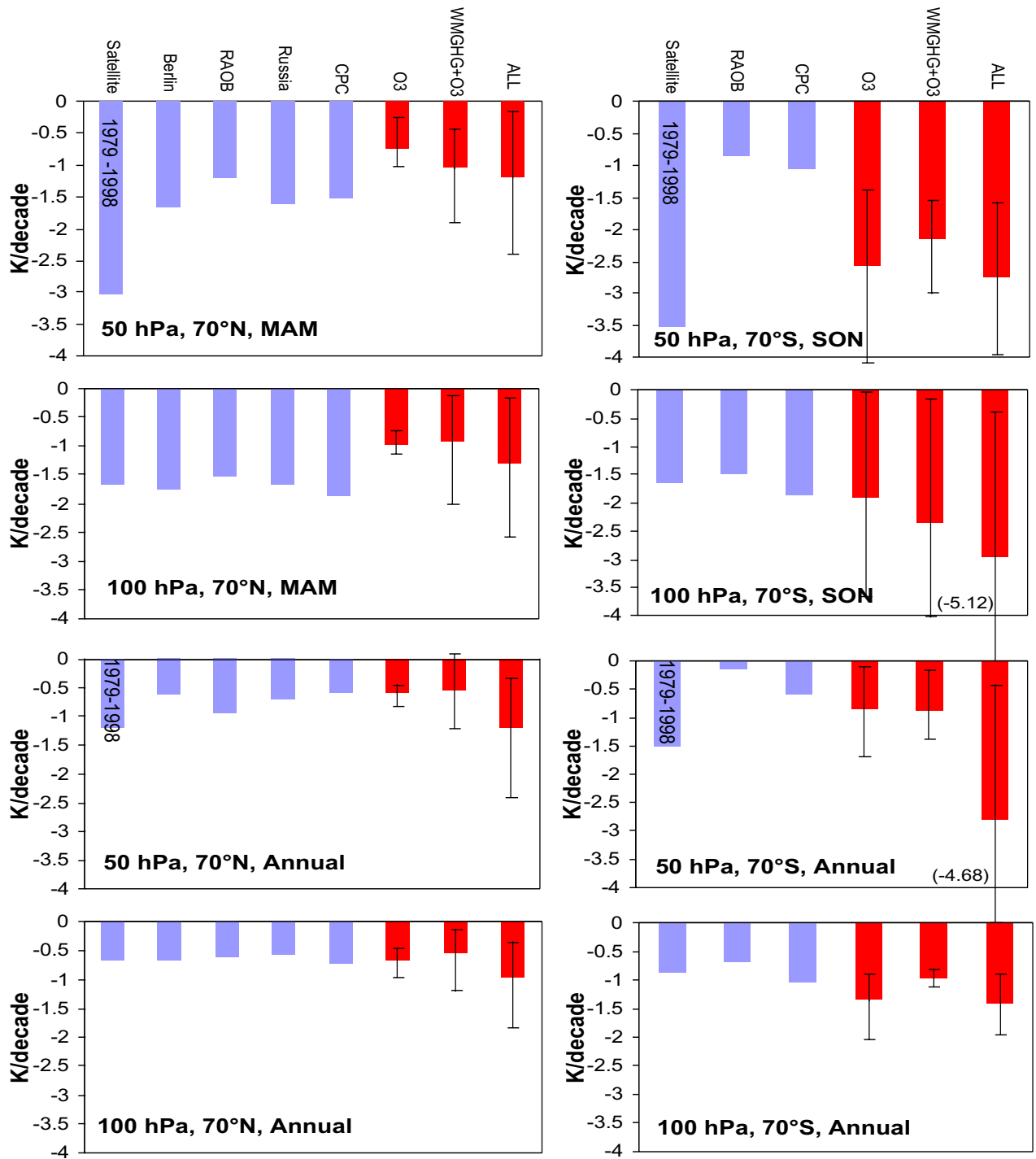


Figure 3-39. Comparison of observed and modeled temperature trends at 70°N and 70°S for the spring seasons and annual averages. Trends are presented at 50 hPa and 100 hPa. Observed trends are represented by blue bars and discussed in Section 3.1.2. All observed trends are significant at, at least, the 1σ level. The average modeled trends from Figure 3-40 are shown as the red bars with the range of model results illustrated by the black “uncertainty bars.” Model trends are shown for ozone changes alone, WMGHG and ozone changes, and “All,” where model estimates of the effects of stratospheric water vapor have been added to the WMGHG and ozone model trends. All observed trends are for 1979-2000 unless otherwise indicated (see Ramaswamy et al. (2001) for details regarding the observational datasets).

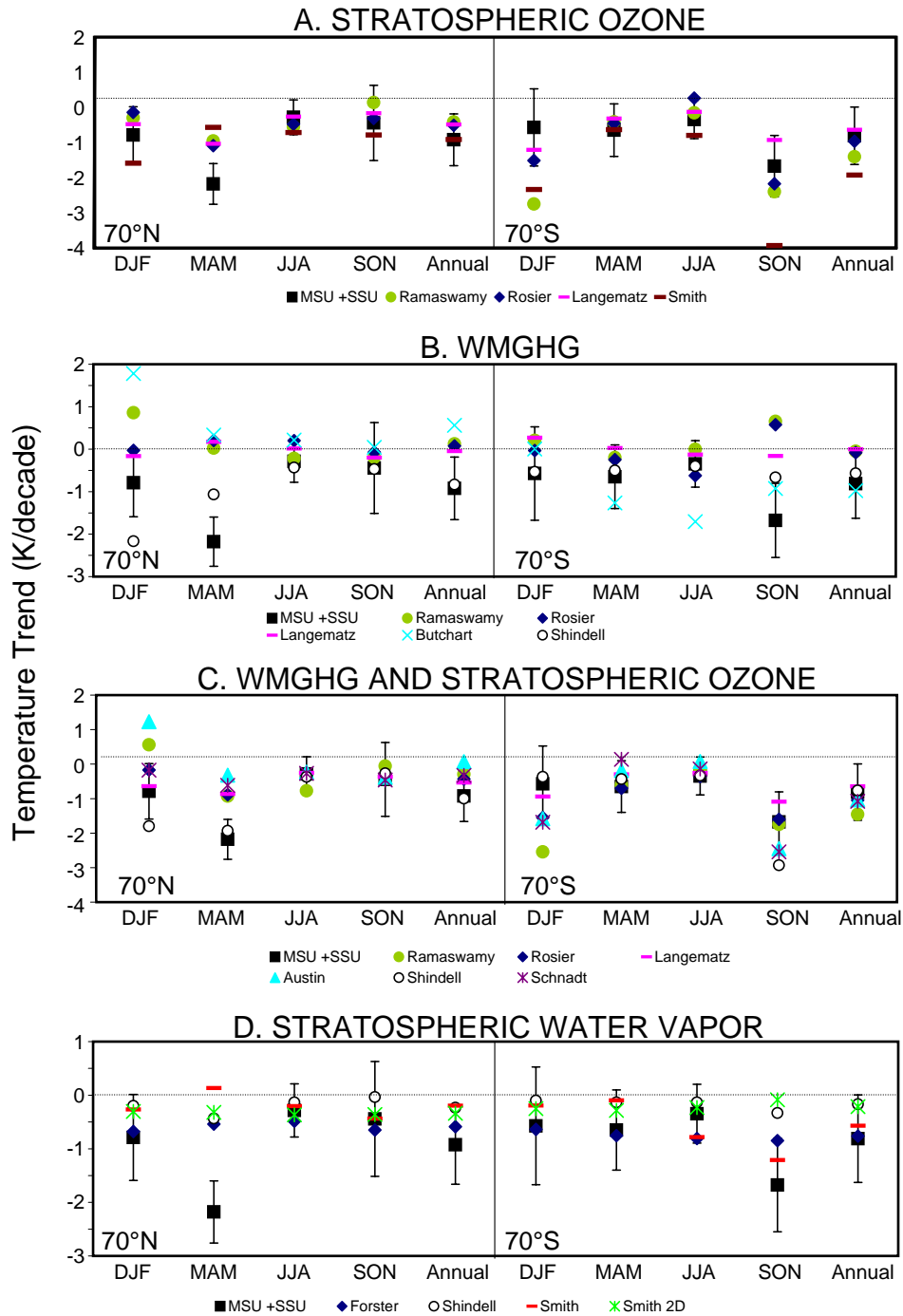


Figure 3-40. The seasonal and annual combined 50- and 100-hPa temperature trends at 70°N and 70°S, corresponding to one-third of the 50-hPa trend added to two-thirds of the 100-hPa trend, using the model-derived trends discussed in this section. The modeled temperature trends are for (a) stratospheric ozone changes; (b) WMGHG changes; (c) WMGHG and stratospheric ozone changes; and (d) stratospheric water vapor changes. On each panel, 2 error bars are plotted for the observed satellite trends, and the horizontal dotted lines indicate the zero trend. References for models are given in Section 3.4.3.

POLAR OZONE

springtime Arctic temperatures and ozone (WMO, 1999; Randel and Wu, 1999a). However, the correlations are not as strong, and the cooling observed during the Arctic winter is not expected from a simple radiative response to the ozone loss (Randel and Wu, 1999a). In addition, reductions of planetary wave driving reduce the strength of the residual circulation, leading to a cooling trend. This also weakens the transport of ozone-rich air to the polar lower stratosphere, and could give larger heterogeneous loss rates. Hence, a correlation of temperature and ozone does not necessarily imply a causal linkage of ozone loss with temperature.

Since the previous Assessment several studies have employed the monthly averaged vertical trend data, based on ozone observations over the period 1979 to 1997 (SPARC, 1998), with most studies employing the combined trend dataset of Randel and Wu (1999b). The results of these prescribed ozone change studies are shown Figure 3-40a for the NH (left panel) and SH (right panel). The calculations presented in the figure had the benefit of more detailed ozone-trend vertical resolution compared with previous work. The ozone dataset employs stratospheric-only trends derived from the Syowa (69°S) and Resolute (75°N) ozonesondes as representative of the polar regions. Figure 3-41 shows an illustration of the annual cycle of model-derived 100-hPa trends from the Berlin model and compares them with trends derived from reanalysis data. It is noted that trends from reanalysis data (Figure 3-41, panel c) must be interpreted with caution (Chapter 5 in WMO, 1999). The Antarctic and Arctic response are discussed separately below.

Antarctic

All model studies report an ozone-induced cooling at 70°S for most seasons, with the largest cooling in all models occurring in September, October, and November (SON) and December, January, and February (DJF) (right panel of Figure 3-40a). Langematz et al. (2002) and Ramaswamy and Schwarzkopf (2002) find that the largest cooling at 100 hPa occurs in DJF not SON (see Section 3.4.4). There is a dynamically induced heating in the middle atmosphere, which adds to the radiative heating owing to more upwelling longwave radiation initiated by the depletion of ozone in the lower stratosphere. This effect is simulated by several models (Kiehl et al., 1988; Mahlman et al., 1994; Ramaswamy et al., 1996; Rosier and Shine, 2000) and is consistent with observations (Ramaswamy et al., 2001), but it is not statistically significant, in either models or observations.

Compared with the observed trends, the Langematz et al. (2002) response underestimates the SON cooling at 50 hPa, but gives a better fit with the MSU-4 observations

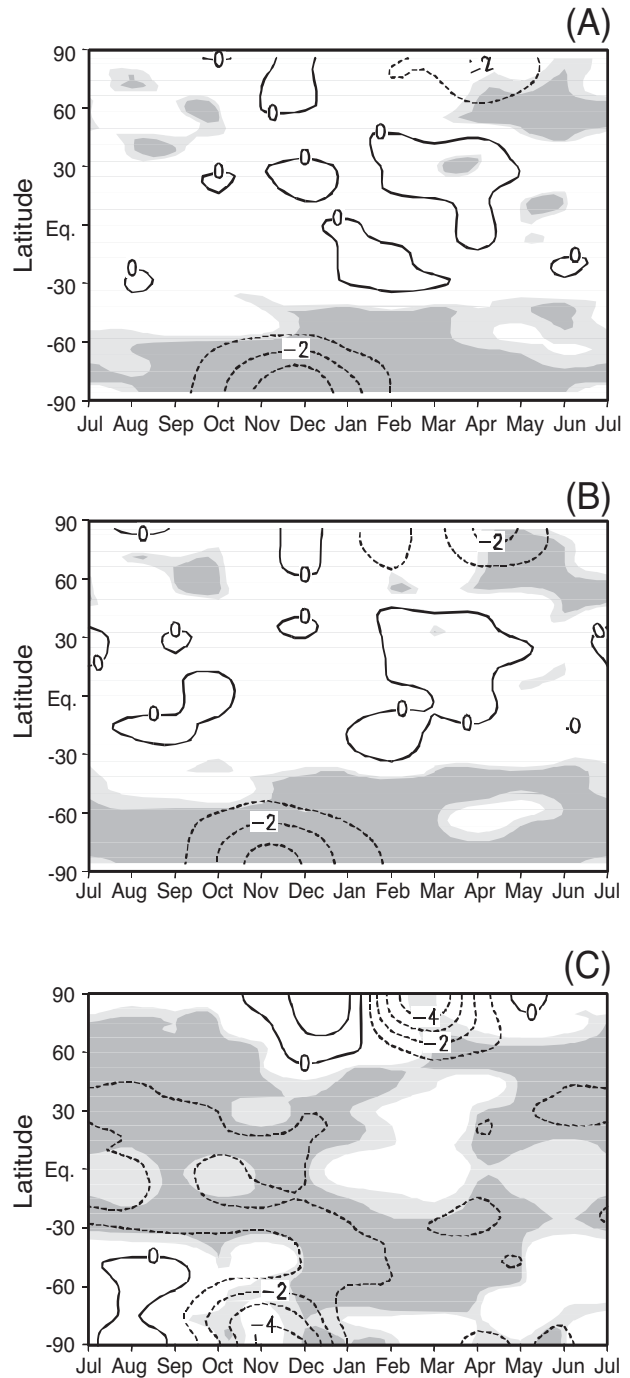


Figure 3-41. Annual cycle of the zonal-mean temperature trend (K/decade) at 100 hPa. (a) Model-derived trends employing the observed 1980 to 2000 ozone trend; (b) same as (a), but with an additional increase in CO₂; and (c) the corresponding 1980 to 2000 linear trend, derived from NCEP reanalysis data. The contour interval is 1.0 K/decade. Dark (light) shaded areas denote regions where the trend is significant at the 99% (95%) confidence level. Adapted from Langematz et al. (2002).

representative of 100 hPa. The other models tend to overestimate the observed spring and summer cooling at 100 hPa, particularly during DJF (see Section 3.4.4). Caution needs to be applied to this satellite-model comparison, because there are uncertainties with regard to the representation of the altitude profile of ozone loss in the models over the winter/spring period, and with regard to the interpretation of seasonal trends at 50 and 100 hPa from satellite data.

Two versions of the same model (Rosier and Shine, 2000, updated; Smith, 2001) produce substantially different trends in SON (Figure 3-40a). Both models are versions of the Reading Intermediate GCM performing 20-year equilibrium experiments. Differences between the simulations are also found in the Arctic (see below), which may imply a difference between the way the ozone trends are implemented and/or differences in the variability of the model.

Arctic

All four models in Figure 3-40a (left panel) find an annually averaged cooling in the Arctic. Three of the four models find the largest cooling in March, April, and May (MAM), which agrees qualitatively well with the satellite data. However, this modeled cooling is only about half the size of the cooling trend in the satellite data. Smith (2001), in contrast, finds a maximum cooling in DJF and smaller cooling in MAM, although differences again may be due to the large variability in the Arctic winter and are of limited significance. When comparing trends, Graf et al. (1998), Waugh et al. (1999), Langematz et al. (2002), and Ramaswamy and Schwarzkopf (2002) make the important point that the large natural variability in the Arctic may mean that the modeled and observed trends are not easily compared (see Figure 3-8).

3.4.3.2 WELL-MIXED GREENHOUSE GASES (WMGHGs)

In general, considering their radiative effects only, WMGHG increases are expected to have a much smaller effect on lower stratospheric temperatures than they do on temperatures above 30 hPa (Forster and Shine, 1997; WMO, 1999; Chapter 4 of this Assessment; Ramaswamy and Schwarzkopf, 2002). This is borne out by the results presented in Figure 3-40b for the NH (left panel) and SH (right panel). The Langematz et al. (2002) trend was derived for CO₂ changes only and has been estimated by taking the difference between the results of their stratospheric-ozone-and-WMGHG experiment and those of their stratospheric-ozone-only experiment. The same

method has been adopted in connection with the Ramaswamy and Schwarzkopf (2002) results. This is in contrast to the updated Rosier and Shine (2000) study where WMGHG effects were studied directly. Few of the modeling studies show significant temperature trends. Some models are seen to cool their annual-mean lower stratospheres in response to WMGHG increases. The magnitude of cooling (~0.3 K/decade) agrees with earlier FDH calculations (e.g., Ramaswamy et al., 2001). For further discussion on the role of WMGHGs in annual-mean trends see Chapter 4.

3.4.3.3 COMBINED CHANGES IN WMGHGs AND STRATOSPHERIC OZONE

Since the previous Assessment (WMO, 1999) several experiments with coupled chemistry-climate models have been performed for different time periods to simulate the combined effect of changes in ozone and WMGHGs. These experiments are discussed in more detail in Section 3.5. Here we only examine how the coupled chemistry-climate modeling studies influence the attribution of high-latitude temperature trends. Results from four coupled chemistry-climate experiments are presented in Figure 3-40c. Temperature trends are also shown for two different prescribed WMGHG and ozone experiments and the updated Rosier and Shine (2000) result, where individual ozone and WMGHG trends have been added.

Antarctic

The agreement between the different models in Figure 3-40c (right panel) is encouraging considering (1) the range of different models employed; (2) the differences between the responses, for models employing the same ozone trend dataset (Section 3.4.3.1); and (3) the large uncertainty in trends derived from transient integrations. Because the overall effect of WMGHG changes on lower stratospheric temperatures is minimal (annual-mean results in Section 3.4.3.2), there is little difference with respect to the annual-mean temperature trends from the stratospheric ozone experiments. Therefore, for all seasons the observed cooling can be explained by either combined WMGHG and stratospheric ozone changes or stratospheric ozone changes alone (see Figure 3-39). Most of the coupled chemistry-climate models and Ramaswamy and Schwarzkopf (2002) tend to overestimate the observed 50- to 100-hPa cooling in SON, although most results are still within the observational uncertainty range. Most of the models presented in Figure 3-40c (right panel) were found to simulate both the annual-mean and SON

POLAR OZONE

change at 50 hPa reasonably well, while all overestimated the 100-hPa trend (not shown). Austin (2002) found that the discrepancies in their model were consistent with systematic biases in the vertical profile of the applied ozone loss. Generally, the models capture Antarctic springtime cooling, but further improvements are needed to simulate the magnitude of the cooling and its vertical extent.

Arctic

The models for the Arctic, like those for Antarctica, are generally consistent with the observed trends, and inter-model differences are generally smaller than the 2σ uncertainty in the observations (left panel of Figure 3-40c). At 50 to 100 hPa, all models underestimate the MAM cooling, which could indicate (1) an underestimate of the ozone-related cooling; (2) a contribution of a missing effect, such as increases in stratospheric water vapor; or (3) an underestimate of the role of natural variability. Some models yield a warming in DJF that is in contrast to the observations, although this may be statistically insignificant in models. In the annual mean, only one of the models (a coupled model) is close to the observations; the rest underestimate the observed cooling.

3.4.3.4 STRATOSPHERIC WATER VAPOR

Since the previous Assessment, a major development has been the burgeoning interest in the role of stratospheric water vapor. Increases in stratospheric water vapor that are roughly twice the expected increase from methane oxidation have now been measured by satellite and ground-based observing systems (see Chapter 4 of this Assessment; Rosenlof et al., 2001; SPARC, 2000). Several recent papers have examined the consequences of this increase for stratospheric temperatures (see Figure 3-40d).

The study of Forster and Shine (1999) used an oversimplified representation of the water vapor change, in both the perturbation and background stratospheric water values (Forster and Shine, 2002) and, perhaps, in its radiative transfer scheme (Oinas et al., 2001). In general, inadequacies of broadband radiative transfer codes are readily accounted for (see Forster et al., 2001; Forster and Shine, 2002). Since the Forster and Shine (1999) study, Smith (2001) (see also Smith et al., 2001) used trends derived from HALOE data over the period 1992 to 1999 to represent better the water vapor change (see also Appendix 3A for HALOE data descriptions). Likewise, Forster and Shine (2002) used an improved representation of the background water vapor and a simulated +1-ppmv water vapor increase, derived from SPARC (2000) data. Shindell

(2001) also modeled the effect on increases in stratospheric water vapor, from methane oxidation, using a coupled chemistry-climate GCM. Although large uncertainties in the water vapor trend remain, these studies indicate a possible cooling of more than 0.5 K/decade at 70°N and 70°S, comparable with that due to ozone (Figure 3-40a). Given the present level of uncertainty in the observational trend analysis and notwithstanding the contribution of WMGHGs and stratospheric ozone to the cooling, one cannot rule out a significant effect due to stratospheric water vapor. There is an indication that a water vapor contribution is required for a quantitative accounting of the observed polar cooling (also see the discussion in Chapter 4).

3.4.3.5 SOLAR CHANGES

Following on from work discussed in the reviews of WMO (1999) and Ramaswamy et al. (2001), van Loon and Labitzke (2000) correlate the solar cycle with stratospheric temperatures and find that the “response” of the Arctic stratosphere depends on the phase of the QBO. During solar maximum, easterly phases of the QBO coincide with a cooler Arctic stratosphere, whereas westerly phases of the QBO give a warmer stratosphere. A model simulation (Cubasch and Voss, 2000) was unable to simulate this response, although their model did not include a modulation of ozone with ultraviolet radiation. Inclusion of this feedback affects the Arctic temperature response (Haigh, 1999; Larkin et al., 2000). Both these modeling studies found a warmer wintertime Arctic stratosphere during solar maximum. Recent studies with coupled chemistry-climate models (Williams et al., 2001; Labitzke et al., 2002) find increased sensitivity of lower stratospheric ozone to the solar cycle, compared with earlier modeling experiments, giving greater consistency with observations (see also EC, 2001). Generally, the latest modeling studies indicate a possible influence of the solar cycle on high-latitude temperatures. However, any effect is still too uncertain to quantify and remains somewhat speculative.

3.4.3.6 VOLCANOES

In the last 20 years the two large volcanic eruptions of Mt. Pinatubo and El Chichón created significant amounts of aerosol in the low-latitude stratosphere. Although several simulations show a low-latitude stratospheric warming, the response at high latitudes is less certain (WMO, 1999). Ramachandran et al. (2000) simulated the Mt. Pinatubo eruption in a GCM and found that the dynamical response to the aerosol forcing led to an

annually averaged cooling at high latitudes of up to 2 K for the 2 years following the eruption. Ramaswamy et al. (2002b) find that the high-latitude simulations of Mt. Pinatubo aerosol effects are affected substantially by the initial conditions in the model ensemble integrations. Timmreck et al. (1999) also found that volcanic aerosol caused a stronger Arctic vortex. Although both model and observations in the Mt. Pinatubo case indicate that polar effects were not statistically significant, the suggestion remains that volcanic eruptions may have contributed to the observed high-latitude stratospheric cooling. Following a volcanic eruption, enhanced ozone loss is expected from heterogeneous chemical reactions on the volcanic aerosol (see WMO, 1999). This ozone loss would cool the stratosphere. Pawson et al. (1999) postulate a stepwise decrease in stratospheric temperatures following volcanic eruptions that may be connected with changes in heterogeneous ozone chemistry (Solomon et al., 1998).

3.4.4 Timing of the Springtime Cooling Trend

Observational evidence shows that the maximum springtime stratospheric cooling trend occurs at roughly the same time as a maximum ozone loss (March in the NH and October–November in the SH (e.g., Randel and Wu, 1999a; see also Figure 3-9). However, most modeling studies of ozone loss and simple radiative arguments would suggest that the maximum cooling lags the ozone loss in the lower stratosphere by a month or more (see Figure 3.41a,b; see also Forster et al., 1997; Ramaswamy et al., 2001; Langematz, 2000; Rosier and Shine, 2000; Graf et al., 1998; Langematz et al., 2002). For example, in Antarctica a number of the models show approximately similar cooling trends in SON and DJF for their stratospheric ozone experiments (Figure 3-40). This is especially true of the 100-hPa level, where radiative relaxation times are longer. The NCEP reanalysis also hints at this feature (Figure 3-41, panel c). This feature is not observed in the satellite record. Graf et al. (1998) investigated whether WMGHG increases could compensate for this lag and found that they could not, at least in their model. Ramaswamy and Schwarzkopf (2002) find that the effects due to ozone and WMGHG over the period 1980 to 2000 in the northern polar region are swamped by the dynamical variability seen in both model and observations. The finding is probably true of the other models (Figure 3-40). Graf et al. (1998) further suggested that the discrepancy could be due to an incorrect modeling of the dynamical response and concluded that, until reasons for this are adequately resolved, it represents a problem in the attri-

bution, of particularly the Arctic cooling, to an anthropogenic cause.

3.4.5 Summary and Conclusions

Generally, modeling studies now demonstrate that the springtime cooling in the Arctic lower stratosphere over the 1980 to 2000 period is, in part, due to stratospheric ozone depletion, but the degree of attribution is hindered by the large dynamical variability in this region. In Antarctica, modeling studies reaffirm that ozone loss is the major cause of the springtime cooling. They also indicate that WMGHG and stratospheric water vapor increases are likely contributors to the annually averaged cooling.

For combined changes in stratospheric ozone and WMGHGs there is generally a reasonable agreement between the various modeling studies; inter-model differences are generally smaller than the uncertainty in observations (the 1σ uncertainty in the observations, if plotted on Figure 3-39, would be substantially larger than the plotted model error bars, which indicate the inter-model range). Including the effects of stratospheric water vapor in models improves the comparison with observations (the “All” scenario of Figure 3-39). However, there is still a large spread in model results, especially for the spring seasons. For the annual mean temperature change, both the agreement between models and the agreement between the satellite and sonde-based observations are encouraging (see Figure 3-39 and Chapter 4).

In summary the cooling of the springtime high-latitude stratosphere is likely influenced to a substantial extent by various mechanisms (WMGHG increases, ozone loss, stratospheric water vapor increases, volcanic eruptions, and natural variability). Attribution of polar temperatures is hampered by the large variability in the polar vortices (see Figure 3-8). This variability not only increases the uncertainty of observational trend analyses, but it also means that either many years of equilibrium studies or many ensemble integrations are needed for reliable statistics. Further, it implies that model studies performed under equilibrium conditions may be inadequate for examination of polar trends, especially in the Arctic, over a time period of two decades. At present, 20 years of an equilibrium GCM run are barely sufficient to resolve temperature changes in the Arctic winter. This would imply that 20-plus-member ensembles would also be needed for transient integrations. Comparison between observations and models, or between different models, is also complicated by uncertainty in the vertical profile of ozone loss, which leads to uncertainty in the temperature response. In models that simulate the chemistry, this

POLAR OZONE

uncertainty could be larger than in those models that prescribe the ozone loss from observations. These coupled-chemistry models are discussed in the next section.

3.5 CHEMICAL-CLIMATE MODELING OF THE PAST AND FUTURE POLAR STRATOSPHERE

3.5.1 Introduction

Section 3.3.2 shows that, while there has been halogen-induced chemical ozone loss in many recent Arctic winters, the extent of this chemical loss in a given year is determined by the meteorological conditions, with severe ozone loss in the colder winters and essentially no loss in the warmer winters. Thus, low temperatures are required to initiate wintertime chemical ozone loss in the Arctic, and the time series of Arctic ozone shown in Figure 3-2 reflects the changes in meteorology much more than it does the changes in halogen loading. This understanding is consistent with the conclusion of Section 3.4.3 (see also Rosier and Shine, 2000; Langematz, 2000) that the observed decrease in Arctic temperature over the last two decades cannot be explained just as a radiative response to the observed ozone decrease (although there is a contribution), and must have occurred for some other reason. In this respect the Arctic is quite different from the Antarctic. In the Antarctic, wintertime temperatures are low enough to initiate severe chemical ozone loss every year, and meteorological variability provides only a small modulation of this loss. The time series of Antarctic ozone shown in Figure 3-2 therefore primarily reflects changes in halogen loading, and the observed late-spring cooling and increased persistence of the Antarctic vortex are understood to be a radiative response to the observed ozone decrease (Section 3.4.3). That this Antarctic cooling is less than the observed Arctic cooling, despite the fact that Antarctic ozone losses are much greater than those in the Arctic, provides further confirmation that the Arctic cooling is a driver of the Arctic ozone decreases (in the presence of anthropogenic halogens), rather than being a response to them.

The difference between the past behavior of Arctic and Antarctic ozone has implications for the future evolution of polar ozone. In the Antarctic, meteorological conditions are so far past the threshold for severe chemical ozone loss that neither natural meteorological variability nor WMGHG-induced climate change are expected to change this situation over the coming decades. Thus, future Antarctic ozone levels are expected primarily to reflect the anticipated decrease in stratospheric halogen loading, as they have reflected the observed increase in

halogen levels in the past. (There is the possibility of more sensitivity for aspects of Antarctic ozone that are closer to threshold conditions, such as ozone losses at the edge of the vortex or in early summer; these may be of more importance for UV impacts than minimum column ozone amounts.) In the Arctic, on the other hand, our expectation for future ozone changes depends on our attribution of the past changes, and in particular on the cause of the observed Arctic cooling over the past two decades. If this cooling represents a forced response to WMGHG changes, then we would expect it to continue in the future and Arctic ozone levels would be expected to decrease further in spite of the decreasing halogen loading. If, on the other hand, the observed cooling represents natural variability, then anything is possible in the future; chemical ozone loss in the Arctic could be essentially zero for the next decade, or it could be severe.

The implication of the above considerations is that we cannot expect future Arctic ozone abundances to follow stratospheric halogen loading, apart from the obvious fact that halogen-induced chemical ozone loss can be expected to become negligible when halogen levels become negligible. Instead, the evolution of Arctic ozone abundances (which reflect both chemistry and transport) will be determined primarily by the evolution of meteorological conditions. In the Arctic, those meteorological conditions are largely determined by dynamical processes (Section 3.2.1), and the effects of WMGHG changes on the lower stratospheric Arctic vortex over the past and through the next few decades are expected to mainly arise from dynamical feedbacks, rather than from direct radiative forcing (Section 3.4). Therefore, in order both to attribute past behavior and predict future behavior of Arctic ozone, it is necessary to use models that are capable of representing those dynamical feedbacks together with a prognostic representation of ozone, namely, coupled chemistry-climate models.

It is important to appreciate what such models can and cannot do. In this respect there is a notable contrast with the CTMs used in Section 3.3. CTMs specify the meteorological conditions (winds and temperatures), and predict the resulting chemical ozone loss without addressing the issue of why those conditions occurred. This prediction is essentially deterministic, because the chemical equations are essentially deterministic; we expect to capture the exact chemical ozone loss on a particular day, within the uncertainties of the calculation. Coupled chemistry-climate models specify the radiative and chemical forcing (WMGHGs, halogens, surface conditions) and predict the resulting state of the chemistry-climate system. However, since the climate system is chaotic and exhibits unforced variability, this prediction

is only stochastic, not deterministic; we do not expect to capture the exact state of the chemistry-climate system on a particular day, or even in a particular year. Therefore, the comparison between such models and observations requires careful thought. On the other hand, chemistry-climate models allow one in principle to draw unambiguous conclusions about the attribution of past changes, and they are the only tool available for prediction of future changes that includes all physical feedbacks.

There are two distinct strategies for assessing the response of a chemistry-climate model to chemical or radiative forcing. The traditional approach is to perform simulations under fixed conditions (so-called “timeslice” experiments) and compare the differences in equilibrium climate resulting from the different forcings. The advantage of this approach is that the simulations can, in principle, be run for a sufficiently long time to obtain good statistics on the differences, which is useful for understanding mechanisms and feedbacks. In this way the unforced variability inherent in the climate system is dealt with explicitly, albeit in an idealized manner. The second approach is to perform simulations under changing conditions (so-called “transient” experiments) over a particular period of time. The advantage of this approach is that it permits a more direct comparison with the real atmosphere, where the forcings are evolving continuously in time. Because of unforced variability, two realizations of the same transient experiment will not evolve in exactly the same way, and an ensemble of experiments is generally required in order to determine a statistically reliable signal.

Yet no matter how good a chemistry-climate model is and how well its climate-change experiments are characterized, the real atmosphere exhibits only a single realization. The best one can expect, even for a perfect model, is that the observations fall within the range of model-predicted behaviors, according to appropriate statistical criteria. Whether this permits a meaningful prediction depends on the relative magnitudes and time scales of the forced signal and the natural noise. As discussed above, we expect the evolution of Antarctic ozone over decadal time scales (past and future) to be a fairly predictable signal, but it is not at all clear whether this is the case in the Arctic. It is known that there is strong interannual variability in the Arctic, extending to multidecadal time scales; even timeslice experiments require several decades of integration to obtain reliable statistics for basic diagnostic quantities (Scaife et al., 2000b). Thus, it is not a priori obvious that even a perfect chemistry-climate model should be able to reproduce the long-term decreases of Arctic ozone observed over the past 20 years, for example.

Chemistry-climate models for stratospheric ozone are probably the most advanced of all chemistry-climate models, but they are still being developed. Early timeslice experiments were performed by Austin et al. (1992) and Pitari et al. (1992) to examine the question of how Arctic ozone might evolve under the conditions of doubled CO₂ expected toward the end of the 21st century, if large halogen abundances were to persist until that time. The results were contradictory, with the former study predicting severe Arctic ozone loss and the latter study predicting only a slight reduction; this at least demonstrated the sensitivity of the response. In the previous Assessment (WMO, 1999, Chapter 12), many of the conclusions were based on the transient experiment of Shindell et al. (1998a), which examined the combined effects of anticipated increasing WMGHGs and decreasing halogens, and predicted increasingly severe Arctic ozone loss over the next couple of decades resulting from Arctic cooling. The stated mechanism for this severe cooling was the dynamical feedback from WMGHG changes, and this represents the key question for the Arctic: namely, are the dynamical feedbacks resulting from WMGHG-induced temperature changes expected to enhance or to reduce the direct radiative stratospheric cooling?

Since the previous Assessment, a number of coupled chemistry-climate models have been developed and run, so there is now considerably more information available than at that time (see Austin et al., 2002). Although these models have improved representations of many processes, they still have many deficiencies, and computational constraints also place severe limitations on the experimental configurations; transient experiments are generally performed singly, not as part of an ensemble, and timeslice experiments are often too short to adequately characterize their variability. In this report, the strategy is therefore adopted of combining the results of the different models, whether the experiments are timeslice or transient, the working assumption being that the differences between the models cover the range of model errors. In this way a current best estimate is obtained of the attribution of past ozone changes in the polar stratosphere and the prediction of future changes over the next half-century.

The models used in the comparisons are indicated in Table 3-3, in order of decreasing horizontal resolution (see Austin et al., 2002). Università degli Studi dell’Aquila (ULAQ) is the only model with a substantial aerosol package and it has reasonably detailed chemistry, albeit diurnally averaged. This model has been run in timeslice mode. Of the other models run in this mode, the Canadian Middle Atmosphere Model (CMAM) and the Middle Atmosphere European Centre Hamburg Model

POLAR OZONE

Table 3-3. Models used in the comparisons. The resolution is given in either degrees latitude × degrees longitude (grid point models), or as T21, T30, and T32, which are the resolutions in spectral models corresponding to triangular truncation of the spectral domain with 21, 30, and 32 wave numbers, respectively. IS92a refers to scenario IS92a of IPCC (1992), and WMO refers to the halogen scenario indicated in Chapter 11 of WMO (1999).

Model	Horizontal Resolution	No. Levels/ Upper Boundary	GHG/ Halogen Scenarios	Reference
UMETRAC	2.5° × 3.75°	64/0.01 hPa	IS92a/WMO	Austin (2002) (Rayleigh friction version)
CMAM	T32	65/0.0006 hPa	Observations, IS92a/WMO	de Grandpré et al. (2000)
MAECHAM/ CHEM	T30	39/0.01 hPa	IS92a/WMO	See details in Austin et al. (2002)
E39/C	T30	39/10 hPa	IS92a/WMO	Schnadt et al. (2002)
UIUC	4° × 5°	25/1 hPa	Observations	Rozanov et al. (2001)
CCSR/NIES	T21	30/0.06 hPa	IS92a/WMO	Takigawa et al. (1999); Nagashima et al. (2002)
GISS	8° × 10°	23/0.002 hPa	IS92a/WMO	Shindell et al. (1998b)
ULAQ	10° × 20°	18/1 hPa	IS92a/WMO	Pitari et al. (2002a)

(ECHAM) with Chemistry (MAECHAM/CHEM) have reasonably detailed chemistry and a high upper boundary (0.01 hPa and above), while the University of Illinois at Urbana-Champaign (UIUC) model and the ECHAM model with chemistry run at DLR (E39/C) have a much lower upper boundary (1 hPa and below). The Unified Model with Eulerian Transport and Chemistry (UMETRAC), Center for Climate System Research (University of Tokyo)/National Institute for Environmental Studies (Japan) (CCSR/NIES), and GISS have been run in transient mode; UMETRAC and CCSR/NIES have reasonably detailed chemistry, whereas the GISS model has parameterized chemistry.

3.5.2 The Uncertainties in Chemistry-Climate Models

3.5.2.1 TEMPERATURE BIASES

As noted in Section 3.4.2.2, many climate models without chemistry but with a fully resolved stratosphere have a cold bias of the order of 5 to 10 K over Antarctica in the lower stratosphere. This suggests that their residual circulations are too weak (Pawson et al., 2000), i.e., there is too little downwelling in high latitudes and too little upwelling in low latitudes. This cold bias would significantly impact model heterogeneous chemistry and

enhance ozone destruction. The “cold-pole problem” extends to higher stratospheric levels, causing a polar night jet that is too strong and too vertically oriented, whereas the observed polar night jet slopes with height toward the equator in the upper stratosphere. The weaker jet and vertical slope allow waves to propagate into higher latitudes and maintain higher polar temperatures. A potentially important component of climate change is whether these waves will be stronger in the future, since this will likely affect the evolution of ozone (see Section 3.5.2.4). A practical solution applied in some models with a cold bias is to increase the temperatures in the heterogeneous chemistry routines (e.g., Austin et al., 2000) by a fixed amount (e.g., 5 K). The strong polar night jet is also associated with a polar vortex that breaks down later in the spring, particularly in the SH. In a chemistry-climate model this can lead to ozone depletion that continues for longer than observed.

Gravity waves generated by processes other than orographic forcing (e.g., convection) are thought to play an important role in the momentum balance of the stratosphere. Non-orographic gravity wave drag (gwd) schemes have now been developed for climate models (e.g., Medvedev and Klaassen, 1995; Hines, 1997a, b; Warner and McIntyre, 1999), and their use has resulted in a significant reduction in the cold-pole problem relative to simulations that rely on Rayleigh friction to decelerate the

polar night jet (e.g., Manzini and McFarlane, 1998). Two of these schemes have also been shown to produce a QBO when run in a climate model (Scaife et al., 2000a). The latest versions of several coupled chemistry-climate models now employ such schemes: CMAM uses the Medvedev-Klaassen scheme (Medvedev et al., 1998) or the Hines scheme (McLandress, 1998); UMETRAC uses the Warner and McIntyre scheme; and MAECHAM/CHEM uses the Hines scheme (see Austin et al., 2002). The GISS GCM has used a non-orographic gravity wave drag scheme for many years (Rind et al., 1988a, b), which is able to reproduce high-latitude temperatures reasonably well (Shindell et al., 1998b) but does not simulate a QBO in the tropics.

Figure 3-42 shows model temperature biases as a function of height for 80°N and 80°S, which are representative of the polar regions, for the winter and spring seasons. To determine the biases, a 10-year temperature climatology determined from UKMO data assimilation fields (Swinbank and O'Neill, 1994) was subtracted from the mean model temperature profiles applicable to the 1990s. The UKMO temperatures are considered to be about 2 K too high at low temperatures (e.g., Pullen and Jones, 1997; Manney et al., 2002; Pommereau et al., 2002; Knudsen et al., 2002), but this bias is smaller than typical model biases. The upper stratospheric cold-pole problem is particularly noticeable in the south in the UMETRAC (with Rayleigh friction), CCSR/NIES (which also uses Rayleigh friction), and MAECHAM/CHEM results. In the results of the UIUC and ULAQ models, a warm bias is present. For the ULAQ model this is likely to be due to the inclusion of vertical diffusion (in addition to Rayleigh friction). As seen in the UMETRAC results, the winter and spring polar temperature bias can be dramatically reduced by the use of non-orographic gwd. Both UMETRAC and CMAM have very similar biases, within a few K of each other in the seasons investigated. The MAECHAM/CHEM model, which uses the Hines non-orographic gwd scheme, is only a slight improvement on the Rayleigh friction results of UMETRAC and CCSR/NIES. The E39/C model is very similar to the MAECHAM/CHEM model, and gives similar results below 30 hPa, but does not have a non-orographic gwd scheme. At 80°N, temperature biases are somewhat smaller than at 80°S and are sometimes positive. The northern lower stratospheric temperature biases would generally lead to insufficient heterogeneous ozone depletion in early winter but excessive ozone depletion in the more important spring period. In the SH, spring cold biases could lead to more extensive PSCs than observed and delayed recovery in Antarctic ozone.

Some indication of the source of the model temperature biases in the lower stratosphere is given by Figure 3-43, which shows the zonal mean heat flux [$v'T'$] at 100 hPa averaged over the domain 40° to 80°N for January and February plotted against temperature averaged at 50 hPa over the domain 60° to 90°N for February and March. As argued by Newman et al. (2001), the heat flux at 100 hPa is indicative of the wave forcing from the troposphere, and this is highly correlated with lower stratospheric temperature slightly later in the year. Newman et al. (2001) chose a 1-15 March temperature average, but here we choose a longer period for the temperature average to smooth model and atmospheric transients. The model results (Figures 3-43 and 3-44) are in general agreement with observations. Table 3-4 shows results of the linear regression between the two variables (see table caption for explanation of the terms T_0 and β). The results indicate that horizontal resolution may have affected the model results; in general the model regression lines were less steep (smaller β in Table 3-4) as the model resolution decreased, particularly in the NH. This could be because low-resolution models capture the low-amplitude-wave, small-heat-flux case, but have difficulty capturing the large-heat-flux case with its significant potential enstrophy cascade to larger wave numbers. The performance of the models might also depend on the dissipation that the models have at short spatial scales, although this is more difficult to compare. The values of β are generally much smaller in the SH, except for the CCSR/NIES and CMAM models. The implication of these results is that models need higher resolution and non-orographic gwd schemes to improve the relationship between heat flux and temperature in order to reduce their polar temperature biases.

3.5.2.2 THE SIMULATION OF POLAR STRATOSPHERIC CLOUDS

PSCs have a significant impact on stratospheric ozone depletion in polar regions, and recent developments in their understanding are discussed in detail in Carslaw et al. (2001) and in Section 3.2.2. Coupled chemistry-climate models have a variety of PSC schemes with and without sedimentation, but such models have in some cases large climatological temperature biases in the polar regions, as indicated in Section 3.5.2.1. If the models are to be effective, the temperature field must give realistic distributions near the PSC temperature thresholds.

The areal coverage of PSCs provides a model comparison diagnostic. We use the temperature at 50 hPa as an indicator of likely PSC amounts, and ignore the effect of HNO_3 and sulfate concentrations on the determination

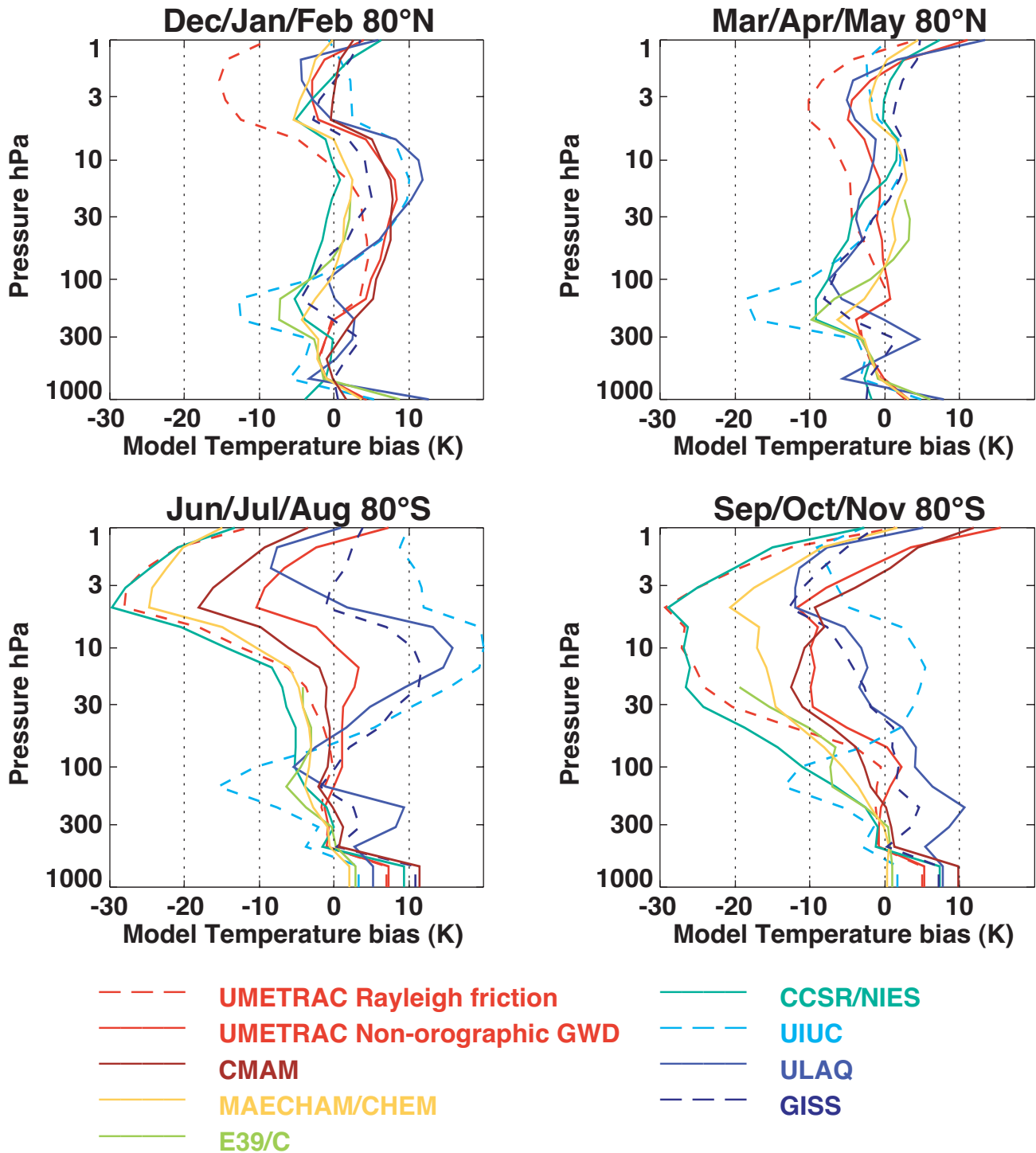


Figure 3-42. Model temperature biases at 80°N and 80°S for the winter and spring seasons, as a function of pressure. To determine the bias, a climatology determined from 10 years of UKMO data assimilation temperatures was subtracted from the model results.

of PSC surface areas (following Pawson and Naujokat, 1997; and Pawson et al., 1999). Figure 3-45 shows for the models and observations the time integral throughout the winter of the PSC area at 50 hPa (A_{τ}). A_{τ} is the sum

throughout the winter of the PSC area (expressed as % fraction of the hemisphere) at 50 hPa. For the ice amount, A_{τ} varies dramatically in the Arctic, between zero and 70% of the hemisphere times days. The models have large

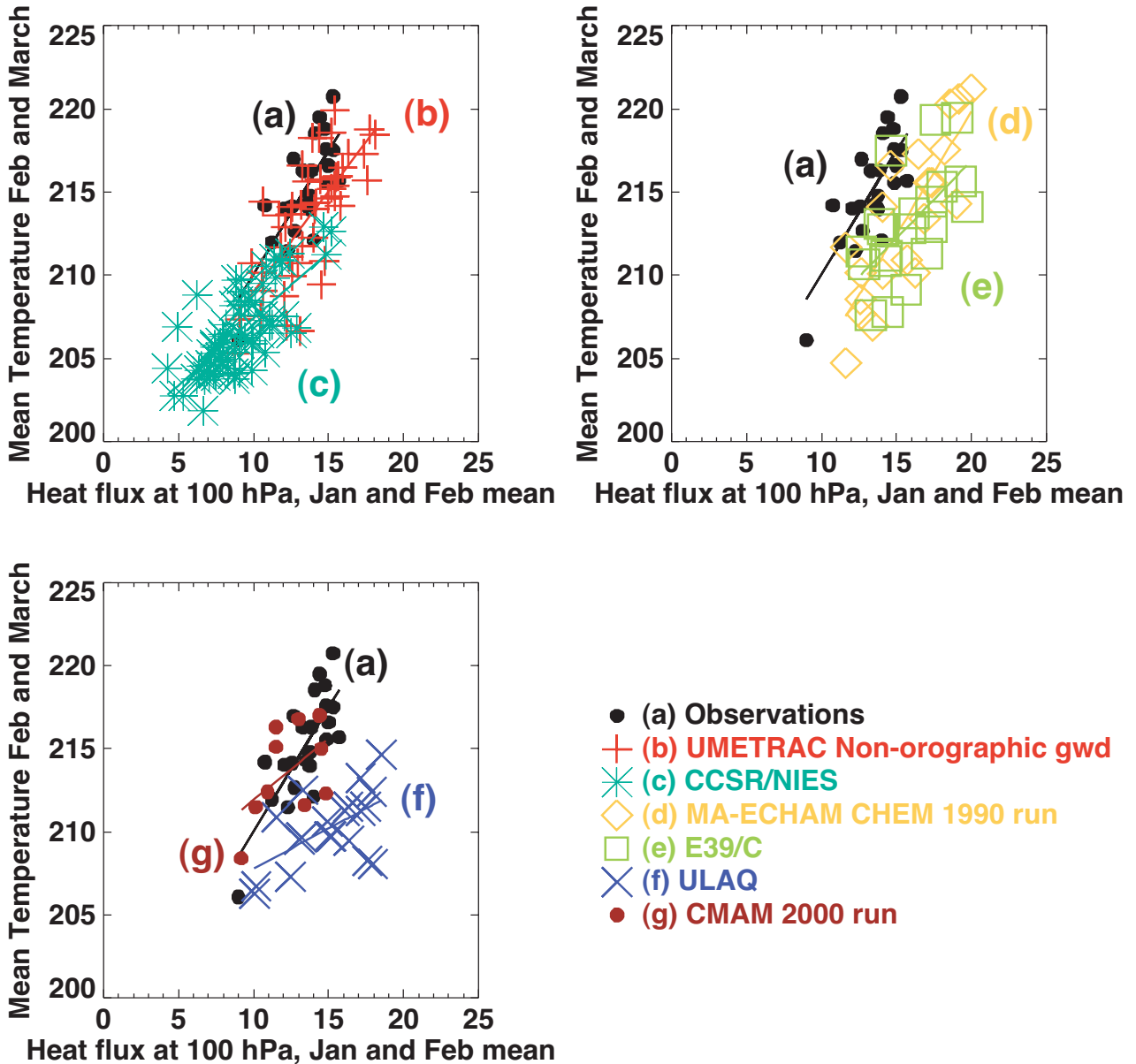


Figure 3-43. Scatter diagrams of the longitudinally averaged (zonal-mean) heat flux (K m/s , averaged for 40° to 80°N , at 100 hPa for January and February) versus temperature (K , averaged for 60° to 90°N , at 50 hPa for February and March) for participating models. The solid lines are linear regression lines between the two variables. The observations are taken from NCEP data.

interannual variability. Arctic NAT also covers a large range, both for different models and in the interannual variability for each simulation. In accordance with their temperature biases, several models have larger areas of NAT than are typically derived from observations. The ULAQ PSCs are in good agreement with observations in both hemispheres, despite a slight positive temperature bias, whereas UMETRAC and CMAM have lower PSC

areas in the Arctic than are derived from observations. In the Antarctic each model has much lower fractional interannual variation for both NAT and ice, but again the results for separate models cover an exceedingly large range for the ice amount. Clearly, the differences between different models will have a profound impact on the amount of chemical ozone depletion calculated. This will be discussed further in Section 3.5.3.

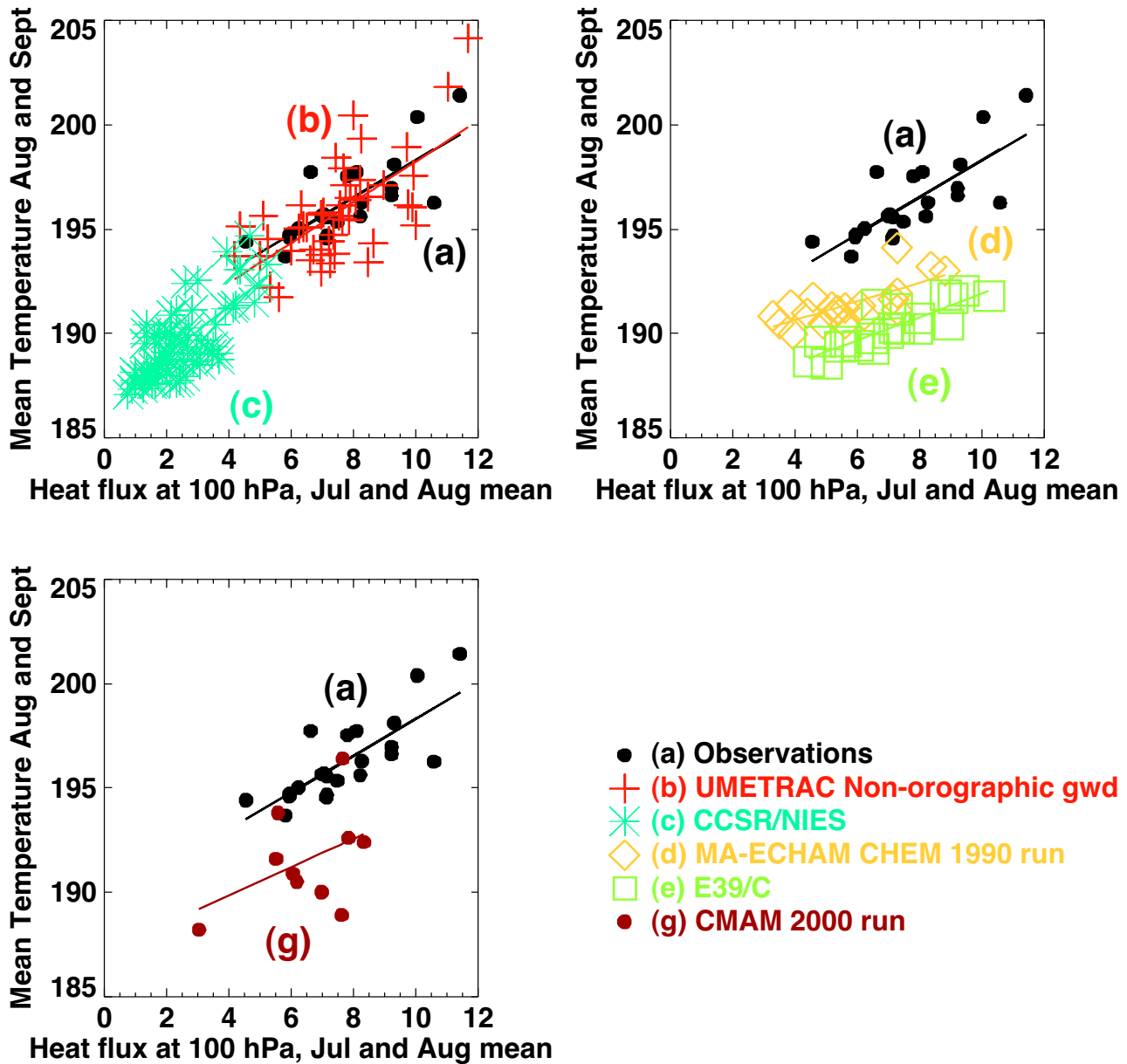


Figure 3-44. As in Figure 3-43, but for heat flux at 40° to 80°S, at 100 hPa for July and August, and temperature at 60° to 90°S, at 50 hPa for August and September.

3.5.2.3 THE POSITION OF THE UPPER BOUNDARY OF THE GCM

There is strong evidence from a number of modeling studies (Garcia and Boville, 1994; Shepherd et al., 1996; Lawrence, 1997; Austin et al., 1997; Rind et al., 1998; Beagley et al., 2000) that the position of the model upper boundary can play a significant role in influencing transport and stratospheric dynamics due to the “downward control principle” (Haynes et al., 1991). The sensitivity of the dynamical fields to the position of the upper

boundary may be larger when non-orographic gwd schemes are used than when Rayleigh friction is used. However, if all the non-orographic gwd that is produced above the model boundary is placed instead in the top model layer, assuming that the upward-propagating waves are not simply absorbed in the top layer, this sensitivity reduces (Lawrence, 1997). Model simulations with an upper boundary as low as 10 hPa have been completed (e.g., Schnadt et al., 2002; Hein et al., 2001; Dameris et al., 1998). Schnadt et al. (2002) show the meridional circulation of the Deutschen Zentrum für Luft- und

Table 3-4. Statistical analysis of the linear regression between the area-averaged temperature (K) at 50 hPa poleward of 60°N for February and March in the NH and 60°S in August and September in the SH, and the heat flux (K m/s) at 100 hPa between 40° and 80°N for January and February in the NH and 40° and 80°S for July and August in the SH. R is the correlation coefficient between the variables, T_0 is the intercept of the line at zero heat flux, and β is the gradient of the line. For ULAQ results in the Southern Hemisphere, the heat flux and temperature are not correlated.

Model/Observations	Northern Hemisphere			Southern Hemisphere		
	R	T_0	β	R	T_0	β
NCEP (observations)	0.77	195.1	1.49	0.78	189.4	0.89
UMETRAC non-orographic gwd	0.74	196.9	1.21	0.66	188.5	0.98
Rayleigh friction	0.67	196.2	1.21	0.51	187.7	0.67
CMAM 2000	0.52	204.5	0.75	0.44	187.2	0.68
MAECHAM/CHEM 1990	0.79	196.3	1.10	0.70	190.0	0.50
E39/C	0.62	198.3	0.93	0.86	186.3	0.56
CCSR/NIES	0.74	199.4	0.80	0.74	186.6	1.17
ULAQ	0.58	203.0	0.48	—	—	—

Raumfahrt (DLR) model. This gives the expected upward motion from the summer hemisphere and downward motion over the winter hemisphere, although modeled meridional circulations are known to extend into the mesosphere (e.g., Butchart and Austin, 1998). Schnadt et al. (2002) argue that it is less important to have a high upper boundary, but more important to have high resolution in the vicinity of the tropopause. At present the evidence appears ambiguous; for example, in the total ozone presented by Hein et al. (2001), insufficient ozone is transported to the North Pole, but there is excessive subtropical ozone transport. This could be related to the cold-pole problem, rather than the position of the upper boundary. While the transport effect on ozone is direct, other considerations are the transport of long-lived tracers such as NO_y and water vapor that have a photochemical impact on ozone. Consequently, it is generally recognized that the upper boundary should be placed at least as high as 1 hPa (e.g., Rozanov et al., 2001; Pitari et al., 2002b); many models are now placing their boundary at about 0.01 hPa (e.g., Shindell et al., 1998b; Austin et al., 2001; Nagashima et al., 2002). In comparison, CMAM (de Grandpré et al., 2000) has an upper boundary somewhat higher (~ 0.0006 hPa) to allow a more complete representation of gwd to reduce the cold-pole problem (Section 3.5.2.1) and to simulate upper atmosphere phenomena.

3.5.2.4 PREDICTIONS OF PLANETARY WAVES

The direct radiative cooling by greenhouse gases at high latitudes in the lower stratosphere causes an increase in the strength of the polar vortex. Planetary wave changes may be a feedback that strengthens or weakens this effect. One proposed planetary wave feedback mechanism (Shindell et al., 2001) works as follows: tropical and subtropical sea surface temperatures increase, leading to a warmer tropical and subtropical upper troposphere via moist convective processes. This results in an increased latitudinal temperature gradient at around 100 to 200 hPa, leading to enhanced lower stratospheric westerly winds that refract upward, propagating tropospheric planetary waves equatorward. This results in a strengthened polar vortex.

The E39/C results (Schnadt et al., 2002) also show a small decrease in planetary wave activity for the period 1960 to 1990. However, results for future simulations differ depending on the model. Without chemical feedback, the Unified Model (UM) (Gillett et al., 2002) predicts a future increase in overall generation of planetary waves, which leads to a greater wave flux to the Arctic stratosphere, and is even able to overcome the radiatively induced increase in the westerly zonal wind so that the overall trend is to weaken westerly flow. This also occurs in the DLR model with chemical feedback (Schnadt et al.,

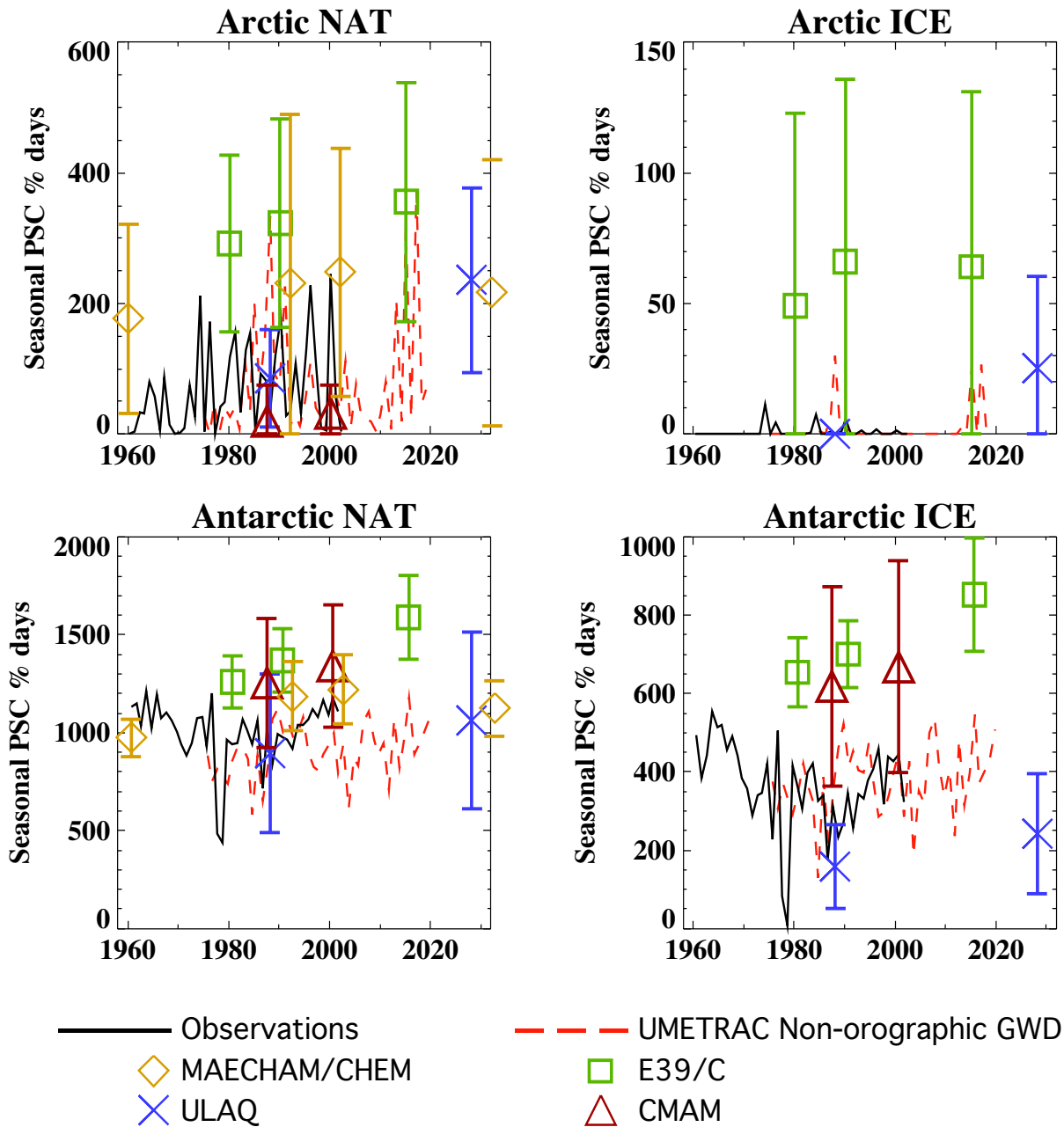


Figure 3-45. Time integral of the percentage area of the hemisphere at 50 hPa covered by temperatures below 195 K (approximate NAT temperature) and below 188 K (approximate ICE temperature) during winter and spring. The error bars for the timeslice runs indicate 95% confidence intervals. For clarity, ULAQ data are plotted 2 years early, and MAECHAM CHEM data for 1990 and 2030 are plotted 2 years late.

2002), whereas in the UM with chemical feedback (UMETRAC) the trend in the heat flux during the period 1975 to 2020 is downward but is not statistically significant. The Center for Climate System Research/National Institute for Environmental Studies (CCSR/NIES) model, of lower resolution than UMETRAC, has systematically

lower heat fluxes but does show a downward trend during the period 1986 to 2050 that is marginally statistically significant. In general, the strengthening of the polar vortex appears to be critically dependent upon the relative importance of changes in wave generation versus wave propagation. These changes are likely to be highly model and

resolution dependent, resulting from the particular wave forcing and drag schemes employed in each climate model. To some degree this sensitivity of the changes in planetary waves to the model simulation reflects similar sensitivities in the atmosphere: for example, in the observations of the last five northern winters, four have been warm with a weaker polar vortex (see Section 3.1.2 and Figure 3-8). As a result, the strengthening of the vortex over the last 20 years noted by some authors (Tanaka et al., 1996; Zurek et al., 1996; Waugh et al., 1999; Hood et al., 1999) will have been modified by recent events.

3.5.2.5 STRATOSPHERIC WATER VAPOR CHANGES

Observations of atmospheric water vapor concentrations have revealed significant increases over the period 1964 to 2000 (Oltmans and Hofmann, 1995; Oltmans et al., 2000; Rosenlof et al., 2001). As discussed further in Chapter 4, these increases are uncertain in magnitude and their causes have not been established.

Increased water vapor directly affects ozone chemistry. It also alters local temperatures by radiative cooling, slowing down the reaction rates of ozone depletion chemistry, which indirectly leads to more ozone. Evans et al. (1998), Dvortsov and Solomon (2001), and Shindell (2001) have studied the effects on homogeneous chemistry. The models all show that increases in water vapor reduce ozone in the upper and lower stratosphere, and increase ozone in the middle stratosphere. The model results differ most in the lower stratosphere where the largest impact on total ozone column occurs. In the model of Evans et al. (1998), lower stratospheric ozone is reduced only in the tropics when water vapor increases, whereas in the other models, ozone reductions extend to midlatitudes or to the poles. Thus, the models of Dvortsov and Solomon (2001) and Shindell (2001) show a slower ozone recovery by about 10 to 20 years, and a 1-2% reduction during the next 50 years due to water vapor increase, assuming that the water vapor increase continues at the current rate. The Evans et al. (1998) model disagrees with these results, presumably due to differences in that model's temperature response to increasing water, which seems to dominate over the chemical impacts.

Water vapor increases also affect heterogeneous chemistry, enhancing the formation of PSCs (see Section 3.2.2). Kirk-Davidoff et al. (1999) calculated a significant enhancement to Arctic ozone loss in a more humid atmosphere. Much of this effect was based on a very large estimate of 6 to 9 K per ppmv radiative cooling induced by increased water vapor. This value has been superseded by newer results showing that the value is almost certainly much smaller, about 1.5 to 2.5 K cooling per ppmv of

water (Section 3.4.3.4). This would in turn imply a reduced role for water vapor in enhancing PSC formation. Tabazadeh et al. (2000) showed that the enhancement of PSC formation due to the addition of 1 ppmv of water vapor is approximately the same as the PSC enhancement due to cooling of about 1 K. This suggests that the radiative impact of water vapor is larger than its effects on chemistry or microphysics but that all these processes should be considered in numerical models. Given the potential for denitrification in the Arctic, and the large ozone losses that could result from a slight cooling there (Tabazadeh et al., 2000), it is important both to understand trends in stratospheric water vapor and to resolve model differences in the radiative impact of those trends.

Model simulations of past water vapor trends do not agree well with observations. In UMETRAC (Austin, 2002), water vapor increases by only about 1% per decade in the stratosphere, despite the inclusion of a methane oxidation scheme. In UMETRAC, the tropical tropopause temperature decreases slightly, counteracting the methane impact. In E39/C (Schnadt et al., 2002), water vapor increases in the lower stratosphere are significantly larger (about 3% per decade) but are still about a factor of 2 to 3 lower than observed. Similar results are also obtained in the GISS model. In general the modeled water vapor trend tends to be driven by methane oxidation and trends in tropical tropopause temperatures, suggesting the need to investigate the microphysics of dehydration and how this is represented in models. (See also Section 4.3.3 of EC (2001).)

3.5.3 Model Assessments

In the Arctic the processes leading to stratospheric ozone depletion may undergo too much natural variability to provide a definite answer to how ozone will actually evolve. Each model may be considered as supplying a single simulation (or range of simulations in the case of the timeslice experiments) of a larger ensemble. Although the mean of the ensemble can be readily computed, the atmosphere may in practice evolve in a manner anywhere within, or even outside, the envelope of the model simulations. In the Antarctic, the dominant processes are less dependent on interannual variability and, hence, the ozone evolution is in principle more predictable.

One of the emphases here has been on spring ozone recovery. In view of the range of results obtained, it is important to define this term carefully. It is here used in two senses: (1) the start of ozone recovery, defined as the date of the minimum spring column ozone as a function of year in the decadal averaged results, and (2) full ozone recovery, defined as the date of the return of the decadal averaged spring column ozone to the value obtained in 1980.

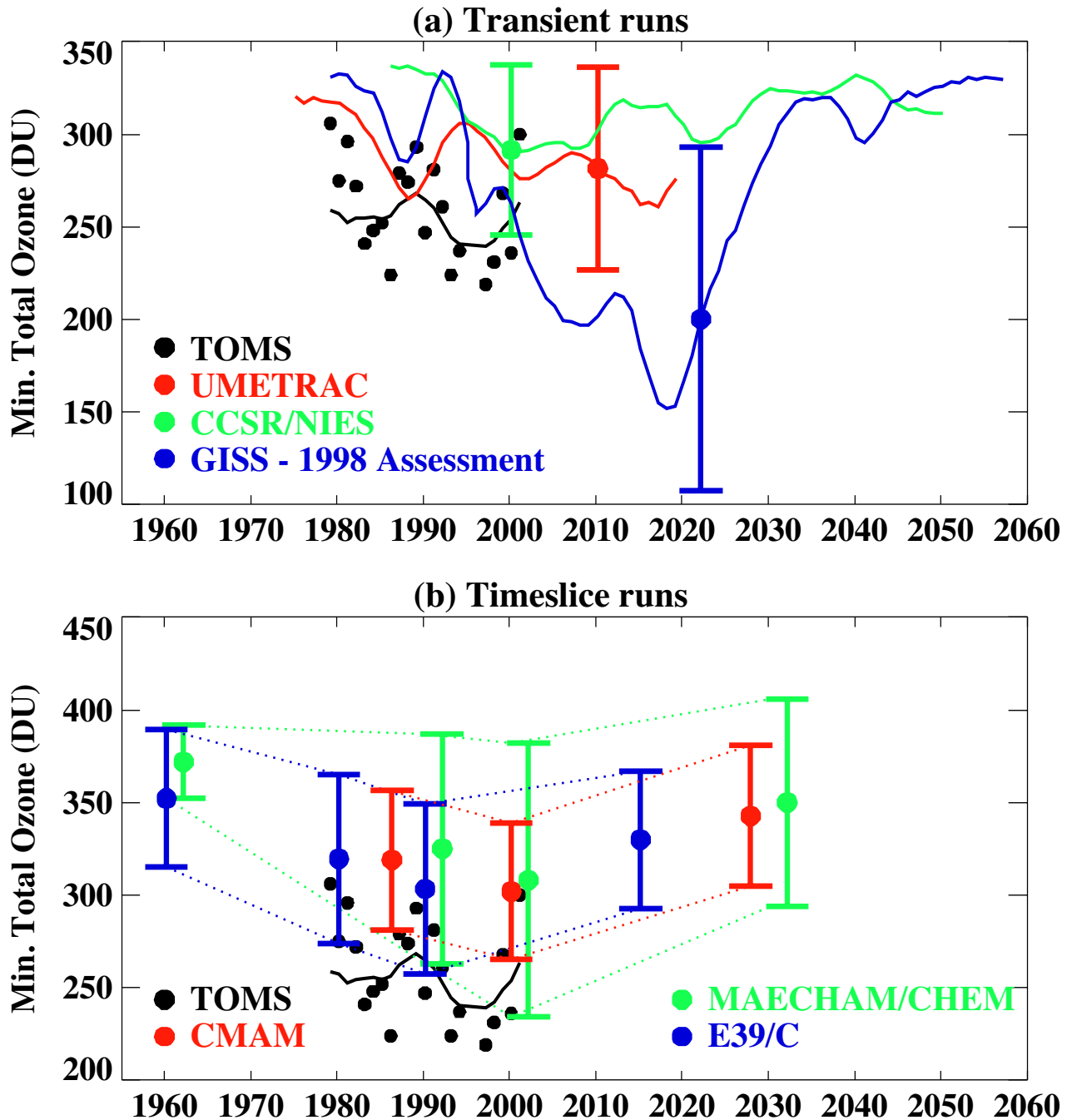


Figure 3-46. Minimum Arctic (March/April) total ozone for the main experiments of this Assessment. (a) Transient runs in comparison with TOMS data. The solid lines show the results of a Gaussian smoothing applied to the individual year's results. The error bars denote twice the standard deviation of the individual years from the smoothed curve. Results from the previous Assessment (the GISS model) are included for comparison. (b) Timeslice runs in comparison with TOMS data. The colored circles and the error bars denote the mean and twice the standard deviation of the individual years within each model sample (10 years for CMAM, 20 years for MAECHAM/CHEM and E39/C). Dotted lines are drawn between the end points of the error bars to assist in estimating trends by eye. For MAECHAM/CHEM only: (1) the values have been plotted 2 years late for clarity, and (2) a standard tropospheric column of 100 DU has been added to the computed stratospheric columns.

3.5.3.1 THE 1960-2000 TIME FRAME: OZONE DEPLETION

As is well established from observations (Section 3.1.1), polar ozone has been decreasing over the last few decades. Figure 3-46 shows the minimum daily ozone throughout the range 60° to 90°N for several of the models of Table 3-3 together with TOMS data. The GISS results are included to provide a comparison with the state of knowledge at the time of the previous Assessment (WMO, 1999). For clarity, the models are separated into two panels according to their mode of simulation (transient or timeslice). For the transient models, a Gaussian low-pass filter is fitted through the results for the individual years, and the error bars denote two standard deviations from the Gaussian filtered curve. For the timeslice experiments, the mean and two standard deviations are plotted, and the dotted lines give an indication of the temporal behavior of the model results. Each model has a large interannual variability, similar to that of the observations, and, hence, detecting a signal is difficult. All the models indicate a slight high bias relative to observations. The trends in the minimum (Table 3-5) are consistent with the observations, although only E39/C, MAECHAM/CHEM, and the observations have statistically significant trends. Averaging the five model results obtained since the previous Assessment gives an Arctic trend that is statistically significant and agrees with observations.

In the Antarctic (Figure 3-47, upper panel), the model runs agree reasonably well with observations for the past and show the steady development of the ozone hole during the period. However, the calculated trends (Table 3-5) depend on the period chosen. CMAM indicates a small trend because the ozone hole was already partially formed in 1987 and the CMAM values for 2000 are higher than observed. The mean trend of the latest five model simulations (Table 3-5) is slightly lower than observed, but if the latest reaction rates for the ClO dimer production (Bloss et al., 2001) had been used, the agreement would have been further improved. While the interannual variability of most of the models is similar to that observed, both CMAM and UMETRAC have a large interannual variability. In the case of UMETRAC, this may to some extent be a product of the non-orographic gwd scheme.

The maximum size of the Antarctic ozone hole during each spring, as given by the area within the 220-DU total ozone contour, is shown in Figure 3-47 (lower panel). The results for GISS, E39/C, and CCSR/NIES are in good agreement with observations, but may indicate a slight underprediction. A much smaller ozone hole is simulated by UMETRAC, but recent model runs with a

revised NO_y distribution consistent with observations show an ozone hole about 50% larger for 1995, which is in close agreement with observations. The size of the ozone hole area for CMAM reflects the bias and large interannual variability noted in Figure 3-47 (upper panel). Errors in the modeling of the size of the ozone hole can have important implications. First, comparisons between models and observations for ozone amounts near 60°S will give poor agreement if the ozone hole area is too small, even though the underlying physics of the model may be correct. Second, a model with a smaller ozone hole may evolve differently from that of the atmosphere due to transport and chemistry effects relating to radiative effects.

3.5.3.2 THE 2000-2020 TIME FRAME: START OF OZONE RECOVERY

The first signs of ozone recovery are expected within the next two decades (Shindell et al., 1998a; Austin et al., 2000; Schnadt et al., 2002; Rosenfield et al., 2002; Nagashima et al., 2002). Two-dimensional (2-D) model simulations (e.g., Rosenfield et al., 2002) indicate a slight delay in Arctic and Antarctic spring ozone recovery following the maximum values in halogen loading. The

Table 3-5. Past trends (1979-2000) in minimum ozone (DU/decade) with 2σ error bars for participating models and TOMS. The MAECHAM/CHEM results cover the period 1960-2000 (Arctic) and 1960-1990 (Antarctic); the E39/C (ECHAM model with chemistry run at DLR) results cover the period 1960-1990 (Arctic) and 1980-1990 (Antarctic); the CCSR/NIES model results cover the period 1986-2000; and the CMAM results cover the period 1987-2000.

Model/Observations	Northern Trend	Southern Trend
UMETRAC	-6 ± 22	-80 ± 31
CMAM	-13 ± 27	-23 ± 28
MAECHAM/CHEM	-16 ± 10	-45 ± 3
E39/C	-16 ± 14	-64 ± 7
CCSR/NIES	-33 ± 38	-41 ± 21
Mean (this Assessment)	-17 ± 12	-51 ± 11
GISS (1998 Assessment)	-21 ± 34	-34 ± 12
TOMS	-21 ± 16	-59 ± 12

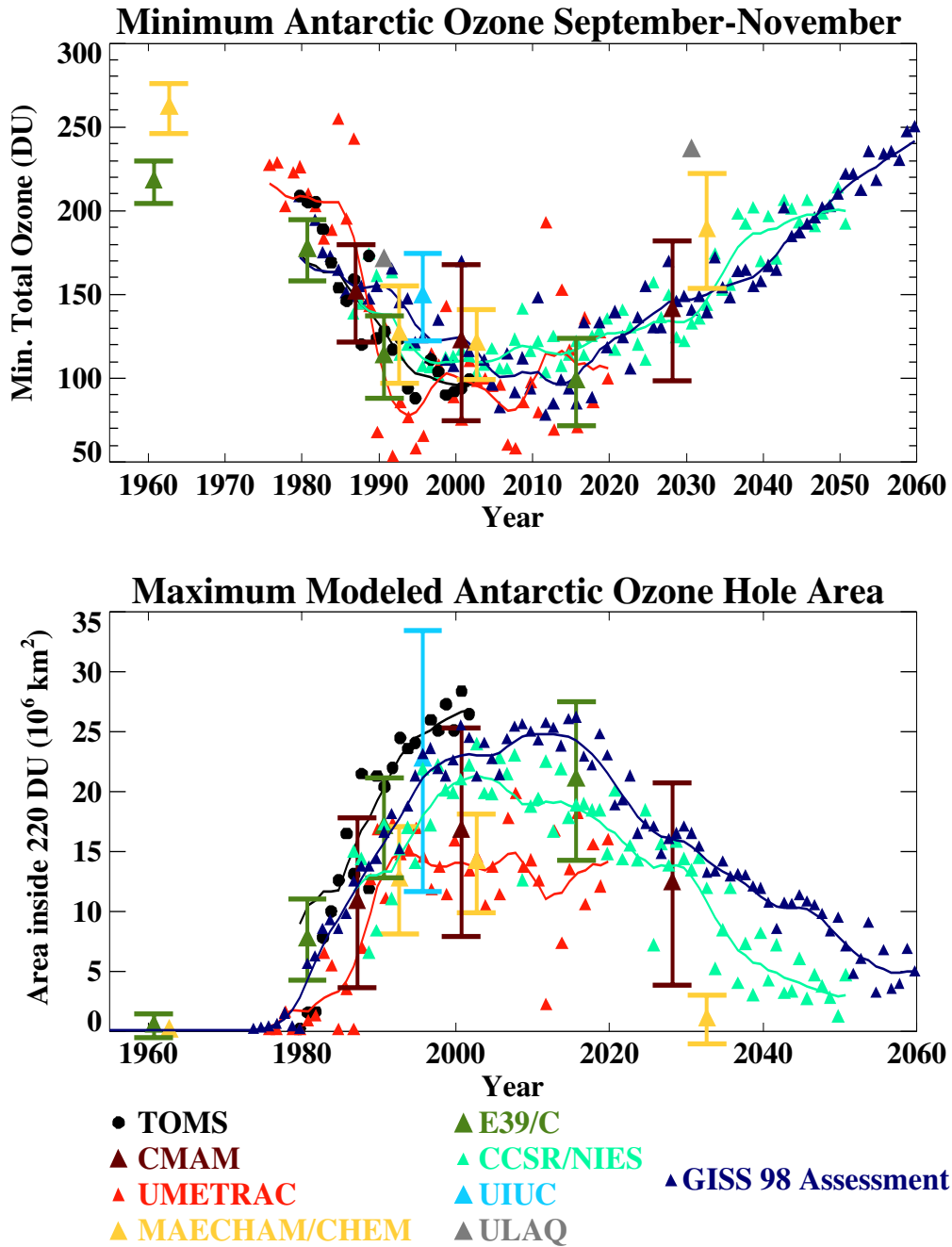


Figure 3-47. Upper panel: Minimum Antarctic total ozone for September to November, as observed by TOMS and as computed by the participating models. For the transient models, the solid lines show the results of a Gaussian smoothing applied to the individual year's results (also plotted). For the timeslice experiments, the mean and twice the standard deviation of the values within each sample are recorded by the colored triangles and the error bars. For MAECHAM/CHEM only: (1) the values have been plotted 2 years late for clarity, and (2) a standard tropospheric column of 40 DU has been added to the computed stratospheric columns. Lower panel: The maximum area of the ozone hole during the period September to November, as given by the 220-DU contour, for TOMS observations and participating models. The TOMS data and transient model results are plotted for each year and with a Gaussian filter applied (solid lines). For the timeslice experiments the means and twice the standard deviations of the model samples are included. For MAECHAM/CHEM only: (1) the values have been plotted 2 years late for clarity, and (2) a standard tropospheric column of 40 DU has been added to the computed stratospheric columns.

GISS model has a larger response than the other models, with the simulation indicating a minimum in the decadal averaged results of about 175 DU compared with almost 100 DU higher in the other transient runs. The date of minimum Arctic ozone, again as indicated by the minimum of the decadal averaged results, varies from 2004 for the CCSR/NIES model to 2019 for the GISS model. UMETRAC indicates a minimum at about the year 2015, but the simulation ends shortly afterwards and the results do not change substantially in the final decade. All three transient runs indicate some delay in the onset of ozone recovery, presumably due to increases in greenhouse gases (GHGs), although such a result is subject to considerable uncertainty because of the large interannual variability. Although the timeslice experiments do not have the temporal resolution to give a precise indication of the timing of future ozone recovery, the E39/C model results (Schnadt et al., 2002) may go against the transient model results by suggesting that increases in planetary waves occur in the Arctic, speeding up ozone recovery. This may be considered the “dynamical effect on chemistry”: increases in planetary waves transport more ozone as well as raise temperatures and decrease heterogeneous chemistry. Therefore, the net effect on ozone is that of the two potentially competing processes of dynamics and radiation. If planetary waves increase, the “dynamical” effect increases ozone and the “radiative” effect decreases ozone, giving a relatively small response. If planetary waves decrease, both the “dynamical” and “radiative” effects are negative, leading to enhanced ozone depletion. To resolve from the timeslice simulations whether increases in GHGs are delaying the onset of ozone recovery would require more results for the period 1990 to 2015.

In the Antarctic, the runs are all in fairly good agreement. Of the transient runs, as in the Arctic, the CCSR/NIES model indicates the earliest start of ozone recovery (2001) followed by UMETRAC (2005) and GISS (2008). The minima in the decadal averaged results are all comparable (109, 86, and 98 DU, respectively). On the basis of the decadal averaged model results this would appear to indicate that ozone recovery would begin earlier in the Antarctic than in the Arctic. Such an earlier start to recovery would also be detectable earlier in observations in Antarctica, because of the smaller interannual variability.

Observations of the size of the ozone hole (Figure 3-47; see also Figure 3-7) do not indicate any clear recovery by October 2001, with interannual variability now dominating over the current trends. For the GISS model the maximum ozone hole is in 2015, whereas for

UMETRAC the maximum occurs in 2007, although any systematic variation is obscured by the large interannual variability noted previously. In contrast the CCSR/NIES results show a peak as early as the year 2002.

3.5.3.3 THE 2020-2060 TIME FRAME: COMPLETE OZONE RECOVERY

Those models that have run beyond the year 2020 indicate some recovery in ozone. Of particular importance is the return to “1980-like conditions,” when the effects of anthropogenic halogen concentrations in the polar regions are negligible. As noted in the previous Assessment (Chapter 12 of WMO, 1999), this recovery would be to a different vertical distribution of ozone, with higher middle and upper stratospheric ozone due to the change in the vertical temperature profile (see Chapter 4). Using a 2-D model, Rosenfield et al. (2002) determined the date for the recovery of total ozone to 1980 levels as a function of day of year and latitude. In the Arctic, this recovery was latest at the end of spring (after 2050) and earliest in autumn (before 2035). Further, the impact of CO₂ increases was shown to accelerate the recovery from that due to chemical changes alone by increasing the downwelling over the poles. In contrast, if methane amounts do not increase at the current rate, ozone recovery could be slowed down in the future by the increased importance of NO_x chemistry (Randeniya et al., 2002). Over Antarctica, downwelling is less important in speeding up the ozone recovery.

Figures 3-46 and 3-47 show similar results for the spring for 3-D models. However, in the Arctic, most models do not show substantial ozone change throughout the period 2020 to 2050, and the low values of the GISS model for the decade 2010 to 2020 are no longer present after 2030 (Figure 3-46). In the Antarctic, the recovery of spring ozone, already under way by 2020, continues in the simulations completed (Figure 3-47). Recovery to 1980-like conditions occurs in the CCSR/NIES and GISS models by about 2045, and perhaps a decade later in the results of Austin et al. (2001). The CCSR/NIES and GISS transient model results suggest a near-monotonic recovery of ozone, but the results of Austin et al. (2001) suggest that ozone could undergo further loss over the period 2025 to 2045. This was identified as due to increases in ice PSCs as the lower stratospheric climate cools (but would need to be confirmed by model simulations with more detailed PSC schemes). Of the timeslice experiments, the MAECHAM/CHEM results indicate a significant (but not “full”) recovery in the Antarctic by 2030, consistent with the transient experiments. In the Arctic this model also simulates full or near-full recovery by 2030.

POLAR OZONE

3.5.3.4 ATTRIBUTION OF MODEL OZONE CHANGES

The contrast between the modeled Antarctic and Arctic ozone behavior is striking in terms of the extent to which the observed behavior can be regarded as a forced response to chlorine loading. There is no question but that this is the case in the Antarctic; the models, despite their various imperfections, together give a clear, statistically significant signal that is in line with the observations. However, this is not the case in the Arctic: although there is a general ozone decrease in the models during the period of chlorine loading, it is not statistically significant. This is partly because of the weaker chemical impact of chlorine loading in the Arctic than in the Antarctic, and partly because of the greater natural variability in the Arctic.

In a coupled chemistry-climate model, the attribution of ozone changes to dynamical and chemical processes may be ambiguous because the dynamical changes themselves may have been caused by chemical changes to the ozone amounts. This is discussed further in Chapter 4. Figure 3-45, illustrating the approximate amounts of PSCs in the model simulations, should in principle reflect the amount of chemical ozone depletion (cf. Figure 3-33). This would suggest, for example, that UMETRAC has slightly less Arctic ozone depletion relative to observations, and this is reflected in the Arctic ozone trend (Figure 3-46; Table 3-5) that is smaller than observed, although the difference is not statistically significant. Also, both MAECHAM/CHEM and E39/C results for PSCs in Figure 3-45 suggest that their chemical ozone depletion is larger than observed in the Arctic, although the net ozone trend is similar to observations. The implication is that transport into the polar regions is enhanced to compensate. However, this does not appear to be consistent with earlier results (e.g., Hein et al., 2001), which if anything indicate reduced transport into the polar regions.

In the Antarctic, many of the models have similar ozone depletion rates, similar amounts of PSCs, and similar ozone trends, when allowance is made for the different periods under consideration (Figure 3-47; Table 3-5). The main exceptions are the GISS model for which PSC diagnostics are not available, and CMAM, which has less ozone depletion than that observed in 2000. These inconsistencies in both hemispheres suggest the need for further investigation of the sizes of the transport versus chemical depletion terms in all the models included herein.

Considering now the future evolution of Arctic ozone, the envelope of ozone variability defined by the timeslice experiments in Figure 3-46b returns to higher values in the future. Thus, the impact of the WMGHGs on Arctic ozone is still uncertain. The two transient exper-

iments performed for this Assessment, shown in Figure 3-46a, are consistent with the timeslice experiments. However, the transient experiment from the previous Assessment falls well outside the envelope of variability defined by the timeslice experiments over the coming several decades, particularly in terms of its lowest values. The prediction of the previous Assessment that changes in WMGHGs could lead to Arctic ozone minima of 100 DU over the coming several decades is not supported by the more recent models. The reason for the difference from the previous Assessment is that the more recent models do not predict the severe decrease in planetary wave drag over the Arctic (leading to essentially Antarctic-like meteorological conditions in the Arctic in some years) predicted by the earlier model. The earlier caveats, including the need for ensemble integrations, should again be borne in mind.

3.5.4 Summary

The main uncertainties of 3-D coupled chemistry-climate models stem from the performance of the underlying dynamical models. Temperature biases lead to errors in the spatial extent of PSCs and the degree of chemical ozone depletion. The model results also suggest significant differences in the transport of ozone to high latitudes, although this is in need of further clarification. At the current stage of model performance, uncertainties in the details of PSC formation and sedimentation are probably less important in simulating ozone amounts than the model temperature biases. Nonetheless, the accurate representation of PSC processes will prove to be increasingly important as temperature biases become smaller by, for example, the inclusion of non-orographic gravity wave parameterizations. Another uncertainty is the amount of aerosol present due to future unpredictable volcanic eruptions. For a large eruption such as that of Mt. Pinatubo, sufficient aerosol would be present to provide additional sites for heterogeneous chemistry and possible severe ozone loss for a period of a few years (see, e.g., Tabazadeh et al., 2002), although this perturbation would not affect the long-term ozone trend. The impact of volcanic eruptions on coupled chemistry-climate model results has not been discussed in this section, but further details may be found in Chapter 4.

For the transient model simulations, the start of ozone recovery, as defined in Section 3.5.3, occurs in the Antarctic within the next decade, depending on the model, and in the Arctic it occurs within the next two decades. In the Antarctic, however, model results suggest that the vertical and horizontal extent of the ozone hole may increase slightly further over the next few years. Thus, the results here suggest that the start of ozone recovery will occur

slightly later in the Arctic than in the Antarctic. Further, since the halogen amounts are thought to have maximized in 2001 (see Chapter 1, Figure 1-7), the start of ozone recovery in the Arctic in the models is delayed by up to almost two decades, probably by greenhouse gas increases. Most of the models come to similar conclusions on this issue, but one of the coupled chemistry-climate model experiments (Schnadt et al., 2002) suggests that greenhouse gas increases would tend to speed up rather than slow down ozone recovery in the Arctic. It should also be recognized that interannual variability on the sub-decadal time scale may still lead to ozone extremes. In the worst-case scenario, therefore, it may take until at least the end of the 2020s before we can be certain that ozone recovery has started in the Arctic. To put this into perspective, most models predict relatively modest changes in future spring Arctic column ozone (under 10%). The one model that does predict a major Arctic ozone change in the near future (described in Shindell et al., 1998a) has lower spatial resolution, simplified ozone transport, and parameterized ozone chemistry. In comparison, the other models have more accurate treatments of these processes.

On the longer time scale, to the middle of the 21st century, model predictions appear to be more uncertain. Hence, although recovery of Antarctic ozone to 1980-like conditions (“full ozone recovery”) is to be expected by about 2050, models will need to have a better representation of the water vapor increase than has hitherto been possible, as well as an accurate specification of methane changes, for full confidence in their predictions. Although the results for the Arctic are less certain, since most models indicate relatively modest change in ozone, it is possible that “full recovery” may occur somewhat earlier there.

REFERENCES

- Abrams, M.C., G.L. Manney, M.R. Gunson, M.M. Abbas, A.Y. Chang, A. Goldman, F.W. Irion, H.A. Michelsen, M.J. Newchurch, C.P. Rinsland, R.J. Salawitch, G.P. Stiller, and R. Zander, ATMOS/ATLAS-3 observations of long-lived tracers and descent in the Antarctic vortex in November 1994, *Geophys. Res. Lett.*, *23*, 2341-2344, 1996.
- Allen, D.R., J.L. Stanford, N. Nakamura, M.A. Lopez-Valverde, M. Lopez-Puertas, F.W. Taylor, and J.J. Remedios, Antarctic polar descent and planetary wave activity observed in ISAMS CO from April to July 1992, *Geophys. Res. Lett.*, *27*, 665-668, 2000.
- Allen, D.R., and N. Nakamura, A seasonal climatology of effective diffusivity in the stratosphere, *J. Geophys. Res.*, *106*, 7917-7935, 2001.
- Ambaum, M.H.P., B.J. Hoskins, and D.B. Stephenson, Arctic oscillation or North Atlantic oscillation?, *J. Clim.*, *14*, 3495-3507, 2001.
- Andersen, S.B., and B.M. Knudsen, The influence of polar vortex ozone depletion on Arctic ozone trends, *Geophys. Res. Lett.*, in press, 2002.
- Appenzeller, C., and J.R. Holton, Tracer lamination in the stratosphere: A global climatology, *J. Geophys. Res.*, *102*, 13555-13569, 1997.
- Atkinson, R.J., and R.A. Plumb, Three-dimensional ozone transport during the ozone-hole breakup in December 1987, *J. Geophys. Res.*, *102*, 1451-1466, 1997.
- Austin, J., A three-dimensional coupled chemistry-climate model simulation of past stratospheric trends, *J. Atmos. Sci.*, *59*, 218-232, 2002.
- Austin, J., N. Butchart, and K.P. Shine, Possibility of an Arctic ozone hole in a doubled-CO₂ climate, *Nature*, *360*, 221-225, 1992.
- Austin, J., N. Butchart, and R.S. Swinbank, Sensitivity of ozone and temperature to vertical resolution in a GCM with coupled stratospheric chemistry, *Quart. J. Roy. Meteorol. Soc.*, *123*, 1405-1431, 1997.
- Austin, J., J. Knight, and N. Butchart, Three-dimensional chemical model simulations of the ozone layer: 1979-2015, *Quart. J. Roy. Meteorol. Soc.*, *126*, 1533-1556, 2000.
- Austin, J., N. Butchart, and J. Knight, Three-dimensional chemical model simulations of the ozone layer: 2015-2055, *Quart. J. Roy. Meteorol. Soc.*, *127*, 959-974, 2001.
- Austin, J., D. Shindell, S. Beagley, C. Brühl, M. Dameris, E. Manzini, T. Nagashima, P. Newman, S. Pawson, G. Pitari, E. Rozanov, C. Schnadt, and T.G. Shepherd, Uncertainties and assessments of chemistry-climate models of the stratosphere, *Atmos. Chem. Phys.*, in press, 2002.
- Avallone, L.M., and D.W. Toohey, Tests of halogen photochemistry using in situ measurements of ClO and BrO in the lower polar stratosphere, *J. Geophys. Res.*, *106*, 10411-10421, 2001.
- Avallone, L.M., D.W. Toohey, S.M. Schauffler, W.H. Pollock, L.E. Heidt, E.L. Atlas, and K.R. Chan, In situ measurements of BrO during AASE-II, *Geophys. Res. Lett.*, *22*, 831-834, 1995.
- Bacmeister, J.T., S.D. Eckermann, A. Tsias, K.S. Carslaw, and T. Peter, Mesoscale temperature fluctuations induced by a spectrum of gravity waves: A comparison of parameterizations and their impact on stratospheric microphysics, *J. Atmos. Sci.*, *56*,

POLAR OZONE

- 1913-1924, 1999.
- Baldwin, M.P., and T.J. Dunkerton, Propagation of the Arctic Oscillation from the stratosphere to the troposphere, *J. Geophys. Res.*, *104*, 30937-30946, 1999.
- Baldwin, M.P., and T.J. Dunkerton, Stratospheric harbingers of anomalous weather regimes, *Science*, *294*, 581-584, 2001.
- Beagley, S.R., C. McLandress, V.I. Fomichev, and W.E. Ward, The extended Canadian middle atmosphere model, *Geophys. Res. Lett.*, *27*, 2529-2532, 2000.
- Becker, G., R. Müller, D.S. McKenna, M. Rex, and K.S. Carslaw, Ozone loss rates in the Arctic stratosphere in the winter 1991/92: Model calculations compared with Match results, *Geophys. Res. Lett.*, *25*, 4325-4328, 1998.
- Becker, G., R. Müller, D.S. McKenna, M. Rex, K.S. Carslaw, and H. Oelhaf, Ozone loss rates in the Arctic stratosphere in the winter 1994/1995: Model simulations underestimate results of the Match analysis, *J. Geophys. Res.*, *105*, 15175-15184, 2000.
- Bertram, A.K., and J.J. Sloan, Temperature-dependent nucleation rate constants and freezing behavior of submicron nitric acid dihydrate aerosol particles under stratospheric conditions, *J. Geophys. Res.*, *103*, 3553-3561, 1998a.
- Bertram, A.K., and J.J. Sloan, The nucleation rate constants and freezing mechanism of nitric acid trihydrate aerosol under stratospheric conditions, *J. Geophys. Res.*, *103*, 13261-13265, 1998b.
- Bevilacqua, R.M., C.P. Aellig, D.J. Debrestian, M.D. Fromm, K. Hoppel, J.D. Lumpe, E.P. Shettle, J.S. Hornstein, C.E. Randall, D.W. Rusch, and J.E. Rosenfield, POAM II ozone observation in the Antarctic ozone hole in 1994, 1995, and 1996, *J. Geophys. Res.*, *102*, 23643-23657, 1997.
- Bevilacqua, R.M., M.D. Fromm, J.M. Alfred, J.S. Hornstein, G.E. Nedoluha, K.W. Hoppel, J.D. Lumpe, C.E. Randall, E.P. Shettle, E.V. Browell, C. Butler, A. Dörnbrack, and A.W. Strawa, Observations and analysis of polar stratospheric clouds detected by POAM III during the 1999/2000 Northern Hemisphere winter, *J. Geophys. Res.*, *107* (D20), 8281, doi: 10.1029/2001JD000477, 2002.
- Biele, J., A. Tsias, B.P. Luo, K.S. Carslaw, R. Neuber, G. Beyerle, and T. Peter, Nonequilibrium coexistence of solid and liquid particles in Arctic stratospheric clouds, *J. Geophys. Res.*, *106*, 22991-23007, 2001.
- Biermann, U.M., T. Presper, T. Koop, J. Mossinger, P.J. Crutzen, and T. Peter, The unsuitability of meteoritic and other nuclei for polar stratospheric cloud freezing, *Geophys. Res. Lett.*, *23*, 1693-1696, 1996.
- Bird, J.C., S.R. Pal, A.I. Carswell, D.P. Donovan, G.L. Manney, J.M. Harris, and O. Uchino, Observations of ozone structures in the Arctic polar vortex, *J. Geophys. Res.*, *102*, 10785-10800, 1997.
- Bloss, W.J., S.L. Nikolaisen, R.J. Salawitch, R.R. Friedl, and S.P. Sander, Kinetics of the ClO self-reaction and 210 nm absorption cross section of the ClO dimer, *J. Phys. Chem A.*, *105*, 11226-11239, 2001.
- Bodeker, G.E., J.C. Scott, K. Kreher, and R.L. McKenzie, Global ozone trends in potential vorticity coordinates using TOMS and GOME intercompared against the Dobson network: 1978-1998, *J. Geophys. Res.*, *106*, 23029-23042, 2001.
- Bodeker, G.E., H. Struthers, and B.J. Connor, Dynamical containment of Antarctic ozone depletion, *Geophys. Res. Lett.*, *29* (7), 1098, doi: 10.1029/2001GL014206, 2002.
- Bonne, G.P., R.M. Stimpfle, R.C. Cohen, P.B. Voss, K.K. Perkins, J.G. Anderson, R.J. Salawitch, J.W. Elkins, G.S. Dutton, K.W. Jucks, and G.C. Toon, An examination of the inorganic chlorine budget in the lower stratosphere, *J. Geophys. Res.*, *105*, 1957-1971, 2000.
- Bowman, K.P., Rossby wave phase speeds and mixing barriers in the stratosphere, 1, Observations, *J. Atmos. Sci.*, *53*, 905-916, 1996.
- Bowman, K.P., and A.J. Krueger, A global climatology of total ozone from the Nimbus-7 Total Ozone Mapping Spectrometer, *J. Geophys. Res.*, *90*, 7967-7976, 1985.
- Brasseur, G.P., The response of the middle atmosphere to long-term and short-term solar variability: A two-dimensional model, *J. Geophys. Res.*, *98*, 23079-23090, 1993.
- Brasseur, G.P., X. Tie, P.J. Rasch, and F. Lefèvre, A three-dimensional simulation of the Antarctic ozone hole: Impact of anthropogenic chlorine on the lower stratosphere and upper troposphere, *J. Geophys. Res.*, *102*, 8909-8930, 1997.
- Bridgeman, A.J., and J. Rothery, Bonding in mixed halogen and hydrogen peroxides, *J. Chem. Soc. Dalton Trans.*, *22*, 4077-4082, 1999.
- Brown, S.S., R.K. Talukdar, and A.R. Ravishankara, Rate constants for the reaction $\text{OH} + \text{NO}_2 + \text{M} \rightarrow \text{HNO}_3 + \text{M}$ under atmospheric conditions, *Chem. Phys. Lett.*, *299*, 277-284, 1999a.
- Brown, S.S., R.K. Talukdar, and A.R. Ravishankara, Reconsideration of the rate constant for the reaction of hydroxyl radicals with nitric acid, *J. Phys.*

- Chem. A.*, 103, 3031-3037, 1999b.
- Brühl, C., P.J. Crutzen, and J.-U. Groö, High-latitude, summertime NO_x activation and seasonal ozone decline in the lower stratosphere: Model calculations based on observations by HALOE on UARS, *J. Geophys. Res.*, 103, 3587-3597, 1998.
- Brune, W.H., D.W. Toohey, J.G. Anderson, W.L. Starr, J.F. Vedder, and E.F. Danielson, In situ northern latitude observations of ClO, O₃, and BrO in the wintertime lower stratosphere, *Science*, 242, 558-562, 1988.
- Brune, W.H., J.G. Anderson, and K.R. Chan, In situ observations of BrO over Antarctica: ER-2 aircraft results from 54°S to 72°S latitude, *J. Geophys. Res.*, 94, 16639-16647, 1989.
- Burrows, J.P., M. Weber, M. Buchwitz, V.V. Rozanov, A. Ladstadter-Weissenmayer, A. Richter, R. de Beek, R. Hoogen, K. Bramstedt, K.-U. Eichmann, M. Eisigner, and D. Perner, The Global Ozone Monitoring Experiment (GOME): Mission concept and first scientific results, *J. Atmos. Sci.*, 56, 151-175, 1999.
- Butchart, N., and J. Austin, Middle atmosphere climatologies from the troposphere-stratosphere configuration of the UKMO's Unified Model, *J. Atmos. Sci.*, 55, 2782-2809, 1998.
- Butchart, N., J. Austin, J.R. Knight, A.A. Scaife, and M.L. Gallani, The response of the stratospheric climate to projected changes in the concentrations of well-mixed greenhouse gases from 1992 to 2051, *J. Clim.*, 13, 2142-2159, 2000.
- Carslaw, K.S., T. Peter, and S.L. Clegg, Modeling the composition of liquid stratospheric aerosols, *Rev. Geophys.*, 35, 125-154, 1997a.
- Carslaw, K.S., T. Peter, and R. Müller, Uncertainties in reactive uptake coefficients for solid stratospheric particles, 2, Effect on ozone depletion, *Geophys. Res. Lett.*, 24, 1747-1750, 1997b.
- Carslaw, K.S., M. Wirth, A. Tsiaras, B.P. Luo, A. Dörnbrack, M. Leutbecher, H. Volkert, W. Renger, J.T. Bacmeister, and T. Peter, Particle microphysics and chemistry in remotely observed mountain polar stratospheric clouds, *J. Geophys. Res.*, 103, 5785-5796, 1998a.
- Carslaw, K.S., M. Wirth, A. Tsiaras, B.P. Luo, A. Dörnbrack, M. Leutbecher, H. Volkert, W. Renger, J.T. Bacmeister, E. Reimer, and T. Peter, Increased stratospheric ozone depletion due to mountain-induced atmospheric waves, *Nature*, 391, 675-678, 1998b.
- Carslaw, K.S., T. Peter, J.T. Bacmeister, and S.D. Eckermann, Widespread solid particle formation by mountain waves in the Arctic stratosphere, *J. Geophys. Res.*, 104, 1827-1836, 1999.
- Carslaw, K.S., H. Oelhaf, J. Crowley, F. Goutail, B. Knudsen, N. Larsen, G. Redaelli, M. Rex, H. Roscoe, R. Ruhnke, and M. Volk, Polar ozone, in *European Research in the Stratosphere 1996-2000: Advances in Our Understanding of the Ozone Layer during THESEO*, edited by G.T. Amanatidis and N.R.P. Harris, EUR 19867, 69-132, European Commission, Luxembourg, 2001.
- Carslaw, K.S., J. Kettleborough, M.J. Northway, S. Davies, R.S. Gao, D.W. Fahey, D.G. Baumgardner, M.P. Chipperfield, and A. Kleinböhl, A vortex-scale simulation of the growth and sedimentation of large nitric acid particles observed during SOLVE/THESEO-2000, *J. Geophys. Res.*, in press, 2002.
- Chen, P., The permeability of the Antarctic vortex edge, *J. Geophys. Res.*, 99, 20563-20571, 1994.
- Chipperfield, M.P., Multiannual simulations with a three-dimensional chemical transport model, *J. Geophys. Res.*, 104, 1781-1805, 1999.
- Chipperfield, M.P., and R.L. Jones, Relative influences of atmospheric chemistry and transport on Arctic ozone trends, *Nature*, 400, 551-554, 1999.
- Chipperfield, M.P., and J.A. Pyle, Model sensitivity studies of Arctic ozone depletion, *J. Geophys. Res.*, 103, 28389-28403, 1998.
- Chipperfield, M.P., D. Cariolle, P. Simon, R. Ramarason, and D.J. Lary, A 3-dimensional modeling study of trace species in the Arctic lower stratosphere during winter 1989-1990, *J. Geophys. Res.*, 98, 7199-7218, 1993.
- Chipperfield, M.P., T. Glassup, I. Pundt, and O.V. Rattigan, Model calculations of stratospheric OBrO indicating very small abundances, *Geophys. Res. Lett.*, 25, 3575-3578, 1998.
- Christiansen, B., Downward propagation of zonal mean zonal wind anomalies from the stratosphere to the troposphere: Model and reanalysis, *J. Geophys. Res.*, 106, 27307-27322, 2001.
- Cohen, R.C., K.K. Perkins, L.C. Koch, R.M. Stimpfle, P.O. Wennberg, T.F. Hanisco, E.J. Lanzendorf, G.P. Bonne, P.B. Voss, R.J. Salawitch, L.A. Del Negro, J.C. Wilson, C.T. McElroy, and T.P. Bui, Quantitative constraints on the atmospheric chemistry of nitrogen oxides: An analysis along chemical coordinates, *J. Geophys. Res.*, 105, 24283-24304, 2000.
- Compagnucci, R.H., M.A. Salles, and P.O. Canziani, The

POLAR OZONE

- spatial and temporal behaviour of the lower stratospheric temperature over the Southern Hemisphere: The MSU view, I, Data methodology and temporal behaviour, *Int. J. Climatol.*, *21*, 419-437, 2001.
- Considine, D.B., A.R. Douglass, P.S. Connell, D.E. Kinnison, and D.A. Rotman, A polar stratospheric cloud parameterization for the global modeling initiative three-dimensional model and its response to stratospheric aircraft, *J. Geophys. Res.*, *105*, 3955-3973, 2000.
- Corlett, G.K., and P.S. Monks, A comparison of total column ozone values derived from the Global Ozone Monitoring Experiment (GOME), the TIROS Operational Vertical Sounder (TOVS), and the Total Ozone Mapping Spectrometer (TOMS), *J. Atmos. Sci.*, *58*, 1103-1116, 2001.
- Cubasch, U., and R. Voss, The influence of total solar irradiance on climate, *Space Sci. Rev.*, *94*, 185-198, 2000.
- Dameris, M., V. Grewe, R. Hein, and C. Schnadt, Assessment of future development of the ozone layer, *Geophys. Res. Lett.*, *25*, 3579-3582, 1998.
- Danilin, M.Y., M.L. Santee, J.M. Rodriguez, M.K.W. Ko, J.M. Mergenthaler, J.B. Kumer, A. Tabazadeh, and N.J. Livesey, Trajectory hunting: A case study of rapid chlorine activation in December 1992 as seen by UARS, *J. Geophys. Res.*, *105*, 4003-4018, 2000.
- Davies, S., M.P. Chipperfield, K.S. Carslaw, B.-M. Sinnhuber, J.G. Anderson, R.M. Stimpfle, D.M. Wilmouth, D.W. Fahey, P.J. Popp, E.C. Richard, P. von der Gathen, H. Jost, and C.R. Webster, Modeling the effect of denitrification on Arctic ozone depletion during winter 1999/2000, *J. Geophys. Res.*, in press, 2002.
- de Grandpré, J., S.R. Beagley, V.I. Fomichev, E. Griffioen, J.C. McConnell, A.S. Medvedev, and T.G. Shepherd, Ozone climatology using interactive chemistry: Results from the Canadian Middle Atmosphere Model, *J. Geophys. Res.*, *105*, 26475-26491, 2000.
- Del Negro, L.A., D.W. Fahey, R.S. Gao, S.G. Donnelly, E.R. Keim, J.A. Neuman, R.C. Cohen, K.K. Perkins, L.C. Koch, R.J. Salawitch, S.A. Lloyd, M.H. Proffitt, J.J. Margitan, R.M. Stimpfle, G.P. Bonne, P.B. Voss, P.O. Wennberg, C.T. McElroy, W.H. Swartz, T.L. Kusterer, D.E. Anderson, L.R. Lait, and T.P. Bui, Comparison of modeled and observed values of NO₂ and J_{NO₂} during the POLARIS mission, *J. Geophys. Res.*, *104*, 26687-26703, 1999.
- DeMore, W.B., S.P. Sander, D.M. Golden, R.F. Hampson, M.J. Kurylo, C.J. Howard, A.R. Ravishankara, C.E. Kolb, and M.J. Molina, *Chemical Kinetics and Photochemical Data for Use in Stratospheric Modeling: Evaluation No. 12, JPL Pub. 97-4*, Jet Propulsion Laboratory, Pasadena, Calif., 1997.
- Deniel, C., J.-P. Pommereau, R.M. Bevilacqua, and F. Lefèvre, Arctic chemical ozone depletion during the 1994/95 winter deduced from POAM II satellite observations and the REPROBUS 3-D model, *J. Geophys. Res.*, *103*, 19231-19244, 1998.
- Deniel, C., J.-P. Pommereau, F. Lefèvre, R.M. Bevilacqua, M. Fromm, and K. Hoppel, Arctic ozone loss deduced by POAM, in *Stratospheric Ozone 1999, Proc. 5th European Symp.*, 27 September-10 October 1999, St. Jean de Luz, France, edited by N.R.P. Harris, M. Guirlet, and G.T. Amanatidis, *Air Pollution Research Report 73, EUR 19340*, 421-424, European Commission, Luxembourg, 2000.
- Deshler, T., and S.J. Oltmans, Vertical profiles of volcanic aerosol and polar stratospheric clouds above Kiruna, Sweden: Winters 1993 and 1995, *J. Atmos. Chem.*, *30*, 11-23, 1998.
- Deshler, T., A. Adriani, D.J. Hofmann, and G.P. Gobbi, Evidence for denitrification in the 1990 Antarctic spring stratosphere, II, lidar and aerosol measurements, *Geophys. Res. Lett.*, *18*, 1999-2002, 1991.
- Deshler, T., T. Peter, R. Müller, and P. Crutzen, The lifetime of leewave-induced ice particles in the Arctic stratosphere, 1, Balloonborne observations, *Geophys. Res. Lett.*, *21*, 1327-1330, 1994.
- Dessler, A.E., J. Wu, M.L. Santee, and M.R. Schoeberl, Satellite observations of temporary and irreversible denitrification, *J. Geophys. Res.*, *104*, 13993-14002, 1999.
- Dhaniyala, S., K.A. McKinney, and P.O. Wennberg, Leewave clouds and denitrification in the polar stratosphere, *Geophys. Res. Lett.*, *29* (9), 1322, doi: 10.1029/2001GL013900, 2002.
- Disselkamp, R.S., S.E. Anthony, A.J. Prenni, T.B. Onasch, and M.A. Tolbert, Crystallization kinetics of nitric acid dihydrate aerosols, *J. Phys. Chem.*, *100*, 9127-9137, 1996.
- Dobson, G.M.B., Annual variation of ozone in Antarctica, *Quart. J. Roy. Meteorol. Soc.*, *92*, 549-552, 1966.
- Donahue, N.M., R. Mohrschladt, T.J. Dransfield, J.G. Anderson, and M.K. Dubey, Constraining the mechanism of OH + NO₂ using isotopically labeled reactants: Experimental evidence for HOONO formation, *J. Phys. Chem. A*, *105*, 1551-1520, 2001.
- Donaldson, D.J., G.J. Frost, K.H. Rosenlof, A.F. Tuck, and V. Vaida, Atmospheric radical production by

- excitation of vibrational overtones via absorption of visible light, *Geophys. Res. Lett.*, *24*, 2651-2654, 1997.
- Dörnbrack, A., M. Leutbecher, J. Reichardt, A. Behrendt, K.-P. Müller, and G. Baumgarten, Relevance of mountain wave cooling for the formation of polar stratospheric clouds over Scandinavia: Mesoscale dynamics and observations for January 1997, *J. Geophys. Res.*, *106*, 1569-1581, 2001.
- Dörnbrack, A., T. Birner, A. Fix, H. Flentje, A. Meister, H. Schmid, E.V. Browell, and M.J. Mahoney, Evidence for inertia gravity waves forming polar stratospheric clouds over Scandinavia, *J. Geophys. Res.*, *107* (D20), 8287, doi: 10.1029/2001JD000452, 2002.
- Douglass, A.R., M.R. Schoeberl, R.S. Stolarski, J.W. Waters, J.M. Russell III, A.E. Roche, and S.T. Massie, Interhemispheric differences in springtime production of HCl and ClONO₂ in the polar vortices, *J. Geophys. Res.*, *100*, 13967-13978, 1995.
- Douglass, A.R., M.R. Schoeberl, S.R. Kawa, and E.V. Browell, A composite view of ozone evolution in the 1995-1996 northern winter polar vortex developed from airborne lidar and satellite observations, *J. Geophys. Res.*, *106*, 9879-9895, 2001.
- Dransfield, T.J., K.K. Perkins, N.M. Donahue, J.G. Anderson, M.M. Sprengnether, and K.L. Demerjian, Temperature and pressure dependent kinetics of the gas-phase reaction of the hydroxyl radical with nitrogen dioxide, *Geophys. Res. Lett.*, *26*, 687-690, 1999.
- Drdla, K., and M.R. Schoeberl, Microphysical modeling of the 1999-2000 winter, 2, Chlorine activation and ozone depletion, *J. Geophys. Res.*, in press, 2002.
- Drdla, K., M.R. Schoeberl, and E. Browell, Microphysical modeling of the 1999-2000 winter, 1, Chlorine activation and ozone depletion, *J. Geophys. Res.*, in press, 2002.
- Dütsch, H.U., Ozone distribution in atmosphere, *Canadian J. Chem.*, *52*, 1491-1504, 1974.
- Dvortsov, V.L., and S. Solomon, Response of the stratospheric temperatures and ozone to past and future increases in stratospheric humidity, *J. Geophys. Res.*, *106*, 7505-7514, 2001.
- Dye, J.E., D. Baumgardner, B.W. Gandrud, S.R. Kawa, K.K. Kelly, M. Loewenstein, G.V. Ferry, K.R. Chan, and B.L. Gary, Particle size distribution in Arctic polar stratospheric clouds, growth and freezing of sulfuric acid droplets, and implications for cloud formation, *J. Geophys. Res.*, *97*, 8015-8034, 1992.
- EC (European Commission), *European Research in the Stratosphere 1996-2000: Advances in Our Understanding of the Ozone Layer during THESEO*, edited by G.T. Amanatidis and N.R.P. Harris, *EUR 19867*, 378 pp., Luxembourg, 2001.
- Engel, A., U. Schmidt, and R.A. Stachnik, Partitioning between chlorine reservoir species deduced from observations in the Arctic winter stratosphere, *J. Atmos. Chem.*, *27*, 107-126, 1997.
- Erle, F., U. Platt, and K. Pfeilsticker, Measurement of OBrO upper limits in the nighttime stratosphere, *Geophys. Res. Lett.*, *27*, 2217-2220, 2000.
- Esler, J.G., and D.W. Waugh, A method for estimating the extent of denitrification of Arctic polar vortex air from tracer-tracer scatter plots, *J. Geophys. Res.*, *107* (13), 4169, doi: 10.1029/2001JD001071, 2002.
- Evans, S.J., R. Toumi, J.E. Harries, M.P. Chipperfield, and J.M. Russell, Trends in stratospheric humidity and the sensitivity of ozone to these trends, *J. Geophys. Res.*, *103*, 8715-8725, 1998.
- Fahey, D.W., and A.R. Ravishankara, Summer in the stratosphere, *Nature*, *285*, 208-210, 1999.
- Fahey, D.W., R.S. Gao, L.A. Del Negro, E.R. Keim, S.R. Kawa, R.J. Salawitch, P.O. Wennberg, T.F. Hanisco, E.J. Lanzendorf, K.K. Perkins, S.A. Lloyd, W.H. Swartz, M.H. Proffitt, J.J. Margitan, J.C. Wilson, R.M. Stimpfle, R.C. Cohen, C.T. McElroy, C.R. Webster, M. Loewenstein, J.W. Elkins, and T.P. Bui, Ozone destruction and production rates between spring and autumn in the Arctic stratosphere, *Geophys. Res. Lett.*, *27*, 2605-2608, 2000.
- Fahey, D.W., R.S. Gao, K.S. Carslaw, J. Kettleborough, P.J. Popp, M.J. Northway, J.C. Holecek, S.C. Ciciora, R.J. McLaughlin, T.L. Thompson, R.H. Winkler, D.G. Baumgardner, B. Gandrud, P.O. Wennberg, S. Dhaniyala, K. McKinney, T. Peter, R.J. Salawitch, T.P. Bui, J.W. Elkins, C.R. Webster, E.L. Atlas, H. Jost, J.C. Wilson, R.L. Herman, A. Kleinböhl, and M. von König, The detection of large HNO₃-containing particles in the winter Arctic stratosphere, *Science*, *291*, 1026-1031, 2001.
- Fels, S.B., Radiative dynamical interactions in the middle atmosphere, *Adv. Geophys.*, *28*, 277-300, 1985.
- Fitzenberger, R., H. Bösch, C. Camy-Peyret, M.P. Chipperfield, H. Harder, U. Platt, B.-M. Sinnhuber, T. Wagner, and K. Pfeilsticker, First profile measurements of tropospheric BrO, *Geophys. Res. Lett.*, *27*, 2921-2924, 2000.
- Flentje, H., W. Renger, M. Wirth, and W.A. Lahoz,

POLAR OZONE

- Validation of contour advection simulations with airborne lidar measurements of filaments during the Second European Stratospheric Arctic and Midlatitude Experiment (SESAME), *J. Geophys. Res.*, *105*, 15417-15437, 2000.
- Forster, P.M. de F., and K.P. Shine, Radiative forcing and temperature trends from stratospheric ozone changes, *J. Geophys. Res.*, *102*, 10841-10855, 1997.
- Forster, P.M. de F., and K.P. Shine, Stratospheric water vapor changes as a possible contributor to observed stratospheric cooling, *Geophys. Res. Lett.*, *26*, 3309-3312, 1999.
- Forster, P.M. de F., and K.P. Shine, Assessing the climate impact and its uncertainty for trends in stratospheric water vapor, *Geophys. Res. Lett.*, *29* (6), 1086, doi: 10.1029/2001GL013909, 2002.
- Forster, P.M. de F., R.S. Freckleton, and K.P. Shine, On the aspects of the concept of radiative forcing, *Clim. Dyn.*, *13*, 547-560, 1997.
- Forster, P.M. de F., M. Ponater, and W.Y. Zhong, Testing broadband radiation schemes for their ability to calculate the radiative forcing and temperature response to stratospheric water vapour and ozone changes, *Meteorol. Z.*, *10*, 387-393, 2001.
- Friess, U., M.P. Chipperfield, H. Harder, C. Otten, U. Platt, J. Pyle, T. Wagner, and K. Pfeilsticker, Inter-comparison of measured and modeled BrO slant column amounts for the Arctic winter and spring 1994/95, *Geophys. Res. Lett.*, *26*, 1861-1864, 1999.
- Fromm, M.D., J.D. Lumpe, R.M. Bevilacqua, E.P. Shettle, J. Hornstein, S.T. Massie, and K.H. Fricke, Observations of Antarctic polar stratospheric clouds by POAM II: 1994-1996, *J. Geophys. Res.*, *102*, 23659-23672, 1997.
- Fromm, M.D., R.M. Bevilacqua, J. Hornstein, E. Shettle, K. Hoppel, and J.D. Lumpe, An analysis of Polar Ozone and Aerosol Measurement (POAM) II Arctic polar stratospheric cloud observations: 1993-1996, *J. Geophys. Res.*, *104*, 24341-24358, 1999.
- Füglister, S., B.P. Luo, C. Vigt, K.S. Carslaw, and T. Peter, NAT-rock formation by mother clouds: A microphysical model study, *Atmos. Chem. Phys.*, *2*, 93-98, 2002.
- Gao, R.S., D.W. Fahey, L.A. Del Negro, S.G. Donnelly, E.R. Keim, J.A. Neuman, E. Teverovskaia, P.O. Wennberg, T.F. Hanisco, E.J. Lanzendorf, M.H. Proffitt, J.J. Margitan, J.C. Wilson, J.W. Elkins, R.M. Stimpfle, R.C. Cohen, C.T. McElroy, T.P. Bui, R.J. Salawitch, S.S. Brown, A.R. Ravishankara, R.W. Portmann, M.K.W. Ko, D.K. Weisenstein, and P.A. Newman, A comparison of observations and model simulations of NO_x/NO_y in the lower stratosphere, *Geophys. Res. Lett.*, *26*, 1153-1156, 1999.
- Gao, R.S., L.A. Del Negro, W.H. Swartz, R.J. Salawitch, S.A. Lloyd, M.H. Proffitt, D.W. Fahey, S.G. Donnelly, J.A. Neuman, R.M. Stimpfle, and T.P. Bui, J_{NO_2} at high solar zenith angles in the lower stratosphere, *Geophys. Res. Lett.*, *28*, 2405-2408, 2001a
- Gao, R.S., E.C. Richard, P.J. Popp, G.C. Toon, D.F. Hurst, P.A. Newman, J.C. Holecck, M.J. Northway, D.W. Fahey, M.Y. Danilin, B. Sen, K. Aikin, P.A. Romashkin, J.W. Elkins, C.R. Webster, S.M. Schauffler, J.B. Greenblatt, C.T. McElroy, L.R. Lait, T.P. Bui, and D. Baumgardner, Observational evidence for the role of denitrification in Arctic stratospheric ozone loss, *Geophys. Res. Lett.*, *28*, 2879-2882, 2001b.
- Garcia, R.R., and B.A. Boville, "Downward control" of the mean meridional circulation and temperature distribution of the polar winter stratosphere, *J. Atmos. Sci.*, *51*, 2238-2245, 1994.
- Gillett, N.P., M.R. Allen, and K.D. Williams, Modelling the atmospheric response to doubled CO_2 and depleted stratospheric ozone using a stratosphere-resolving coupled GCM, *Quart. J. Roy. Meteorol. Soc.*, in press, 2002.
- Gleghorn, J.T., A G1 study of the isomers of ClOOBr and related systems, *Chem. Phys. Lett.*, *271*, 296-301, 1997.
- Gobbi, P.G., G.D. Donfrancesco, and A. Adriani, Physical properties of stratospheric clouds during the Antarctic winter of 1995, *J. Geophys. Res.*, *103*, 10859, 1998.
- Godin, S., V. Bergeret, S. Bekki, C. David, and G. Mégie, Study of the interannual ozone loss and the permeability of the Antarctic polar vortex from long-term aerosol and ozone lidar measurements in Dumont d'Urville (66.4°S, 140°E), *J. Geophys. Res.*, *106*, 1311-1330, 2001.
- Golden, D.M., and G.P. Smith, Reaction of $\text{OH} + \text{NO}_2 + \text{M}$: A new view, *J. Phys. Chem. A*, *104*, 3991-3997, 2000.
- Gomez, P.C., and L.F. Pacios, Bromine and mixed bromine chlorine oxides: Wave function (CCSD(T) and MP2) versus density functional theory (B3LYP) calculations, *J. Phys. Chem. A*, *103*, 739-743, 1999.

- Goutail, F., J.-P. Pommereau, C. Phillips, C. Deniel, A. Sarkissian, F. Lefèvre, E. Kyrö, M. Rummukainen, P. Ericksen, S.B. Andersen, B.A. Kåstad-Høiskar, G.O. Braathen, V. Dorokhov, and V.U. Khattatov, Depletion of column ozone in the Arctic during the winters of 1993-94 and 1994-95, *J. Atmos. Chem.*, *32*, 1-34, 1999.
- Graf, H.F., I. Kirchner, and J. Perlwitz, Changing lower stratospheric circulation: The role of ozone and greenhouse gases, *J. Geophys. Res.*, *103*, 11251-11261, 1998.
- Gray, L.J., S.J. Phipps, T.J. Dunkerton, M.P. Baldwin, E.F. Drysdale, and M.R. Allen, A data study of the influence of the equatorial upper stratosphere on Northern-Hemisphere stratospheric sudden warmings, *Quart. J. Roy. Meteorol. Soc.*, *127*, 1985-2003, 2001.
- Grewe, V., and M. Dameris, Heterogeneous PSC ozone loss during an ozone mini-hole, *Geophys. Res. Lett.*, *24*, 2503-2506, 1997.
- Grooß, J.-U., G. Günther, P. Konopka, R. Müller, D.S. McKenna, F. Stroh, B. Vogel, A. Engel, M. Müller, K. Hoppel, R. Bevilacqua, E. Richard, C.R. Webster, J.W. Elkins, D.F. Hurst, P.A. Romashkin, and D.G. Baumgardner, Simulation of ozone depletion in spring 2000 with the Chemical Lagrangian Model of the Stratosphere (CLaMS), *J. Geophys. Res.*, in press, 2002.
- Guirlet, M., M.P. Chipperfield, J.A. Pyle, F. Goutail, J.-P. Pommereau, and E. Kyrö, Modeled Arctic ozone depletion in winter 1997/1998 and comparison with previous winters, *J. Geophys. Res.*, *105*, 22185-22200, 2000.
- Gunson, M.R., M.C. Abrams, L.L. Lowes, E. Mahieu, R. Zander, C.P. Rinsland, M.K.W. Ko, N.D. Sze, and D.K. Weisenstein, Increase in levels of stratospheric chlorine and fluorine loading between 1985 and 1992, *Geophys. Res. Lett.*, *21*, 2223-2226, 1994.
- Hadjinicolaou, P., A. Jrrar, J.A. Pyle, and L. Bishop, The dynamically-driven long-term trend in stratospheric ozone over high latitudes, *Quart. J. Roy. Meteorol. Soc.*, in press, 2002.
- Haigh, J.D., The role of stratospheric ozone in modulating the solar radiative forcing of climate. *Nature*, *370*, 544-546, 1994.
- Haigh, J.D., A GCM study of climate change in response to the 11-year solar cycle, *Quart. J. Roy. Meteorol. Soc.*, *125*, 871-892, 1999.
- Hamilton, K., Effects of an imposed quasi-biennial oscillation in a comprehensive troposphere-stratosphere-mesosphere general circulation model, *J. Atmos. Sci.*, *55*, 2393-2418, 1998.
- Hamilton, K., R.J. Wilson, and R.S. Hemler, Middle atmosphere simulated with high vertical and horizontal resolution versions of a GCM: Improvements in the cold pole bias and generation of a QBO-like oscillation in the tropics, *J. Atmos. Sci.*, *56*, 3829-3846, 1999.
- Hanisco, T.F., J.B. Smith, R.M. Stimpfle, D.M. Wilmouth, K.K. Perkins, J.R. Spackman, J.G. Anderson, D. Baumgardner, B. Gandrud, C.R. Webster, S. Dhaniyala, K.A. McKinney, and T.P. Bui, Quantifying the rate of heterogeneous processing in the Arctic polar vortex with in situ observations of OH, *J. Geophys. Res.*, *107* (D20), 8278, doi: 10.1029/2001JD000425, 2002.
- Hansen, G., T. Svenøe, M.P. Chipperfield, A. Dahlback, and U.-P. Hoppe, Evidence of substantial ozone depletion in winter 1995/96 over northern Norway, *Geophys. Res. Lett.*, *24*, 799-802, 1997.
- Hansen, G., A. Dahlback, F. Tonnessen, and T. Svenøe, Validation of GOME total ozone by means of the Norwegian ozone monitoring network, *Annales Geophysicae*, *17*, 430-436, 1999.
- Hanson, D., and K. Mauersberger, Vapor pressures of HNO₃/H₂O solutions at low temperatures, *J. Phys. Chem.*, *92*, 6167-6170, 1988.
- Harder, H., C. Camy-Peyret, F. Ferlemann, R. Fitzenberger, T. Hawat, H. Osterkamp, M. Schneider, D. Perner, U. Platt, P. Vradelis, and K. Pfeilsticker, Stratospheric BrO profiles measured at different latitudes and seasons: Atmospheric observations, *Geophys. Res. Lett.*, *25*, 3843-3846, 1998.
- Harris, N.R.P., M. Rex, F. Goutail, B.M. Knudsen, G.L. Manney, R. Müller, and P. von der Gathen, Comparison of empirically derived ozone losses in the Arctic vortex, *J. Geophys. Res.*, *107* (D20), 8264, doi: 10.1029/2001JD000482, 2002.
- Hartmann, D.L., J.M. Wallace, V. Limpasuvan, D.W.J. Thompson, and J.R. Holton, Can ozone depletion and global warming interact to produce rapid climate change?, *Proc. Natl. Acad. Sci.*, *97*, 1412-1417, 2000.
- Haynes, P.H., C.J. Marks, M.E. McIntyre, T.G. Shepherd, and K.P. Shine, On the "downward control" of extratropical diabatic circulations by eddy-induced mean zonal forces, *J. Atmos. Sci.*, *48*, 651-678, 1991.
- Hein, R., M. Dameris, C. Schnadt, C. Land, V. Grewe, I. Kohler, M. Ponater, R. Sausen, B. Steil, J.

POLAR OZONE

- Landgraf, and C. Brühl, Results of an interactively coupled atmospheric chemistry-general circulation model: Comparison with observations, *Annales Geophysicae*, 19, 435-457, 2001.
- Hendricks, J., F. Baier, G. Gunther, B.C. Kruger, and A. Ebel, Stratospheric ozone depletion during the 1995-1996 Arctic winter: 3-D simulations on the potential role of different PSC types, *Annales Geophysicae*, 19, 1163-1181, 2001.
- Herman, R.L., K. Drdla, J.R. Spackman, D.F. Hurst, P.J. Popp, C.R. Webster, J.W. Elkins, E.M. Weinstock, B.W. Gandrud, G.C. Toon, M.R. Schoeberl, H. Jost, E.L. Atlas, and T.P. Bui, Hydration, dehydration, and the total hydrogen budget of the 1999-2000 winter Arctic stratosphere, *J. Geophys. Res.*, in press, 2002.
- Hines, C.O., Doppler-spread parameterization of gravity-wave momentum deposition in the middle atmosphere, 1, Basic formulation, *J. Atmos. Sol.-Terr. Phys.*, 59, 371-386, 1997a.
- Hines, C.O., Doppler-spread parameterization of gravity-wave momentum deposition in the middle atmosphere, 2, Broad and quasi-monochromatic spectra and implementation, *J. Atmos. Sol.-Terr. Phys.*, 59, 387-400, 1997b.
- Hints, H.J., P.A. Newman, H.H. Jonsson, C.R. Webster, R.D. May, R.L. Herman, L.R. Lait, M.R. Schoeberl, J.W. Elkins, P.R. Wamsley, G.S. Dutton, T.P. Bui, D.W. Kohn, and J.G. Anderson, Dehydration and denitrification in the Arctic polar vortex during the 1995-1996 winter, *Geophys. Res. Lett.*, 25, 501-504, 1998.
- Hipler, H., S. Nasterlack, and F. Striebel, Reaction of OH + NO₂ + M: Evidence for isomer formation, *Phys. Chem. Chem. Phys.*, 4, 2959-2964, 2002.
- Hofmann, D.J., and T. Deshler, Stratospheric cloud observations during formation of the Antarctic ozone hole in 1989, *J. Geophys. Res.*, 96, 2897-2912, 1991.
- Hofmann, D.J., S.J. Oltmans, J.M. Harris, B.J. Johnson, and J.A. Lathrop, Ten years of ozonesonde measurements at the South Pole: Implication for recovery of springtime Antarctic ozone, *J. Geophys. Res.*, 102, 8931-8943, 1997.
- Holton, J.R., Meridional distribution of stratospheric trace constituents. *J. Atmos. Sci.*, 43, 1238-1242, 1986.
- Hood, L.L., and S. Zhou, Stratospheric effects of 27-day solar ultraviolet variations: The column ozone response and comparisons of solar cycles 21 and 22, *J. Geophys. Res.*, 104, 26473-26479, 1999.
- Hood, L., S. Rossi, and M. Beulen, Trends in lower stratospheric zonal winds, Rossby wave breaking behavior, and column ozone at northern midlatitudes, *J. Geophys. Res.*, 104, 24321-24339, 1999.
- Hood, L.L., B.E. Soukharev, M. Fromm, and J.P. McCormack, Origin of extreme ozone minima at middle to high northern latitudes, *J. Geophys. Res.*, 106, 20925-20940, 2001.
- Hoogen, R., V.V. Rozanov, and J.P. Burrows, Ozone profiles from GOME satellite data: Algorithm description and first validation, *J. Geophys. Res.*, 104, 8263-8280, 1999.
- Hopfner, M., C.E. Blom, H. Fischer, N. Glatthor, T. Gulde, C. Piesch, W. Renger, and M. Wirth, HNO₃ and PSC measurements from the TRANSALL: Sequestering of HNO₃ in the winter of 1994/95, *J. Atmos. Chem.*, 30, 61-79, 1998.
- Hoppel, K.W., R.M. Bevilacqua, G. Nedoluha, C. Deniel, F. Lefèvre, J.D. Lumpe, M.D. Fromm, C.E. Randall, J. Rosenfield, and M. Rex, POAM III observations of Arctic ozone loss for the 1999/2000 winter, *J. Geophys. Res.*, 107 (D20), 8262, doi: 10.1029/2001JD000476, 2002.
- Hu, R., K.S. Carslaw, C. Hostetler, L.R. Poole, B.P. Luo, T. Peter, S. Füglistaler, T.J. McGee, and J.F. Burris, The microphysical properties of wave PSCs retrieved from lidar measurements during SOLVE, *J. Geophys. Res.*, in press, 2002.
- Huder, K.J., and W.B. DeMore, Absorption cross sections of the ClO dimer, *J. Phys. Chem.*, 99, 3905-3908, 1995.
- Ionov, D.V., Y.M. Timofeev, V.V. Ionov, A.M. Shalamyanskii, O.M. Johannessen, and J.P. Burrows, Comparison of measurements of total ozone by the GOME (ERS-2) spectrometer with data from the Russian ozonometric network, *Earth Obs. Remote Sens.*, 16, 527-539, 2001.
- IPCC (Intergovernmental Panel on Climate Change), *Climate Change 1992: The Supplementary Report to the IPCC*, edited by J.T. Houghton, B.A. Callander, and S.K. Varney, 205 pp., Cambridge University Press, Cambridge, U.K., 1992.
- IPCC (Intergovernmental Panel on Climate Change), *Climate Change 1995: The Science of Climate Change*, edited by J.T. Houghton, L.G. Meira Filho, J. Bruce, H. Lee, B.A. Callander, E. Haites, N. Harris, and K. Maskell, 572 pp., Cambridge University Press, Cambridge, U.K., 1996.
- IPCC (Intergovernmental Panel on Climate Change), *Climate Change 2001: The Scientific Basis: Contribution of Working Group I to the Third Assessment Report of the Intergovernmental Panel*

- on *Climate Change*, edited by J.T. Houghton, Y. Ding, D.J. Griggs, M. Noguer, P.J. van der Linden, X. Dai, K. Maskell, and C.A. Johnson, 881 pp., Cambridge University Press, Cambridge, U.K., 2001.
- Iraci, L.T., A.M. Middlebrook, M.A. Wilson, and M.A. Tolbert, Growth of nitric-acid hydrates on thin sulfuric-acid films, *Geophys. Res. Lett.*, *21*, 867-870, 1994.
- Iraci, L.T., A.M. Middlebrook, and M.A. Tolbert, Laboratory studies of the formation of polar stratospheric clouds: Nitric acid condensation on thin sulfuric acid films, *J. Geophys. Res.*, *100*, 20969-20977, 1995.
- Iraci, L.T., T.J. Fortin, and M.A. Tolbert, Dissolution of sulfuric acid tetrahydrate at low temperatures and subsequent growth of nitric acid trihydrate, *J. Geophys. Res.*, *103*, 8491-8498, 1998.
- Irie, H., M. Koike, Y. Kondo, G.E. Bodeker, M.Y. Danilin, and Y. Sasano, Redistribution of nitric acid in the Arctic lower stratosphere during the winter of 1996-1997, *J. Geophys. Res.*, *106*, 23139-23150, 2001.
- Irie, H., Y. Kondo, M. Koike, M.Y. Danilin, C. Camy-Peyret, S. Payan, J.-P. Pommereau, F. Goutail, H. Oelhaf, G. Wetzell, G.C. Toon, B. Sen, R.M. Bevilacqua, J.M. Russell, J.B. Renard, H. Kanzawa, H. Nakajima, T. Yokota, T. Sugita, and Y. Sasano, Validation of NO₂ and HNO₃ measurements from the Improved Limb Atmospheric Spectrometer (ILAS) with the version 5.20 retrieval algorithm, *J. Geophys. Res.*, *107* (D24), 8206, doi: 10.1029/2001JD001304, 2002.
- Jensen, E.J., O.B. Toon, A. Tabazadeh, and K. Drdla, Impact of polar stratospheric cloud particle composition, number density, and lifetime on denitrification, *J. Geophys. Res.*, *107* (D20), 8284, doi: 10.1029/2001JD000440, 2002.
- Johnsson, K., A. Engdahl, J. Kolm, J. Nieminen, and B. Nelander, The ClOClO, BrOClO, and IOClO molecules and their photoisomerization: A matrix isolation study, *J. Chem. Phys.*, *99*, 3902-3904, 1995.
- Jones, R.L., and A.R. MacKenzie, Observational studies of the role of the polar regions in mid-latitude ozone loss, *Geophys. Res. Lett.*, *22*, 3485-3488, 1995.
- Juckes, M.N., and M.E. McIntyre, A high-resolution, one-layer model of breaking planetary waves in the stratosphere, *Nature*, *328*, 590-596, 1987.
- Jucks, K.W., D.G. Johnson, K.V. Chance, W.A. Traub, J.J. Margitan, G.B. Osterman, R.J. Salawitch, and Y. Sasano, Observations of OH, HO₂, H₂O, and O₃ in the upper stratosphere: Implications for HO_x photochemistry, *Geophys. Res. Lett.*, *25*, 3935-3938, 1998.
- Jucks, K.W., D.G. Johnson, K.V. Chance, W.A. Traub, and R.J. Salawitch, Nitric acid in the middle stratosphere as a function of altitude and aerosol loading, *J. Geophys. Res.*, *104*, 26715-26723, 1999.
- Kaledin, A., and K. Morokuma, An ab initio direct study of the photodissociation of ClOCl, *J. Chem. Phys.*, *113*, 5750-5762, 2000.
- Kanzawa, H., C. Schiller, J. Ovarlez, C. Camy-Peyret, S. Payan, P. Jeseck, H. Oelhaf, M. Stowasser, W.A. Traub, K. Jucks, D.G. Johnson, G.C. Toon, J.H. Park, G. Bodeker, L. Pan, T. Sugita, H. Nakajima, T. Yokota, M. Suzuki, M. Shiotani, and Y. Sasano, Validation and data characteristics of water vapor profiles observed by the Improved Limb Atmospheric Spectrometer (ILAS) and processed with version 5.20 algorithm, *J. Geophys. Res.*, in press, 2002.
- Kawamoto, N., and M. Shiotani, Interannual variability of the vertical descent rate in the Antarctic polar vortex, *J. Geophys. Res.*, *105*, 11935-11946, 2000.
- Kettleborough, J.A., and J.R. Holton, Limitations of a diagnostic of stratospheric tracer lamination, *J. Geophys. Res.*, *104*, 21621-21628, 1999.
- Kiehl, J.T., B.A. Boville, and B.P. Briegleb, Response of a general-circulation model to a prescribed Antarctic ozone hole, *Nature*, *332*, 501-504, 1988.
- Kilbane-Dawe, I., N.R.P. Harris, J.A. Pyle, M. Rex, A.M. Lee, and M.P. Chipperfield, A comparison of Match ozonesonde-derived and 3-D model ozone loss rates in the Arctic polar vortex during the winters of 1994/95 and 1995/96, *J. Atmos. Chem.*, *39*, 123-138, 2001.
- Kirchner, I., G.L. Stenchikov, H.-F. Graf, A. Robock, and J.C. Antuna, Climate model simulation of winter warming and summer cooling following the 1991 Mt. Pinatubo eruption, *J. Geophys. Res.*, *104*, 19039-19055, 1999.
- Kirk-Davidoff, D.B., E.J. Hints, J.G. Anderson, and D.W. Keith, The effect of climate change on ozone depletion through changes in stratospheric water vapour, *Nature*, *402*, 399-401, 1999.
- Klein, U., K. Linder, I. Wohltmann, and K.F. Künzi, Winter and spring observations of stratospheric chlorine monoxide from Ny-Ålesund, Spitsbergen, in 1997/98 and 1998/99, *Geophys. Res. Lett.*, *27*, 4093-4096, 2000.
- Knudsen, B.M., N. Larsen, I.S. Mikkelsen, J.-J. Morcrette,

POLAR OZONE

- G.O. Braathen, E. Kyrö, H. Fast, H. Gernandt, H. Kanzawa, H. Nakane, V. Dorokhov, V. Yushkov, G. Hansen, M. Gil, and R.J. Shearman, Ozone depletion in and below the Arctic vortex for 1997, *Geophys. Res. Lett.*, *25*, 627-630, 1998.
- Knudsen, B.M., J.-P. Pommereau, A. Garnier, M. Nunes-Pinharanda, L. Denis, P.A. Newman, G. Letrenne, and M. Durand, Accuracy of analyzed stratospheric temperatures in the winter Arctic vortex from infrared Montgolfier long-duration balloon flights, II, Results, *J. Geophys. Res.*, *107* (D20), 4316, doi: 10.1029/2001JD001329, 2002.
- Kodera, K., Influence of volcanic eruptions on the troposphere through stratospheric dynamical processes in the Northern Hemisphere winter, *J. Geophys. Res.*, *99*, 1273-1282, 1994.
- Kodera, K., and Y. Kuroda, Tropospheric and stratospheric aspects of the Arctic oscillation, *Geophys. Res. Lett.*, *27*, 3349-3352, 2000.
- Kodera, K., M. Chiba, H. Koide, A. Kitoh, and Y. Nikaidou, Interannual variability of the winter stratosphere and troposphere in the Northern Hemisphere, *J. Meteorol. Soc. Japan*, *74*, 365-382, 1996.
- Kodera, K., Y. Kuroda, and S. Pawson, Stratospheric sudden warmings and slowly propagating zonal-mean wind anomalies, *J. Geophys. Res.*, *105*, 12351-12359, 2000.
- Koike, M., Y. Kondo, H. Irie, F.J. Murcray, J. Williams, P. Fogal, R. Blatherwick, C. Camy-Peyret, S. Payan, H. Oelhaf, G. Wetzel, W. Traub, D. Johnson, K. Jucks, G.C. Toon, B. Sen, J.-F. Blavier, H. Schlager, H. Ziereis, N. Toriyama, M.Y. Danilin, J.M. Rodriguez, H. Kanzawa, and Y. Sasano, A comparison of Arctic HNO₃ profiles measured by ILAS and balloon-borne sensors, *J. Geophys. Res.*, *105*, 6761-6771, 2000.
- Kondo, Y., H. Irie, M. Koike, and G.E. Bodeker, Denitrification and nitrification in the Arctic stratospheric during the winter of 1996-1997, *Geophys. Res. Lett.*, *27*, 337-340, 2000.
- Koop, T., U.M. Biermann, W. Raber, B.P. Luo, P.J. Crutzen, and T. Peter, Do stratospheric aerosol droplets freeze above the ice frost point?, *Geophys. Res. Lett.*, *22*, 917-920, 1995.
- Koop, T., B. Luo, U.M. Biermann, P.J. Crutzen, and T. Peter, Freezing of HNO₃/H₂SO₄/H₂O solutions at stratospheric temperatures: Nucleation statistics and experiments, *J. Phys. Chem. A*, *101*, 1117-1133, 1997.
- Kopp, G., H. Berg, T. Blumenstock, H. Fischer, F. Hase, G. Hochschild, M. Hoepfner, W. Kouker, I. Langbein, T. Reddmann, R. Ruhnke, U. Raffalski, and Y. Kondo, Evolution of ozone and ozone related species over Kiruna during the THESEO 2000-SOLVE campaign retrieved from ground-based millimeter wave and infrared observations, *J. Geophys. Res.*, in press, 2002.
- Kuroda, Y., and K. Kodera, Interannual variability in the troposphere and stratosphere of the Southern Hemisphere winter, *J. Geophys. Res.*, *103*, 13787-13799, 1998.
- Kuroda, Y., and K. Kodera, Role of planetary waves in the stratosphere-troposphere coupled variability in the Northern Hemisphere winter, *Geophys. Res. Lett.*, *26*, 2375-2378, 1999.
- Labitzke, K., On the interannual variability of the middle stratosphere during the northern winters, *J. Meteorol. Soc. Japan*, *60*, 124-139, 1982.
- Labitzke, K., and H. van Loon, The southern oscillation, IX, The influence of volcanic-eruptions on the southern oscillation in the stratosphere, *J. Clim.*, *2*, 1223-1226, 1989.
- Labitzke, K., and H. van Loon, A note on the distribution of trends below 10 hPa: The extratropical Northern Hemisphere, *J. Meteorol. Soc. Japan*, *73*, 8883-8889, 1995.
- Labitzke, K., and H. van Loon, The signal of the 11-year solar cycle in the upper troposphere-lower stratosphere, *Space Sci. Rev.*, *80*, 393-410, 1997.
- Labitzke, K., J. Austin, N. Butchart, J. Knight, J. Haigh, and V. Williams, The global signal of the 11-year solar cycle in the stratosphere, *J. Atmos. Sol.-Terr. Phys.*, in press, 2002.
- Langematz, U., An estimate of the impact of observed ozone losses on stratospheric temperature. *Geophys. Res. Lett.*, *27*, 2077-2080, 2000.
- Langematz, U., M. Kunze, K. Krueger, K. Labitzke, and G.L. Roff, Thermal and dynamical changes of the stratosphere since 1979 and their link to ozone and CO₂ changes, *J. Geophys. Res.*, in press, 2002.
- Larkin, A., J.D. Haigh, and S. Djavidnia, The effect of solar UV irradiance variations on the Earth's atmosphere, *Space Sci. Rev.*, *94*, 199-214, 2000.
- Larsen, N., I. Mikkelsen, B.M. Knudsen, J. Schreiner, C. Voigt, K. Mauersberger, J.M. Rosen, and N.T. Kjome, Comparison of chemical and optical in situ measurements of polar stratospheric clouds, *J. Geophys. Res.*, *105*, 1491-1502, 2000.
- Larsen, N., S. Høyer Svendsen, B.M. Knudsen, C. Voigt, A. Kohlmann, J. Schreiner, K. Mauersberger, T. Deshler, C. Kröger, J.M. Rosen, N.T. Kjome, A.

- Adriani, F. Cairo, G. Di Donfrancesco, J. Ovarlez, H. Ovarlez, A. Dörnbrack, and T. Birner, Microphysical mesoscale simulations of polar stratospheric cloud formation constrained by in situ measurements of chemical and optical cloud properties, *J. Geophys. Res.*, in press, 2002.
- Lawrence, B.N., Some aspects of the sensitivity of stratospheric climate simulation to model lid height, *J. Geophys. Res.*, *102*, 23805-23811, 1997.
- Lee, A.M., H.K. Roscoe, and S. Oltmans, Model and measurements show Antarctic ozone loss follows edge of polar night, *Geophys. Res. Lett.*, *27*, 3845-3848, 2000.
- Lee, A.M., H.K. Roscoe, A.E. Jones, P.H. Haynes, E.F. Shuckburgh, M.W. Morrey, and H.C. Pumphrey, The impact of the mixing properties within the Antarctic stratospheric vortex on ozone loss in spring, *J. Geophys. Res.*, *106*, 3203-3211, 2001.
- Lefèvre, F., F. Figarol, K.S. Carslaw, and T. Peter, The 1997 Arctic ozone depletion quantified from three-dimensional model simulations, *Geophys. Res. Lett.*, *25*, 2425-2428, 1998.
- Li, S., E.C. Cordero, and D.J. Karoly, Transport out of the Antarctic polar vortex from a three-dimensional transport model, *J. Geophys. Res.*, *107* (D11), 4132, doi: 10.1029/2001JD000508, 2002.
- Liley, J.B., P.V. Johnston, R.L. McKenzie, A.J. Thomas, and I.S. Boyd, Stratospheric NO₂ variations from a long time series at Lauder, New Zealand, *J. Geophys. Res.*, *105*, 11633-11640, 2000.
- Lloyd, S., W.H. Swartz, T. Kusterer, D. Anderson, C.T. McElroy, C. Midwinter, R. Hall, K. Nassim, D. Jaffe, W. Simpson, J. Kelley, D. Nicks, D. Griffin, B. Johnson, R. Evans, D. Quincy, S. Oltmans, P. Newman, R. McPeters, G. Labow, L. Moy, C. Seftor, G. Toon, B. Sen, and J.-F. Blavier, Intercomparison of total ozone observations at Fairbanks, Alaska, during POLARIS, *J. Geophys. Res.*, *104*, 26767-26778, 1999.
- Lucic, D., N.R.P. Harris, J.A. Pyle, and R.L. Jones, A technique for estimating polar ozone loss: Results from the northern 1991/92 winter using EASOE data, *J. Atmos. Chem.*, *34*, 365-383, 1999.
- Lucke, R.L., D.R. Korwan, R.M. Bevilacqua, J.S. Hornstein, E.P. Shettle, D.T. Chen, M. Dähler, J.D. Lumpe, M.D. Fromm, D. Debrestian, B. Neff, M. Squire, G. König-Langlo, and J. Davies, The Polar Ozone and Aerosol Measurement (POAM) III instrument and early validation results, *J. Geophys. Res.*, *104*, 18785-18799, 1999.
- Lumpe, J.D., M. Fromm, K. Hoppel, R.M. Bevilacqua, C.E. Randall, E.V. Browell, W.B. Grant, T. McGee, J. Burris, L. Twigg, E. Richard, G.C. Toon, J.J. Margitan, B. Sen, K. Pfeilsticker, H. Boesch, R. Fitzenberger, F. Goutail, and J.-P. Pommereau, Comparison of POAM III ozone measurements with correlative aircraft and balloon data during SOLVE, *J. Geophys. Res.*, in press, 2002.
- Mahlman, J.D., J.P. Pinto, and L.J. Umscheid, Transport radiative and dynamical effects of the Antarctic ozone hole: A GFDL SKYHI model experiment, *J. Atmos. Sci.*, *51*, 489-508, 1994.
- Mann, G.W., S. Davies, K.S. Carslaw, M.P. Chipperfield, and J. Kettleborough, Influence of vortex baroclinicity on Arctic denitrification, *J. Geophys. Res.*, in press, 2002.
- Manney, G.L., L. Froidevaux, J.W. Waters, R.W. Zurek, W.G. Read, L.S. Elson, J.B. Kumer, J.L. Mergenthaler, A.E. Roche, A. O'Neill, R.S. Harwood, I. MacKenzie, and R. Swinbank, Chemical depletion of ozone in the Arctic lower stratosphere during winter 1992-93, *Nature*, *370*, 429, 1994.
- Manney, G.L., R.W. Zurek, L. Froidevaux, J.W. Waters, A. O'Neill, and R. Swinbank, Lagrangian transport calculations using UARS data, II, Ozone, *J. Atmos. Sci.*, *52*, 3069-3081, 1995a.
- Manney, G.L., R.W. Zurek, L. Froidevaux, and J.W. Waters, Evidence for Arctic ozone depletion in late February and early March 1994, *Geophys. Res. Lett.*, *22*, 2941-2944, 1995b.
- Manney, G.L., M.L. Santee, L. Froidevaux, J.W. Waters, and R.W. Zurek, Polar vortex conditions during the 1995-96 Arctic winter: Meteorology and MLS ozone, *Geophys. Res. Lett.*, *23*, 3203-3206, 1996a.
- Manney, G.L., L. Froidevaux, J.W. Waters, M.L. Santee, W.G. Read, D.A. Flower, R.F. Garnet, and R.W. Zurek, Arctic ozone depletion observed by UARS MLS during the 1994-95 winter, *Geophys. Res. Lett.*, *23*, 85-88, 1996b.
- Manney, G.L., L. Froidevaux, M.L. Santee, R.W. Zurek, and J.W. Waters, MLS observations of Arctic ozone loss in 1996-1997, *Geophys. Res. Lett.*, *24*, 2697-2700, 1997.
- Manney, G.L., J.C. Bird, D.P. Donovan, T.J. Duck, J.A. Whiteway, S.R. Pal, and A.I. Carswell, Modeling ozone laminae in ground-based Arctic wintertime observations using trajectory calculations and satellite data, *J. Geophys. Res.*, *103*, 5797-5814, 1998.
- Manney, G.L., W.A. Lahoz, R. Swinbank, A. O'Neill, P.M. Connex, and R.W. Zurek, Simulation of the

POLAR OZONE

- December 1998 stratospheric major warming, *Geophys. Res. Lett.*, *26*, 2733-2736, 1999.
- Manney, G.L., H.A. Michelsen, F.W. Irion, G.C. Toon, M.R. Gunson, and A.E. Roche, Lamination and polar vortex development in fall from ATMOS long-lived trace gases observed during November 1994, *J. Geophys. Res.*, *105*, 29023-29038, 2000.
- Manney, G.L., J.L. Sabutis, and R. Swinbank, A unique stratospheric warming event in December 2000, *Geophys. Res. Lett.*, *28*, 2629-2632, 2001.
- Manney, G.L., J.L. Sabutis, S. Pawson, M.L. Santee, B. Naujokat, R. Swinbank, M.E. Gelman, and W. Ebisuzaki, Lower stratospheric temperature differences between meteorological analyses in two cold Arctic winters and their impact on polar processing studies, *J. Geophys. Res.*, in press, 2002.
- Manzini, E., and N.A. McFarlane, The effect of varying the source spectrum of a gravity wave parameterization in a middle atmosphere general circulation model, *J. Geophys. Res.*, *103*, 31523-31539, 1998.
- Massie, S.T., X. Tie, G.P. Brasseur, R.M. Bevilacqua, M.D. Fromm, and M.L. Santee, Chlorine activation during the early 1995-1996 Arctic winter, *J. Geophys. Res.*, *105*, 7111-7132, 2000.
- Matheu, D.M., and W.H. Green, A priori falloff analysis for OH + NO₂, *Int. J. Chem. Kinet.*, *32*, 245-262, 2000.
- McCormick, M.P., W.P. Chu, G.W. Grams, P. Hamill, B.M. Herman, L.R. McMaster, T.J. Pepin, P.B. Russell, H.M. Steele, and T.J. Swissler, High-latitude stratospheric aerosols measured by the SAM II satellite system in 1978 and 1979, *Science*, *214*, 328-331, 1981.
- McGrath, M.P., and F.S. Rowland, Determination of the barriers to internal-rotation in ONOOX (X = H, Cl) and characterization of the minimum energy conformers, *J. Phys. Chem.*, *98*, 1061-1067, 1994.
- McKenna, D., R.L. Jones, J. Austin, E.V. Browell, M.P. McCormick, A.J. Krueger, and A.F. Tuck, Diagnostic studies of the Antarctic vortex during the 1987 Airborne Antarctic Ozone Experiment: Ozone mini-holes, *J. Geophys. Res.*, *94*, 11641-11668, 1989.
- McKinney, K.A., J.M. Pierson, and D.W. Toohey, A wintertime in situ profile of BrO between 17 and 27 km in the Arctic vortex, *Geophys. Res. Lett.*, *24* (8), 853-856, 1997.
- McLandress, C., On the importance of gravity waves in the middle atmosphere and their parameterization in general circulation models, *J. Atmos. Sol.-Terr. Phys.*, *60*, 1357-1383, 1998.
- McLinden, C.A., S.C. Olsen, M.J. Prather, and J.B. Liley, Understanding trends in stratospheric NO_y and NO₂, *J. Geophys. Res.*, *106*, 27787-27793, 2001.
- Medvedev, A.S., and G.P. Klaassen, Vertical evolution of gravity wave spectra and the parameterization of associated wave drag, *J. Geophys. Res.*, *100*, 25841-25853, 1995.
- Medvedev, A.S., G.P. Klaassen, and S.R. Beagley, On the role of anisotropic gravity wave spectrum in maintaining the circulation of the middle atmosphere, *Geophys. Res. Lett.*, *25*, 509-512, 1998.
- Meilinger, S.K., T. Koop, B.P. Luo, T. Huthwelker, K.S. Carslaw, U. Kreiger, P.J. Crutzen, and T. Peter, Size-dependent stratospheric droplet composition in lee wave temperature fluctuations and their potential role in PSC freezing, *Geophys. Res. Lett.*, *22*, 3031-3034, 1995.
- Mergenthaler, J.L., J.B. Kumer, A.E. Roche, and S.T. Massie, Distribution of Antarctic polar stratospheric clouds as seen by the CLAES experiment, *J. Geophys. Res.*, *102*, 19161-19170, 1997.
- Michelsen, H.A., G.L. Manney, M.R. Gunson, and R. Zander, Correlations of stratospheric abundances of NO_y, O₃, N₂O, and CH₄ derived from ATMOS measurements, *J. Geophys. Res.*, *103*, 28347-28359, 1998.
- Michelsen, H.A., C.R. Webster, G.L. Manney, D.C. Scott, J.J. Margitan, R.D. May, F.W. Irion, M.R. Gunson, J.M. Russell III, and C.M. Spivakovsky, Maintenance of high HCl/Cl_y and NO_x/NO_y in the Antarctic vortex: A chemical signature of confinement during spring, *J. Geophys. Res.*, *104*, 26419-26436, 1999.
- Mickley, L.J., J.P.D. Abbatt, J.E. Frederick, and J.M. Russell III, Evolution of chlorine and nitrogen species in the lower stratosphere during Antarctic spring: Use of tracers to determine chemical change, *J. Geophys. Res.*, *102*, 21479-21491, 1997.
- Millard, G.A., A.M. Lee, and J.A. Pyle, A model study of the connection between polar and midlatitude ozone loss in the Northern Hemisphere lower stratosphere, *J. Geophys. Res.*, in press, 2002.
- Miller, H.L., R.W. Sanders, and S. Solomon, Observations and interpretation of column OClO seasonal cycles at polar sites, *J. Geophys. Res.*, *104*, 18769-18783, 1999.
- Mo, R.P., O. Buhler, and M.E. McIntyre, Permeability of the vortex edge: On the mean mass flux due to thermally dissipating, steady, non-breaking Rossby waves, *Quart. J. Roy. Meteorol. Soc.*, *124*, 2129-2148, 1998.

- Moore, T.A., M. Okumura, J.W. Seale, and T.K. Minton, UV photolysis of ClOOCl, *J. Phys. Chem. A*, *103*, 1691-1695, 1999.
- Müller, R., P.J. Crutzen, J.-E. Grooß, C. Brühl, J.M. Russell III, and A.F. Tuck, Chlorine activation and ozone depletion in the Arctic vortex: Observations by the Halogen Occultation Experiment on the Upper Atmosphere Research Satellite, *J. Geophys. Res.*, *101*, 12531-12554, 1996.
- Müller, R., P.J. Crutzen, J.-U. Grooß, C. Brühl, J.M. Russell, H. Gernandt, D.S. McKenna, and A.F. Tuck, Severe chemical ozone loss in the Arctic during the winter 1995-96, *Nature*, *389*, 709-712, 1997.
- Müller, R., J.-U. Grooß, D.S. McKenna, P.J. Crutzen, C. Brühl, J.M. Russell III, L.L. Gordley, J.P. Burrows, and A.F. Tuck, Chemical ozone loss in the Arctic vortex in the winter 1995-96: HALOE measurements in conjunction with other observations, *Annales Geophysicae*, *17*, 101-114, 1999.
- Müller, R., S. Tilmes, J.-U. Grooß, D.S. McKenna, M. Müller, U. Schmidt, G.C. Toon, R.A. Stachnik, J.J. Margitan, J.W. Elkins, J. Arvelius, and J.M. Russell III, Chlorine activation and chemical ozone loss deduced from HALOE and balloon measurements in the Arctic during the winter of 1999/2000, *J. Geophys. Res.*, in press, 2002.
- Nagashima, T., M. Takahashi, M. Takigawa, and H. Akiyoshi, Future development of the ozone layer calculated by a general circulation model with fully interactive chemistry, *Geophys. Res. Lett.*, *29* (8), 1162, doi: 10.1029/2001GL014026, 2002.
- Nakajima, H., M. Suzuki, A. Matsuzaki, T. Ishigaki, K. Waragai, Y. Mogi, N. Kimura, N. Araki, T. Yokota, H. Kanzawa, T. Sugita, and Y. Sasano, Characteristics and performance of the Improved Limb Atmospheric Spectrometer (ILAS) in orbit, *J. Geophys. Res.*, in press, 2002.
- Nash, E.R., P.A. Newman, J.E. Rosenfield, and M.R. Schoeberl, An objective determination of the polar vortex using Ertel's potential vorticity, *J. Geophys. Res.*, *101*, 9471-9478, 1996.
- Nedoluha, G.E., R.M. Bevilacqua, K.W. Hoppel, M. Dähler, E.P. Shettle, J.H. Hornstein, M.D. Fromm, J.D. Lumpe, and J.E. Rosenfield, POAM III measurements of dehydration in the Antarctic lower stratosphere, *Geophys. Res. Lett.*, *27*, 1683-1686, 2000.
- Newman, P.A., and M.R. Schoeberl, A reinterpretation of the data from the NASA Stratosphere-Troposphere Exchange Project, *Geophys. Res. Lett.*, *22*, 2501-2504, 1995.
- Newman, P.A., L.R. Lait, and M.R. Schoeberl, The morphology and meteorology of Southern-Hemisphere spring total ozone mini-holes, *Geophys. Res. Lett.*, *15*, 923-926, 1988.
- Newman, P.A., L.R. Lait, M. Seablom, L. Coy, R. Rood, R. Swinbank, M. Proffitt, M. Loewenstein, J.R. Podolske, J.W. Elkins, C.R. Webster, R.D. May, D.W. Fahey, G.S. Dutton, and K.R. Chan, Measurements of polar vortex air in the midlatitudes, *J. Geophys. Res.*, *101*, 12879-12891, 1996.
- Newman, P.A., J.F. Gleason, R.D. McPeters, and R.S. Stolarski, Anomalous low ozone over the Arctic, *Geophys. Res. Lett.*, *24*, 2689-2692, 1997.
- Newman, P.A., D. Fahey, W. Brune, M. Kurylo, and S.R. Kawa, Preface: Photochemistry of Ozone Loss in the Arctic Region in Summer (POLARIS), *J. Geophys. Res.*, *104*, 26481-26496, 1999.
- Newman, P.A., E.R. Nash, and J.E. Rosenfield, What controls temperature of the Arctic stratosphere during spring?, *J. Geophys. Res.*, *106*, 19999-20010, 2001.
- Newman, P.A., N.R.P. Harris, A. Adriani, G.T. Amanatidis, J.G. Anderson, G.O. Braathen, W.H. Brune, K.S. Carslaw, M.S. Craig, P.L. DeCola, M. Guirlet, R.S. Hipskind, M.J. Kurylo, H. Küllmann, N. Larsen, G.J. Mégie, J.-P. Pommereau, L.R. Poole, M.R. Schoeberl, F. Stroh, O.B. Toon, C.R. Trepte, and M. Van Roozendael, An overview of the SOLVE/THESEO 2000 campaign, *J. Geophys. Res.*, *107* (020), doi: 10.1029/2001JD001303, in press, 2002.
- Niwano, M., and M. Takahashi, The influence of the equatorial QBO on the Northern Hemisphere winter circulation of a GCM, *J. Meteorol. Soc. Japan*, *76*, 453-461, 1998.
- Nizkorodov, S.A., and P.O. Wennberg, First spectroscopic observations of gas-phase HOONO, *J. Phys. Chem. A*, *106*, 855-859, 2002.
- Northway, M.J., R.-S. Gao, P.J. Popp, J.C. Holecek, D.W. Fahey, K.S. Carslaw, M.A. Tolbert, L.R. Lait, S. Dhaniyala, R.C. Flagan, P.O. Wennberg, M.J. Mahoney, R.L. Herman, G.C. Toon, and T.P. Bui, An analysis of large HNO₃-containing particles sampled in the Arctic stratosphere during the winter of 1999-2000, *J. Geophys. Res.*, in press, 2002a.
- Northway, M.J., P.J. Popp, R.S. Gao, D.W. Fahey, G.C. Toon, and T.P. Bui, Relating inferred HNO₃ flux values to the denitrification of the 1999-2000 Arctic vortex, *Geophys. Res. Lett.*, *29* (16), 1816, doi: 10.1029/2002GL015000, 2002b.
- Norton, W.A., and M.P. Chipperfield, Quantification of

POLAR OZONE

- the transport of chemically processed air from the Northern Hemisphere polar vortex, *J. Geophys. Res.*, *100*, 25817-25840, 1995.
- Oinas, V., A.A. Lacis, D. Rind, D.T. Shindell, and J.E. Hansen, Radiative cooling by stratospheric water vapor: Big differences in GCM results, *Geophys. Res. Lett.*, *28*, 2791-2794, 2001.
- Oltmans, S.J., and D.J. Hofmann, Increase in lower-stratospheric water vapour at a mid-latitude Northern Hemisphere site from 1981 to 1994, *Nature*, *374*, 146-149, 1995.
- Oltmans, S.J., H. Vömel, D.J. Hofmann, K.H. Rosenlof, and D. Kley, The increase in stratospheric water vapor from balloonborne, frostpoint hygrometer measurements at Washington, DC, and Boulder, Colorado, *Geophys. Res. Lett.*, *27*, 3453-3456, 2000.
- Orsolini, Y.J., Long-lived tracer patterns in the summer polar stratosphere, *Geophys. Res. Lett.*, *28*, 3855-3858, 2001.
- Orsolini, Y.J., and V. Limpasuvan, The North Atlantic Oscillation and the occurrences of ozone mini-holes, *Geophys. Res. Lett.*, *28*, 4099-4102, 2001.
- Orsolini, Y.J., G. Hansen, U.P. Hoppe, G.L. Manney, and K.H. Fricke, Dynamical modeling of wintertime lidar observations in the Arctic: Ozone laminae and ozone depletion, *Quart. J. Roy. Meteorol. Soc.*, *123*, 785-800, 1997.
- Osterman, G.B., B. Sen, G.C. Toon, R.J. Salawitch, J.J. Margitan, J.-F. Blavier, D.W. Fahey, and R.S. Gao, The partitioning of reactive nitrogen species in the summer Arctic stratosphere, *Geophys. Res. Lett.*, *26*, 1157-1160, 1999.
- Pan, L.L., W.J. Randel, H. Nakajima, S.T. Massie, H. Kanzawa, Y. Sasano, T. Yokota, T. Sugita, S. Hayashida, and S. Oshchepkov, Satellite observation of dehydration in the Arctic polar stratosphere, *Geophys. Res. Lett.*, *29* (8), 1184, doi: 10.1029/2001GL014147, 2002.
- Papayannis, D.K., A.M. Kosmas, and V.S.R. Melissas, Quantum mechanical studies on the BrO plus ClO reaction, *J. Phys. Chem.*, *105*, 2209-2215, 2001.
- Pawson, S., and B. Naujokat, Trends in daily wintertime temperatures in the northern stratosphere, *Geophys. Res. Lett.*, *24*, 575-578, 1997.
- Pawson, S., and B. Naujokat, The cold winters of the middle 1990s in the northern lower stratosphere, *J. Geophys. Res.*, *104*, 14209-14222, 1999.
- Pawson, S., B. Naujokat, and K. Labitzke, On the polar stratospheric cloud formation potential of the northern stratosphere, *J. Geophys. Res.*, *100*, 23215-23225, 1995.
- Pawson, S., K. Kruger, R. Swinbank, M. Bailey, and A. O'Neill, Intercomparison of two stratospheric analyses: Temperatures relevant to polar stratospheric cloud formation, *J. Geophys. Res.*, *104*, 2041-2050, 1999.
- Pawson, S., K. Kodera, K. Hamilton, T.G. Shepherd, S.R. Beagley, B.A. Boville, J.D. Farrara, T.D.A. Fairlie, A. Kitoh, W.A. Lahoz, U. Langematz, E. Manzini, D.H. Rind, A.A. Scaife, K. Shibata, P. Simon, R. Swinbank, L. Takacs, R.J. Wilson, J.A. Al-Saadi, M. Amodei, M. Chiba, L. Coy, J. de Grandpré, R.S. Eckman, M. Fiorino, W.L. Grose, H. Koide, J.N. Koshyk, D. Li, J. Lerner, J.D. Mahlman, N.A. McFarlane, C.R. Mechoso, A. Molod, A. O'Neill, R.B. Pierce, W.J. Randel, R.B. Rood, and F. Wu, The GCM-Reality Intercomparison Project for SPARC (GRIPS): Scientific issues and initial results, *Bull. Amer. Meteorol. Soc.*, *81*, 781-796, 2000.
- Perez, A., E. de Crino, I.A. de Carcer, and F. Jaque, Low ozone events and three-dimensional transport at midlatitudes of South America during springs of 1996 and 1997, *J. Geophys. Res.*, *105*, 4553-4561, 2000.
- Perkins, K.K., T.F. Hanisco, R.C. Cohen, L.C. Koch, R.M. Stimpfle, P.B. Voss, G.P. Bonne, E.J. Lanzendorf, J.G. Anderson, P.O. Wennberg, R.S. Gao, L.A. Del Negro, R.J. Salawitch, C.T. McElroy, E.J. Hintsa, M. Loewenstein, and T.P. Bui, The NO_x-HNO₃ system in the lower stratosphere: Insights from in situ measurements and implications of the J_{HNO₃}⁻[OH] relationship, *J. Phys. Chem. A.*, *105*, 1521-1534, 2001.
- Perlwitz, J., and H.-F. Graf, The variability of the horizontal circulation in the troposphere and stratosphere: A comparison, *Theor. Appl. Clim.*, *69*, 149-161, 2001.
- Pfeilsticker, K., W.T. Sturges, H. Bösch, C. Camy-Peyret, M.P. Chipperfield, A. Engel, R. Fitzenberger, M. Müller, S. Payan, and B.-M. Sinnhuber, Lower stratospheric organic and inorganic bromine budget for the Arctic winter 1998/99, *Geophys. Res. Lett.*, *27*, 3305-3308, 2000.
- Pfenniger, M., A.Z. Liu, G.C. Papen, and C.S. Gardner, Gravity wave characteristics in the lower atmosphere at South Pole, *J. Geophys. Res.*, *104*, 5963-5984, 1999.
- Pierce, R.B., J.A. Al-Saadi, T.D. Fairlie, J.R. Olson, R.S. Eckman, W.L. Grose, G.S. Lingenfelter, J.-U. Groöß, and J.M. Russell III, Large-scale strato-

- spheric ozone photochemistry and transport during the POLARIS campaign, *J. Geophys. Res.*, *104*, 26525-26545, 1999.
- Pierce, R.B., J. Al-Saadi, T.D. Fairlie, M. Natarajan, V.L. Harvey, W.L. Grose, J.M. Russell, R.M. Bevilacqua, S. Eckermann, D.W. Fahey, R.-S. Gao, G.C. Toon, E. Richard, R. Stimpfle, C.R. Webster, and J.W. Elkins, Large-scale chemical evolution of the Arctic vortex during the 1999-2000 winter: HALOE/POAM3 Lagrangian photochemical modeling for the SAGE III Ozone Loss and Validation Experiment (SOLVE) campaign, *J. Geophys. Res.*, in press, 2002.
- Pierson, J.M., K.A. McKinney, D.W. Toohey, J.J. Margitan, U. Schmidt, A. Engel, and P.A. Newman, An investigation of ClO photochemistry in the chemically perturbed Arctic vortex, *J. Atmos. Chem.*, *32*, 61-81, 1999.
- Pitari, G., S. Palermi, G. Visconti, and R.G. Prinn, Ozone response to a CO₂ doubling: Results from a stratospheric circulation model with heterogeneous chemistry, *J. Geophys. Res.*, *97*, 5953-5962, 1992.
- Pitari, G., E. Mancini, and D. Shindell, Feedback of future climate and sulfur emission changes on stratospheric aerosols and ozone, *J. Atmos. Sci.*, in press, 2002a.
- Pitari, G., E. Mancini, V. Rizi, and D. Shindell, Impact of future climate and emission changes on stratospheric aerosols and ozone, *J. Atmos. Sci.*, in press, 2002b.
- Piters, A.J.M., P.F. Levelt, M.A.F. Allaart, and H.M. Kelder, Validation of GOME total ozone column with the assimilation model KNMI, *Adv. Space Res.*, *22* (11), 1501-1504, 1999.
- Plumb, R.A., and M.K.W. Ko, Interrelationships between mixing ratios of long-lived stratospheric constituents, *J. Geophys. Res.*, *97*, 10145-10156, 1992.
- Plumb, R.A., D.W. Waugh, and M.P. Chipperfield, The effects of mixing on tracer-tracer relationships in the polar vortices, *J. Geophys. Res.*, *105*, 10047-10062, 2000.
- Pommereau, J.-P., A. Garnier, B.M. Knudsen, G. Letrenne, M. Durand, M. Nunes-Pinharanda, L. Denis, F. Vial, A. Hertzog, and F. Cairo, Accuracy of analyzed stratospheric temperature in the winter Arctic vortex from infrared Montgolfier long-duration balloon flights, 1, Measurements, *J. Geophys. Res.*, *107* (D20), 8260, doi: 10.1029/2001JD001379, 2002.
- Popp, P.J., M.J. Northway, J.C. Holecek, R.S. Gao, D.W. Fahey, J.W. Elkins, D.F. Hurst, P.A. Romashkin, G.C. Toon, B. Sen, S.M. Schauffler, R.J. Salawitch, C.R. Webster, R.L. Herman, H. Jost, T.P. Bui, P.A. Newman, and L.R. Lait, Severe and extensive denitrification in the 1999-2000 Arctic winter stratosphere, *Geophys. Res. Lett.*, *28*, 2875-2878, 2001.
- Portmann, R.W., S. Solomon, R.R. Garcia, L.W. Thomason, L.R. Poole, and M.P. McCormick, Role of aerosol variations in anthropogenic ozone depletion in the polar regions, *J. Geophys. Res.*, *101*, 22991-23006, 1996.
- Prezzi, A.J., T.B. Onasch, R.T. Tisdale, R.L. Siefert, and M.A. Tolbert, Composition-dependent freezing nucleation rates for HNO₃-H₂O aerosols resembling gravity-wave-perturbed stratospheric particles, *J. Geophys. Res.*, *103*, 28439-28450, 1998.
- Proffitt, M.H., J.J. Margitan, K.K. Kelly, M. Loewenstein, J.R. Podolske, and K.R. Chan, Ozone loss in the Arctic polar vortex inferred from high altitude aircraft measurements, *Nature*, *347*, 31-36, 1990.
- Pullen, S., and R.L. Jones, Accuracy of temperatures from UKMO analyses of 1994/95 in the Arctic winter stratosphere, *Geophys. Res. Lett.*, *24*, 845-848, 1997.
- Pundt, I., Étude de la distribution verticale des oxydes d'iode et de bromine dans la basse stratosphère à l'aide de sonde SAOZ-Ballon, Ph.D. thesis, University of Paris VI, France, 1997.
- Raffalski, U., U. Klein, B. Franke, J. Langer, B.-M. Sinnhuber, J. Trentmann, K.F. Künzi, and O. Schrems, Ground-based millimeter-wave observations of Arctic chlorine activation during winter and spring 1996/97, *Geophys. Res. Lett.*, *25*, 3331-3334, 1998.
- Ramachandran, S., V. Ramaswamy, G.L. Stenchikov, and A. Robock, Radiative impact of the Mount Pinatubo volcanic eruption: Lower stratospheric response, *J. Geophys. Res.*, *105*, 24409-24429, 2000.
- Ramaswamy, V., and M.D. Schwarzkopf, Effects of ozone and well-mixed gases on annual-mean stratospheric temperature trends, *Geophys. Res. Lett.*, in press, 2002.
- Ramaswamy, V., M.D. Schwarzkopf, and W.J. Randel, Fingerprint of ozone depletion in the spatial and temporal pattern of recent lower-stratospheric cooling, *Nature*, *382*, 616-618, 1996.
- Ramaswamy, V., M.-L. Chanin, J. Angell, J. Barnett, D. Gaffen, M. Gelman, P. Keckhut, Y. Koshelkov, K. Labitzke, J.J.R. Lin, A. O'Neill, J. Nash, W. Randel, R. Rood, K. Shine, M. Shiotani, and R. Swinbank, Stratospheric temperature trends:

POLAR OZONE

- Observations and model simulations, *Rev. Geophys.*, *39*, 71-122, 2001.
- Ramaswamy, V., M. Gelman, M.D. Schwarzkopf, and R. Lin, An update of stratospheric temperature trends, *SPARC Newslett.*, *18*, 7-9, January 2002a.
- Ramaswamy, V., S. Ramachandran, G. Stenchikov, and A. Robock, A model study of the effect of Pinatubo volcanic aerosols on stratospheric temperatures, in *Frontiers in the Science of Climate Modeling*, edited by J.T. Kiehl and V. Ramanathan, Cambridge University Press, U.K., in press, 2002b.
- Randall, C.E., J.D. Lumpe, R.M. Bevilacqua, K.W. Hoppel, M.D. Fromm, R.J. Salawitch, W.H. Swartz, S.A. Lloyd, E. Kyrö, P. von der Gathen, H. Claude, J. Davies, H. De Backer, H. Dier, M.J. Molyneux, and J. Sancho, Reconstruction of 3-D ozone fields using POAM III during SOLVE, *J. Geophys. Res.*, in press, 2002.
- Randel, W.J., and P.A. Newman, The stratosphere in the Southern Hemisphere, in *The Meteorology of the Southern Hemisphere*, edited by D.J. Karoly and D.G. Vincent, *AMS Meteorol. Monogr. Ser.*, *27* (49), 243-282, Amer. Meteorol. Soc., Boston, Mass., 1998.
- Randel, W.J., and F. Wu, Cooling of the Arctic and Antarctic polar stratospheres due to ozone depletion, *J. Clim.*, *12*, 1467-1479, 1999a.
- Randel, W.J., and F. Wu, A stratospheric ozone trends data set for global modeling studies. *Geophys. Res. Lett.*, *26*, 3089-3092, 1999b.
- Randeniya, L.K., P.F. Vohralik, and I.C. Plumb, Stratospheric ozone depletion at northern mid-latitudes in the 21st century: The importance of future concentrations of greenhouse gases nitrous oxide and methane, *Geophys. Res. Lett.*, *29* (4), 1051, doi: 10.1029/2001GL014295, 2002.
- Rathman, W., P.S. Monks, D. Llewellyn Jones, and J.P. Burrows, A preliminary comparison between TOVS and GOME level 2 ozone data, *Geophys. Res. Lett.*, *24*, 2191-2194, 1997.
- Ray, E.A., F.L. Moore, J.W. Elkins, D.F. Hurst, P.A. Romashkin, G.S. Dutton, and D.W. Fahey, Descent and mixing in the 1999-2000 northern polar vortex inferred from in situ tracer measurements, *J. Geophys. Res.*, *107* (D20), 8285, doi: 10.1029/2001JD000961, 2002.
- Renard, J.-B., M. Pirre, C. Robert, and D. Huguenin, Is OBrO present in the stratosphere?, *C. R. Acad. Sci. Paris, Sci. Terre Planet.*, *325*, 921-924, 1997.
- Renard, J.-B., M. Pirre, C. Robert, and D. Huguenin, The possible detection of OBrO in the stratosphere, *J. Geophys. Res.*, *103*, 25383-25395, 1998.
- Rex, M., N.R.P. Harris, P. von der Gathen, R. Lehmann, G.O. Braathen, E. Reimer, A. Beck, M.P. Chipperfield, R. Alfier, M. Allaart, F. O'Connor, H. Dier, V. Dorokhov, H. Fast, M. Gil, E. Kyrö, Z. Litynska, I.S. Mikkelsen, M.G. Molyneux, H. Nakane, J. Notholt, M. Rummukainen, P. Viatte, and J. Wenger, Prolonged stratospheric ozone loss in the 1995-96 Arctic winter, *Nature*, *389*, 835-838, 1997.
- Rex, M., P. von der Gathen, N.R.P. Harris, D. Lucic, B.M. Knudsen, G.O. Braathen, S.J. Reid, H. De Backer, H. Claude, R. Fabian, H. Fast, M. Gil, E. Kyrö, I.S. Mikkelsen, M. Rummukainen, H.G. Smit, J. Stähelin, C. Varotsos, and I. Zaitcev, In situ measurements of stratospheric ozone depletion rates in the Arctic winter 1991/1992: A Lagrangian approach, *J. Geophys. Res.*, *103*, 5843-5853, 1998.
- Rex, M., R.J. Salawitch, G.C. Toon, B. Sen, J.J. Margitan, G.B. Osterman, J.F. Blavier, R.-S. Gao, S. Donnelly, E. Keim, J. Neuman, D.W. Fahey, C.R. Webster, D.C. Scott, R.L. Herman, R.D. May, E.J. Moyer, M.R. Gunson, F.W. Irion, A.Y. Chang, C.P. Rinsland, and T.P. Bui, Subsidence, mixing, and denitrification of Arctic polar vortex air measured during POLARIS, *J. Geophys. Res.*, *104*, 26611-26623, 1999a.
- Rex, M., P. von der Gathen, G.O. Braathen, N.R.P. Harris, E. Reimer, A. Beck, R. Alfier, R. Krüger-Carstensen, M. Chipperfield, H. De Backer, D. Balis, F. O'Connor, H. Dier, V. Dorokhov, H. Fast, A. Gamma, M. Gil, E. Kyrö, Z. Litynska, I.S. Mikkelsen, M. Molyneux, G. Murphy, S.J. Reid, M. Rummukainen, and C. Zerefos, Chemical ozone loss in the Arctic winter 1994/95 as determined by the Match technique, *J. Atmos. Chem.*, *32*, 35-39, 1999b.
- Rex, M., R.J. Salawitch, N.R.P. Harris, P. von der Gathen, G.O. Braathen, A. Schulz, H. Deckelman, M. Chipperfield, B.-M. Sinnhuber, E. Reimer, R. Alfier, R. Bevilacqua, K. Hoppel, M. Fromm, J. Lumpe, H. Küllmann, A. Kleinböhl, H. Bremer, M. von König, K. Künzi, D. Toohey, H. Vömel, E. Richard, K. Aikin, H. Jost, J.B. Greenblatt, M. Loewenstein, J.R. Podolske, C.R. Webster, G.J. Flesch, D.C. Scott, R.L. Herman, J.W. Elkins, E.A. Ray, F.L. Moore, D.F. Hurst, P. Romashkin, G.C. Toon, B. Sen, J.J. Margitan, P. Wennberg, R. Neuber, M. Allaart, R.B.R. Bojkov, H. Claude, J. Davies, W. Davies, H. De Backer, H. Dier, V. Dorokhov, H. Fast, Y. Kondo, E. Kyrö, Z. Litynska,

- I.S. Mikkelsen, M.J. Molyneux, E. Moran, T. Nagai, H. Nakane, C. Parrondo, F. Ravegnani, P. Skrivankova, P. Viatte, and V. Yushkov, Chemical depletion of Arctic ozone in winter 1999/2000, *J. Geophys. Res.*, *107* (D20), 8276, doi: 10.1029/2001JD000533, 2002a.
- Rex, M., R.J. Salawitch, M.L. Santee, J.W. Waters, K. Hoppel, and R. Bevilacqua, On the unexplained stratospheric ozone losses during cold Arctic Januaries, *Geophys. Res. Lett.*, in press, 2002b.
- Ricaud, P., E. Monnier, F. Goutail, J.-P. Pommereau, C. David, S. Godin, L. Froidevaux, J.W. Waters, J. Mergenthaler, A.E. Roche, H. Pumphrey, and M.P. Chipperfield, Stratosphere over Dumont d'Urville, Antarctica, in winter 1992, *J. Geophys. Res.*, *103*, 13267-13284, 1998.
- Richard, E.C., K.C. Aikin, A.E. Andrews, B.C. Daube, C. Gerbig, S.C. Wofsy, P.A. Romashkin, D.F. Hurst, E.A. Ray, F.L. Moore, J.W. Elkins, T. Deshler, and G.C. Toon, Severe chemical ozone loss inside the Arctic polar vortex during winter 1999-2000 inferred from in situ airborne measurements, *Geophys. Res. Lett.*, *28*, 2197-2200, 2001.
- Rind, D., R. Suozzo, N.K. Balachandran, A. Lacis, and G. Russell, The GISS global climate/middle atmosphere model, I, Model structure and climatology, *J. Atmos. Sci.*, *45*, 329-370, 1988a.
- Rind, D., R. Suozzo, and N.K. Balachandran, The GISS global climate/middle atmosphere model, II, Model variability due to interactions between planetary waves, the mean circulation, and gravity wave drag, *J. Atmos. Sci.*, *45*, 371-386, 1988b.
- Rind, D., D. Shindell, P. Lonergan, and N.K. Balachandran, Climate change and the middle atmosphere, III, The doubled CO₂ climate revisited, *J. Clim.*, *11*, 876-894, 1998.
- Robock, A., Volcanic eruptions and climate, *Rev. Geophys.*, *38*, 191-219, 2000.
- Roehl, C.M., T.L. Mazely, R.R. Friedl, Y.M. Li, J.S. Francisco, and S.P. Sander, NO₂ quantum yield from the 248-nm photodissociation of peroxyacetic acid (HO₂NO₂), *J. Phys. Chem.*, *105*, 1592-1598, 2001.
- Rood R.B., A.R. Douglass, M.C. Cerniglia, and W.G. Read, Synoptic-scale mass exchange from the troposphere to the stratosphere, *J. Geophys. Res.*, *102*, 23467-23485, 1997.
- Roscoe, H.K., A.E. Jones, and A.M. Lee, Midwinter start to Antarctic ozone depletion: Evidence from observations and models, *Science*, *278*, 93-96, 1997.
- Rosenfield, J.E., and M.R. Schoeberl, On the origin of polar vortex air, *J. Geophys. Res.*, *106*, 33485-33497, 2001.
- Rosenfield, J.E., A.R. Douglass, and D.B. Considine, The impact of increasing carbon dioxide on ozone recovery, *J. Geophys. Res.*, *107* (D6), 4049, doi: 10.1029/2001JD000824, 2002.
- Rosenlof, K.H., Estimates of the seasonal cycle of mass and ozone transport at high northern latitudes, *J. Geophys. Res.*, *104*, 26511-26523, 1999.
- Rosenlof, K.H., S.J. Oltmans, D. Kley, J.M. Russell III, E.-W. Chiou, W.P. Chu, D.G. Johnson, K.K. Kelly, H.A. Michelsen, G.E. Nedoluha, E.E. Remsberg, G.C. Toon, and M.P. McCormick, Stratospheric water vapor increases over the past half-century, *Geophys. Res. Lett.*, *28*, 1195-1198, 2001.
- Rosier, S.M., and K.P. Shine, The effect of two decades of ozone change on stratospheric temperatures as indicated by a general circulation model, *Geophys. Res. Lett.*, *27*, 2617-2620, 2000.
- Rozanov, E.V., M.E. Schlesinger, and V.A. Zubov, The University of Illinois at Urbana-Champaign three-dimensional stratosphere-troposphere general circulation model with interactive ozone photochemistry: Fifteen-year control run climatology, *J. Geophys. Res.*, *106*, 27233-27254, 2001.
- Russell, J.M. III, M.Z. Luo, R.J. Cicerone, and L.E. Deaver, Satellite confirmation of the dominance of chlorofluorocarbons in the global stratospheric chlorine budget, *Nature*, *379*, 526-529, 1996.
- Saitoh, N., S. Hayashida, Y. Sasano, and L.L. Pan, Characteristics of Arctic polar stratospheric clouds in winter of 1996/1997 inferred from ILAS measurements, *J. Geophys. Res.*, *107* (D24), 8205, doi: 10.1029/2001JD000595, 2002.
- Salawitch, R.J., J.J. Margitan, B. Sen, G.C. Toon, G.B. Osterman, M. Rex, J.W. Elkins, E.A. Ray, F.L. Moore, D.F. Hurst, P.A. Romashkin, R.M. Bevilacqua, K.W. Hoppel, E.C. Richard, and T.P. Bui, Chemical loss of ozone during the Arctic winter of 1999-2000: An analysis based on balloonborne observations, *J. Geophys. Res.*, *107* (D20), 8269, doi: 10.1029/2001JD000620, 2002a.
- Salawitch, R.J., P.O. Wennberg, G.C. Toon, B. Sen, and J.-F. Blavier, Near IR photolysis of HO₂NO₂: Implications for HO_x, *Geophys. Res. Lett.*, *29* (16), 1762, doi: 10.1029/2002GL015006, 2002b.
- Salcedo, D., L.T. Molina, and M.J. Molina, Homogeneous freezing of concentrated aqueous nitric acid solutions at polar stratospheric temperatures, *J. Phys. Chem. A*, *105*, 1433-1439, 2001.
- Sander, S.P., A.R. Ravishankara, R.R. Friedl, W.B.

POLAR OZONE

- DeMore, D.M. Golden, C.E. Kolb, M.J. Kurylo, M.J. Molina, R.F. Hampson, R.E. Huie, and G.K. Moortgat, *Chemical Kinetics and Photochemical Data for Use in Stratospheric Modeling (Supplement to Evaluation 12: Update of Key Reactions): Evaluation Number 13, JPL Publ. 00-3*, Jet Propulsion Laboratory, Pasadena, Calif., 2000.
- Santee, M.L., G.L. Manney, L. Froidevaux, W.G. Read, and J.W. Waters, Six years of UARS microwave limb sounder HNO₃ observations: Seasonal, inter-hemispheric, and interannual variations in the lower stratosphere, *J. Geophys. Res.*, *104*, 8225-8246, 1999.
- Santee, M.L., G.L. Manney, N.J. Livesey, and J.W. Waters, UARS Microwave Limb Sounder observations of denitrification and ozone loss in the 2000 Arctic late winter, *Geophys. Res. Lett.*, *27*, 3213-3216, 2000.
- Santee, M.L., A. Tabazadeh, G.L. Manney, M.D. Fromm, R.M. Bevilacqua, J.W. Waters, and E.J. Jensen, A Lagrangian approach to studying Arctic polar stratospheric clouds using UARS MLS HNO₃ and POAM II aerosol extinction measurements, *J. Geophys. Res.*, *107* (D10), 4098, doi: 10.1029/2000JD000227, 2002.
- Sasano, Y., M. Suzuki, T. Yokota, and H. Kanzawa, Improved Limb Atmospheric Spectrometer (ILAS) for stratospheric ozone layer measurements by solar occultation technique, *Geophys. Res. Lett.*, *26*, 197-200, 1999.
- Sasano, Y., Y. Terao, H.L. Tanaka, T. Yasunari, H. Kanzawa, H. Nakajima, T. Yokota, H. Nakane, S. Hayashida, and N. Saitoh, ILAS observations of chemical ozone loss in the Arctic vortex during early spring 1997, *Geophys. Res. Lett.*, *27*, 213-216, 2000.
- Sato, K., K. Yamada, and I. Hirota, Global characteristics of medium-scale tropopause waves observed in ECMWF operational data, *Mon. Wea. Rev.*, *128*, 3808-3823, 2000.
- Scaife, A.A., N. Butchart, C.D. Warner, D. Stainforth, W. Norton, and J. Austin, Realistic quasi-biennial oscillations in a simulation of the global climate, *Geophys. Res. Lett.*, *27*, 3481-3484, 2000a.
- Scaife, A.A., J. Austin, N. Butchart, S. Pawson, M. Keil, J. Nash, and I.N. James, Seasonal and interannual variability of the stratosphere diagnosed from UKMO TOVS analyses, *Quart. J. Roy. Meteorol. Soc.*, *126*, 2585-2604, 2000b.
- Schauffler, S.M., E.L. Atlas, F. Flocke, R.A. Lueb, V. Stroud, and W. Travnicek, Measurement of bromine-containing organic compounds at the tropical tropopause, *Geophys. Res. Lett.*, *25*, 317-320, 1998.
- Schnadt, C., M. Dameris, M. Ponater, R. Hein, V. Grewe, and B. Steil, Interaction of atmospheric chemistry and climate and its impact on stratospheric ozone, *Clim. Dyn.*, *18*, 501-517, 2002.
- Schoeberl, M.R., and P.A. Newman, A multi-level trajectory analysis of vortex filaments, *J. Geophys. Res.*, *100*, 25801-25815, 1995.
- Schoeberl, M.R., M.H. Proffitt, K.K. Kelly, L.R. Lait, P.A. Newman, J.E. Rosenfield, M. Loewenstein, J.R. Podolske, S.E. Strahan, and K.R. Chan, Stratospheric constituent trends from ER-2 profile data, *Geophys. Res. Lett.*, *17*, 469-472, 1990.
- Schoeberl, M.R., M.Z. Lu, and J.E. Rosenfield, An analysis of the Antarctic Halogen Occultation Experiment trace gas observations, *J. Geophys. Res.*, *100*, 5159-5172, 1995.
- Schoeberl, M.R., A.R. Douglass, S.R. Kawa, A.E. Dessler, P.A. Newman, R.S. Stolarski, A.E. Roche, J.W. Waters, and J.M. Russell III, Development of the Antarctic ozone hole, *J. Geophys. Res.*, *101*, 20909-20924, 1996.
- Schoeberl, M.R., P.A. Newman, L.R. Lait, T.J. McGee, J.F. Burris, E.V. Browell, W.B. Grant, E.C. Richard, P. von der Gathen, R. Bevilacqua, and I.S. Mikkelsen, An assessment of the ozone loss during the 1999-2000 SOLVE/THESEO 2000 Arctic campaign, *J. Geophys. Res.*, *107* (D20), 8261, doi: 10.1029/2001JD000412, 2002.
- Schreiner, J., C. Voigt, A. Kohlmann, F. Arnold, K. Mauersberger, and N. Larsen, Chemical analysis of polar stratospheric cloud particles, *Science*, *283*, 968-970, 1999.
- Schreiner, J., C. Voigt, C. Weisser, A. Kohlmann, K. Mauersberger, T. Deshler, C. Kröger, J. Rosen, N. Kjöme, N. Larsen, A. Adriani, F. Cairo, G. Di Donfrancesco, J. Ovarlez, H. Ovarlez, and A. Dörnbrack, Chemical, microphysical and optical properties of polar stratospheric clouds, *J. Geophys. Res.*, in press, 2002.
- Schulz, A., M. Rex, J. Steger, N.R.P. Harris, G.O. Braathen, E. Reimer, R. Alfier, A. Beck, M. Alpers, J. Cisneros, H. Claude, H. De Backer, H. Dier, V. Dorokhov, H. Fast, S. Godin, G. Hansen, H. Kanzawa, B. Kois, Y. Kondo, E. Kosmidis, E. Kyrö, Z. Litynska, M.J. Molyneux, G. Murphy, H. Nakane, C. Parrondo, F. Ravegnani, C. Varotsos, C. Vialle, P. Viatte, V. Yushkov, C. Zerefos, and P.

- von der Gathen, Match observations in the Arctic winter 1996/97: High stratospheric ozone loss rates correlate with low temperatures deep inside the polar vortex, *Geophys. Res. Lett.*, *27*, 205-208, 2000.
- Schulz, A., M. Rex, N.R.P. Harris, G.O. Braathen, E. Reimer, R. Alfier, I. Kilbane-Dawe, S. Eckermann, M. Allaart, M. Alpers, B. Bojkov, J. Cisneros, H. Claude, E. Cuevas, J. Davies, H. De Backer, H. Dier, V. Dorokhov, H. Fast, S. Godin, B. Johnson, B. Kois, Y. Kondo, E. Kosmidis, E. Kyrö, Z. Litynska, I.S. Mikkelsen, M.J. Molyneux, G. Murphy, T. Nagai, H. Nakane, F. O'Connor, C. Parrondo, F.J. Schmidlin, P. Skrivankova, C. Varotsos, C. Vialle, P. Viatte, V. Yushkov, C. Zerefos, and P. von der Gathen, Arctic ozone loss in threshold conditions: Match observations in 1997/1998 and 1998/1999, *J. Geophys. Res.*, *106*, 7495-7503, 2001.
- Sen, B., G.B. Osterman, R.J. Salawitch, G.C. Toon, J.J. Margitan, J.-F. Blavier, A.Y. Chang, R.D. May, C.R. Webster, R.M. Stimpfle, G.P. Bonne, P.B. Voss, K.K. Perkins, J.G. Anderson, R.C. Cohen, J.W. Elkins, G.S. Dutton, D.F. Hurst, P.A. Romashkin, E.L. Atlas, S.M. Schauffler, and M. Loewenstein, The budget and partitioning of stratospheric chlorine during the 1997 Arctic summer, *J. Geophys. Res.*, *104*, 26653-26665, 1999.
- Shepherd, T.G., K. Semeniuk, and J.N. Koshyk, Sponge-layer feedbacks in middle atmosphere models, *J. Geophys. Res.*, *101*, 23447-23464, 1996.
- Shindell, D.T., Climate and ozone response to increased stratospheric water vapor, *Geophys. Res. Lett.*, *28*, 1551-1554, 2001.
- Shindell, D.T., and R.L. de Zafra, The chlorine budget of the lower polar stratosphere: Upper limits on ClO and implications of new Cl₂O₂ photolysis cross-sections, *Geophys. Res. Lett.*, *22*, 3215-3218, 1995.
- Shindell, D.T., D. Rind, and P. Lonergan, Increased polar stratospheric ozone losses and delayed eventual recovery owing to increasing greenhouse-gas concentrations, *Nature*, *392*, 589-592, 1998a.
- Shindell, D.T., D. Rind, and P. Lonergan, Climate change and the middle atmosphere, IV, Ozone response to doubled CO₂, *J. Clim.*, *11*, 895-918, 1998b.
- Shindell, D., D.H. Rind, N. Balachandran, J. Lean, and P. Lonergan, Solar cycle variability, ozone, and climate, *Science*, *284*, 305-308, 1999a.
- Shindell, D.T., D. Rind, and N. Balachandran, Interannual variability of the Antarctic ozone hole in a GCM, II, A comparison of unforced and QBO-induced variability, *J. Atmos. Sci.*, *56*, 1873-1884, 1999b.
- Shindell, D.T., G.A. Schmidt, R.L. Miller, and D. Rind, Northern Hemisphere winter climate response to greenhouse gas, volcanic, ozone and solar forcing, *J. Geophys. Res.*, *106*, 7193-7210, 2001.
- Shine, K.P., On the modeled thermal response of the Antarctic stratosphere to a depletion of ozone, *Geophys. Res. Lett.*, *13*, 1331-1334, 1986.
- Sinnhuber, B.-M., M.P. Chipperfield, S. Davies, J.P. Burrows, K.-U. Eichmann, M. Weber, P. von der Gathen, M. Guirlet, G.A. Cahill, A.M. Lee, and J.A. Pyle, Large loss of total ozone during the Arctic winter of 1999/2000, *Geophys. Res. Lett.*, *27*, 3473-3476, 2000.
- Sinnhuber, B.-M., D.W. Arlander, H. Bovensmann, J.P. Burrows, M.P. Chipperfield, C.-F. Enell, U. Friess, F. Hendrick, P.V. Johnston, R.L. Jones, K. Kreher, N. Mohamed-Tahrin, R. Mueller, K. Pfeilsticker, U. Platt, J.-P. Pommereau, I. Pundt, A. Richter, A. South, K.K. Tørnkvist, M. Van Roozendaal, T. Wagner, and F. Wittrock, Comparison of measurements and model calculations of stratospheric bromine monoxide, *J. Geophys. Res.*, *107* (D19), 4398, doi: 10.1029/2001JD000940, 2002.
- Smith, C.A., The radiative effects of observed trends in stratospheric water vapour, Ph.D. thesis, Imperial College, London, 2001.
- Smith, C.A., J.D. Haigh, and R. Toumi, Radiative forcing due to trends in stratospheric water vapour, *Geophys. Res. Lett.*, *28*, 179-182, 2001.
- Sobel, A., and R.A. Plumb, Quantitative diagnostics of mixing in a shallow water model of the stratosphere, *J. Atmos. Sci.*, *56*, 2811-2829, 1999.
- Solomon, P., J. Barrett, B. Connor, S. Zoonematkermani, A. Parrish, A. Lee, J. Pyle, and M. Chipperfield, Seasonal observations of chlorine monoxide in the stratosphere over Antarctica during the 1996-1998 ozone holes and comparison with the SLIMCAT three-dimensional model, *J. Geophys. Res.*, *105*, 28979-29001, 2000.
- Solomon, P., B. Connor, J. Barrett, T. Mooney, A. Lee, and A. Parrish, Measurements of stratospheric ClO over Antarctica in 1996-2000 and implications for ClO dimer chemistry, *Geophys. Res. Lett.*, *29* (15), 1708, doi: 10.1029/2002GL015232, 2002.
- Solomon, S., Stratospheric ozone depletion: A review of concepts and history, *Rev. Geophys.*, *37*, 275-316, 1999.
- Solomon, S., R.W. Portmann, R.R. Garcia, W.J. Randel, F. Wu, R. Nagatani, J. Gleason, L. Thomason, L.R. Poole, and M.P. McCormick, Ozone depletion at

POLAR OZONE

- midlatitudes: Coupling of volcanic aerosols and temperature variability to anthropogenic chlorine, *Geophys. Res. Lett.*, *25*, 1871-2874, 1998.
- Spang, R., M. Riese, and D. Offermann, CRISTA-2 observations of the south polar vortex in winter 1997: A new dataset for polar process studies, *Geophys. Res. Lett.*, *28*, 3159-3162, 2001.
- SPARC (Stratospheric Processes and Their Role in Climate), *SPARC/IOC/GAW Assessment of Trends in the Vertical Distribution of Ozone*, edited by N. Harris, R. Hudson, and C. Phillips, *SPARC Report No. 1, WMO Global Ozone Research and Monitoring Project Report No. 43*, 289 pp., Verrières le Buisson, France, 1998.
- SPARC (Stratospheric Processes and Their Role in Climate), *SPARC Assessment of Upper Tropospheric and Stratospheric Water Vapour*, edited by D. Kley, J.M. Russell, III, and C. Phillips, *World Climate Research Program Report 113, SPARC Report 2*, 312 pp., Verrières le Buisson, France, 2000.
- Stachnik, R.A., R.J. Salawitch, A. Engel, and U. Schmidt, Measurements of chlorine partitioning in the winter Arctic stratosphere, *Geophys. Res. Lett.*, *26*, 3093-3096, 1999.
- Steele, H.M., K. Drdla, R.P. Turco, J.D. Lumpe, and R.M. Bevilacqua, Tracking polar stratospheric cloud development with POAM II and a microphysical model, *Geophys. Res. Lett.*, *26*, 287-290, 1999.
- Steinbrecht, W., H. Claude, U. Kohler, and K.P. Hoinka, Correlations between tropopause height and total ozone: Implications for long-term changes, *J. Geophys. Res.*, *103*, 19183-19192, 1998.
- Stimpfle, R.M., R.C. Cohen, G.P. Bonne, P.B. Voss, K.K. Perkins, L.C. Koch, J.G. Anderson, R.J. Salawitch, S.A. Lloyd, R.S. Gao, L.A. Del Negro, E.R. Keim, and T.P. Bui, The coupling of ClONO₂, ClO, and NO₂ in the lower stratosphere from in situ observations using the NASA ER-2 aircraft, *J. Geophys. Res.*, *104*, 26705-26714, 1999.
- Stone, E.M., A. Tabazadeh, E.J. Jensen, H.C. Pumphrey, K.L. Santee, and J.L. Mergenthaler, Onset, extent, and duration of dehydration in the Southern Hemisphere polar vortex, *J. Geophys. Res.*, *106*, 22979-22990, 2001.
- Strawa, A.W., K. Drdla, M. Fromm, R.F. Pueschel, K.W. Hoppel, E.V. Browell, P. Hamill, and D.P. Dempsey, Discriminating type Ia and Ib polar stratospheric clouds in POAM satellite data, *J. Geophys. Res.*, in press, 2002.
- Sugita, T., Y. Kondo, H. Nakajima, U. Schmidt, A. Engel, H. Oelhaf, G. Wetzel, M. Koike, and P.A. Newman, Denitrification observed inside the Arctic vortex in February 1995, *J. Geophys. Res.*, *103*, 16221-16233, 1998.
- Sugita, T., T. Yokota, H. Nakajima, H. Kanzawa, H. Nakane, H. Germandt, V. Yushkov, K. Shibasaki, T. Deshler, Y. Kondo, S. Godin, F. Goutail, J.-P. Pommereau, C. Camy-Peyret, S. Payan, P. Jeseck, J.B. Renard, H. Bosch, R. Fitzenberger, K. Pfeilsticker, M. Von König, H. Bremer, H. Küllmann, H. Schlager, J.J. Margitan, R. Stachnik, G. Toon, K. Jucks, W. Traub, D.G. Johnson, I. Murata, H. Fukunishi, and Y. Sasano, Validation of ozone measurements from the Improved Limb Atmospheric Spectrometer (ILAS), *J. Geophys. Res.*, in press, 2002.
- Swinbank, R., and A. O'Neill, A stratosphere-troposphere data assimilation system, *Mon. Wea. Rev.*, *122*, 686-702, 1994.
- Tabazadeh, A., M.L. Santee, M.Y. Danilin, H.C. Pumphrey, P.A. Newman, P.J. Hamill, and J.L. Mergenthaler, Quantifying denitrification and its effect on ozone recovery, *Science*, *288*, 1407-1411, 2000.
- Tabazadeh, A., E.J. Jensen, O.B. Toon, K. Drdla, and M.R. Schoeberl, Role of the stratospheric polar freezing belt in denitrification, *Science*, *291*, 2591, 2001.
- Tabazadeh, A., K. Drdla, M.R. Schoeberl, P. Hamill, and O.B. Toon, Arctic "ozone hole" in a cold volcanic stratosphere, *Proc. Natl. Acad. Sci.*, *99*, 2609-2612, 2002.
- Takigawa, M., M. Takahashi, and H. Akiyoshi, Simulation of ozone and other chemical species using a Center for Climate Systems Research/National Institute for Environmental Studies atmospheric GCM with coupled stratospheric chemistry, *J. Geophys. Res.*, *104*, 14003-14018, 1999.
- Tanaka, H.L., R. Kanohgi, and T. Yasunari, Recent abrupt intensification of the northern polar vortex since 1988, *J. Meteorol. Soc. Japan*, *74*, 947-954, 1996.
- Teitelbaum, H., M. Moustou, P.F.J. van Velthoven, and H. Kelder, Decrease of total ozone at low latitudes in the Southern Hemisphere by a combination of linear and non-linear processes, *Quart. J. Roy. Meteorol. Soc.*, *124*, 2625-2644, 1999.
- Teitelbaum, H., C. Basdevant, and M. Moustou, Explanations of simultaneous laminae in water vapor and aerosols profiles found during the SESAME experiment, *Tellus*, *52A*, 442-455, 2000.
- Teitelbaum, H., M. Moustou, and M. Fromm, Exploring polar stratospheric cloud and ozone minihole for-

- mation: The primary importance of synoptic-scale flow perturbations, *J. Geophys. Res.*, *106*, 28173-28188, 2001.
- Terao, Y., Y. Sasano, H. Nakajima, H.L. Tanaka, and T. Yasunari, Stratospheric ozone loss in the 1996/1997 Arctic winter: Evaluation based on multiple trajectory analysis for double-sounded air parcels by ILAS, *J. Geophys. Res.*, *107* (D24), 8210, doi: 10.1029/2001JD000615, 2002.
- Thompson, D.W.J., and J.M. Wallace, The Arctic Oscillation signature in the wintertime geopotential height and temperature fields, *Geophys. Res. Lett.*, *25*, 1297-1300, 1998.
- Thompson, D.W.J., and J.M. Wallace, Annular modes in the extratropical circulation, I, Month-to-month variability, *J. Clim.*, *13*, 1000-1016, 2000.
- Thompson, D.W.J., J.M. Wallace, and G.C. Hegerl, Annular modes in the extratropical circulation, II, Trends, *J. Clim.*, *13*, 1018-1036, 2000.
- Thuburn, J., and V. Lagneau, Eulerian mean, contour integral, and finite-amplitude wave activity diagnostics applied to a single-layer model of the winter stratosphere, *J. Atmos. Sci.*, *56*, 689-710, 1999.
- Timmreck, C., H.-F. Graf, and I. Kirchner, A one-and-half-year interactive MA/ECHAM4 simulation of Mount Pinatubo aerosol, *J. Geophys. Res.*, *104*, 9337-9359, 1999.
- Tolbert, M.A., and O.B. Toon, Solving the PSC mystery, *Science*, *292*, 61-63, 2001.
- Toniolo, A., M. Persico, and D. Pitea, Theoretical photoabsorption spectra of ClOOCl and Cl₂O, *J. Phys. Chem.*, *104*, 7278-7283, 2000.
- Toohey, D.W., J.G. Anderson, W.H. Brune, and K.R. Chan, In situ measurements of BrO in the Arctic stratosphere, *Geophys. Res. Lett.*, *17* (4), Suppl. S, 513-516, 1990.
- Toon, G.C., J.-F. Blavier, B. Sen, R.J. Salawitch, G.B. Osterman, J. Notholt, M. Rex, C.T. McElroy, and J.M. Russell III, Ground-based observations of Arctic O₃ loss during spring and summer 1997, *J. Geophys. Res.*, *104*, 26497-26510, 1999.
- Toon, O.B., A. Tabazadeh, E.V. Browell, and J. Jordan, Analysis of lidar observations of Arctic polar stratospheric clouds during January 1989, *J. Geophys. Res.*, *105*, 20589-20615, 2000.
- Tsias, A., M. Wirth, K.S. Carslaw, J. Biele, H. Mehrstens, J. Reichardt, C. Wedekind, V. Weiss, W. Renger, R. Neuber, U. von Zahn, B. Stein, V. Santacesaria, L. Stefanutti, F. Fierli, J. Bacmeister, and T. Peter, Aircraft lidar observations of an enhanced type Ia polar stratospheric clouds during APE-POLECAT, *J. Geophys. Res.*, *104*, 23961-23969, 1999.
- Tuck, A.F., K.K. Kelly, C.R. Webster, M. Loewenstein, R.M. Stimpfle, M.H. Proffitt, and R.K. Chan, Airborne chemistry and dynamics at the edge of the 1994 Antarctic vortex, *J. Chem. Soc. Faraday Trans.*, *91*, 3063-3071, 1995.
- Tzvetkova, N.D., H. Nakane, A.N. Lukyanov, V.A. Yushkov, V.M. Dorokhov, I.G. Zaitsev, and V.I. Sitnikova, Estimation of the winter-spring rates of ozone depletion within the stratospheric Arctic cyclon in Siberia in 1995-2000 from balloon measurements, *Izvestia, Atmos. Ocean. Phys.*, *38*, 211-219, 2002.
- Uchino, O., R.D. Bojkov, D.S. Balis, K. Akagi, M. Hayashi, and R. Kajiwara, Essential characteristics of the Antarctic ozone decline: Update to 1998, *Geophys. Res. Lett.*, *26*, 1377-1380, 1999.
- van den Broek, M.M.P., A. Bregman, and J. Lelieveld, Model study of stratospheric chlorine activation and ozone loss during the 1996-1997 winter, *J. Geophys. Res.*, *105*, 28961-28977, 2000.
- van Loon, H., and K. Labitzke, The Southern Oscillation, V, The anomalies in the lower stratosphere of the Northern Hemisphere in winter and comparison with the quasi-biennial oscillation, *Mon. Wea. Rev.*, *115*, 357-369, 1987.
- van Loon, H., and K. Labitzke, The influence of the 11-year solar cycle on the stratosphere below 30 km: A review, *Space Sci. Rev.*, *94*, 259-278, 2000.
- Vincent, A.P., and B.J.S. Tranchant, Anisotropic diffusion for ozone transport at 520 K, *J. Geophys. Res.*, *104*, 27209-27215, 1999.
- Voigt, C., J. Schreiner, A. Kohlmann, P. Zink, K. Mauersberger, N. Larsen, T. Deshler, C. Kroger, J. Rosen, A. Adriani, F. Cairo, G. Di Donfrancesco, M. Viterbini, J. Ovarlez, H. Ovarlez, C. David, and A. Dörnbrack, Nitric acid trihydrate (NAT) in polar stratospheric clouds, *Science*, *290*, 1756-1758, 2000a.
- Voigt, C., A. Tsias, A. Dörnbrack, S. Meilinger, B. Luo, J. Schreiner, N. Larsen, K. Mauersberger, and T. Peter, Non-equilibrium compositions of liquid polar stratospheric clouds in gravity waves, *Geophys. Res. Lett.*, *27*, 3873-3876, 2000b.
- Volkert, H., and D. Intes, Orographically forced stratospheric waves over northern Scandinavia, *Geophys. Res. Lett.*, *19*, 1205-1208, 1992.
- Vömel, H., M. Rummukainen, R. Kivi, J. Karhu, T. Turunen, E. Kyrö, J. Rosen, N. Kjöme, and S. Oltmans, Dehydration and sedimentation of ice particles in the Arctic stratospheric vortex,

POLAR OZONE

- Geophys. Res. Lett.*, 24, 795-798, 1997.
- Vömel, H., D.W. Toohey, T. Deshler, and C. Kröger, Sunset observations of ClO in the Arctic polar vortex and implications for ozone loss, *Geophys. Res. Lett.*, 28, 4183-4186, 2001.
- von Clarmann, T., A. Linden, H. Oelhaf, H. Fischer, F. Friedl-Vallon, C. Piesch, M. Seefeldner, W. Völker, R. Bauer, A. Engel, and U. Schmidt, Determination of the stratospheric organic chlorine budget in the spring Arctic vortex from MIPAS B limb emission spectra and air sampling experiments, *J. Geophys. Res.*, 100, 13979-13997, 1995.
- von der Gathen, P., M. Rex, N.R.P. Harris, D. Lucic, B.M. Knudsen, G.O. Braathen, H. De Backer, R. Fabian, H. Fast, M. Gil, E. Kyrö, I.S. Mikkelsen, M. Rummukainen, J. Stähelin, and C. Varotsos, Observational evidence for chemical ozone depletion over the Arctic winter 1991-92, *Nature*, 375, 131-134, 1995.
- Voss, P.B., R.M. Stimpfle, R.C. Cohen, T.F. Hanisco, G.P. Bonne, K.K. Perkins, E.J. Lanzendorf, J.G. Anderson, R.J. Salawitch, C.R. Webster, D.C. Scott, R.D. May, P.O. Wennberg, P.A. Newman, L.R. Lait, J.W. Elkins, and T.P. Bui, Inorganic chlorine partitioning in the summer lower stratosphere: Modeled and measured [ClONO₂]/[HCl] during POLARIS, *J. Geophys. Res.*, 106, 1713-1732, 2001.
- Wagner, R.E., and K.P. Bowman, Wavebreaking and mixing in the Northern Hemisphere summer stratosphere, *J. Geophys. Res.*, 105, 24799-24807, 2000.
- Wagner, T., C. Leue, K. Pfeilsticker, and U. Platt, Monitoring of the stratospheric chlorine activation by Global Ozone Monitoring Experiment (GOME) OClO measurements in the austral and boreal winters 1995 through 1999, *J. Geophys. Res.*, 106, 4971, 2001.
- Wagner, T., F. Wittrock, A. Richter, M. Wenig, J.P. Burrows, and U. Platt, Continuous monitoring of the high and persistent chlorine activation during the Arctic winter 1999/2000 by the GOME instrument on ERS-2, *J. Geophys. Res.*, 107 (D20), 8267, doi: 10.1029/2001JD000466 2002.
- Wahner, A., and C. Schiller, Twilight variation of vertical column abundances of OClO and BrO in the North Polar region, *J. Geophys. Res.*, 97, 8047-8055, 1992.
- Waibel, A.E., T. Peter, K.S. Carslaw, H. Oelhaf, G. Wetzel, P.J. Crutzen, U. Poschl, A. Tsias, E. Reimer, and H. Fischer, Arctic ozone loss due to denitrification, *Science*, 283, 2064-2069, 1999.
- Wamsley, P.R., J.W. Elkins, D.W. Fahey, G.S. Dutton, C.M. Volk, R.C. Meyers, S.A. Montzka, J.H. Butler, A.D. Clarke, P.J. Fraser, L.P. Steele, M.P. Lucarelli, E.L. Atlas, S.M. Schauffler, D.R. Blake, F.S. Rowland, W.T. Sturges, J.M. Lee, S.A. Penkett, A. Engel, R.M. Stimpfle, K.R. Chan, D.K. Weisenstein, M.K.W. Ko, and R.J. Salawitch, Distribution of halon-1211 in the upper troposphere and lower stratosphere and the 1994 total bromine budget, *J. Geophys. Res.*, 103, 1513-1526, 1998.
- Warner, C.D., and M.E. McIntyre, Toward an ultra-simple spectral gravity wave parameterization for general circulation models, *Earth Planets Space*, 51, 475-484, 1999.
- Waters, J.W., W.G. Read, L. Froidevaux, R.F. Jarnot, R.E. Cofield, D.A. Flower, G.K. Lau, H.M. Pickett, M.L. Santee, D.L. Wu, M.A. Boyles, J.R. Burke, R.R. Lay, M.S. Loo, N.J. Livesey, T.A. Lungu, G.L. Manney, L.L. Nakamura, V.S. Perun, B.P. Ridenoure, Z. Shippony, P.H. Siegel, R.P. Thurstans, R.S. Harwood, H.C. Pumphrey, and M.J. Filipiak, The UARS and EOS Microwave Limb Sounder experiments, *J. Atmos. Sci.*, 56, 194-218, 1999.
- Waugh, D.W., and D.G. Dritschel, The dependence of Rossby wave breaking on the vertical structure of the polar vortex, *J. Atmos. Sci.*, 56, 2359-2375, 1999.
- Waugh, D.W., R.A. Plumb, J.W. Elkins, D.W. Fahey, K.A. Boering, G.S. Dutton, C.M. Volk, E. Keim, R.-S. Gao, B.C. Daube, S.C. Wofsy, M. Loewenstein, J.R. Podolske, K.R. Chan, M.H. Proffitt, K.K. Kelly, P.A. Newman, and L.R. Lait, Mixing of polar vortex air into middle latitudes as revealed by tracer-tracer scatterplots, *J. Geophys. Res.*, 102, 13119-13134, 1997.
- Waugh, D.W., W.J. Randel, S. Pawson, P.A. Newman, and E.R. Nash, Persistence of the lower stratospheric polar vortices, *J. Geophys. Res.*, 104, 27191-27201, 1999.
- Weber, M., K.-U. Eichmann, F. Wittrock, K. Bramstedt, L. Hild, A. Richter, J.P. Burrows, and R. Müller, The cold Arctic winter 1995/96 as observed by GOME and HALOE: Tropospheric wave activity and chemical ozone loss, *Quart. J. Roy. Meteorol. Soc.*, 128, 1293-1319, 2002.
- Wennberg, P.O., R.J. Salawitch, D.J. Donaldson, T.F. Hanisco, E.J. Lanzendorf, K.K. Perkins, S.A. Lloyd, V. Vaida, R.S. Gao, E.J. Hints, R.C. Cohen, W.H. Swartz, T.L. Kusterer, and D.E. Anderson,

- Twilight observations suggest unknown sources of HO_x, *Geophys. Res. Lett.*, *26*, 1373-1376, 1999.
- Whiteway, J.A., and T.J. Duck, Enhanced stratospheric gravity wave activity above a tropospheric jet, *Geophys. Res. Lett.*, *26*, 2453-2456, 1999.
- Williams, V., J. Austin, and J.D. Haigh, Model simulations of the impact of the 27-day solar rotation period on stratospheric ozone and temperatures: Ozone variations of the solar origin, *Adv. Space Res.*, *27*, 1933-1942, 2001.
- Wirth, M., A. Tsias, A. Dörnbrack, V. Weiss, K.S. Carslaw, M. Leutbecher, W. Renger, H. Volkert, and T. Peter, Model-guided Lagrangian observation and simulation of mountain polar stratospheric clouds, *J. Geophys. Res.*, *104*, 23971-23981, 1999.
- WMO (World Meteorological Organization), *Scientific Assessment of Ozone Depletion: 1989, Global Ozone Research and Monitoring Project—Report No. 20*, Geneva, 1990.
- WMO (World Meteorological Organization), *Scientific Assessment of Ozone Depletion: 1994, Global Ozone Research and Monitoring Project—Report No. 37*, Geneva, 1995.
- WMO (World Meteorological Organization), *Scientific Assessment of Ozone Depletion: 1998, Global Ozone Research and Monitoring Project—Report No. 44*, Geneva, 1999.
- Wofsy, S.C., R.J. Salawitch, J.H. Yatteau, M.B. McElroy, B.W. Gandrud, J.E. Dye, and B. Baumgardner, Condensation of HNO₃ on falling ice particles: Mechanism for denitrification of the polar stratosphere, *Geophys. Res. Lett.*, *17*, 449-452, 1990.
- Woyke, T., R. Müller, F. Stroh, D.S. McKenna, A. Engel, J.J. Margitan, M. Rex, and K.S. Carslaw, A test of our understanding of the ozone chemistry in the Arctic polar vortex based on in situ measurements of ClO, BrO, and O₃ in the 1994/1995 winter, *J. Geophys. Res.*, *104*, 18755-18768, 1999.
- Wu, J., and A.E. Dessler, Comparison between measurements and models of Antarctic ozone loss, *J. Geophys. Res.*, *106*, 3195-3201, 2001.
- Yoden, S., T. Yamaga, S. Pawson S, and U. Langematz, A composite analysis of the stratospheric sudden warmings simulated in a perpetual January integration of the Berlin TSM GCM, *J. Meteorol. Soc. Japan*, *77*, 431-445, 1999.
- Yoshiki, M., and K. Sato, A statistical study of gravity waves in the polar regions based on operational radiosonde data, *J. Geophys. Res.*, *105*, 17995-18011, 2000.
- Zander, R., M.R. Gunson, C.B. Farmer, C.P. Rinsland, F.W. Irion, and E. Mahieu, The 1985 chlorine and fluorine inventories in the stratosphere based on ATMOS observations at 30° north latitude, *J. Atmos. Chem.*, *15*, 171-186, 1992.
- Zander, R., E. Mahieu, M.R. Gunson, M.C. Abrams, A.Y. Chang, M. Abbas, C. Aellig, A. Engel, A. Goldman, F.W. Irion, N. Kämpfer, H.A. Michelsen, M.J. Newchurch, C.P. Rinsland, R.J. Salawitch, G.P. Stiller, and G.C. Toon, The 1994 northern midlatitude budget of stratospheric chlorine derived from ATMOS/ATLAS-3 observations, *Geophys. Res. Lett.*, *23*, 2357-2360, 1996.
- Zhou, S.T., M.E. Gelman, A.J. Miller, and J.P. McCormack, An inter-hemisphere comparison of the persistent stratospheric polar vortex, *Geophys. Res. Lett.*, *27*, 1123-1126, 2000.
- Zink, F., and R.A. Vincent, Wavelet analysis of stratospheric gravity wave packets over Macquarie Island, 2, Intermittency and mean-flow accelerations, *J. Geophys. Res.*, *106*, 10289-10297, 2001.
- Zurek, R.W., G.L. Manney, A.J. Miller, M.E. Gelman, and R.M. Nagatani, Interannual variability of the north polar vortex in the lower stratosphere during the UARS mission, *Geophys. Res. Lett.*, *23*, 289-292, 1996.

Appendix 3A

SATELLITE MEASUREMENTS IN THE ANTARCTIC AND ARCTIC

In this appendix, we update information on satellite instruments that measure ozone and other species that are pertinent to polar ozone issues. We briefly review the status of a variety of ozone and related measurements for the Antarctic and Arctic. Total ozone observations and ozonesondes have been extensively discussed in previous reports, and are further reviewed in Chapter 4 of this Assessment.

Earth Probe (EP) Total Ozone Mapping Spectrometer (TOMS): Data from the TOMS instrument have been extensively used to track Arctic and Antarctic ozone changes. The TOMS data are discussed in Chapter 4, Appendix 4A. The EP/TOMS operational processing configuration has recently been changed in order to apply a correction to a cross-track bias error that has grown since 2000. Although 2001 data are included herein, they are of slightly greater uncertainty (see discussion in the Earth Probes TOMS description in Chapter 4, Appendix 4A).

Microwave Limb Sounder (MLS): MLS observations started in September 1991 with the launch of the Upper Atmosphere Research Satellite (UARS). It gives column and profile data on ozone, ClO, and HNO₃. Recently, the satellite and instrument have experienced problems, and the instrument is turned on only when there are situations of particular interest. In particular, MLS was taken out of standby mode on 31 January 2000 and was operated during the 2-13 February and 27-29 March periods in conjunction with the SOLVE/THESEO 2000 campaign (Santee et al., 2000).

Halogen Occultation Experiment (HALOE): HALOE observations also started in September 1991 with the launch of UARS. HALOE is a solar occultation instrument that makes measurements in the IR at both sunset and sunrise. HALOE measurements are used to retrieve profiles of ozone, HF, HCl, CH₄, H₂O, NO, NO₂, and aerosol extinction. HALOE occultation latitudes are variable over the course of the northern winter, but do not reach the high northern latitudes. During the winter of 1999/2000, the maximum latitude sampled by HALOE was approximately 63°N in mid-March. HALOE typically has difficulty sampling the polar vortex during midwinter, but does sample the vortex edge region in the fall (Pierce et al., 2002).

Global Ozone Monitoring Experiment (GOME): The GOME instrument was launched in 1995 aboard the second European Remote Sensing (ERS-2) satellite. It measures column ozone, NO₂, BrO, and OCIO, and ozone profiles. Details on the GOME instrument can be found in Burrows et al. (1999). The GOME data have been subject to validation exercises (Hansen et al., 1999; Hoogen et al., 1999; Corlett and Monks, 2001; Ionov et al., 2001; Piters et al., 1999; Rathman et al., 1997).

Polar Ozone and Aerosol Measurement (POAM): POAM is a solar occultation instrument that provides ozone, water vapor, NO₂, and aerosol extinction profiles in the polar regions. POAM II was launched in 1993 aboard the French Satellite Pour l'Observation de la Terre (SPOT)-3 satellite. These measurements were interrupted by the failure of the SPOT-3 satellite in November 1996. POAM III was subsequently launched on the French SPOT-4 satellite in March 1998 and is currently operational.

Lucke et al. (1999), Lumpe et al. (2002), and Randall et al. (2002) have published intercomparisons between POAM III and other instruments. Results from POAM III include studies on dehydration (Nedoluha et al., 2000), ozone loss (Randall et al., 2002; Hoppel et al., 2002), and PSCs (Bevilacqua et al., 2002).

Improved Limb Atmospheric Spectrometer (ILAS): ILAS is a satellite instrument that uses the solar occultation technique (Sasano et al., 1999; Nakajima et al., 2002). ILAS was launched onboard the ADvanced Earth Observing Satellite (ADEOS) on 17 August 1996. ILAS made measurements over high-latitude regions from 57°N to 71°N and from 64°S to 88°S from late October 1996 until late June 1997.

ILAS consists of an infrared spectrometer that covers the wavelength region from about 6 to 12 μm. ILAS made vertical profile measurements of ozone, HNO₃, NO₂, N₂O, CH₄, and H₂O from the infrared spectrometer, as well as vertical profiles of aerosol extinction coefficient at 780 nm from the visible spectrometer. Ozone data are validated by correlative and coincident measurements from several instrumental techniques (Sugita et al., 2002). Nitric acid, NO₂, and H₂O data have also been validated (Koike et al., 2000; Kanzawa et al., 2002; Irie et al., 2002).